Segmented Flow Coil Equilibrator for Continuous Measurement of Volatile Organic Compounds in Seawater of the Polar Oceans

Submitted by Charel Wohl

as a thesis for the degree of Doctor of Philosophy

to the University of East Anglia

School of Environmental Sciences

In April 2021

Supervised by Dr. Mingxi Yang, Prof. Philip Nightingale, Prof. William Sturges and Dr. Anna Jones

Abstract

Volatile organic compounds (VOCs) are a group of molecules that influence aspects of atmospheric chemistry such as oxidation chemistry and particle formation. Most VOCs are produced from a variety of anthropogenic and natural sources; with emissions from the oceans least well known/ quantified. In this thesis I focus on methanol, acetone, acetaldehyde, DMS and isoprene. Uncertainty persists as to the factors influencing their variability in seawater concentrations. The polar oceans are particularly undersampled regions with few to no measurements of these compounds, which is partially due to a lack of suitable instrumentation.

To increase available instrumentation, this thesis describes the development of a Segmented Flow Coil Equilibrator coupled to a commercially available Proton Transfer Reaction-Mass Spectrometer for measurements of VOCs in seawater. Its main advantage lies in its ability to measure underway and discrete samples.

The method is used to make depth profile and underway measurements in the Canadian Arctic Archipelago during sea ice melt season. Highest VOC concentrations are generally observed at the surface, apart from DMS and isoprene which sometimes display a subsurface maximum. Generally, highest surface concentrations of VOCs are observed in partial ice cover. Concentrations of acetone and acetaldehyde were about 30 – 50 % higher in partial ice cover compared to ice-free waters.

This thesis also presents ambient air, underway and depth profile measurements from a transect in the subpolar Southern Ocean, used to calculate surface saturations and air – sea fluxes. Correlations with other biogeochemical data allowed me to elucidate factors controlling seawater concentrations of these VOCs. This dataset contains the first evidence of a statistically significant, but small diel change (on the order of 8 – 26 %) in seawater isoprene, acetone and acetaldehyde concentrations in the open ocean.

The measurements presented in this thesis will be useful to constrain ocean source/sink strength. The analysis points towards factors controlling the global variability of these compounds in the ocean.

Table of Contents

List of Tables

List of Figures

Acknowledgements

I am very thankful to the Foundation for Young Scientists in Luxembourg for giving me positive values as a person and a scientist at young age. Many thanks to Carlo Hansen and his wife Simone Hansen for their hard work reviving the annual contest “Jonk Fuerscher”. I am also thankful to the Mérite Jeunesse in Luxembourg for igniting a sense of exploration and adventure in me that made me go for this amazing PhD project.

Hans Pfalzgraf encouraged me to ask whether I might be qualified for this PhD because it was so different from my previous experience and I expressed interest to him. Thank you ever so much for this prod.

I am very thankful that my supervisors have been amazingly supportive and such excellent scientists. Thank you very much for all the time you spent on my supervision, which must have been frustrating at times. It has been a pleasure to work with you. Many thanks for your continued support until the end and detailed/rapid paper comments throughout. I dearly hope other PhD students will have the pleasure to be supervised by them as well.

To all the people involved in the cruise logistics - thank you very much for making this PhD project possible. Thanks to the crew of the CCGS Amundsen and RRS James Clark Ross for accommodating the PTR-MS on board. Many thanks also to the chief scientists for the successful cruises.

Many thanks to all those at PML working with the PTR-MS for sharing their time on the instrument and sharing other equipment such as thermometers (Dr. Tom Bell, Dr. Richard Sims), syringe pumps (Dr. Tom Bell), DMS (Dr. Frankie Hopkins) and isoprene (Paul Hackett) standards.

Many thanks to all those that made it so much fun living in Plymouth. The PML PhD students are really a nice cohort. Thank you to the Bluegrass players from the Bread and Roses for having me at their jams with my banjo. Thank you to the sport of climbing which provided an exciting distraction from the PhD, especially my new friends from the South Devon Mountaineering Club.

Thanks to my family in Luxembourg for always letting me do what I wanted and supporting me while doing it. Many thanks also to Emily’s family for their support while doing the PhD corrections. Final thanks are to Emily Alcock for her continuous emotional support throughout this adventure. Here is to a wonderful life together!

1 Literature review and open research questions

1.1 Introduction

Volatile Organic Compounds (VOCs), a subgroup of non-methane hydrocarbons (NMHC) (Carpenter and Nightingale, 2015; Heald et al., 2008), are comprised of numerous organic compounds of biological and anthropogenic origins. They are present ubiquitously throughout the lower atmosphere (Heald et al., 2008; Singh et al., 2004) and are important for the atmospheric oxidative capacity (Lewis et al., 2005) and particle formation (Arnold et al., 2009; Charlson et al., 1987). In this thesis, I focus on measuring seawater concentrations of the most ubiquitous oxygenated VOCs in the marine atmosphere, namely methanol, acetone and acetaldehyde (Lewis et al., 2005) and the biogenic VOCs dimethyl sulfide (DMS) and isoprene.

There exist relatively few oceanic measurements of these dissolved gases in the ocean. Modelling and observational studies show a large discrepancy as to whether the ocean is a source or a sink of methanol, acetone and acetaldehyde. Estimates of the oceanic emission of isoprene vary widely (Arnold et al., 2009; Luo and Yu, 2010), while DMS emissions are also poorly constrained globally (Lana et al., 2011; Land et al., 2014). This gap in oceanic observations is in part due to a paucity of suitable, automated measurement systems.

Thus, further thorough methodological development is required to improve the accuracy and automation of dissolved gas measurements. These measurements are necessary to build an understanding of what influences the variability of these VOCs in the ocean to inform global atmospheric models of the oceanic source or sink strength. The polar oceans are particularly under-sampled due to their remoteness. The effect of the unique environment of the high latitudes on these gases, including the melting of sea ice, has not been previously assessed. Furthermore, air – sea fluxes in these areas likely have a very substantial impact on the atmosphere due to the absence of other sources.

1.2 This thesis

This PhD thesis describes the development of an air – sea equilibrator (coined the Segmented Flow Coil Equilibrator, SFCE) coupled to a Proton Transfer Reaction-Mass Spectrometer (PTR-MS). The deployments of this setup in the Canadian Arctic sea ice zone and during a subpolar Southern Ocean transect are described. Measurements from these cruises are presented, which illustrate the effect of marine biogeochemistry on the

dissolved VOC concentrations. The thesis concludes with a brief comparison of the observations from both polar oceans.

The design of the SFCE is different to previous equilibrators as it allows for both underway high resolution and discrete measurements. Another novel aspect of this technique is that it has been incorporated into an automated setup which allows for fast alternation between underway seawater and ambient air measurement. This enables the calculation of high resolution air – sea fluxes.

Chapter 2 presents the optimisation and calibration of the PTR-MS instrument for the measurement of these gases in ambient air and equilibrator headspace. A discussion of the effect of humidity on the PTR-MS measurement is provided.

In Chapter 3, I present a very detailed characterisation of the analytical chemistry of the Segmented Flow Coil Equilibrator and share how the dissolved gas concentrations and ambient air mole fractions from the deployments are calculated. I share the results of a multitude of different laboratory tests to determine equilibration efficiencies. The chapter is rounded up by a discussion of the instrument background and the potential uncertainty of the measurement.

In Chapter 4, I share measurements of methanol, acetone, acetaldehyde, isoprene and DMS in the Arctic sea ice zone. Depth profiles and high resolution underway measurements allowed an assessment on the effect of sea ice cover on the seawater concentrations of these compounds.

Chapter 5 presents seawater and ambient air measurements of the same VOCs in the Southern Ocean. These are used to calculate high resolution saturations and fluxes. The large number of surface underway measurements enabled me to resolve a subtle diurnal change in the seawater concentrations of some of these VOCs. Using depth profiles, I estimate the importance of air sea exchange in controlling seawater concentrations of these VOCs in the Southern Ocean.

The concentrations, mole fractions and air – sea fluxes reported in this thesis improve our understanding of what influences the variability of these gases in the marine environment and help to constrain the impact of air – sea exchange. The measurements are useful model inputs to assess the effect of these gases on the oxidative capacity and particle formation potential in the polar atmosphere.

1.3 Sources and sinks of VOCs in the marine environment and the role of the ocean in their global cycling

In this section, I present what is known about the biogeochemical cycling of these gases in the marine environment and point out key gaps in our understanding. Further, I lay out the discrepancies between global air – sea exchange estimates. The compounds are grouped in this discussion based on similarities in their biogeochemical cycling.

1.3.1 Oxygenated VOCs; methanol, acetone and acetaldehyde

The oxygenated VOCs methanol, acetone and acetaldehyde share many similar sources (e.g. terrestrial emissions, photochemistry) and sinks (e.g. oxidation by OH) in the atmosphere. Therefore, I present them together in this section to compare and contrast their production mechanism in seawater and uncertainties in global ocean air – sea exchange.

1.3.1.1 Cycling in the marine environment and vertical profiles

Figure 1.1 illustrates the biogeochemical cycling of these oxygenated VOCs in the marine environment.

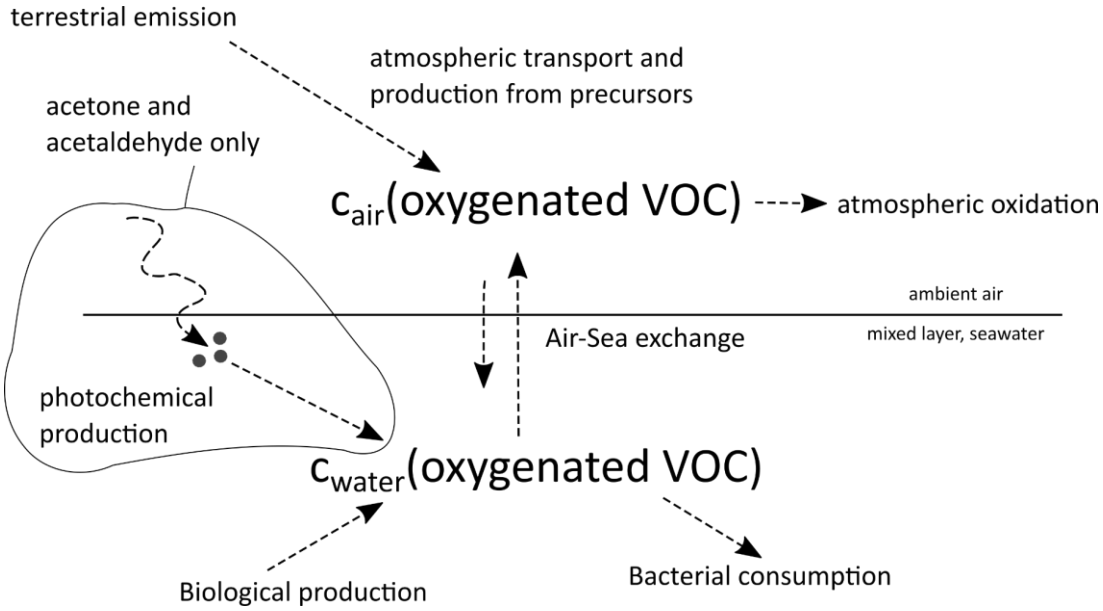

Figure 1.1 Diagram illustrating the biogeochemical cycling of the oxygenated VOCs, methanol, acetone and acetaldehyde in the marine environment. Arrows indicate the main known processes to date.

Methanol

The largest source of methanol to the atmosphere is terrestrial plant growth (Heikes, 2002; Stavrakou et al., 2011) and photochemical production from precursors (Müller et al.,

2016a). Methanol is released during phases of intense plant growth as part of the normal metabolism of higher plants (Fall, 2003). The mean lifetime in the lower atmosphere of methanol to all its sinks is estimated to be around 6 days (Stavrakou et al., 2011). The largest sinks for methanol are atmospheric oxidation and deposition to the ocean (Stavrakou et al., 2011).

Methanol concentrations in seawater typically range from 15 to 360 nmol dm^{-3} (Beale et al., 2013, 2015; Kameyama et al., 2010; Yang et al., 2013c, 2014a). This makes methanol the most abundant of the VOCs monitored here. Substantial concentrations of methanol in the surface ocean may seem surprising given the high biological turnover (Dixon et al., 2013), comparable to the lifetime of isoprene in seawater (Booge et al., 2018). This implies that the in situ biological production of methanol in seawater is also rapid. At the same time, the high solubility of methanol (Burkholder et al., 2015) disfavours substantial outgassing and probably helps methanol to accumulate in seawater. There are no measurements of methanol at the high latitudes. In the Labrador Sea (Yang et al., 2014a) and in the South Atlantic (Yang et al., 2013a) at latitudes of approximately 50° N and approximately 50° S, respectively, concentrations of methanol are generally lower and displayed a smaller range from 7 to 28 nmol dm^{-3} compared to other parts of the ocean. It is currently unclear which processes dominate and control the variability of methanol in surface seawater concentrations.

Methanol is thought to be produced biologically in seawater from phytoplankton and by the breakdown of marine algal cells (Heikes, 2002; Mincer and Aicher, 2016). Mincer and Aicher (2016) measured substantial methanol concentrations in a large range of phytoplankton cultures. Similarly, Kameyama et al. (2011) observed methanol in the headspace of a culture of the marine diatom *Thalassiosira pseudonana.* During a trans-Atlantic transect, Beale et al. (2013) and Yang et al. (2014c) found no correlation in surface methanol concentrations with chlorophyll *a* (Chl *a*) or primary productivity. This suggests that methanol may be produced only by some phytoplankton, and surface concentrations could also be influenced by removal processes. Dixon et al. (2013) did not observe any photochemical production of methanol in seawater.

During an Atlantic Meridional Transect through several oceanic provinces with distinct marine productivity, microbial oxidation was found to account for 10-50 % of methanol loss in the surface waters. This gave it a biological lifetime in upwelling areas of less than 7 days and 10 to 26 days in the open ocean (Dixon et al., 2013). Biological lifetimes of less than 1

day have also been reported (Dixon et al., 2011b). Methanol serves as sole carbon and energy source for a type of microbes coined methylotrophs (Stacheter et al., 2013). Methanol was found to be used by other bacteria as well as a source of energy and to a lesser extent carbon (Dixon et al., 2011a, 2011b).

There are generally few depth profile measurements of methanol. During a trans-Atlantic crossing, Yang et al. (2014c) find generally higher concentrations of methanol in the surface than at 500 m. During a similar crossing, Beale et al. (2013) found no consistent trend in concentrations down to 200 m. Williams et al. (2004) observed generally highest concentrations of methanol in the mixed layer near the tropical Atlantic. Concentrations of methanol within the mixed layer can be very variable, possibly due to stark variations in the biological consumption rates with depth (Dixon and Nightingale, 2012) or due to the large measurement noise (Beale et al., 2011). During an annual study at a coastal site near the UK where the water column was ≈ 50 m deep, methanol concentration was found to be relatively consistent throughout the water column (Beale et al., 2015). Higher concentrations at the surface than below the mixed layer in the open ocean support a biological source of methanol in seawater.

Acetone

The biggest source of acetone to the atmosphere is direct emission by terrestrial plants and oxidation of organic precursors (Fischer et al., 2012). Terrestrial plants emit acetone as part of their metabolic activity (Sharkey, 1996). Hence it is mostly emitted during times of intense plant growth in spring (Schade and Goldstein, 2006). Mostly anthropogenic isoalkanes are oxidised to acetone, representing a global source of acetone (Fischer et al., 2012). The mean atmospheric lifetime of acetone to its sinks is estimated as 18 days (Khan et al., 2015), with removal dominated by OH oxidation in the atmosphere (Fischer et al., 2012).

Typical acetone concentrations in seawater range from 2 to 25 nmol dm^{-3} (Beale et al., 2013; Hudson et al., 2007; Kameyama et al., 2010; Marandino et al., 2005a; Williams et al., 2004; Yang et al., 2013c). At higher latitudes, lower seawater concentrations have been observed in the Labrador sea of 3 to 9 nmol dm^{-3} (Yang et al., 2014a) and in the far North Atlantic of less than 9 nmol dm^{-3} (Hudson et al., 2007). Early measurements suggested higher concentrations of acetone in the sea surface microlayer (Zhou and Mopper, 1997). However, this might have been an artefact associated with sampling the microlayer and has

not been repeated to my knowledge. It is unclear which processes dominate in controlling the variability of acetone in surface seawater.

Acetone is thought to be produced in the oceans primarily by photochemical degradation of organic carbon (Dixon et al., 2013; Mopper and Stahovec, 1986; Zhou and Mopper, 1997). During a series of incubation experiments covering a wider range of marine productivity areas, Dixon et al. (2013) found that photochemical production accounts for up to 100 % of the observed acetone in seawater, hence dominating over biological production in the open ocean. De Bruyn et al. (2011) suggest that acetone production may proceed via a OH/O_2 mediated mechanism requiring UV light. Qualitatively consistent with a photochemical source, higher surface acetone concentrations in the summer compared to winter have been observed at a coastal site in UK (Beale et al., 2015). At the same site, Dixon et al. (2014) report a much higher oxidation rate from bacteria in winter compared to summer, which could also account for this seasonality. More recently, biological sources for acetone have also been suggested from field measurements (Schlundt et al., 2017), laboratory phytoplankton cultures (Halsey et al., 2017), and bacterial cultures (Nemecek-Marshall et al., 1995). Also Taddei et al. (2009) find highest emissions of acetone in the South Atlantic in areas of higher Chl *a* concentrations compared to the rest of the cruise track. It is unclear whether most of the acetone in seawater is produced from photochemical or biological sources.

In the oceans, acetone is thought to be consumed by microbes (Dixon et al., 2013, 2014). By addition of small amounts of ^{14}C-labelled acetone to seawater from the Atlantic, Dixon et al. (2013) found that microbial consumption was responsible for 0.5-13 % of the total observed losses of acetone. However, this method could represent an underestimate as it does not account for acetone incorporated into the cells (Carpenter and Nightingale, 2015). The typical open ocean lifetimes of acetone range between 5 and 55 days (Dixon et al., 2013). In coastal seawater, De Bruyn et al. (2017) estimated a much shorter half-life of acetone of (5.8 ± 2.4) h, where abiotic loss accounted for less than 10 % of that.

Relatively few investigators have measured acetone depth profiles. Highest concentrations of acetone are generally measured in the mixed layer, while concentrations of acetone below the mixed layer are low, but still detectable (Beale et al., 2013; Williams et al., 2004; Yang et al., 2014c). Acetone concentrations within the mixed layer appear very homogenous (Williams et al., 2004). Higher concentrations at the surface than below the mixed layer are consistent with photochemical production from degrading organic matter

(Dixon et al., 2013; Kieber et al., 1990) or a light dependent production by phytoplankton (Halsey et al., 2017; Schlundt et al., 2017).

Acetaldehyde

Millet et al. (2010) modelled the biggest atmospheric source of acetaldehyde to be photochemical oxidation of organic precursors such as short chain alkanes (>C1), alkenes (>C2) and ethanol. In the atmosphere, acetaldehyde has a very short lifetime of 0.8 days (Millet et al., 2010). This is due to its rapid atmospheric oxidation through reaction with OH – its largest sink (Millet et al., 2010).

Typical acetaldehyde concentrations in seawater range from 3 to 9 nmol dm^{-3} (Beale et al., 2013; Schlundt et al., 2017; Yang et al., 2013c, 2014a; Zhu and Kieber, 2019), but concentrations as high as 30 nmol dm^{-3} have been reported near the coast (Beale et al., 2015) and river outflows (Mopper and Stahovec, 1986; Takeda et al., 2014). Acetaldehyde is thought to be produced predominantly in the ocean by photodegradation of chromophoric dissolved organic matter (CDOM) (Dixon et al., 2013; Zhou and Mopper, 1997; Zhu and Kieber, 2019). The mechanism appears to be dominated by direct photolysis of CDOM by UV light (De Bruyn et al., 2011). Zhu and Kieber (2018) find that acetaldehyde production from CDOM coincides with a loss of absorption of CDOM, so called CDOM "bleaching" which in turn also reduces the rate of acetaldehyde production (De Bruyn et al., 2011). During a series of incubation experiments with small additions of ^{14}C-labelled acetaldehyde, Dixon et al. (2013) found that photochemical production accounts for about 16-68 % of acetaldehyde production in seawater. More recently, using laboratory cultures of diatoms, Halsey et al. (2017) argue for a strong light dependent biological source of acetaldehyde in seawater. Field deployment of the same setup further led the authors to suggest a strong biological source of acetaldehyde (Davie-Martin et al., 2020). Zhu and Kieber (2019) estimate that photochemical production can only explain for 7-53 % of the observed acetaldehyde concentrations in surface seawater at their sampling stations. Thus, there appears to be more evidence for biological production of acetaldehyde, compared to acetone. Acetaldehyde is likely produced from a combination of biological and photochemical sources. It is unclear what are the dominant production processes of acetaldehyde in the polar oceans in particular.

Microbial consumption of acetaldehyde has been found to be very fast with reported biological lifetimes in seawater of less than 1 day (Beale et al., 2015; Dixon et al., 2013). De Bruyn et al. (2017) and Dixon et al. (2014) found even faster acetaldehyde consumption rates in unfiltered coastal seawater, giving lifetimes of about one hour only. The abiotic loss of acetaldehyde in seawater appears to be negligible (De Bruyn et al. (2017)).

Depth profile measurements of acetaldehyde are rare. During a trans-Atlantic crossing, Beale et al. (2013) and Yang et al. (2014c) generally observe similar concentrations of acetaldehyde from the surface and from 200 or 500 m. During an annual study in temperate coastal waters, Beale et al. (2015) observe a rapid decline of acetaldehyde concentrations with depth. In the Black Sea, Mopper and Kieber (1991) found very heterogenous concentrations of acetaldehyde up to 4 nmol dm^{-3} in the surface mixed layer and concentrations of around 2 nmol dm^{-3} at depths down to 2000 m. Using a similar method in the Atlantic, Zhu and Kieber (2019) find highest concentrations in the mixed layer and very homogenous, near zero concentrations below the mixed layer. The rapid biological consumption of acetaldehyde at the surface (Dixon et al., 2013) likely prevents accumulation of substantial concentrations in the mixed layer most of the time. Consumption below the mixed layer is thought to be slower (Dixon et al., 2013; Kieber et al., 1990) and production at these depths in the absence of light (Zhu and Kieber, 2020) could be due to microbial activity (Zhu and Kieber, 2019).

1.3.1.2 Air – sea fluxes: comparing global budgets and observations

Methanol

To explain high methanol mole fractions observed in the marine boundary layer, earlier global atmospheric budgets suggest that the ocean is emitting methanol (Heikes, 2002) which is partly balanced by a large ocean uptake (Heikes, 2002; Millet et al., 2008; Stavrakou et al., 2011). Müller et al. (2016a) suggest that the reaction of CH_3O_2 + OH represents a substantial source of methanol in the remote marine atmosphere. Using these insights and recently measured seawater concentrations, Bates et al. (2021) calculate an oceanic source of 24 Tg a^{-1} and an oceanic sink of -38 Tg a^{-1}, resulting in a net ocean sink of -14 Tg a^{-1}. In contrast to previous methanol budgets (Müller et al., 2016b; Stavrakou et al., 2011), which suggested outgassing in some regions, this budget (Figure 1.2, Bates et al. (2021)) suggests that the net flux of methanol is consistently into the ocean, in all ocean regions. The polar oceans are modelled to be a net weak sink. Largest uptake is modelled in equatorial regions and coastal areas.

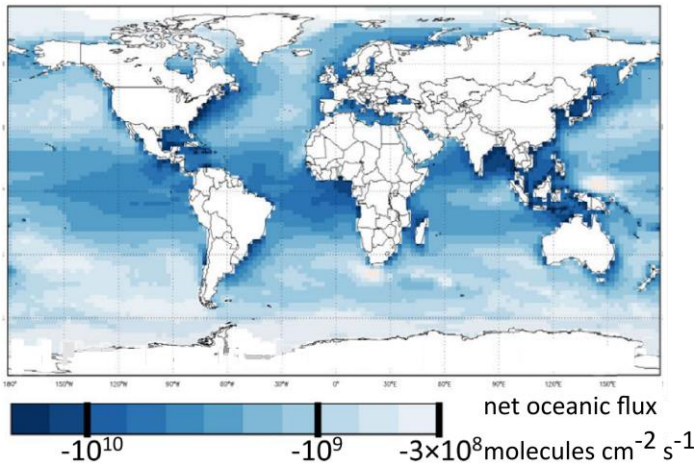

Figure 1.2 Annual mean modelled emission fluxes of methanol over the oceans. (10^9 cm^{-2} s^{-1} / N_A = µmol m^{-2} d^{-1}). Figure taken from Bates et al. (2021) with adaptations of the annotation.

There are relatively few observations of methanol ocean flux. Direct air – sea flux measurements of methanol during a trans-Atlantic crossing (Yang et al., 2013a) and in the Labrador Sea (Yang et al., 2014a) have found that the flux of methanol is exclusively into the ocean. Beale et al. (2015) calculate that the English Channel was strongly undersaturated in methanol throughout the year. From direct air – sea flux measurements in the Atlantic, Yang et al. (2013a) extrapolated that the global ocean represent a net sink of -42 Tg a^{-1}. Thus, the few in situ observations predominantly suggest that the ocean is consistently a sink of methanol.

Acetone

The biggest uncertainty in global atmospheric acetone budget is the role of the ocean as a net source or sink of acetone. The most recent global atmospheric budget of acetone (CAM-Chem) calculates that the ocean is both a large source (33.4 Tg a^{-1}) and a large sink of acetone (-41.5 Tg a^{-1}) (Wang et al., 2020a). This results in a net oceanic sink of -8.1 Tg a^{-1} (Wang et al., 2020a). Using an older model, Wang et al. (2020) estimate that the largest ocean emissions of acetone occur at the lower latitudes, while the high northern latitudes are modelled to be a year round sink (Figure 1.3). The Southern Ocean is modelled to be a weak sink most of the year, but a weak source during austral summer. Outgassing is predicted for the lower latitudes year round.

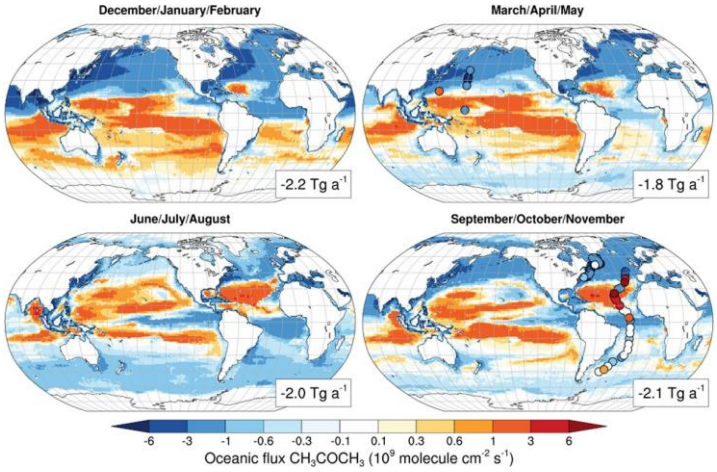

Figure 1.3 : This figure illustrates the net average modelled flux of acetone from the ocean. A positive flux indicates a flux from the sea to the air. Some observationally based flux estimates are included as coloured markers. (10^9 cm^{-2} s^{-1} / N_A = 1.4 µmol m^{-2} d^{-1}). Figure taken from Wang et al. (2020a).

There are relatively few air – sea flux measurements of acetone. Direct flux observations during a transatlantic transect (Yang et al., 2014c) and in the Labrador Sea (Yang et al., 2014a) showed that the acetone flux can be either in or out of the ocean, depending on location. This leads to highly uncertain global extrapolations as these observations (Yang et al., 2014c) imply the ocean to be a net sink of -1 Tg a^{-1} with a propagated uncertainty of 19 Tg a^{-1}. Beale et al. (2015) estimate that the UK shelf seas are a sink of acetone year round. Measurements in the South China/Sulu Sea also showed that the ocean is a large sink of acetone (Schlundt et al., 2017), likely due to high atmospheric mole fractions near continental outflow.

Acetaldehyde

Air – sea exchange represents a large uncertainty in the global budget of acetaldehyde. Constrained by aircraft measurements, Wang et al. (2019) estimate the global oceanic source of acetaldehyde to be 34 Tg a^{-1}. They suggest that the strongest outgassing of acetaldehyde occurs in the tropics (Figure 1.4) while the polar oceans represent a weak sink or are near equilibrium year round (Wang et al., 2019).

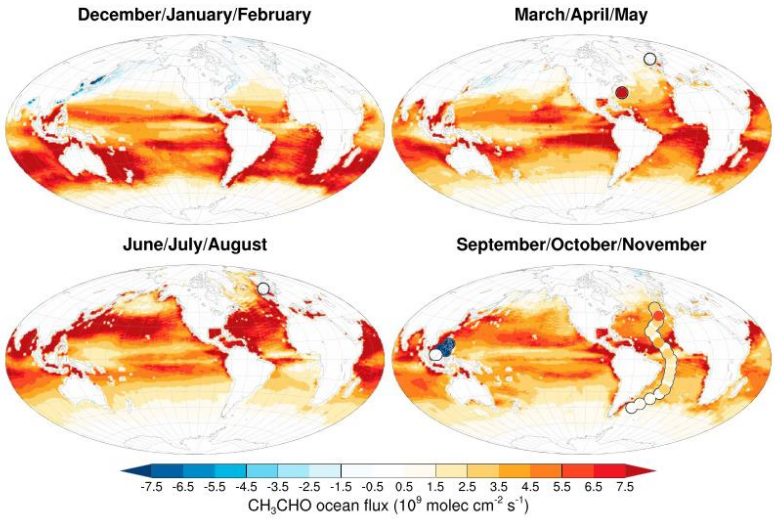

Figure 1.4 Modelled ocean-to-air flux of acetaldehyde.

Figure taken from Wang et al. (2019). Markers represent comparison to flux observations. Positive values indicate sea to air flux. (10^9 cm^{-2} s^{-1} / N_A = 1.4 µmol m^{-2} d^{-1}).

There are few direct ocean flux measurements of acetaldehyde. Using direct flux measurements over the Atlantic, Yang et al. (2014c) found that the ocean absorbs or emits acetaldehyde depending on location. Extrapolating their measurements, Yang et al. (2014c) estimate the net oceanic emission of acetaldehyde to be around (3 ±14) Tg a^{-1} (Yang et al., 2014c). Similar to the case for acetone, the large propagated uncertainty is because the fluxes are highly variable in direction as well as in magnitude. During an annual study at a UK coastal site, Beale et al. (2015) also found that the ocean can be both a source and a sink of acetaldehyde. Measurements from a cruise in the South China/Sulu sea showed that this region is a strong sink of acetaldehyde, which is likely due to high atmospheric mole fractions in areas of continental outflow (Schlundt et al., 2017).

1.3.2 Biogenic VOCs; dimethyl sulfide and isoprene

DMS and isoprene are both produced from phytoplankton-related sources and consumed by microbes in seawater. DMS and isoprene in the marine atmosphere are heavily influenced by their sea-to-air fluxes, and not generally influenced by terrestrial emissions. They are thus discussed together in this section.

1.3.2.1 Cycling in the marine environment and vertical profiles

The following Figure 1.5 is a schematic illustrating the biogeochemical cycling of these biogenic VOCs in the marine environment.

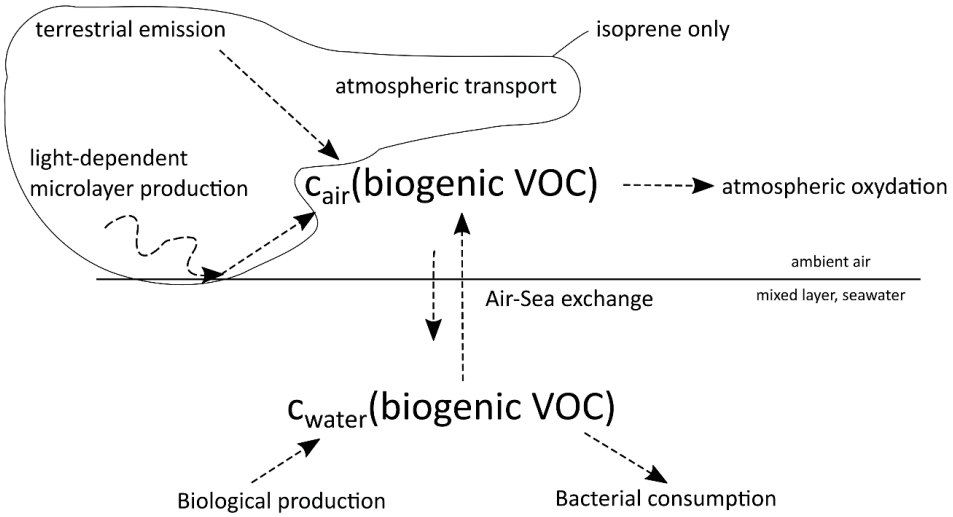

Figure 1.5 Diagram illustrating the biogeochemical cycling of the biogenic VOCs DMS and isoprene in the marine environment. Arrows indicate the main known processes to date.

DMS

There are very few terrestrial sources of DMS (Lana et al., 2011). Typical oceanic concentrations of DMS range between 1 and 7 nmol dm^{-3} (Lana et al., 2011), where concentrations above this threshold are generally labelled as extreme events (Lana et al., 2011). Production of DMS in seawater is complex but relatively well-studied (Zhang et al., 2019). The main production pathway is cleavage of dimethyl sulfoniopropionate (DMSP), which is produced by phytoplankton (Ksionzek et al., 2016). Phytoplankton produce DMSP and DMS at widely different rates (Sheehan and Petrou, 2020). Literature suggests that generally haptophytes and some dinoflagellates have higher intracellular levels of DMSP than diatoms (Malin and Steinke, 2010). Recently it has been discovered that some heterotrophic bacteria can also synthesise DMSP (Curson et al., 2017).

DMSP is converted to DMS from cleavage of DMSP by heterotrophic bacteria in seawater (Simo et al., 2000) or by phytoplankton themselves with the DMSP cleaved inside the cell (Alcolombri et al., 2015; Lizotte et al., 2017). Only a small fraction of the total DMSP is cleaved to DMS (between 2 % and 21 % (Kiene et al., 2000)). A large fraction of the DMSP is catabolised by bacteria and some of it is transformed to methanethiol by bacteria (Kiene et al., 2000). This makes DMS production highly variable and dependent on biological conditions (Archer et al., 2002). Most of the DMS is thought to be produced following the release of DMSP into the water column from events such as viral lysis (Barak-Gavish et al., 2018), zooplankton grazing (Simó et al., 2018) or senescence of phytoplankton (Merzouk et al., 2008). Only about 10 % or less of the DMS in the water column is lost due to emission

to the atmosphere (Archer et al., 2002; Yang et al., 2013b). In the atmosphere, DMS is rapidly oxidised by OH to various sulfur containing compounds (Boucher and Pham, 2002). The largest sink of DMS in seawater is biological consumption by bacteria (Kiene and Bates, 1990; Yang et al., 2013b). In surface seawater, the biological turnover time of DMS is generally between 0.5 and 2 days (Simo et al., 2000).

Depth profiles of DMS generally show highest concentrations in the mixed layer, in line with predominant biological cycling of DMS in the oceans (Rellinger et al., 2009; Royer et al., 2016). In the sea ice zone, Galí and Simó (2010), Matrai and Vernet (1997) and Bouillon et al. (2002) observe higher DMS concentrations at the deep Chl *a* maximum only at some of the stations, which is likely species and growth condition dependent (Galí and Simó, 2010). Concentrations below the mixed layer are generally found to be near zero due to bacterial consumption and a lack of production (Rellinger et al., 2009).

Isoprene

The largest source of isoprene to the atmosphere is from terrestrial plants, which is estimated at around 410 Tg a^{-1} (Müller et al., 2008). This emission has a large effect on the oxidative capacity of the terrestrial atmosphere (Sinha et al., 2010). Isoprene has an extremely short lifetime in the atmosphere of less than 1 hour (Wells et al., 2020) due to its rapid reaction with OH (Medeiros et al., 2018). Thus, atmospheric isoprene over the remote ocean cannot be explained by atmospheric transport but suggests a marine origin.

Isoprene concentrations in seawater range typically between 0 and 0.05 nmol dm^{-3} (Hackenberg et al., 2017; Rodríguez-Ros et al., 2020). Higher concentrations of up to 0.1 nmol dm^{-3} have been observed in phytoplankton blooms (Ooki et al., 2015; Rodríguez-Ros et al., 2020). Isoprene is mainly produced in seawater by a broad range of phytoplankton, where different phytoplankton functional groups show different production rates (Shaw et al., 2010). The marine production of isoprene is less growth condition and species dependent compared to DMS. As a consequence, numerous studies show a correlation between surface concentrations of isoprene and Chl *a* in the oceans (Bonsang et al., 2010; Gantt et al., 2009; Hackenberg et al., 2017; Kameyama et al., 2014; Ooki et al., 2015).

The largest removal mechanism of isoprene from the water column is emission to the atmosphere (Booge et al., 2018). The net flux of isoprene is predominantly from the ocean to the atmosphere due to the low solubility of isoprene and the generally low isoprene mole fraction in the atmosphere (Baker et al., 2000). A likely smaller sink of isoprene in the

water column is bacterial consumption (Booge et al., 2018). Alvarez et al. (2009) observed isoprene consumption by various bacteria from a temperate estuary. In the open ocean, recent budget calculations by Booge et al. (2018) have suggested a loss term of isoprene due to bacterial consumption or degradation varying between 10 and 100 days. The lifetime of isoprene in seawater due to air – sea exchange has been estimated as 7 days (Palmer and Shaw, 2005) or 10 days (Booge et al., 2018).

Depth profile concentrations of isoprene generally show higher concentrations in the mixed layer and very low concentrations well below the mixed layer (Booge et al., 2018; Moore and Wang, 2006; Tran et al., 2013). Booge et al. (2018), Hackenberg et al. (2017) and Tran et al. (2013) found that the subsurface isoprene maximum is found either at, above or below the Chl *a* maximum. Thus, in contrast to DMS, isoprene more reliably shows higher concentrations near the deep Chl *a* maximum.

1.3.2.2 Ocean emissions

DMS

In an effort to estimate global ocean DMS emissions from in situ measurements, Lana et al. (2011) assembled a global climatology and used it to estimate an annual global DMS emission of 54 Tg a^{-1} (expressed in this thesis as actual mass flux rather than S mass, which is more common in the field). Figure 1.6 shows that highest seawater DMS concentrations are typically observed during times of high biological productivity. As such, DMS concentrations show a strong seasonality, especially in the Southern Ocean and North Atlantic. This map (Figure 1.6) also illustrates that for many months of the year, the Arctic and Antarctic oceans are severely undersampled in DMS.

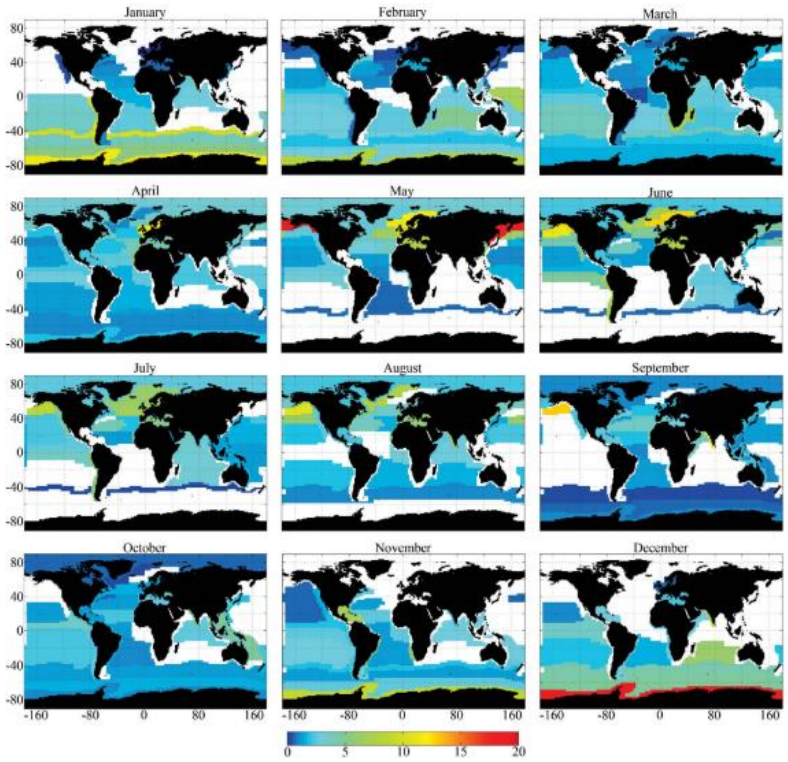

Figure 1.6 Monthly average DMS seawater concentration (nmol dm^{-3}) in different biogeochemical provinces.

Provinces in white contain no data for that calendar month. Figure taken from Lana et al. (2011).

Land et al. (2014) use an updated air – sea exchange parametrisations and estimated a lower global DMS flux of 38 Tg a^{-1}. Lana et al. (2011) suggest that the uncertainty of the seawater DMS concentrations due to lack of measurements contributes at least as much uncertainty to DMS flux as the uncertainty in the air – sea exchange parametrisations (Lana et al., 2011) (see Sect. 1.8 for air – sea exchange parametrisations). Further in situ concentration measurements, particularly in the Southern Ocean (Jarníková and Tortell, 2016) and the Arctic (Abbatt et al., 2019), will reduce the uncertainty of this estimate (Mungall et al., 2016).

Isoprene

Global oceanic isoprene emissions have been estimated to be (0.31±0.08) Tg a^{-1} (Arnold et al., 2009) (more than 100 fold smaller than terrestrial emissions). This estimate was created using modelled seawater concentrations based on phytoplankton specific production rates and satellite derived phytoplankton composition (bottom-up approach (Arnold et al., 2009)). With a similar bottom-up approach, although a different model, Booge et al. (2016) calculate an oceanic isoprene source of 0.21 Tg for the year 2014. In contrast, using measured atmospheric concentrations and the lifetime of isoprene in the atmosphere,

Arnold et al. (2009) estimate an oceanic source of 1.9 Tg a^{-1} (top-down approach). Using the same top-down approach, Luo and Yu (2010) estimate an even bigger oceanic isoprene source of 11.6 Tg a^{-1}. This discrepancy between bottom-up and top-down estimate could be due to inaccurate representation of sea surface isoprene concentrations in these models, highlighting a lack of understanding of isoprene cycling in the surface ocean (Booge et al., 2016, 2018; Hackenberg et al., 2017). Annual mean ocean fluxes calculated by Booge et al. (2016) are shown here (Figure 1.7). Booge et al. (2016) calculate highest fluxes of isoprene in the North Atlantic and the Southern Ocean, with smaller fluxes in the tropics. In their model, Southern Ocean isoprene emissions appear to be dominated by patch-like episodes. These could be related to deep hydrothermal vents (Ardyna et al., 2019) or island effects (Ardelan et al., 2010), creating phytoplankton blooms by supplying iron (Wingenter et al., 2004).

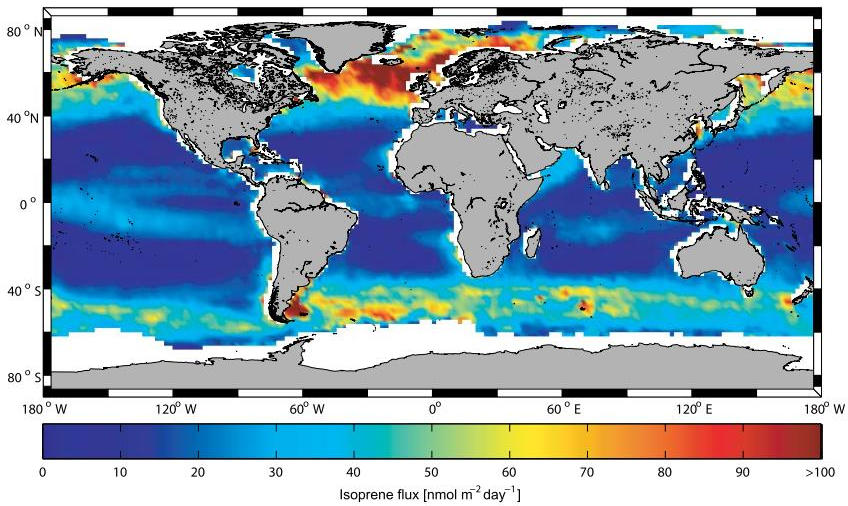

Figure 1.7 Map of the global isoprene flux modelled for 2014 by Booge et al. (2016). These fluxes are calculated using a bottom-up modelling approach, where the seawater concentrations are modelled based on in situ production rates.

Photochemical production within the sea surface microlayer has been suggested to be a substantial source of isoprene and could partly account for the discrepancy between bottom-up and top-down estimates (Ciuraru et al., 2015). Brüggemann et al. (2018) estimate that this process contributes around 1.11 Tg a^{-1} to the oceanic isoprene source. However, the importance of this process is highly debated (Rodríguez-Ros et al., 2020). The only direct air – sea flux measurement (in the Labrador sea in autumn) showed no evidence for an enhanced flux under increased light levels (Kim et al., 2017b). Ambient air concentrations of isoprene in the Arctic also did not correlate with other compounds known to be produced in the sea surface microlayer (Mungall et al., 2017).

1.3.3 Diurnal changes

Dixon et al. (2013) estimated that photochemical production accounts for up to 100 % and 68 % of the gross production rates of acetone and acetaldehyde respectively in seawater. Halsey et al. (2017) suggested a light-dependent biological source, which is stronger for acetaldehyde and weaker for acetone. It might therefore be expected that these VOCs would display diurnal variability in their seawater concentrations. Zhou and Mopper (1997) and Mopper and Stahovec (1986) have reported diurnal changes in seawater acetaldehyde concentrations off the West Coast of Florida, with highest concentrations reported after solar zenith. Similarly, Takeda et al. (2014) have observed a diurnal change in acetaldehyde concentrations in an enclosed coastal area. Zhu and Kieber (2019) found a statistically insignificant difference between mean day and night acetaldehyde concentrations of 1 nmol dm^{-3} in the coastal Northwest Atlantic Ocean. Also, Beale et al. (2013) and Yang et al. (2014c) have observed no significant difference in seawater acetone and acetaldehyde concentrations between samples collected at predawn and solar noon during crossings of the Atlantic Ocean. In general, it seems that in coastal areas acetone and acetaldehyde are more likely to display a diel change compared to in the open ocean. Similarly, diurnal variability in seawater isoprene concentrations has not been observed previously (Booge et al., 2018; Hackenberg et al., 2017; Moore and Wang, 2006; Tran et al., 2013) despite modelling studies suggesting the existence of a diurnal change (Gantt et al., 2009). Hackenberg et al. (2017) have suggested that the absence of diurnal isoprene variability could be due to production at the deep Chl *a* max and gradual replenishment of the surface waters through ocean mixing.

Using round the clock measurements, the existence of a diurnal change in the surface concentrations of these compounds will be investigated in this thesis.

1.3.4 Summary table: previous seawater measurements

Table 1.1 has been compiled to provide an overview of previous measurements of surface seawater concentrations of these VOCs in the polar oceans and other ocean basins.

Table 1.1 Table summarising previous surface (< 5 m) seawater measurements of DMS, isoprene, methanol, acetone and acetaldehyde in the polar oceans and other regions. (BLD = Below Limit of Detection)

	location	c(mean or median)/(nmol/dm^{-3})	c(range)/(nmol/dm^{-3})	date	study
DMS	Canadian Arctic Archipelago, Baffin Bay	1.78		Jul-Aug 2017	This study
	Canadian subarctic and Arctic marine waters	2.7	0.2-12	Jul-Aug 2015	Jarnikova et al. (2018)
	Canadian Arctic		5.0-10.0	Jul-Aug 2014	Mungall et al. (2016)
	Canadian Arctic		5.1-10.9	July-August 2014 and 2016	Abbatt et al. (2019)
	Canadian Arctic		0.05-0.8	Sep 2007	Luce et al. (2011)
		1.3	0.5-4.8	Sep 2008	Motard-Côté et al. (2012)
	Northern Baffin Bay	0.64	BLD-0.72	April 1998	Bouillon et al. (2002)
	Northern Baffin Bay	2.12	0.07-6.74	May 1998	Bouillon et al. (2002)
	Northern Baffin Bay	2.95	0.04-4.59	June 1998	Bouillon et al. (2002)
	far South Atlantic	1.6	0.5-3.2	Mar 2008	Yang et al. (2011)
	Ryder Bay, West Antarctic Peninsula		0.1-30	Annual study	Webb et al. (2019)
	Southern Ocean, near South Georgia	2.2	0.5-3.5	Feb-Apr 2008	Yang et al. (2013b)
isoprene	East Atlantic		0.021-0.046	May 1997	Baker et al. (2000)
	Southern Ocean	0.002		Jan 2002	Wingenter et al. (2004)
	Arctic and Atlantic	0.026	0.001-0.541	Jun-July 2010	Tran et al. (2013)
	Arctic	0.004	0.002-0.0106	March 2013	Hackenberg et al. (2017)
	Arctic	0.024	0.003-0.066	Jul-Aug 2013	Hackenberg et al. (2017)
	Atlantic	0.026	0.008-0.063	Nov-Oct 2012	Hackenberg et al. (2017)

Table 1.1 continued

location		c(mean or median)/(nmol/dm^{-3})	c(range)/(nmol/dm^{-3})	date	study
	Atlantic	0.018	0.001-0.038	Nov-Oct 2013	Hackenberg et al. (2017)
	Polar Basin	0.004	0.001-0.06	Sep-Oct 2012	Ooki et al. (2015)
	Polar Slope	0.004	0.002-0.014	Sep-Oct 2012	Ooki et al. (2015)
	Polar Shelf	0.013	0.003-0.031	Sep-Oct 2012	Ooki et al. (2015)
	North West Pacific	0.07	0.036-0.118	Jul-Aug 2008	Kameyama et al. (2010)
	Southern Ocean	0.078	0.000-0.348	Dec 2010-Jan 2011	Kameyama et al. (2014)
methanol	trans-Atlantic		48-361	Oct-Nov 2009	Beale et al. (2013)
	UK Coast shelf waters	49	16-78	Annual study	Beale et al. (2015)
	Tropical Atlantic	118.4	50-250	Oct-Nov 2002	Williams et al. (2004)
	trans-Atlantic	29	15-62	Oct-Nov 2012	Yang et al. (2013)
	North west Atlantic	16.3	7-28	Nov-Oct 2013	Yang et al. (2014)
	North West Pacific	158.9	77.9-325	Jul-Aug 2008	Kameyama et al. (2010)
acetone	trans-Atlantic		2-24	Oct-Nov 2009	Beale et al. (2013)
	South China/Sulu Sea	21.33	2.47-67.76	Nov 2011	Schlundt et al. (2017)
	Tropical Pacific Ocean	14.5	3-65	May-July 2004	Marandino et al. (2005)
	UK Coast shelf waters	6	2-10	Annual study	Beale et al. (2015)
	Tropical Atlantic	17.6	10-20	Oct-Nov 2002	Williams et al. (2004)
	UK Coast shelf waters	5	2-10	Annual study	Beale et al. (2015)
	trans-Atlantic	13.7	3-36	Oct-Nov 2012	Yang et al. (2014)
	North west Atlantic	5.7	3-9	Nov-Oct 2013	Yang et al. (2014)
	North West Pacific	19	4.4-41.3	Jul-Aug 2008	Kameyama et al. (2010)
	North East Atlantic	7.0	5.5-9.6	June-July 2006	Hudson et al. (2007)

Table 1.1 continued

	location	c(mean or median)/(nmol/dm^{-3})	c(range)/(nmol/dm^{-3})	date	study
acetaldehyde	trans-Atlantic		3-9	Oct-Nov 2009	Beale et al. (2013)
	South China/Sulu Sea	4.11	0.35-14.45	Nov 2011	Schlundt et al. (2017)
	Southwest Coast Florida		2-30	April 1985	Mopper and Stahovec (1986)
	100 km east of the Bahamas	1.38		April 1989	Zhou and Mopper (1997)
	North West Pacific	BLD	BLD-5.9	Jul-Aug 2008	Kameyama et al. (2010)
	trans-Atlantic	5.3	3-9	Oct-Nov 2012	Yang et al. (2014)
	UK Coast shelf waters	13	4-37	Annual study	Beale et al. (2015)
	North west Atlantic	3.02	1.0-7.1	Sep-Oct 2016	Zhu and Kieber (2019)

There have been comparatively many previous measurements of DMS. Therefore, the table here summarises some of the previous measurements from the polar oceans. Surface seawater DMS concentrations in the polar regions are governed by a strong seasonality with highest concentrations generally in summer/spring and lower concentrations in autumn/winter. Episodes of high DMS concentrations (around 10 nmol dm^{-3}) have been measured in the polar oceans, particularly in the sea ice zone.

There exist a large number of isoprene seawater measurements in the temperate and tropical oceans. The polar oceans appear highly undersampled, especially the Southern Ocean and Arctic ocean during the productive spring/summer season. Isoprene concentrations are generally higher in the summer and near the coast.

There are very few measurements of methanol in seawater and I note that all these measurements were carried out using PTR-MS. So it is possible that the measurements suffer from analytical artefacts. There exist no measurements in the polar regions of methanol in seawater. Methanol concentrations display a very large range. The concentrations appear to be lower at the high latitudes compared to tropical waters. Methanol concentrations appear to be higher in the open ocean than in coastal waters.

There exist relatively few measurements of acetone in the surface seawater. Nevertheless, it is the most commonly sampled one out of the oxygenated VOCs investigated in this thesis. There are essentially no measurements of acetone in the polar regions, although previous measurements at high latitude indicate very low concentrations compared to measurements at lower latitudes.

Acetaldehyde has also been measured only a few times in the ocean, with no measurements in the polar regions. Concentrations measured near the coast generally appear to be higher compared to open ocean measurements.

1.3.5 Summary table: production and consumption processes

A summary table is presented to sum up the relative importance of the different production and consumption processes in seawater for the compounds presented here (Table 1.2).

Table 1.2 Summary table summarising current knowledge of the relative importance of different production and consumption processes in seawater for the VOCs discussed here. (NA = Not Applicable)

	Biological production/(% of gross)	in situ Photochemical production/(% of gross)	$\tau_{biological\ consumption}$/(d)	$\tau_{air-sea\ exchange}$/(d)
methanol	100	NA	7[a]	uncertain
acetone	uncertain, but likely < 10 % [a]	48-100 [a]	80 [a]	uncertain
acetaldehyde	Uncertain, but up to 85 % [d]	16-68 [a]	1 [a]	uncertain
DMS	100[b]	NA	1-3 [b-]	10-100[b]
isoprene	100 [c]	uncertain	estimated 10-100[c]	10[c]

[a] Dixon et al. (2013) [b] Kiene and Linn (2000) [c] Booge et al. (2016) [d]Zhu and Kieber (2018)

Evidences of a biological source for acetone and acetaldehyde stem largely from corelations from field measurements (Schlundt et al., 2017) and laboratory cultures (Halsey et al., 2017; Nemecek-Marshall et al., 1999). To my knowledge, there are no reliable direct in situ estimates of the biological production rate of these compounds. Recent measurements by Davie-Martin (2020) potentially suffer from analytical artefacts related to the background. Using rates from Halsey et al. (2017), Zhu and Kieber (2018) calculate that biological acetaldehyde production rates may be very high in coastal areas, but negligible in the open ocean. The contribution of air – sea exchange is uncertain in sign and magnitude for most VOCs due to a paucity of flux estimates and variability in the flux. Some investigators suggest the influence of air – sea exchange on in situ VOC concentrations is likely small (Beale et al., 2015; Dixon et al., 2013; Yang et al., 2013a). The biogenic VOCs DMS and isoprene are produced exclusively from biological activity. The largest sink for DMS is biological consumption, while for isoprene air – sea exchange appears to be the largest sink, but it remains poorly quantified. Isoprene biological consumptions rates presented here are estimated from model calculations. Mixed layer depth (MLD) has been shown to influence DMS surface water concentrations on a global scale (Vallina and Simó, 2007), while the impact of MLD on other VOCs remains largely unquantified.

1.4 Marine biogeochemistry of the polar regions

In this section, I discuss a range of biogeochemical processes unique to the polar regions that are relevant to VOC production and consumption. These processes could influence seawater concentrations of these VOCs. This section provides important background for the measurements and insights presented in this thesis.

1.4.1 Contrasting the Arctic and the Southern Ocean

The Arctic and the Southern Ocean both experience periods of total darkness and 24 h daylight, which influence the seasonality in primary productivity and photochemistry (DeVries and Steffensen, 2005). Nevertheless, they are very different environments.

The Arctic ocean typically experiences lower wind speeds, a large fraction of ice covered ocean and is influenced by nearby landmass (DeVries and Steffensen, 2005). The landmass in the Arctic is partly inhabited and covered in sparse vegetation, depending on the latitude (Mungall et al., 2017). Being situated in the Northern Hemisphere, it is also under a substantial anthropogenic influence (Zou et al., 2017).

In contrast, the Southern Ocean generally experiences very high wind speeds, and consists of a large fraction of open ocean (DeVries and Steffensen, 2005). Hence, the Southern Ocean is characterised by relatively high gas transfer velocities (Yang et al., 2011). The landmass in the Antarctic is generally at the very high latitudes and thus presents essentially no vegetation and is uninhabited (DeVries and Steffensen, 2005). Nevertheless, small islands in the Southern Ocean exert a large influence on the local biogeochemistry (Ardelan et al., 2010; Blain et al., 2001). As a consequence, the Southern Ocean is extremely remote and represents a pristine marine environment (DeVries and Steffensen, 2005).

These environmental settings are bound to influence VOC abundances in water and air. Although, the specific patterns are currently unknown. A comparison of measurements in both oceans will provide a deeper understanding of their production processes.

1.4.2 Seasonality of the water column in the Arctic sea ice zone and the Southern Ocean

The Arctic and the Antarctic are both governed by strong seasonality and variations in mixed layer depth leading to pulses of high primary productivity, which influences the upper water column (DeVries and Steffensen, 2005). In both oceans, the density profile is

generally shaped by the salinity profile, due to the low seawater temperatures (Rudels et al., 1991).

In the marginal ice zone of the Arctic in summer, sea ice melt leads to freshwater input and formation of a very shallow mixed layer (Rudels et al., 1991; Shadwick et al., 2011). Characterised by a very low salinity, this shallow mixed layer (0- 40 m) warms up (Shadwick et al., 2013) the longer it is exposed to air during the spring/summer (Ahmed et al., 2019). The mixed layer isolates phytoplankton near the sunlit surface, leading to phytoplankton blooms (Barber et al., 2015; Perrette et al., 2011). Once the ice has retreated, a well-defined deep Chl *a* maximum forms below the pycnocline, typically between 20 and 35 m (Ardyna et al., 2013; Barber et al., 2015; Martin et al., 2010). Higher wind speeds in winter create a deeper mixed layer, which disfavours phytoplankton growth (Shadwick et al., 2013).

In the open ocean zone in the Antarctic in summer, it is partly ice berg melt that leads to the formation of a deep mixed layer (40-100 m), which is characterised by a low salinity and elevated temperature. This mixed layer enables phytoplankton growth in the spring/summer (Deppeler and Davidson, 2017). The Southern Ocean is predominantly characterised by low Chl *a* concentrations (Deppeler and Davidson, 2017; Shadwick et al., 2013). A colder layer of water is typically found below the surface mixed layer, coined the winter cooled layer at about 100 m (Venables and Meredith, 2014). This is caused by warming of surface in the summer (Rellinger et al., 2009), when winds decrease and freshwater stabilises a 40-100 m deep mixed layer (Pellichero et al., 2017). Most of the Chl *a* is homogenously distributed within the mixed layer, and a subsurface Chl *a* maximum is generally not observed (Deppeler and Davidson, 2017). In winter, stronger winds create a 150-200 m deep colder mixed layer (Deppeler and Davidson, 2017; Pellichero et al., 2017).

The effect of these biogeochemical processes on dissolved VOC concentrations are currently unknown. Measurement of dissolved gases at distinct depths will allow me to investigate the importance of different biogeochemical processes that control these VOCs.

1.5 Role of Volatile Organic Compounds in the atmosphere

In this section, I briefly discuss the atmospheric importance of the VOCs measured here.

VOCs influence the oxidative capacity of the marine atmosphere

The atmospheric lifetimes of CH_4, CO and many non-methane organic compounds are controlled by the oxidative capacity of the atmosphere (Derwent et al., 2018). The

reactions of these compounds with OH radicals initiate a cascade of reactions that ultimately leads to complete oxidation to CO_2 and H_2O (Bloss et al., 2005; Derwent et al., 2018).

From measurements of marine air at an observatory at Mace Head, Lewis et al. (2005) found that acetone, acetaldehyde and methanol constituted 85 % of non-methane hydrocarbons in marine air. Using simple modelling, they showed that methanol, acetone and acetaldehyde represented the third largest sink of OH radicals in marine air after carbon monoxide and methane (Lewis et al., 2005). Lewis et al. (2005) also found that only during periods of intense isoprene emission could isoprene become the locally dominant OH sink in marine air. DMS was calculated to be a very small OH sink (Lewis et al., 2005). Read et al. (2012) find that their Geos-Chem model severely underrepresents atmospheric methanol, acetone and acetaldehyde mole fractions in marine air, which results in an underestimation of methane atmospheric lifetime of up to 8 %.

VOCs can lead to production of ozone

VOCs play a role in air quality and influence ozone mole fractions in marine air as they affect the cycling of ozone with NO_x (=NO +NO_2) in the atmosphere (Atkinson, 2000). In the presence of VOCs, the light driven cycling of NO_x leads to production of ozone.

VOCs are precursor molecules to other important atmospheric gases

At high NO_x, acetaldehyde reacts with NO_x to form peroxyacetyl nitrate (PAN) (Atkinson, 2000), for example in urban polluted air (Lee et al., 2012). PAN is decomposed slowly over the remote ocean, releasing NO_x. Therein it represents a means of long-range transport of NO_x to the remote marine atmosphere (Lee et al., 2012). Methanol is an important precursor to carbon monoxide (Read et al., 2009) and formaldehyde (Zhu et al., 2016).

VOCs can be sources of OH to the troposphere

It has been suggested that acetone and acetaldehyde are chemical precursors of OH radials in the higher troposphere (Singh et al., 1995). Based on their model calculations, Schlundt et al (2017) predicted that at least 0.4 nmol mol^{-1} of oceanic acetone can reach the troposphere above the South China/Sulu Seas. Similarly, isoprene can enter the upper troposphere during convective outflow events, where it dominates OH reactivity (Apel et al., 2012).

VOCs can lead to particle formation

Atmospheric particles influence the earth's climate as they scatter radiation (aerosol direct effect) and influence cloud properties (aerosol indirect effect), which could lead to cooling or warming (Liss and Lovelock, 2007; Udisti et al., 2020). VOCs released by the ocean could have a large impact on the particle concentration and size distribution because of a lower influence of terrestrial emission in the marine environment. At the same time, their effect is poorly constrained (Carslaw et al., 2013), particularly over the Southern Ocean (Hyder et al., 2018). This misrepresentation of the Southern Ocean can lead to biases of the modelled properties of clouds (Thomas et al., 2010). During boreal winter, the Arctic atmosphere is strongly influenced by anthropogenic emissions – a phenomenon called "Arctic haze" (Zou et al., 2017). In the Arctic summer, local sources, especially biogenic sulfate, dominate particle formation (Abbatt et al., 2019; Collins et al., 2017).

DMS is a key gas that contributes to particle formation and growth in the marine atmosphere (Charlson et al., 1987; Woodhouse et al., 2013). DMS has been a long standing topic of research due to the CLAW hypothesis (Charlson et al., 1987), which suggested a feedback role of DMS in regulating climate. These days, it is generally accepted that DMS is important for cloud formation and cooling of the planet (Korhonen et al., 2008; Woodhouse et al., 2013), but the feedback loop has been largely dismissed (Liss and Lovelock, 2007). The Southern Ocean (Jarníková and Tortell, 2016) and the Arctic Ocean (Abbatt et al., 2019; Udisti et al., 2020) are highly under-sampled for DMS. To give an appreciation of the sensitivity of the models to errors in these emissions, Woodhouse et al. (2013) calculate a 4-6 % change in global cloud condensation nuclei (CCN) for a 10 % change in DMS flux (relative to Kettle and Andreae (2000)) in a patch of the Atlantic sector of the Southern Ocean for December alone. CCN over the Southern Ocean show clear seasonal variability with highest concentrations typically observed in austral summer (Kim et al., 2017a), suggesting, amongst others, a role of biological productivity in the formation of CCN.

It is debatable whether isoprene represents a substantial source of particles in the marine environment. Large amounts of organic carbon are detected in marine aerosol (Miyazaki et al., 2016). The organic content in particles is found to increase during intense biological productivity (Ito and Kawamiya, 2010; Spracklen et al., 2008). The mechanism for this is currently unclear and could either be due to primary organic matter from the sea surface being suspended in aerosol phase (O'Dowd et al., 2004) or due to formation of new particles from organic gases (Claeys, 2004; Collins et al., 2017). Isoprene is suggested to be a significant source of organic aerosol in the marine atmosphere (Henze and Seinfeld, 2006)

and could thus be a key molecule that is responsible for the high organic carbon content in areas of high marine biological activity. By including isoprene as a source of secondary organic aerosols, Henze and Seinfeld (2006) found the largest increases in the predicted secondary organic aerosol in the remote marine environment. However, using results from modelled global isoprene emissions (bottom-up), Arnold et al. (2009) suggested that the contribution of marine isoprene to secondary organic aerosols is less than 2 %. Similarly, McFiggans et al. (2019) argued that isoprene can suppress organic aerosol formation by scavenging OH radicals from other particle forming gases. These estimates rely on global isoprene emission estimates that are highly uncertain, in part due to a lack of in situ measurements.

Methanol, acetone and acetaldehyde are suspected to be a source of particles or play a role in particle growth (Blando and Turpin, 2000). This estimate is based purely on their physical properties and observational evidence for this hypothesis is still lacking.

1.6 Methods and gas equilibrators for measuring VOCs in seawater

As mentioned before, observations of dissolved seawater VOC concentrations are scarce, mostly because only a small number of methods allow for in situ, automated quantification of VOCs in seawater. For example, derivatisation methods have been used, which require the synthesis of toxic chemicals to determine aldehyde concentrations in seawater with detection by high performance liquid chromatography (Zhu and Kieber, 2018). Such methods are not suitable for continuous measurements. Most methods of detection require the analyte to be in the gas phase, necessitating an adequate extraction or equilibration device.

Some dissolved gas concentration measurements have been made using purge and trap (PT) systems coupled to Gas Chromatograph – Mass Spectrometers (De Bruyn et al., 2011). This method is sensitive enough to allow detection in seawater (quantification down to nmol dm^{-3}), but it requires manual handling and is often more suitable for discrete measurements. A Gas Chromatograph - Mass Spectrometer has been coupled to a PT system to measure benzene and toluene, among other compounds (Huybrechts et al., 2000). Others have coupled PT systems to a Gas Chromatograph - Flame Ionisation Detector to measure isoprene (Exton et al., 2012), ethanol, and propanol in seawater (Beale et al., 2010). These setups are again only suitable for discrete samples with a sample treatment time of under 2 h, and care must be taken to avoid wall adsorption and desorption effects in the setup. A ship-based PT Gas Chromatograph - Mass Spectrometer

has been used to measure a broad range of VOCs in discrete surface water samples with a three-hour frequency; this required two people and represented a considerable workload (Schlundt et al., 2017). Some purge and trap systems have been automated to allow for underway measurements of halocarbons, DMS and isoprene semi-continuously ca. every 30 minutes (Andrews et al., 2015). The long measurement time preclude high-resolution measurements of these biologically reactive and short lived gases. This highlights the need for continuous, fast, and automated measurement techniques that do not require pre-treatment.

Two types of equilibrators are commonly used for continuous measurements of dissolved gases. One type allows for direct exchange between the carrier gas and the water, while the other uses a membrane to extract gases. Directly exchanging equilibrators such as the Weiss-style showerhead equilibrator (Johnson, 1999) enable underway CO_2 measurements with a <35 minute interval. This has been used widely to measure CO_2 and short lived halocarbons (Arévalo-Martínez et al., 2013; Butler et al., 2007). However, spray generated from the showerhead lengthens the equilibrator's response time for highly soluble gases, making it less suitable for high frequency measurements of highly soluble VOCs such as methanol (Kameyama et al., 2010). Membrane equilibrators avoid spray formation and allow for selective diffusion. Hollow fibre membranes have previously been used for measurement of dissolved CO_2 (Hales et al. , 2005; Sims et al., 2017) and DMS (Tortell, 2005; Yang et al., 2011). By using a hydrophobic membrane, the amount of water vapor in the detector can be reduced. For example membrane inlet mass spectrometers have been used to measure DMS and inorganic gases in seawater with a measurement frequency of more than once per minute (Tortell, 2005). Underway measurements of seawater DMS concentrations have been made with a 1 minute frequency using a Chemical Ionisation Mass Spectrometer (CIMS) coupled to a porous Teflon membrane (Saltzman et al, 2009). One disadvantage of membrane equilibrators is that the equilibration efficiency could be affected by biological growth on the membrane surface (biofouling), especially in biologically productive areas where some VOCs are known to have strong sources.

The choice of detector that the equilibrator is coupled to is crucial as well. Proton Transfer Reaction - Mass Spectrometry (PTR-MS) is a widely used instrument that allows high-frequency (0.1–1s) measurement of a broad range of trace gases in the atmosphere (Lindinger and Jordan, 1998; Blake et al., 2009). It is similarly suitable for high-resolution ship-based measurements of VOCs. In the following sub-sections I lay out existing equilibrators for VOCs in seawater. There are currently only two well characterised

equilibrators that allow measurement of VOCs in seawater using PTR-MS. These are presented here, as well as a coil equilibrator. The design of the segmented flow coil equilibrator used in this thesis is based on this coil equilibrator.

1.6.1 Membrane equilibrators

A simple schematic of the membrane inlet system developed by Beale et al. (2011) is presented in Figure 1.8. Their setup consists of a 3m long ¼ "diameter Fluorinated Ethylene Propylene (FEP) tube with a single silicone membrane (permeable to OVOCs) running in the centre. Seawater is flowing outside of the membrane and a nitrogen carrier gas is flowing inside the membrane. Water and carrier gas flow in opposite directions, which maintains a higher concentration difference between the water and gas phase. The membrane is heated to 50 ºC in a water bath, which is expected to increase the mole fraction of the gases of interest in the carrier gas due to reduced gas solubility. After passing through the membrane inlet system, the carrier gas is analysed by PTR-MS.

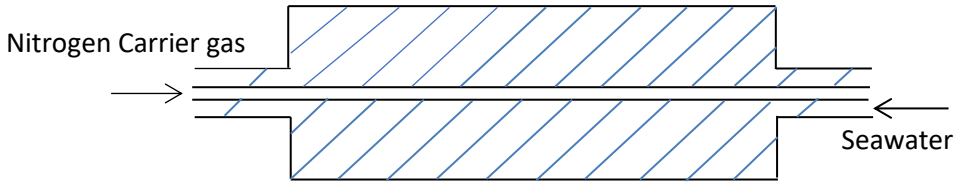

Figure 1.8 Schematic representation of the Membrane Inlet which is coupled to a PTR-MS and presented in Beale et al. (2011).

This system has been developed to measure methanol, acetone and acetaldehyde in seawater. It has been deployed on cruises to measure discrete samples (Beale et al., 2013; Yang et al., 2014a).

1.6.2 Bubble column equilibrator

Kameyama et al. (2009) present a bubble column equilibrator for measurements of dissolved DMS, isoprene, methanol, acetone, acetaldehyde and propene in seawater. The equilibrator consists of a brown (to prevent photochemistry) glass cylinder with a continuous flow of seawater (Figure 1.9). A thin bubble mesh is installed at the bottom to bubble the carrier gas (VOC-free N_2) through the seawater. The bubble mesh creates small bubbles with relatively large surface area for exchange. The carrier gas is measured by a PTR-MS (Kameyama et al., 2010). This equilibrator has been successfully used on research cruises (Kameyama et al. 2009, 2014).

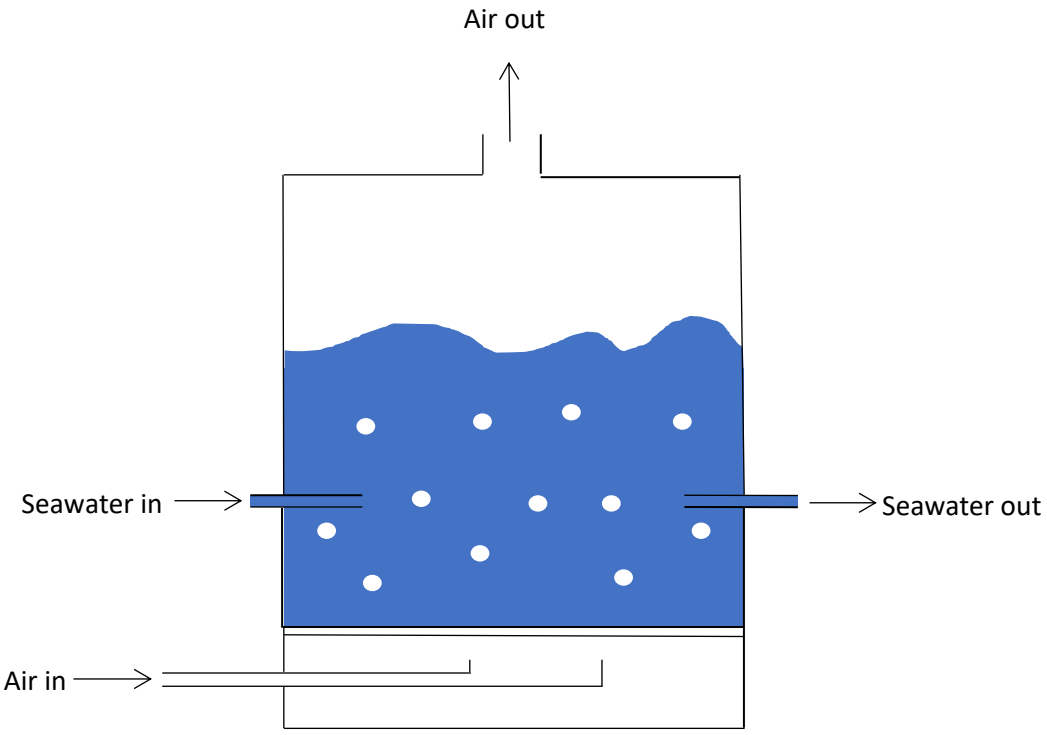

Figure 1.9 Schematic representation of the equilibrator used by Kameyama et al. (2009).

1.6.3 Coil equilibrator

A different design for a continuous air – sea equilibration system has been developed by Xie et al. (2001) for measurement of carbon monoxide. Tran et al. (2013) used this equilibrator design to measure a variety of non-methane hydrocarbons, including isoprene. Blomquist et al. (2017) adopted this design for measurement of DMS.

In this initial design (Xie et al., 2001) use a 6.1 m long glass coil (Figure 1.10). A continuous flow of seawater and carrier gas meet in a Teflon T-piece and automatically, by fluid dynamics, distinct and regularly spaced sections of seawater and carrier gas form. While travelling through the glass coil, each section of seawater equilibrates with the neighbouring section of carrier gas. Wall-induced longitudinal mixing facilitates gas exchange by surface renewal shown in the zoom in Figure 1.10. At the end, the carrier gas is separated from the seawater in a bubble separator and the gas phase is analysed. This equilibrator has been automated and used on a cruise e.g. by Xie et al. (2001) to measure CO.

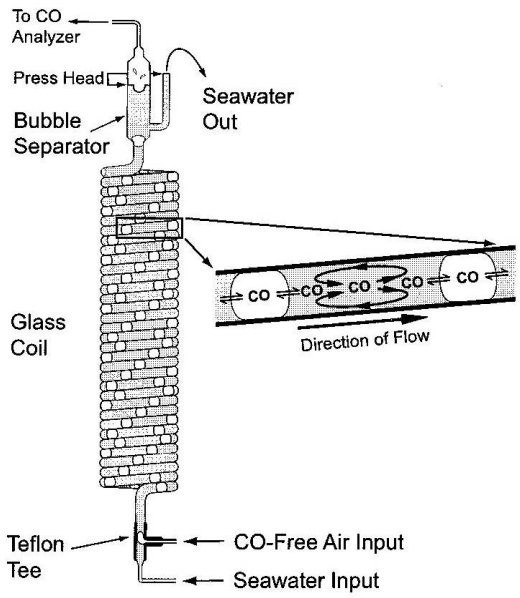

Figure 1.10 A schematic of the coil equilibrator from Xie et al. (2001). Reprinted with permission from Xie et al. (2001). Copyright 2001 American Chemical Society.

The design by Blomquist et al. (2017) is very similar. It uses a longer, Teflon equilibration tube of at 15 m, thus achieving full equilibration for DMS. Tran et al. (2013) used a 7.1 m-long coil to achieve 73 % equilibration for isoprene and use it to measure a variety of VOCs.

1.7 Considerations when designing an air – sea gas equilibrator for continuous measurements

The following section describes a few considerations when designing directly exchanging air – sea equilibrators for continuous. By directly exchanging, I refer to equilibrators that do not use a membrane.

It is preferable to develop an equilibrator that achieves fully equilibration for gases of interest. For partially equilibrating gases, if an unknown factor changes slightly during long term deployment, the degree of equilibration could change a lot. This would introduce error in the measured waterside concentration.

The thermodynamics of equilibration depend on temperature, salinity, and pressure as well as the ratio of water and air volumes or flows in the equilibrator (Atkins and Paula, 2009; Johnson, 1999).

The speed of attaining equilibrium, i.e. the kinetics of equilibration, depend on the gas solubility, the surface of exchange, and thus the equilibrator design (Johnson, 1999).

The response time of an equilibrator is crucial to determine at what resolution the data can be presented. The response time of an equilibrator for continuous sampling is commonly

defined as the time for the signal to reach $1 - \frac{1}{e}$ i.e. about 68 % of the full signal (Sims et al., 2017). The response time depends on flow rates and the design of the equilibrator.

Extracted or equilibrated air from seawater contains a large amount of water vapour, which could cause condensation in the downstream sample tube. A dryer is often used to reduce the humidity in the sample air for measurement of gases including DMS and CO_2. Measurement of very soluble/sticky gases such as methanol or acetone is problematic with this approach due to gas adsorption and desorption on the dryer or tubing material (Beale et al., 2011; Kameyama et al., 2010). Thus, the effects of high sample humidity and condensation need to be considered in the design of the measurement system.

1.8 Flux calculations

The aim of this section is to introduce the two layer model of air – sea exchange (Liss and Slater, 1974) and share the equations and solubilities used to calculate the fluxes and saturations in this thesis.

In the two layer model, the difference in gas concentrations below and above the sea surface drives the air – sea flux (Nightingale, 2009; Wanninkhof et al., 2009). Simplistically, the gas is thought to be well mixed within the bulk water and bulk air (i.e. away from the interface) due to rapid turbulent mixing. Just above and below the interface, molecular diffusion is the dominant force driving the movement of molecules as turbulence vanishes (Liss and Slater, 1974; Nightingale, 2009). This means that the biggest concentration difference exists in these boundary layers, as illustrated in Figure 1.11. Depending on the gas solubility, transfer across one of these boundary layers by diffusion is often the rate limiting step in air – sea gas exchange. Exchange of highly soluble gases is limited on the airside, while poorly soluble gases are limited on the waterside.

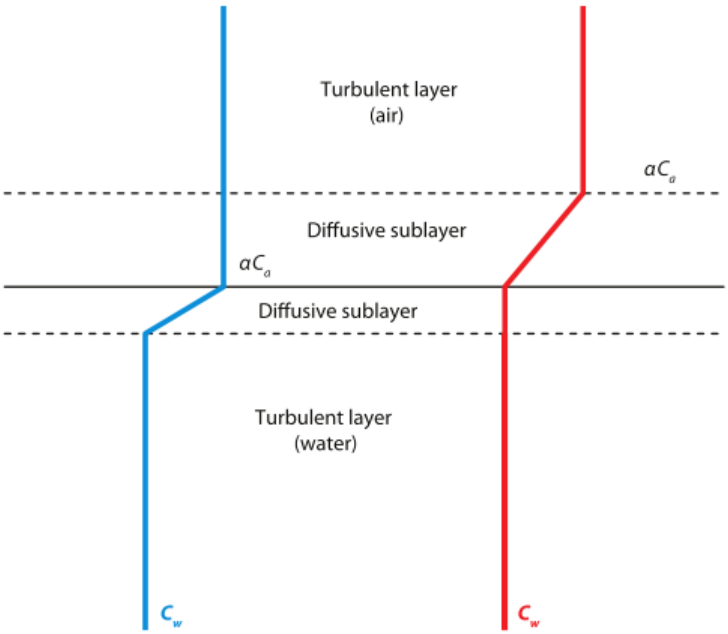

Figure 1.11 Air and water boundary layer distribution profile where the resistance for gas exchange is in the diffusive sublayer. Ca and Cw are concentration in air and water respectively, α is solubility in this figure only. On the left (blue line) the distribution profile for an low solubility (e.g. DMS, isoprene) gas is represented. The largest gradient is across the aqueous diffusive sublayer. On the right (red line) the distribution gradient of a high solubility gas (e.g. methanol, acetone, acetaldehyde) is represented. For a highly soluble gas, the resistance and largest gradient are in the airside diffusive sublayer. Figure taken from Wanninkhof et al. (2009).

Figure 1.11 illustrates that the air – sea exchange constants has two components, an airside resistance and a waterside resistance for which independent parametrisations exist (Nightingale et al., 2000; Yang et al., 2013a). In this thesis, I use parametrisations of air – sea exchange velocity as a function of wind speed.

Before I dive into details regarding the flux calculations in this thesis, I share my solubility values used for different VOCs monitored here. Where possible, values for Henry solubility (water over gas) recommended by Burkholder et al. (2015) are used for calculations presented here. The reference of Burkholder et al. (2015) is used as it represents a critical tabulation of the latest experimental data (Table 1.3). Methanol and acetone concentrations, fluxes and saturations are calculated using the experimentally determined solubility presented in Sect. 3.5.2.2. These freshwater solubilities in Table 1.3 are converted to seawater solubilities by accounting for the "salting out effect" as laid out by Johnson (2010).

Table 1.3: Dimensionless Henry solubility literature values (water over gas, reference listed) in freshwater and seawater referred to throughout this thesis

	***H*(20 ºC, freshwater)**	**reference**	***H*(20 ºC, seawater)**
methanol	6716	Burkholder et al. (2015)	6494
acetone	901	Burkholder et al. (2015)	819
acetaldehyde	444	Burkholder et al. (2015)	400
DMS	15.78	Burkholder et al. (2015)	13.28
benzene	5.44	Leighton and Calo (1981)	4.52
toluene	4.77	McCarty and Reinhard (1980)	3.92
isoprene	0.638	solubility from Karl et al. (2003) using temperature dependence from Leng et al. (2013)	0.510

Saturation provides a measure of the thermodynamic drive behind the flux. It can be used to assess whether the ocean is emitting or absorbing a certain compound (ocean source/sink). In this thesis, the saturation (s / (%)) of the surface ocean relative to the atmosphere is calculated using Eqn. 1.1.

$$s = C_w / C_a \, H \qquad \text{Eqn. 1.1}$$

A saturation above 100 % corresponds to oceanic emission. C_w and C_a are the concentrations in water and air respectively and H is the dimensionless water over liquid form of the Henry solubility. Measured ambient air mole fractions are converted to a concentration using the ideal gas law.

The net air – sea flux (F, positive from sea to air) is determined in this thesis using the two layer model flux equation (Liss and Slater, 1974) illustrated in Eqn. 1.2.

$$f = k\ (\ C_w - H * C_a) \qquad \text{Eqn. 1.2}$$

Where the gas transfer velocity (k) is defined by Eqn. 1.3.

$$k = \frac{1}{\frac{1}{k_w} + \frac{H}{k_a}} \qquad \text{Eqn. 1.3}$$

To calculate the airside (k_a) transfer velocity, we use the following parametrization derived from direct measurements of air – sea methanol transfer (Yang et al., 2013a) (Eqn. 1.4).

$$k_a/(\mathrm{cm\ h^{-1}}) = 8814\ u_*/(\mathrm{m\ s^{-1}}) + 6810\ [u_*/(\mathrm{m\ s^{-1}})]^2 \qquad \text{Eqn. 1.4}$$

Other authors propose more complex and molecule specific parametrisations of k_a which reveal that k_a depends slightly on the airside Schmidt number (Sc_a) and thus in turn on diffusivity and molecular weight. The airside Schmidt number of the compounds presented here does not differ by much e.g. Sc_a(methanol) ≈ 1.1, Sc_a(acetone) ≈ 1.6, Sc_a(acetaldehyde) ≈ 1.3 and Sc_a(DMS) ≈ 1.5 (for 10 ºC). Thus, using a parametrisation based on methanol alone is expected to introduce an error of less than 10 % in my calculated fluxes.

Here the friction velocity u_* is simplistically calculated using the parameterization from Johnson (2010) (Eqn. 1.5).

$$u_* = u_{10} * \sqrt{1.3 * 10^{-3}} \qquad \text{Eqn. 1.5}$$

Wind speed was adjusted to 10 m height (u_{10}). For isoprene, the waterside transfer velocity (k_w) is calculated using the parameterisation by Nightingale et al. (2000) (Eqn. 1.6).

$$k_w/(\mathrm{cm\ h^{-1}}) = \{0.222\ [u_{10}/(\mathrm{m\ s^{-1}})]^2 + 0.333\ u_{10}/(\mathrm{m\ s^{-1}})\} * \left(\frac{Sc}{600}\right)^{-0.5} \qquad \text{Eqn. 1.6}$$

Sc_w is the waterside Schmidt number and Sc_{600} is the Schmidt number of 600. This parametrisation most likely represents an overestimation of k_w for gases that have similar

or greater solubility to DMS because of the solubility dependence in bubble-mediated gas exchange (Yang et al., 2011). Thus for DMS, acetaldehyde, acetone and methanol, the mean k_w presented in Yang et al. (2011) was used here. This parametrisation is derived from direct air – sea exchange measurements of DMS from five different open ocean cruises.

The water phase Schmidt numbers (Sc_w) of methanol, acetone, acetaldehyde and DMS are determined following Johnson (2010). The Schmidt number of isoprene is calculated using the equation presented in Palmer and Shaw (2005).

As illustrated in Figure 1.11, the relative importance of the waterside and airside resistance depends on the solubility of the compound. This is because the solubility in Eqn. 1.3 changes the relative importance of the airside and waterside resistance. For sparingly soluble gases (i.e. low H), transfer velocity is dominated by transfer through the waterside diffusive sublayer i.e. $k \approx k_w$. Using the equations stated in this section, I calculate that the contribution of the waterside resistance to the overall resistance is ≈ 100 % for isoprene, ≈ 95 % for DMS, ≈ 26 % for acetaldehyde, ≈ 23 % for acetone and ≈ 3 % for methanol at 1 ºC seawater temperature. The compounds have been arranged by increased solubility in this list to illustrate the decreasing contribution of the waterside resistance.

An highly detailed discussion of the uncertainty of the gas transfer velocity, a topic of active research by many investigators, is beyond the scope of this thesis. In this paragraph, I would like to convey a rough estimate of the potential uncertainty of the gas transfer velocity for illustrative purposes. These uncertainties are a consequence of the parametrisations I am using. Any uncertainty in these parametrisations is expected to translate directly to the calculated fluxes reported in this thesis. First of all, the relative uncertainty in the gas transfer velocity varies at different wind speeds (greatest at high and low wind speeds and smallest at intermediate wind speeds (Wanninkhof et al., 2009)) and is different for each compound. Waterside transfer velocities for DMS, determined by eddy covariance, tend to be typically within 20 % of each other (Bell et al., 2013, 2015; Yang et al., 2011). No such measurements have been made for isoprene, but the Nightingale (2000) parametrisation is probably within 50 % of the true value. As for the airside transfer velocity (dominant term for the oxygenated VOCs), recent measurements of methanol are fairly close (< 20 %) to the prediction of the COARE model (Yang et al., 2013a, 2014b). How much uncertainties Sc_w and H contribute to the gas transfer velocity depends on the gas. DMS and isoprene are largely influenced by Sc_w, while H matters more for the soluble

oxygenated VOCs. Uncertainties in Sc_w and H are thought to contribute a further 30 % uncertainty within the constraint of the airside and waterside transfer velocity (Johnson, 2010).

1.9 Open research questions and the aims of this thesis

This literature review chapter has presented our current knowledge about the cycling of methanol, acetone, acetaldehyde, DMS and isoprene in the marine environment. The review moved on by mentioning relevant biogeochemical processes in the polar regions and by illustrating the role of these gases in the atmosphere. The second part of the review focused on how dissolved gases have been measured in seawater using air – sea equilibrators and what issues need to be addressed when designing such an equilibrator in my opinion. Further, the equations used to calculate air – sea fluxes in this thesis are presented.

This review highlights that ocean cycling of volatile organic compounds is poorly understood. As a consequence many large uncertainties remain as to what controls the variability of these gases in surface seawater. Additionally, progress has been limited by a lack of suitable measurement techniques. With these uncertainties and shortcomings in mind, this thesis aims to address the following points;

- **Extending and improving measurement techniques in seawater**

This thesis describes an equilibrator coupled to PTR-MS that achieves a high degree of equilibration and is rugged enough for deployment at sea. The analytical chemistry of the PTR-MS measurement and the equilibrator are thoroughly characterised. The PTR-MS operation and calibration are laid out in chapter 2. The equilibrator is a Segmented Flow Coil Equilibrator, which is described in detail in chapter 3.

- **Measurement of VOCs in the sea ice zone to improve our understanding of the variability in the Arctic sea ice zone**

Research has shown that the sea ice zone represents a source for some marine trace gases such as DMS or methylamines. There exist few to no measurements of many of the VOCs discussed here in the sea ice zone. The unique biogeochemistry of the Arctic sea ice zone could provide new insights to the production processes of these VOCs. To investigate the effect of sea ice on these VOCs, chapter 4 presents depth profiles and underway measurements from the sea ice zone in the Canadian Arctic in July 2017.

- **Measuring VOCs in ambient air and seawater of the undersampled Southern Ocean to calculate air – sea fluxes and improve our understanding in the variability of VOCs in the marine environment**

The impact of emissions in the Southern Ocean on atmospheric mole fractions in the Southern Hemisphere is particularly important due to the lower land to sea ratio in the Southern Hemisphere. In this thesis, ambient air and seawater VOC measurements from a transect in the Southern Ocean are described. Hourly seawater and ambient air measurements are used to calculate the air – sea exchange at high resolution. Simultaneous measurement of a broad range of gases provides indication for common sources and sinks. Continuous measurements will enable detection of diel changes in VOC abundances, which could highlight the importance of light in controlling the cycling of these compounds. Measurements of depth profiles yield further clues about the what factors influence seawater concentrations in the water column and the importance of air – sea exchange. These results are presented in chapter 5.

The thesis is rounded up with a conclusion chapter 6, which contrasts the two polar waters and summarises my major findings. I also highlight the remaining important questions and provide recommendations for future work.

2 PTR-MS operation and gas-phase calibration

I would like to measure VOCs in seawater and ambient air using a commercially available PTR-MS instrument. In this chapter, I provide an overview of the PTR-MS instrumentation and the reactions taking place inside the PTR-MS. I also share the PTR-MS instrument settings used during both deployments and explain the rationale. Regular gas phase calibrations during the deployment show that the instrument drift is relatively small, about 10 %. Equilibrator headspace is laden with humidity, which affects the background and signal of the PTR-MS for some VOCs. I show calibrations which allowed me to account for this effect.

2.1 PTR-MS instrumentation

The following section briefly discusses the components inside the Proton Transfer Reaction-Mass Spectrometer (PTR-MS). PTR-MS is a type of mass spectrometer which uses chemical ionisation by a hydronium ion (H_3O^+) and is equipped with a drift tube (Lindinger et al., 1998). The components of the PTR-MS are illustrated in Figure 2.1.

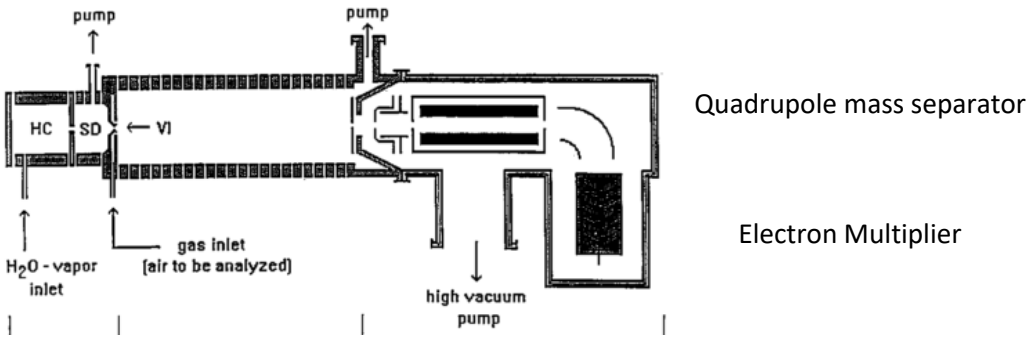

Figure 2.1 Schematic representation of the PTR-MS. HC: Hollow cathode, SD: Source Drift Chamber, VI: Venturi type inlet. Figure reproduced from Lindinger et al. (1998).

In the PTR-MS, water vapour is directed to a hollow cathode (HC), which discharges to the positively charged water vapour (de Gouw and Warneke, 2007). The ionised water molecules are accelerated by an electric field to the source drift chamber (SD) (Blake et al., 2009). Between the SD chamber and the drift tube, the sample gas is inserted through a Venturi-type inlet (VI) (Blake et al., 2009). The drift tube is kept at a low pressure of typically 2.2 mbar and consists of a series of voltage plates. The homogeneously increasing drift tube voltage accelerates hydronium ions and makes them collide with the analyte in the sample gas (Blake et al., 2009). The electric field strength and the pressure in the drift tube are extremely important and are typically combined as a ratio E/N, with a lower E/N indicating a “softer” ionisation regime. The drift tube is separated from the mass separator

through a nose cone with a small orifice, which allows a fraction of the ions to pass to the mass separator (Lindinger et al., 1998).

A quadrupole mass separator in vacuum is used to separate ions of different masses with a mass resolution of one amu (Aston, 2008). The quadrupole accelerates the ions to the electron multiplier which measures the ions in counts per second (Douglas, 2009).

2.2 The proton transfer reaction

In this section, I provide background on the proton transfer reaction that is occurring in the PTR-MS and the advantages thereof.
In the drift flow tube, the hydronium ions transfer a proton to the analyte according to Eqn. 2.1.

$$H_3O^+ + R \rightarrow RH^+ + H_2O \qquad \text{Eqn. 2.1}$$

In Eqn. 2.1, H_3O^+ is the hydronium ion and R is the analyte. PTR-MS uses a drift tube to allow for a controlled reaction between the analyte and the hydronium ions (Lindinger et al., 1998). By maintaining stable reaction conditions in the drift tube, well-studied reaction kinetics (Cappellin et al., 2012; Zhao and Zhang, 2004) can be used to calculate the mole fraction of the analyte with relatively good accuracy (Cappellin et al., 2012). Mole fractions computed using this method are labelled “raw”. In this thesis, these “raw” mole fractions are further corrected based on gas phase calibrations with a certified gas.

The PTR-MS is well suited for measuring VOCs in air for many reasons: (i) the soft chemical ionisation means that most VOCs are ionised at their parent mass, while common inorganic species in air are generally not ionised (Blake et al., 2009); limited fragmentation allows for a fairly straightforward compound identification (de Gouw and Warneke, 2007). (ii) the hydronium ions react at near collision rate or known reaction rates, which allows for a reasonable estimate of the mole fractions of the analytes without calibration (Yang et al., 2013c); (iii) not needing an internal standard makes PTR-MS compact and convenient for field deployment (Lindinger et al., 1998). The PTR-MS also allows (iv) high sampling frequency, which makes it ideal for continuous measurements (Yang et al., 2013a).

Water vapour affects PTR-MS measurements, and a common side reaction in the flow drift tube is hydronium cluster formation Eqn. 2.2 (Blake et al., 2009).

$$H_3O^+ + n\,H_2O \rightarrow H_3O^+ (H_2O)_n \qquad \text{Eqn. 2.2}$$

The hydronium clusters have a higher proton affinity than the hydronium ions alone. Hence they do not protonate some VOCs, such as benzene and toluene (Blake et al., 2009). An excess of hydronium clusters in the drift tube could invalidate the assumption that the majority of the protonation reactions are carried out by hydronium ions (de Gouw and Warneke, 2007). Furthermore, sample humidity affects the backgrounds of some of the VOCs monitored (de Gouw and Warneke, 2007). Hydronium cluster formation can be avoided by heating the drift tube, reducing the humidity in the sample air or increasing the E/N (de Gouw and Warneke, 2007).

2.3 PTR-MS operation and settings

This section gives an overview of the PTR-MS settings for measurement of VOCs in ambient air and equilibrator headspace.

I use a commercially available high sensitivity Proton-Transfer-Reaction Mass Spectrometer Ionicon QMS-500 from circa 2008. For laboratory experiments and the Arctic deployment, the PTR-MS drift tube was operated at 160 Td (1 Td = 10^{-17} V cm^2) (700 V, 2.2 mbar and 80 ºC in the drift tube, drift tube length 9.2 cm). The water vapor flow into the source was set to 5 cm^3 min^{-1}, the source current at 3 mA and the source valve to 35 %. At these settings, the amount of hydronium water clusters is below 5 % when measuring equilibrator headspace and the amount of O_2^+ ions is below 0.7 % of the hydronium ion counts – ideal for minimizing both the water vapor sensitivity and interference in the methanol signal by the oxygen isotope. The disadvantages of this relatively high drift tube voltage are increased fragmentation of isoprene and a reduced reaction time in the drift tube, leading to suboptimal sensitivity. In this case these are acceptable trade-offs since the focus of these measurements are low molecular weight VOCs that generally do not fragment, and the decrease in sensitivity is captured through gas phase calibrations. Following reviewer comments on the published manuscript on the methods, the PTR-MS was operated at 147 Td during the Antarctic deployment (640 V, other settings kept the same). This lower voltage was chosen to reduce the fragmentation of isoprene and increase sensitivity, while still keeping hydronium ions below 5 % when measuring equilibrator headspace.

The PTR-MS is deployed in selective ion mode. Ions monitored at mass to charge ratio (*m/z*) 33, 45, 59, 63, 69, 79 and 93 are attributed to methanol, acetaldehyde, acetone, dimethyl sulfide, isoprene, benzene and toluene in accordance with previous mass assignments (Williams et al., 2001; Warneke et al., 2003). Due to the unit mass resolution of this PTR-

MS, some interferences due to compounds with similar molecular weights are possible. Propanal has previously been shown to have a generally minor (< 10 %) contribution to m/z 59 in seawater (Beale et al., 2013). For methanol, I correct for the oxygen isotope ($^{16}O^{17}O^{+}$) interference by monitoring O_2^+ in the drift tube and applying a theoretical isotopic distribution ratio, which is 0.076 % of the O_2^+ signal. It is possible that some of the mass 79 measured here contains a contribution from fragmenting toluene, but these aromatic compounds are not the focus of my thesis.

2.4 PTR-MS gas phase calibrations

In this section, I present details on how the gas phase calibrations are carried out. In the second part, I show the gas calibrations obtained during different deployments.

2.4.1 Methodology

To improve the accuracy of the PTR-MS measurements, gas phase calibrations are carried out by dynamically diluting a gas canister with known amounts of VOCs in scrubbed BTCA (British Technical Council Approved) synthetic air (zero air). For the gas calibration before the Arctic deployment, the gas standard contained 478 nmol mol^{-1} methanol, 534 nmol mol^{-1} acetone, 480 nmol mol^{-1} isoprene, 499 nmol mol^{-1} DMS, 492 nmol mol^{-1} toluene, 465 nmol mol^{-1} MVK and 492 nmol mol^{-1} a-pinene. All other gas calibrations are carried out using a gas standard from Apel-Riemer Environmental Inc., Miami, Florida, USA containing 517 nmol mol^{-1} acetaldehyde, 490 nmol mol^{-1} methanol, 512 nmol mol^{-1} acetone, 491 nmol mol^{-1} isoprene, 527 nmol mol^{-1} DMS, 500 nmol mol^{-1} benzene, 483 nmol mol^{-1} toluene in N_2. The gas standards were dynamically diluted using two Bronkhorst mass flow controllers. PTFE gas lines were arranged to allow for the shortest line possible from the gas canister to the PTR-MS. A vent was installed downstream of the tee-piece mixing gas standard and zero air. All connection pieces used were Swagelok PTFE which are routinely used for ambient air sampling. This dynamic gas mixture was directly measured by the PTR-MS. To avoid any hysteresis effects, the tubing was left to clean out for 1 h before and after the calibration. Between each step change, the system was left to adjust for 5 min before recording a measurement.

2.4.2 Gas phase calibrations

2.4.2.1 Gas phase calibrations before and after the Arctic deployment

In the Arctic, a gas phase calibration was carried out on board of the CGCS *Amundsen* prior to the shipboard deployment. The original aim was to make weekly gas calibrations during the deployment to capture small drifts in the instrument performance. However due to

logistical constrains and my inexperience, I did not carry out any gas calibration during the Arctic deployment.

To assess the likely drift in the PTR-MS and thus some of the measurement uncertainty during this deployment, a series of gas phase calibrations were carried out in the laboratory after the deployment over a similar timespan. These calibrations are plotted here along with the one obtained on board prior to the deployment (Figure 2.2).

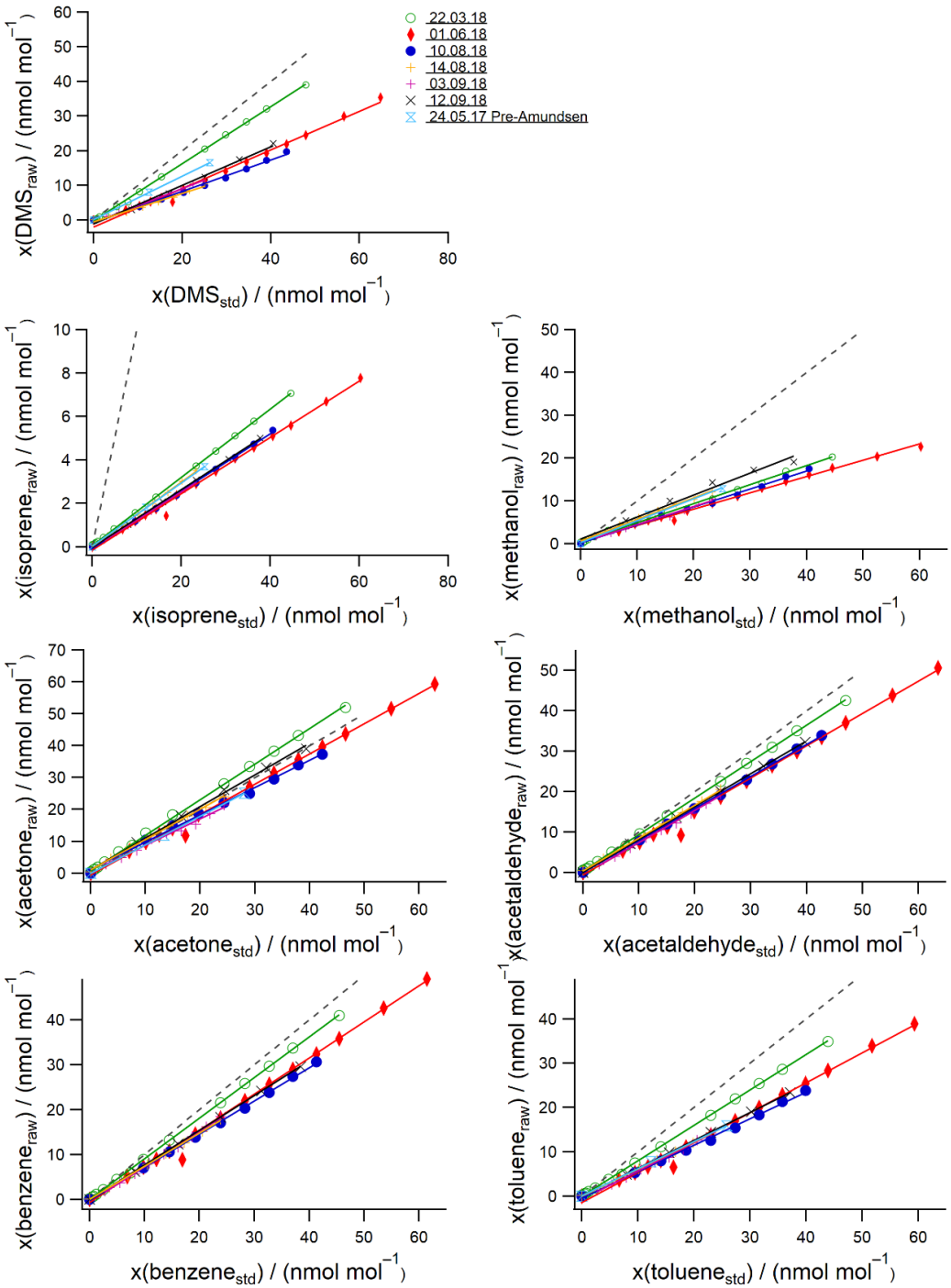

Figure 2.2 Gas calibrations from before the deployment in the Arctic and in the laboratory after the deployment. Mole fractions calculated before applying gas phase calibrations are labelled as "raw" and known mole fractions of gas standard are labelled as "std".

Figure 2.2 shows that the gas phase calibrations are very linear. The calibration slopes are typically within 10 % of each other.

Isoprene was found to fragment significantly, where only 17 % of the isoprene molecules were observed at the primary ion (*m/z* 69, monitored in Figure 2.2), while 30 % and 53 %

were observed at the fragment ions *m/z* 41 and 39 respectively. This is in general agreement with Schwarz et al. (2009). This fragmentation ratio was very stable (standard deviation < 2 %) over three months. As expected for a fragmenting compound, the fragmentation ratio is highly dependent on the drift tube voltage (and so E/N) with a higher fraction of isoprene parent ion (i.e. m/z 69) present at lower voltages. The yield of parent ion is about 30 % higher in air of the same humidity as equilibrator headspace compared to dry air, due to the influence of humidity.

The pre- and post-cruise calibrations generally have similar slopes. This suggests that the PTR-MS had a similar sensitivity during the deployment and later in the lab. It was thus decided to apply the gas phase calibration obtained before the Arctic deployment to compute the dissolved gas concentrations from the Arctic deployment. For acetaldehyde, no gas phase calibration was obtained before the deployment in the Arctic. Thus, the average slope of the post-cruise calibration is applied to the measurements. The regular post-cruise calibrations over a similar period suggests that the random measurement uncertainty due to missing gas calibrations from the Arctic deployment is about 10 %.

2.4.2.2 Gas phase calibrations during the Antarctic deployment

The following Figure 2.3 displays the gas phase calibrations that were carried out roughly weekly during the Antarctic deployment at 640 V. The average PML laboratory gas phase calibration slope at 700 V drift tube voltage from Figure 2.2 is also shown.

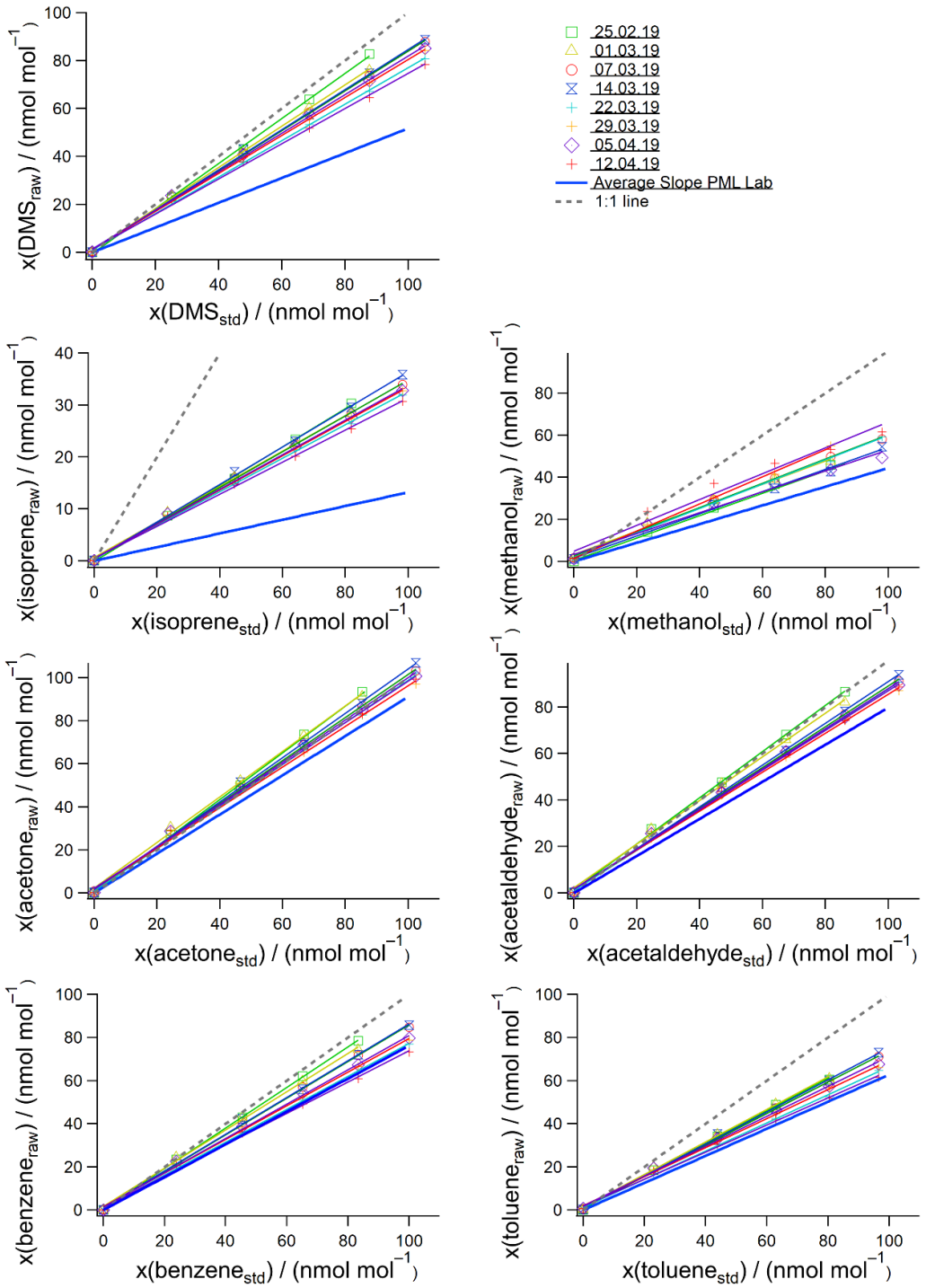

Figure 2.3 Gas calibration curves during the deployment in the Antarctic. Also shown is the average slope from calibrations between 22.03.18 and 12.09.18 in the laboratory, labelled as "Average Slope PML Lab". Mole fractions calculated before applying gas phase calibrations are labelled as "raw" and known mole fractions of gas standard are labelled as "std".

The gas phase calibrations from the Antarctic deployment are generally within 10 % of each other, illustrating the stability of the instrument. The sensitivity is generally slightly better during the Antarctic deployment compared to the calibrations obtained at PML. This is

likely due to the lower drift tube voltage used. The starkest increase in sensitivity was observed for isoprene. The lower drift tube voltage led to less isoprene fragmentation. The following Figure 2.4 shows the interpolation of the calibration slopes over the duration of the Antarctic deployment. Error bars indicate the confidence interval of the linear regression of the calibration slope. Figure 2.4 illustrates that the sensitivity of the PTR-MS is very stable. A cubic interpolation of these slopes was used to compute the seawater VOC concentrations for the entire deployment.

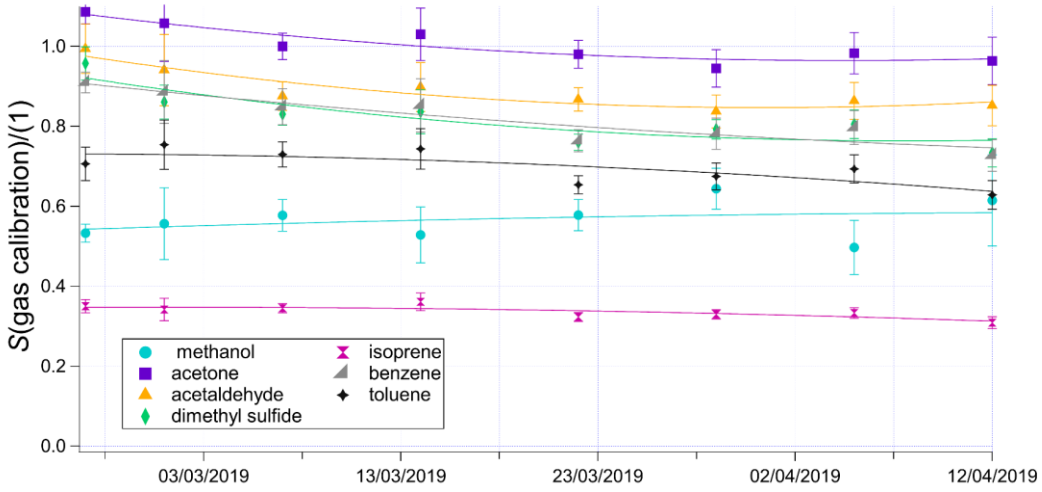

Figure 2.4 Time series of gas calibration slopes interpolated over the duration of the Antarctic deployment. Markers represent the slope from each of the calibrations and error bars represent the confidence interval of the slope.

2.5 Effect of humidity on the PTR-MS

Humidity of the sample air affects the PTR-MS sensitivity and backgrounds of some of the VOCs (de Gouw and Warneke, 2007). To account for these effects, I maintain a constant humidity in the equilibrator headspace by keeping the equilibrator in a water bath at 20 ºC. The equilibrator headspace is thus fully saturated in water vapour at 20 ºC. This greatly simplifies the humidity corrections. Additionally, the humidity in the PTR-MS is monitored by continuously measuring the hydronium cluster as a ratio of the hydronium ion (R_I(37/21)/(%)). Due to the unique design of the equilibrator, I was able to experimentally determine humidity correction factors, in the laboratory as well as in the field, without the need for additional instrumentation. In the following sections I discuss separately the effect of humidity on the PTR-MS background and sensitivity.

2.5.1 Effect of humidity on the background

To investigate the effect of humidity on the background, zero air at different humidity levels was measured. VOC-free air saturated in water was generated by passing synthetic air (BTCA (British Technical Council Approved) grade) through the equilibrator that had been wetted with MilliQ water at 20 ºC. The wetted equilibrator did not dry out over the duration of this experiment and the humidity should be 19.1 mmol mol^{-1} (as a result of the 20 cm^3 min^{-1} dry zero air dilution flow). This humid air was scrubbed with a Pt-Catalyst to oxidize all VOCs to CO_2. The high efficiency of this catalyst at oxidizing VOCs in wet and dry air was demonstrated elsewhere (Yang and Fleming, 2019) and it was found that the catalyst did not affect the humidity level. This flow of scrubbed moist air was dynamically diluted with dry zero air to generate VOC-free air at different humidity levels. This experiment was carried out in the laboratory after the deployment in the Arctic at 700 V and repeated during the deployment in the Antarctic at 640 V drift tube voltage. Only the data obtained in the laboratory is shown here to avoid repetition.

Measurement of zero air at different humidity levels showed that DMS (*m/z* 63), toluene (*m/z* 79) and methanol (*m/z* 33) backgrounds are sensitive to moisture (Figure 2.5). The background of the other compounds monitored here remained unaffected by humidity. In this experiment, a measured R_I(37/21) of 1 % corresponds to dry zero air measurement. A R_I(37/21) between 1.4 % and 2.0 % corresponds to ambient air measurements in the Antarctic and R_I(37/21) of 2.2 % corresponds to measurements of equilibrator headspace. Water vapor mole fraction and R_I(37/21) correlate linearly within the range of settings tested, thus both variables can be plotted on the same axis for comparison.

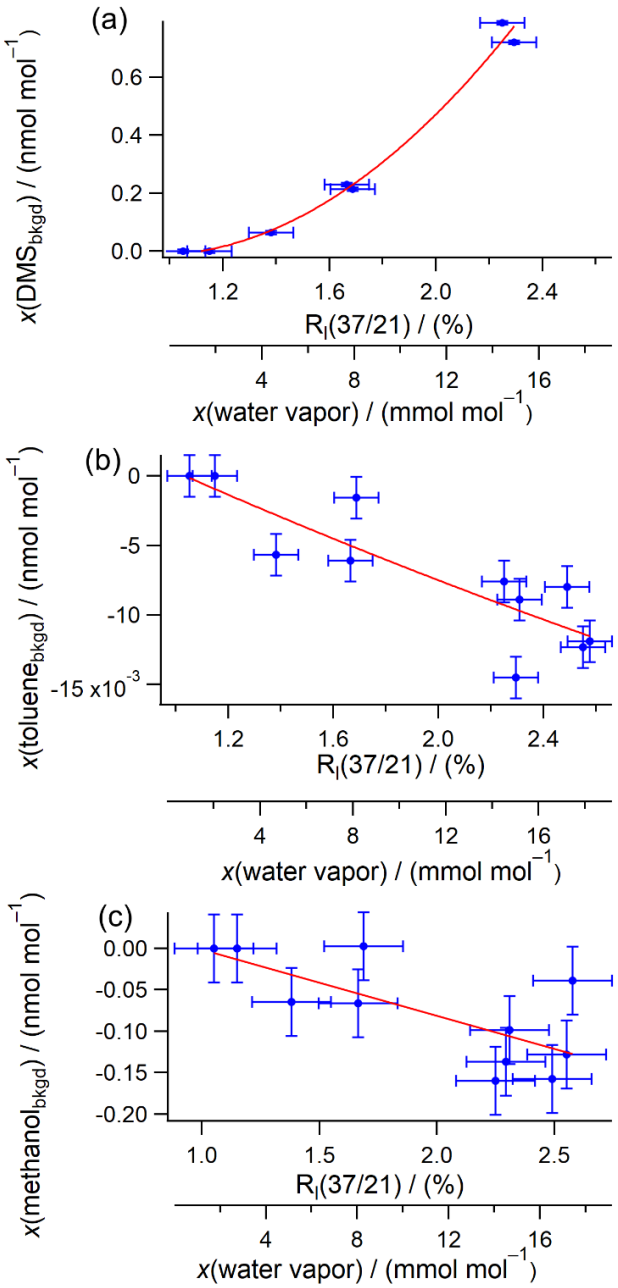

Figure 2.5 Background dependence of (a) DMS, (b) toluene and (c) methanol signal on the humidity in the sample air at 700 V. For this analysis, dry zero air has been subtracted and thus these figures show additional contributions to the background due to sample humidity. Error bars represent the standard deviation of ten consecutive blanks.

Toluene and methanol backgrounds decrease with increasing humidity, while the opposite trend was observed for DMS. These results suggest that using zero air as the background could lead to overestimations of dissolved DMS (by 0.7 nmol dm^{-3}) and underestimations of dissolved toluene (by 0.0321 nmol dm^{-3}) and methanol (by 46 nmol dm^{-3}). I use this change in background of 0.13 nmol mol^{-1} between dry and humid air to compute seawater methanol concentrations from the Arctic deployment.

This experiment suggests that for the compounds that show a strong humidity dependence in the background, a blank of comparable humidity to the equilibrator headspace should be used for the seawater measurements.

2.5.2 Effect of humidity on the sensitivity

To test the effect of humidity on PTR-MS sensitivity, gas calibrations were carried out at different humidity levels. To produce zero air at different humidity levels, a flow of moist air saturated in humidity at 20 ºC was generated by passing zero air through a wetted equilibrator. This was diluted by varying amounts of dry zero air using three Bronkhorst mass flow controllers. The mixture was scrubbed by the Pt-catalyst and then added to the flow of VOC gas standard. This experiment was repeated in the laboratory after the deployment in the Arctic (700 V) and during the deployment in the Antarctic (640 V). Only the data obtained in the laboratory is shown here to avoid repetition. For most of the VOCs, the calibration slopes did not vary with humidity. However, benzene, toluene and isoprene did show some humidity dependence of the slope (Figure 2.6-Figure 2.8).

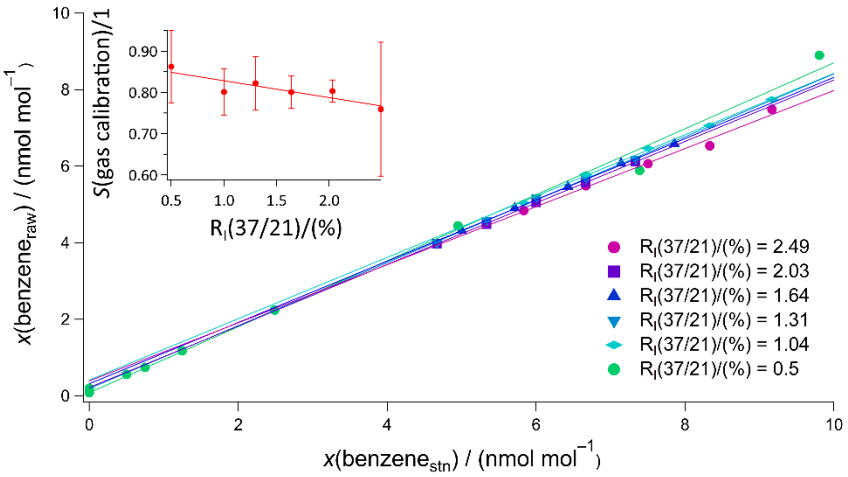

Figure 2.6 Benzene gas phase calibrations at different humidities and an inset displaying the dependency of the slope on the measured humidity.

Error bars on the slope and intercept represent 95% confidence intervals of the linear regression. S=slope

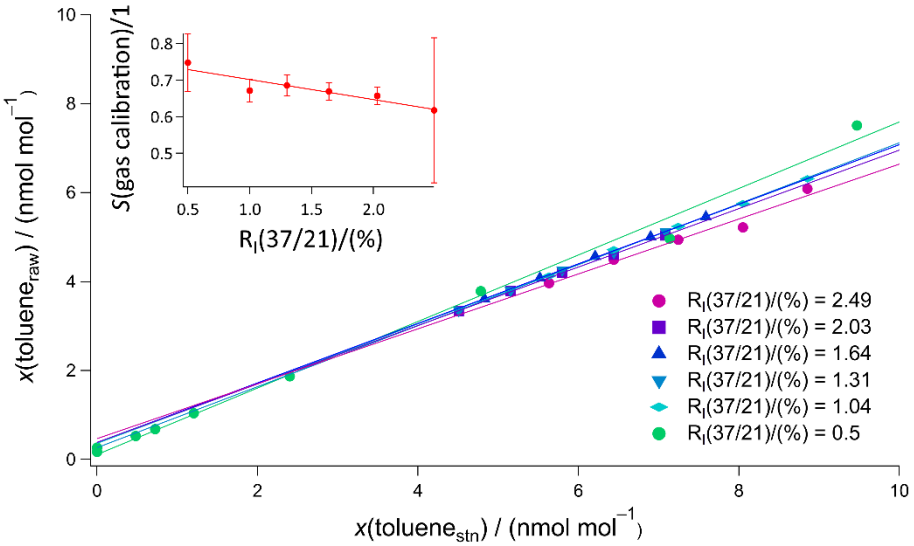

Figure 2.7 Toluene gas phase calibrations at different humidities and an inset displaying the dependency of the slope on the measured humidity. Error bars on the slope and intercept represent 95% confidence intervals of the linear regression. S=slope

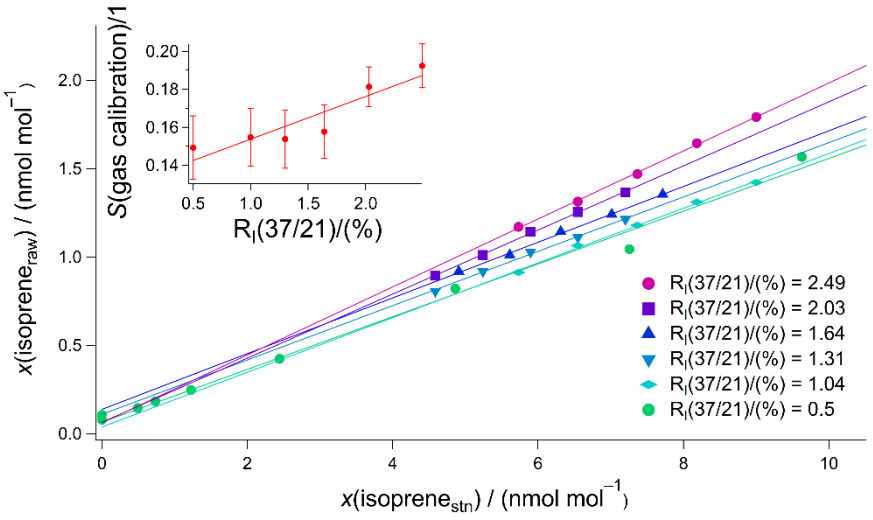

Figure 2.8 Isoprene (*m/z* 69) gas phase calibrations at different humidities and an inset displaying the dependency of the slope on the measured humidity. Error bars on the slope and intercept represent 95% confidence intervals of the linear regression. S=slope

For benzene and toluene, the calibration slopes were found to decrease with increasing humidity (Figure 2.6 and Figure 2.7). The total decrease in sensitivity going from dry to humidity expected in equilibrator headspace is 11 % and 14 % for benzene and toluene respectively. This decrease is due to their relatively low proton affinities, which means that they are ionized by the hydronium ion but not by the hydronium ion water cluster, whose abundance increases as the humidity increases (Warneke et al., 2001).

For isoprene (monitored at *m/z* 69), the calibration slope increases with increasing humidity (Figure 2.8). Nevertheless, the *m/z* 69 signal remains well below the expected mole fraction of the parent ion due to fragmentation. Increasing the sample humidity from dry to the levels expected in the equilibrator headspace, the sensitivity increases by about 30 %. The additional water clusters in the drift tube appear to reduce the fragmentation of isoprene. Schwarz et al. (2009) explained this by suggesting that the additional water molecules stabilise the isoprene primary ion in the drift tube by solvating it.

These changes in gas phase calibration are accounted for in the computation of dissolved gas concentrations.

2.6 Conclusion

This chapter presents the optimisation and calibration of a PTR-MS instrument for measurement of VOCs in ambient air and humid equilibrator headspace. The effect of the humidity on the measurement is investigated. The main advantage of these settings is that I was able to minimise the effect of humidity on the measurement. Additionally, I was able to parametrise any remaining effects experimentally. These humidity effects could differ between deployments or when changing the settings. However, I was able to repeat the experiments during a deployment. To determine the effect of humidity on the measurement, I present methods which only require the equilibrator and the Pt-catalyst. Thus, there is no need for new expensive equipment that could break in the field.

3 Development of a segmented flow coil equilibrator for measuring dissolved VOCs in seawater

In this chapter, I present a technique that utilises a segmented flow coil equilibrator to measure a broad range of dissolved volatile organic compounds in seawater. Thanks to its design, the equilibrator is highly efficient for gas exchange and fully equilibrates for gases that are similarly soluble or more soluble than toluene. It has a fast response time of under 1 min. The system allows for both continuous and discrete measurements of volatile organic compounds in seawater due to its low sample water flow (100 cm^3 min^{-1}) and the ease of changing sample intake. Details on the data processing and calibration of the equilibrator are provided. Extensive calibrations are used to assess the equilibration efficiency and enable me to suggest an updated solubility for methanol and acetone. A discussion is also provided on the most suitable measurement blank and on the uncertainties associated with the seawater measurement.

3.1 Introduction

One of the main aims of this thesis is the development of an equilibrator coupled to PTR-MS for measurement of VOCs in seawater. In this chapter, I present the equilibrator I developed and characterise it in detail. I assess the degrees of equilibration for the VOCs measured by extensive calibrations and at the same time investigate their solubilities. This is important for calculating their dissolved concentrations. I lay out in detail how the data from the SFCE are processed. I also assess the sensitivity of the measurement towards changes in the air to water flow ratio and determine the measurement response time. I move on by discussing the choices of seawater blanks for the compounds monitored, which have not been investigated quantitatively before. I finish the chapter by estimating the measurement uncertainties.

3.2 System description

This section describes the segmented flow coil equilibrator (SFCE), which is shown schematically in Figure 3.1a.

The SFCE is coupled to PTR-MS to measure methanol, acetone (2-propanone), acetaldehyde (ethanal), dimethyl sulfide (DMS), isoprene (2-methyl-1,3-butadiene), benzene and toluene (methyl benzene), demonstrating the versatility of the SFCE. The main advantage of this equilibrator lies in its design. Briefly, the segmented flow allows for a large surface area for gas exchange, ample equilibration time, and thus a high degree of

equilibration. The simple headspace and seawater separation system has a small internal volume, which allows for rapid separation of the headspace from seawater without spray or droplet formation. This enables a fast response time. Due to the ease of changing the seawater sample intake and low seawater flow requirements, the equilibrator can conveniently be used for both continuous underway and discrete seawater sampling. The equilibrator is entirely made up of commercially available Polytetrafluoroethylene (PTFE) tubing and fittings, which should minimise adsorptive loss and make the equilibrator relatively inexpensive and easy to replicate. The constant flow of water and smooth surfaces facilitate occasional cleaning.

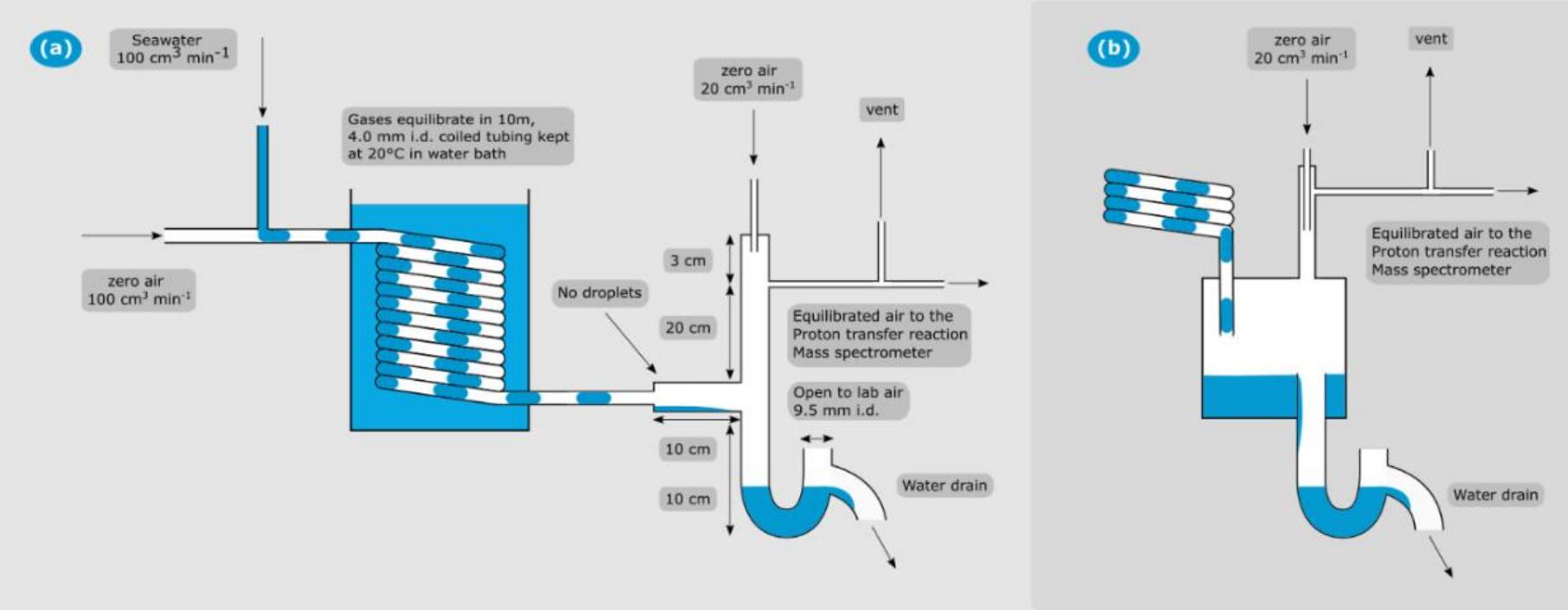

Figure 3.1 (a) Schematic of the segmented flow coil equilibrator coupled to PTR-MS. (b) Schematic of the jar trap that was used during the Arctic deployment for air – water separation. All other aspects of the SFCE are the same for the two designs.

In my setup, the SFCE takes approximately equal, continuous flows of high purity zero air and unfiltered seawater. The zero air flow is controlled by a Bronkhorst mass flow controller set to 100 cm^3 min^{-1} (0 ºC, 1 atm) (all gas flows from mass flow controllers reported in this thesis are reported normalised to these conditions). The seawater flow of (100±5) cm^3 min^{-1} is controlled by a peristaltic pump (Watson Marlow 120 S/DV) with 8 cm long Pumpsil platinum cured silicone tubing (4.4 mm i.d.). I used either ultra-low VOC zero air (Praxair) scrubbed by a hydrocarbon trap (Agilent) or BTCA (British Technical Council Approved) grade zero air (BOC) oxidized by a custom-made Platinum-catalyst (heated to 450 ºC) as the carrier gas for the SFCE.

The seawater is sampled either from the ship's underway water system or, in the case of discrete measurements, from 900 cm^3 glass sample bottles. The carrier gas and seawater meet in a PTFE tee piece (4 mm inner diameter), which naturally leads to the formation of distinct segments of zero air and seawater. The segments travel through a coiled, 10 m long PTFE tube (outer diameter 6.35 mm, wall thickness, 1.19 mm). Each segment of carrier gas or water is approximately 1.5 cm long, giving an approximate total surface of exchange of 82 cm^2 in the coil. The coil is immersed in a water bath kept at a temperature of about 20 ºC. The residence time in the 10 m coiled tube is 37 s (calculated from the internal volume of the coil and the combined air and water flows). Laboratory measurements indicate that regardless of the initial water temperature (0-25 ºC), the water exiting the equilibrator has a temperature of (20±1) ºC if the carrier gas is at room temperature. During the Antarctic deployment when the carrier gas was kept outdoors (about 0 ºC ambient air temperature on average), the water exiting the equilibrator had a temperature of (18±1) ºC despite the water bath being set to 25 deg.

Keeping the equilibrator temperature essentially constant has the benefits of (i) simplifying calibrations/calculations of aqueous concentration, and (ii) in the case of cold high latitude seawater samples, increasing the VOC signal in the headspace as warming to 20 ºC reduces the gas solubility. A rapid biological response to this warming is not expected in the segmented flow coil due to the very short residence time (37 s).

In the initial design, after transiting through the coil, the equilibrated air – water mixture is separated in a 200 cm^3 PTFE jar (Savillex) (Figure 3.1b). The sampled seawater drains away via a U-shaped drain. The U-shaped drain prevents intrusion of lab air and also encourages the sample air to go towards the PTR-MS, rather than escaping via the water drain. I estimate a response time of about 2 minutes with the PTFE jar as the air – water separator.

This is due to a combination of its sizable internal volume and the production of spray inside of the jar from falling droplets. The latter buffers the headspace to step-changes in seawater concentration of highly soluble gases. The PTFE jar was found to slightly outgas some VOCs during the Arctic field deployment (see Sect. 3.8.1 for further information), and was afterwards replaced by a PTFE tee piece (Swagelok, outer diameter: 12.7 mm, wall thickness 1.6 mm). This modification eliminated the outgassing contamination and also shortened the system response time to less than 1 minute by greatly reducing the volume of the air – water separator and allowing for a smooth separation of the equilibrated air – water mixture without droplet formation. Thus, the finalised SFCE consists of high quality, readily available PTFE tubing and fittings used routinely for ambient air sampling.

On the top end of the air – water separator, the humid equilibrator headspace air (100 cm^3 min^{-1}) is diluted with dry zero air (20 cm^3 min^{-1}, same as the carrier gas, controlled by another Bronkhorst mass flow controller). This addition of dry zero air prevents condensation in the approximately 2 m PTFE tubing between the equilibrator and the heated (80 ºC) inlet of the PTR-MS (Figure 3.1). The SFCE system is operated at a slight overpressure (approx. 0.98 mbar above atmospheric pressure) in order to reduce the likelihood of lab air contamination (e.g. due to leaks). An excess-flow vent is installed upstream of the PTR-MS to avoid pressurizing the PTR-MS. The vent flow is typically about 20 cm^3 min^{-1} – the residual between the carrier gas flow (100 cm^3 min^{-1}), the dilution flow (20 cm^3 min^{-1}), as well as the PTR-MS intake flow (approximately 100 cm^3 min^{-1}).

The entire SFCE system fits on a flat bench space of about 40 cm by 40 cm. Importantly, the SFCE is designed such that a failure of an individual component does not result in a catastrophic over- or under-pressurization of the system. For example, if the carrier gas is stopped (e.g. gas supply runs out), the PTR-MS simply measures lab air via the vent and the water is drained from the SFCE as usual. If the water flow from the underway sampling stops, the peristaltic pump will simply pump lab air into the equilibrator. These unexpected failures can be easily identified as lab air has typically much higher mole fractions of VOCs than equilibrator headspace. If the PTR-MS fails, the headspace gas simply exits via the vent.

Due to the smooth, inert surfaces and constant and complete water renewal, the equilibrator should not be very prone to biofouling. As a precautionary measure, I typically cleaned the SFCE every few days during the shipboard cruises by passing 0.037 kg kg^{-1} HCl

solution through the coil for 10 min, followed by a MilliQ water rinse (carrier gas flow to the SFCE was stopped during this procedure).

3.3 Data processing

The PTR-MS measures VOCs in the gas phase. In this section, I explain how a) the PTR-MS raw signal is processed to obtain mole fractions in air/equilibrator headspace, and b) how these mole fractions are converted to dissolved gas concentrations. To calculate dissolved gas concentrations, a purging factor is necessary, which I derive. The section is rounded up with a data flow diagram summarising the data processing steps.

3.3.1 Calculating mole fractions measured by PTR-MS

The mole fractions of the VOC (x) can be reasonably estimated from the PTR-MS signals (in counts per second) (de Gouw and Warneke, 2007; Yang et al., 2013c) using Eqn. 3.1. This is possible given the relatively well-studied reaction rates between VOCs and hydronium ions (Zhao and Zhang, 2004) and mass spectrometer specific parameters (Yang et al., 2013c).

$$x = \frac{1}{\rho_{\mathrm{N}}(\mathrm{air})} \frac{1}{k_{\mathrm{C+}}\ t_{\mathrm{drift}}} \frac{N_{\mathrm{C+}}}{N_{\mathrm{H_3O+}}} \frac{T_{\mathrm{H_3O+}}}{T_{\mathrm{C+}}} \qquad \text{Eqn. 3.1}$$

In this equation, $\rho_N(air)$ is the number density of atoms in ambient air and t_{drift} is the reaction time between H_3O^+ and the VOC in the drift tube (calculated for our instrument in Yang et al. (2013c)). The variable k_{c+} is the kinetic rate constant of the specific VOC with the hydronium ion. The measured values N_{C+} and N_{H3O+} are the signals of the protonated VOC and H_3O^+ in counts per second. The variables T_{H3O+} and T_{C+} are the transmission efficiencies of the $H_3O^+$and the protonated VOC. Transmission efficiency is mainly dependent on the mass of the compound, but also varies between instruments (Taddei et al., 2009). Transmission efficiencies are determined by the manufacturer during annual services.

Some authors suggest that the kinetic rate constants between VOCs and hydronium ions have a reported error margin of up to 50% (Blake et al., 2009; Ellis and Mayhew, 2014). Additionally, the rate constants display a temperature dependence which is not accounted for in this computation (Cappellin et al., 2012; Ellis and Mayhew, 2014). To account for this remaining uncertainty, dynamic gas phase calibrations are carried out using a certified gas standard. These gas phase calibrations are applied to the mole fractions calculated from Eqn. 3.1.

3.3.2 Deriving dissolved VOC concentrations from SFCE-PTR-MS measurements

To calculate dissolved VOC concentrations from the mole fractions, I need to know the equilibration efficiency. The equilibration efficiency for each gas in the SFCE is determined experimentally and is presented in Sect. 3.5.

For compounds that fully equilibrate in the equilibrator (i.e. equilibration efficiency of 100%), the following Eqn. 3.2 is used to compute the measured dissolved gas concentrations (note that simple unit conversions (e.g. m^3 to dm^3) are not explicitly shown):

$$c_w = \left([x_{\mathrm{a}} - x_{\mathrm{a_o}}] \, \frac{P}{R\,T} \right) H \, F \, 1.2 \, 10^{-3} \mathrm{m^3 dm^{-3}} \qquad \text{Eqn. 3.2}$$

Where c_w represents the dissolved gas concentration, x_a represents the measured headspace mole fraction, x_{a_o} represents the background mole fraction (see Sect. 3.8 for a discussion on the measurement background). The ideal gas law is applied to convert from mole fraction to a dissolved gas concentration. Here, P represents the ambient pressure, R is the gas constant and T is the equilibrator temperature (nominally ≈ 293 K). H represents the dimensionless liquid-over-gas form of the Henry solubility. The factor of 1.2 is applied to account for the dilution of these gases in the headspace of the equilibrator, and *F* represents a purging factor (derived in Sect. 3.3.3).

The purging factor arises because a solubility-dependent fraction of dissolved VOCs is transferred into the gas phase during the equilibration process. Thus, the dissolved gas concentration at equilibrium will be somewhat lower than the initial concentrations.

For compounds that partially equilibrate, a calibration slope estimated from liquid standards diluted in MilliQ water is used to determine dissolved gas concentrations. As with Eqn. 1.2, a background is subtracted to account for nonzero blanks (Sect. 3.8).

$$c_{\mathrm{w}} = \left(x_{\mathrm{a}} - x_{\mathrm{a_o}} \right) \frac{1}{S} \qquad \text{Eqn. 3.3}$$

Technically, using a freshwater calibration to calculate gas concentrations in seawater will introduce an uncertainty (nominally within 10% (Johnson, 2010)) due to the effect of salinity on gas solubility. Of all the VOCs studied here, the highly insoluble isoprene is the

only one that does not completely equilibrate in the SFCE. The salting out effect of isoprene seems small relative to the variability in the isoprene calibration slopes (Sect. 3.5.1) and is thus neglected here.

3.3.3 Calculating the Purging Factor

The purging factor (*F*) is the ratio between the dissolved gas concentration before and after complete equilibration in the coil:

$$F = \frac{c_{\mathrm{w}}(\mathrm{VOC}_{\text{before equilibration}})}{c_{\mathrm{w}}(\mathrm{VOC}_{\text{after equilibration}})} \qquad \text{Eqn. 3.4}$$

where;

$$c_w(\mathrm{VOC}_{\text{before equilibration}}) = \frac{n_{\mathrm{tot}}}{V_{\mathrm{W}}} \qquad \text{Eqn. 3.5}$$

Here n_{tot} is the total number of moles in the system for the VOC of interest (entirely in the water phase prior to equilibration) and V_W is the volume of water. The carrier gas is assumed to be free of VOCs.

The dissolved gas concentration after equilibration in the coil is calculated based on mass conservation. In the following derivation, $n_{a_{fin}}$ and $n_{w_{fin}}$ are the number of moles in the gas phase and dissolved phase after equilibration respectively, while V_a is the volume of carrier gas. At equilibrium:

$$c_{\mathrm{w}}(\mathrm{VOC}_{\text{after equilibration}}) = H\, c_{\mathrm{a}}(\mathrm{VOC}_{\text{after equilibration}}) \qquad \text{Eqn. 3.6}$$

$$n_{\mathrm{a_{fin}}} = \frac{n_{w_{fin}}}{H\,\frac{V_w}{V_a}} \qquad \text{Eqn. 3.7}$$

Mass conservation is expressed by the following equation:

$$n_{\mathrm{tot}} = n_{\mathrm{w_{fin}}} + n_{\mathrm{a_{fin}}} \qquad \text{Eqn. 3.8}$$

Combining Eqn. 3.7 and Eqn. 3.8 and rearranging, we have:

$$n_{\mathrm{w_{fin}}} = \frac{n_{\mathrm{tot}}}{1 + \frac{1}{H\,\frac{V_w}{V_a}}} \qquad \text{Eqn. 3.9}$$

with:

$$c_w(\mathrm{VOC}_{\text{after equilibration}}) = \frac{n_{\mathrm{w_{fin}}}}{V_{\mathrm{w}}} \qquad \text{Eqn. 3.10}$$

Combining Eqn. 3.10 and Eqn. 3.9, we have:

$$c_{\mathrm{w}}(\mathrm{VOC}_{\text{after equilibration}}) = \frac{n_{\mathrm{tot}}}{1 + \frac{1}{H\,\frac{V_{\mathrm{w}}}{V_{\mathrm{a}}}}} \quad \frac{1}{V_{\mathrm{w}}} \qquad \text{Eqn. 3.11}$$

Finally, combining Eqn. 3.5 and Eqn. 3.11 with Eqn. 3.4, and rearranging gives:

$$F = 1 + \frac{1}{H\,\frac{V_{\mathrm{w}}}{V_{\mathrm{a}}}} \qquad \text{Eqn. 3.12}$$

At equal zero air/water flow rates (and hence volumes), this is simplified to:

$$F = \frac{c_w(\mathrm{VOC}_{\text{before equilibration}})}{c_w(\mathrm{VOC}_{\text{after equilibration}})} = \frac{1}{H} + 1 \qquad \text{Eqn. 3.13}$$

The precision of the purging factor depends on the precision of the solubility measurement. Since solubilities are reported here to two significant figures, purging factor is reported here to two significant figures as well. For freshwater, computed purging factors assuming full equilibration and equal zero air and water flows are: 1.00 for methanol, 1.00 for acetone, 1.00 for acetaldehyde, 1.06 for DMS, 1.18 for benzene, 1.21 for toluene and 2.57 for isoprene. The same computation in seawater gives the following purging factors: 1.00 for methanol, 1.00 for acetone, 1.00 for acetaldehyde, 1.08 for DMS, 1.22 for benzene, 1.26 for toluene and 2.96 for isoprene. I note that F varies from being insignificant (= 1) for highly soluble VOCs to quite large (>> 1) for the sparingly soluble gases.

3.3.4 Data flow diagram

The following figure presents a data flow diagram summarising the steps involved in the data analysis of fieldwork data (Figure 3.2).

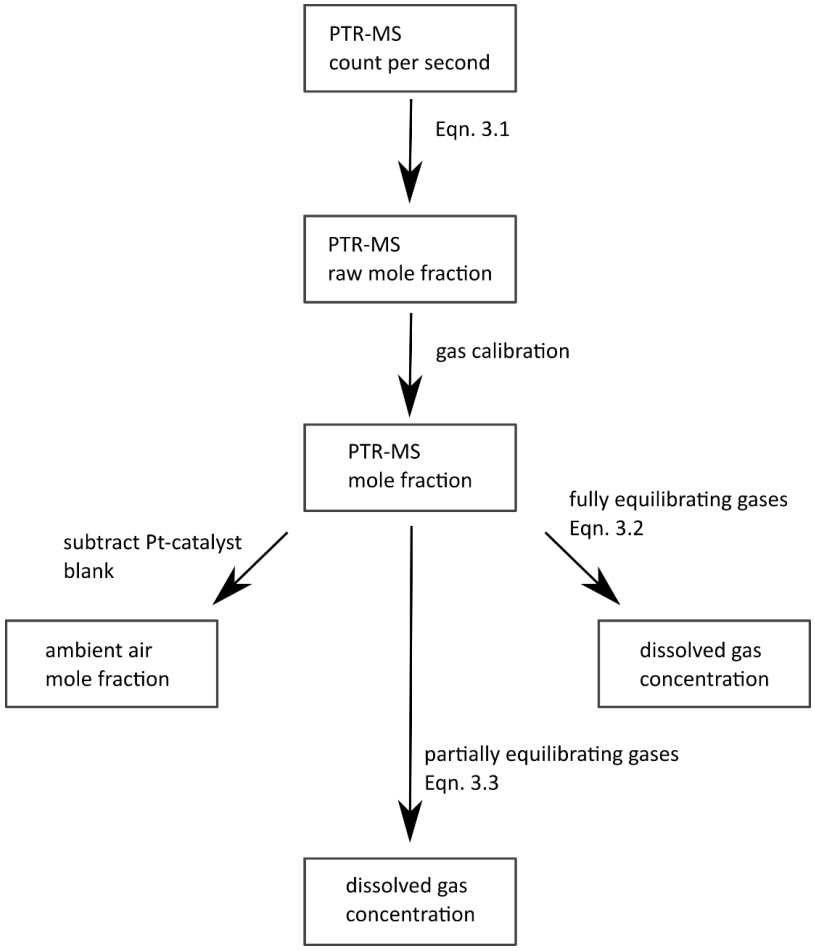

Figure 3.2 Data flow diagram illustrating the data analysis process. In this chapter, raw mole fraction refers to the mole fraction calculated with Eqn. 3.1, before applying gas calibration factors.

Figure 3.2 recapitulates that the PTR-MS measures counts per second in the electron multiplier/detector. Using Eqn. 3.1, this is converted to a "raw" mole fraction, which is then calibrated using gas phase calibration factors. Depending on whether the gas is fully equilibrating in the equilibrator or not, either Eqn. 3.2 (fully equilibrating gases) or Eqn. 3.3 (partially equilibrating gases) is applied to obtain dissolved gas concentrations. The PTR-MS is also used to measure VOC mole fractions in ambient air. The Pt-catalyst is used as a blank for these ambient air measurements (Sect.3.8.1).

3.4 Methods for calibrating the SFCE

In this section I present how the SFCE is calibrated and how the equilibration efficiency is determined at the same time. I also share details about how to calculate the expected mole fractions for the calibrations.

To calibrate the SFCE, I use an innovative way of matching up the results from "evasion" and those from "invasion" calibrations. Evasion calibrations refer to equilibration of VOC

water standards with zero air, whereas invasion calibrations refer to equilibration of VOC gas standards with MilliQ water. Both evasion and invasion should theoretically give the same equilibration efficiency, which in turn relates to the solubility of the compound. By matching up evasion and invasion equilibration efficiency, I can determine the solubility values and compare them against published values.

Some previous investigators (Beale et al., 2011; Williams et al., 2004) rely on serially-diluted liquid standards alone. I found these hard to prepare reliably at environmentally relevant concentrations (Sect. 3.5.2.1). By using both methods of calibration, I can compare serially diluted liquid standards with a certified gas standard. This increases confidence in my serial dilution procedure.

3.4.1 Experimental setup for evasion calibrations

In evasion experiments, liquid standards of methanol, acetone and acetaldehyde were prepared by 3-stage serial dilution of the pure solvent in the same batch of syphoned MilliQ water (or seawater during the Antarctic deployment). This water was also used as the blank for the calibrations. Aliquots of pure, undiluted methanol (for spectroscopy Uvasol) and acetone (HPLC standard) were dispensed using volumetric pipettes, while a 1 cm^3 volumetric flask was used to aliquot pure acetaldehyde (>=99.5 %, A.C.S. Reagent). Subsequent dilutions utilised a volumetric pipette and volumetric flasks to prepare liquid standards ranging from 3 to 30 nmol dm^3 for acetone and acetaldehyde and 30 to 300 nmol dm^3 for methanol in discrete sampling bottles. These diluted standards were measured with the SFCE-PTR-MS system using the same procedure as for discrete seawater samples. Concentrated liquid standards of isoprene and DMS were prepared gravimetrically airtight each day from the pure compound. A syringe pump (New Era Pump Systems) was used to dynamically dilute the concentrated DMS and isoprene liquid standards in a flow of MilliQ water. The syringe pump was installed upstream of the peristaltic pump and set to add 0.1-1 cm^3 min^{-1} to the main flow of 100 cm^3 min^{-1} water through a T-piece. This yielded DMS standards of up to 7 nmol dm^{-3} and isoprene standards of up to 2 nmol dm^3. For this calibration, the flow of MilliQ water is measured at the water drain.

3.4.2 Experimental setup for invasion calibrations

During invasion calibrations, a flow of certified VOC gas standard was diluted to varying degrees with VOC-free zero air using mass flow controllers. This diluted VOC gas standard was then equilibrated with essentially VOC-free MilliQ water. The assumption of no VOCs present in the initial MilliQ water is reasonable as I used relatively high carrier gas VOC

mole fractions (up to 50 nmol mol^{-1} during experiments in the lab and up to 250 nmol mol^{-1} during the Antarctic deployment). The more soluble VOCs are absorbed by the MilliQ water by a greater degree due to their higher solubility.

Due to practical reasons, the equilibration efficiency of benzene and toluene were determined from invasion calibrations only, while that of methanol was determined from evasion calibrations only. The other compounds were calibrated using both evasion and invasion.

3.4.3 Calculating expected mole fractions for invasion and evasion experiments

For evasion calibrations, to compute the expected headspace mole fractions assuming full equilibration, the following Eqn. 3.14 is used.

$$x_{\mathrm{a}}(\mathrm{VOC}_{\mathrm{headspace}}) = \frac{c_{\mathrm{w}}(\mathrm{VOC}_{\mathrm{liquid\ standard}})}{H\ F\ 1.2\ \frac{P}{R\ T}} \qquad \text{Eqn. 3.14}$$

For invasion calibrations, the expected number of moles in the gas phase at equilibrium is calculated by combining the mass conservation equation (Eqn. 3.8) with a rearranged version of Eqn. 3.7 to give:

$$n_{\mathrm{tot}} = n_{\mathrm{a_{fin}}} + H\ n_{\mathrm{a_{fin}}}\ \frac{V_{\mathrm{w}}}{V_{\mathrm{a}}}$$

$$n_{\mathrm{a_{fin}}} = \frac{n_{\mathrm{tot}}}{1 + H\ \frac{V_{\mathrm{w}}}{V_{\mathrm{a}}}} \qquad \text{Eqn. 3.15}$$

Dividing this by the volume of air and using the ideal gas law yields the expected mole fraction in the equilibrated head space. In Eqn. 3.15, n_{tot} is calculated from the known carrier gas VOC mole fraction.

For both evasion and invasion calibrations, the equilibration efficiency is calculated as the measured change in headspace mole fraction (blank corrected) divided by the expected change in headspace mole fraction assuming full equilibration.

3.5 Equilibration efficiencies

In this section, I present the results from the calibrations and the derived equilibration efficiencies.

Ideally, I want to maintain a stable equilibration efficiency of 100 %. This would maximise the signal to noise ratio and minimise the measurement uncertainty. This may also reduce the need for frequent calibrations.

3.5.1 Equilibration efficiency of DMS, isoprene, benzene and toluene

Prior experimentations with a similar setup suggest that the 10 m segmented flow tube presented here is at least a factor of two longer than required for full equilibration of DMS (Blomquist et al., 2017). Hence I expect the more soluble VOCs (methanol, acetone, acetaldehyde and DMS) to fully equilibrate due to their higher solubility (Liss and Slater, 1974). Figure 3.3 shows evasion calibrations for DMS and isoprene using liquid standards over a three week period in the laboratory.

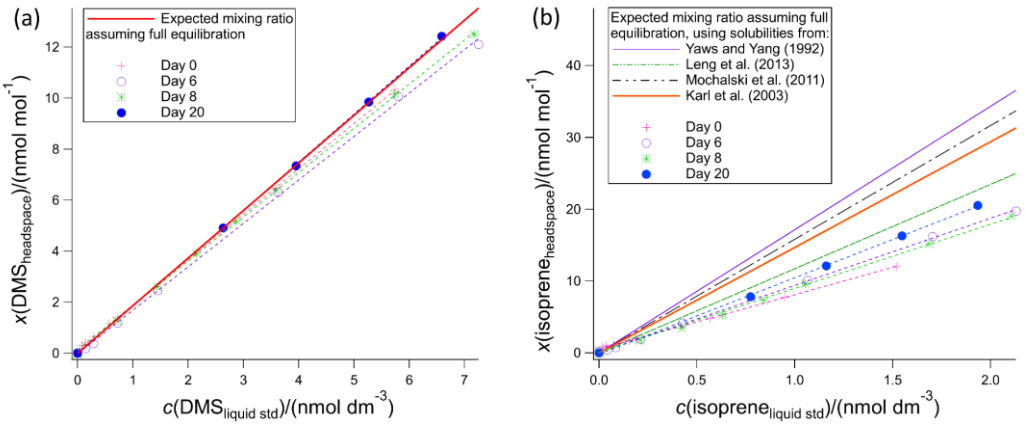

Figure 3.3 Evasion calibration curves for (a) DMS and (b) isoprene. The mean slope of the experimental calibration curve is 1.77 dm^3 mol^{-1} ±4 % and 9.12 dm^3 mol^{-1} ±14 % for DMS and isoprene respectively where errors represent relative standard deviation. Full equilibration slope is computed to be 1.87 dm^3 mol^{-1} for DMS, and 14.69 dm^3 mol^{-1} for isoprene using Karl et al. (2003) solubility with Leng et al. (2013) temperature dependence. This suggests approximately 100 % and 62 % equilibration efficiency for DMS and isoprene respectively in the lab.

The calibrations for DMS suggest full equilibration (Figure 3.3a), where a 5 % underestimation of DMS in the mean is within the uncertainty of the solubility (Burkholder et al., 2015). The DMS calibrations show very little scatter and low weekly variability (±4 % std. dev.), suggesting that the SFCE-PTR-MS setup is very stable. The calibrations for isoprene suggest a mean 62 % equilibration efficiency (Figure 3.3b). Greater variability on a weekly basis (±14 % std. dev.) is observed in the isoprene calibrations, likely in part due to incomplete (and hence less consistent) equilibration.

Results from the invasion experiments obtained in the laboratory are displayed in Figure 3.4.

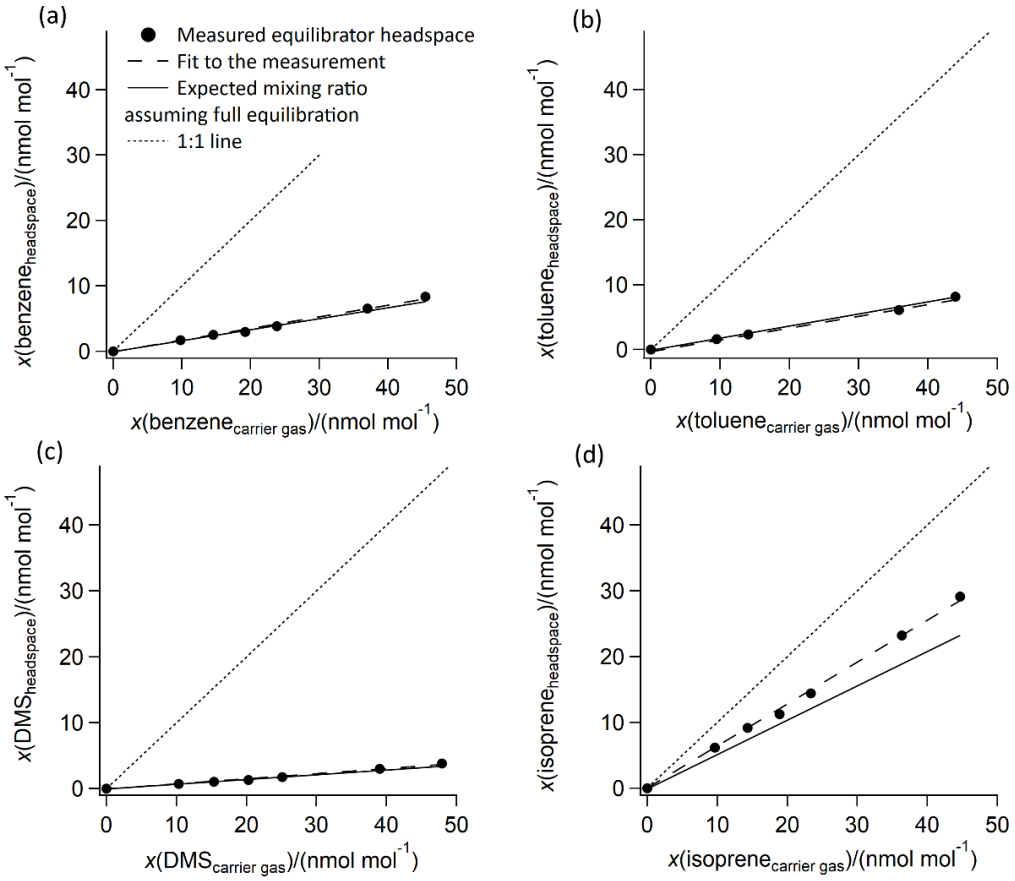

Figure 3.4 Invasion calibration curves for (a) benzene, (b) toluene, (c) DMS and (d) isoprene. A 1:1 line is included to illustrate the role of the water phase in absorbing these compounds.

Invasion experiments (Figure 3.4) confirm that the equilibrator fully equilibrates for DMS, as the measured and expected gas phase mole fractions of DMS match. The equilibration efficiencies of the less soluble gases benzene and toluene are (94±1) % and (95±2) % respectively. The approximately 5 % difference from 100% is within the uncertainty of the solubility of these compounds (Burkholder et al., 2015). This justifies the use of Eqn. 3.2 for VOCs no less soluble than toluene.

For isoprene (the least soluble compound that I measure by far), the equilibration efficiency of 69 % from invasion is similar to that determined in the evasion experiments (62 %) if I use the isoprene solubility from Karl et al. (2003) and the temperature dependence from Leng et al. (2013). I note that there is a large range (40 %) in the values for isoprene solubility in the literature. Using the solubility values from Yaws and Yang (1992), Leng et al. (2013) or Mochalski et al (2011) would result in a large and unexpected discrepancy between evasion and invasion experiments, which I do not expect. Therefore, I use the isoprene solubility from Karl et al. (2003) and the temperature dependence from Leng et al. (2013) throughout this thesis.

These invasion calibrations are also carried out during the Antarctic deployment, which confirm complete equilibration of DMS, benzene and toluene in the equilibrator. During that cruise, I use surface seawater and seawater from well below the mixed layer in addition to MilliQ water for invasion calibration. Complete equilibration for these compounds is achieved regardless of the water used. For isoprene, I determine an average equilibration efficiency of 80 % during the Antarctic cruise with a standard deviation of 15 %. The higher isoprene equilibration efficiency on the ship than in the laboratory is due to the higher seawater flow rate used (see Sect. 3.6 on the sensitivity of the measurement on the air to water flow ratio).

3.5.2 Estimation of the equilibration efficiency of methanol, acetone and acetaldehyde and recommendation of their solubility values

Both theoretical considerations related to the high solubility of these compounds (e.g. Liss and Slater (1974)) and experiments with varying air: water flow ratio (Sect. 3.6) indicate that the oxygenated VOCs (methanol, acetone and acetaldehyde) fully equilibrate within the SFCE. To calculate the dissolved concentrations of these compounds, I need to know their solubility.

A widely used technique for determining solubility is the headspace analysis (Karl et al., 2003; Vitenberg et al., 1975), which relies on measuring the headspace mole fraction from an equilibrated, closed system by usually gas chromatography. However, especially for compounds of high solubility and thus low headspace mole fractions, adsorptive loss on surfaces could lead to an overestimation of the true solubility (Karl et al., 2003; Vitenberg et al., 1975). This might be one reason why the highly soluble oxygenated VOCs show relatively large scatter in the published solubility values (Sect. 3.5.2.1).

Additionally, the above method relies on serial dilution of the pure solvent in water (Benkelberg et al., 1995; Clayton McAuliffe, 1971; Snider and Dawson, 1985; Zhou and Mopper, 1990), which is challenging to do reliably at environmentally relevant concentrations because of the volatility and ease of contamination of these VOCs (Sect. 3.5.2.1).

In this section I match up evasion and invasion calibrations of acetone to test the robustness of my calibrations and recommend a different solubility for acetone and methanol (Sect. 3.5.2.2). Considering these challenges, solubility determined from my works may be more applicable to environmental studies due to the low concentrations used.

3.5.2.1 Large variability in OVOC evasion calibrations

Evasion calibrations of methanol, acetone and acetaldehyde over a long period in the laboratory prior to the Antarctic deployment show substantial variability, likely due to the challenges in producing liquid standards of these gases from serial dilution of pure chemicals. The average slope of 11 evasion calibrations for acetaldehyde and 14 evasion calibrations for methanol and acetone over a three-months period are shown (Figure 3.5). Results are compared to the expected mole fractions computed using every experimentally determined solubility listed in the compilation by Sander (2015) as well as using the solubility recommended by Burkholder et al. (2015). The latter is chosen as a critical evaluation of published solubility values.

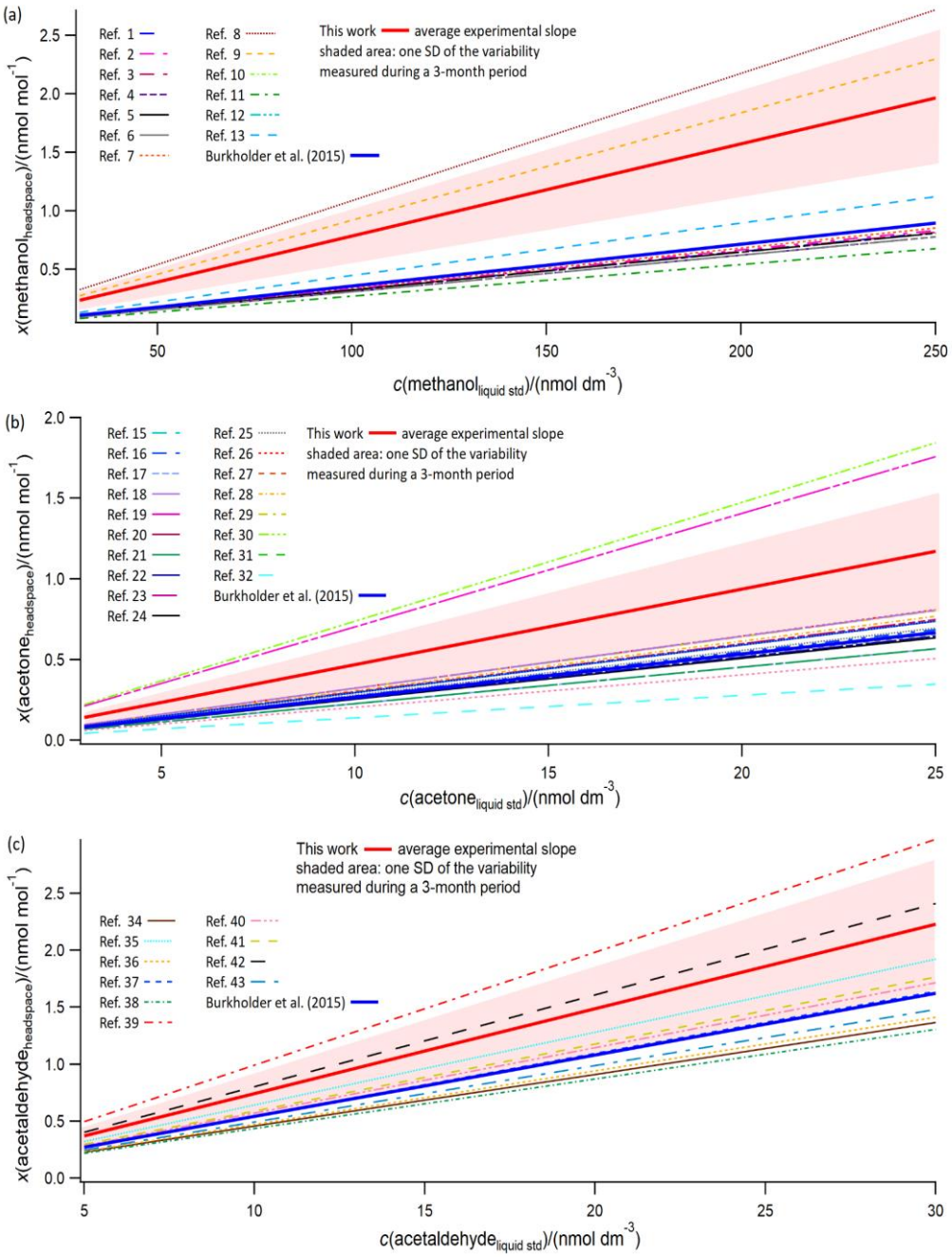

Figure 3.5 Evasion calibrations of methanol (a) and acetone (b) and acetaldehyde (c) in the laboratory. Displayed are the average experimentally determined slopes of 14 calibration curves of methanol (a) and acetone (b) and 11 calibration curves of acetaldehyde (c). These calibrations suggest that these compounds are less soluble than literature values suggest. Shaded area indicates 1 σ standard deviation of the variance in the slope during this three-month period. Average experimentally determined calibration slope for methanol, acetone and acetaldehyde are (0.00786 ±0.00115) dm^3 mol^{-1}, (0.0469 ±0.0145) dm^3 mol^{-1} and (0.0743 ±0.0190) dm^3 mol^{-1}. Plotted along this are the predicted slopes using all experimentally determined solubilities as listed in Sander (2015). The recommended solubility by Burkholder et al. (2015) is plotted as a solid thick line in dark blue. The key to the figure is listed in Table A1 in the appendix, listing the in-figure reference followed by the dimensionless water over air Henry solubility in MilliQ water at 20 ºC and the predicted slope using the listed experimentally determined solubility. For full reference of the cited solubilities, please refer to Sander (2015).

I note that there is a large range in published solubility values of these compounds (Figure 3.5). The experimentally determined calibration slopes for methanol, acetone and acetaldehyde carried out in the laboratory are highly linear (typical R^2 above 0.95). However, they are on average about 50% times higher than the solubilities recommended by Burkholder et al (2015). Nevertheless, my experimental mean slopes are within the range of published solubility values. The relative standard deviation in the slopes of the methanol, acetone and acetaldehyde calibrations (about 25 %) are much larger than that in the DMS calibrations (4 %), with the latter indicating the stability of the SFCE-PTR-MS system. On a weekly basis, the individual calibration slopes of different OVOCs correlate with each other, and these compounds were diluted together from pure reagents. This suggests that most of the observed variability from week to week might be due to errors or contamination in the serial dilution procedure. Possible artefacts include the ubiquity and relatively high mole fractions of these VOCs in lab air as well as their low vapour pressures (especially acetaldehyde). This large variability illustrates the value of deriving solubility by matching up evasion with invasion calibrations, which is presented next.

3.5.2.2 Matching up invasion and evasion calibrations for OVOCs

Evasion calibrations for methanol, acetone and acetaldehyde during the Antarctic deployment are shown in Figure 3.6, Figure 3.8 and Figure 3.9. Invasion calibrations during the Antarctic deployment of acetone and acetaldehyde are shown in Figure 3.7 and Figure 3.10. By matching up the invasion and evasion equilibration efficiencies, I suggest an updated solubility for acetone, and by extension also for methanol.

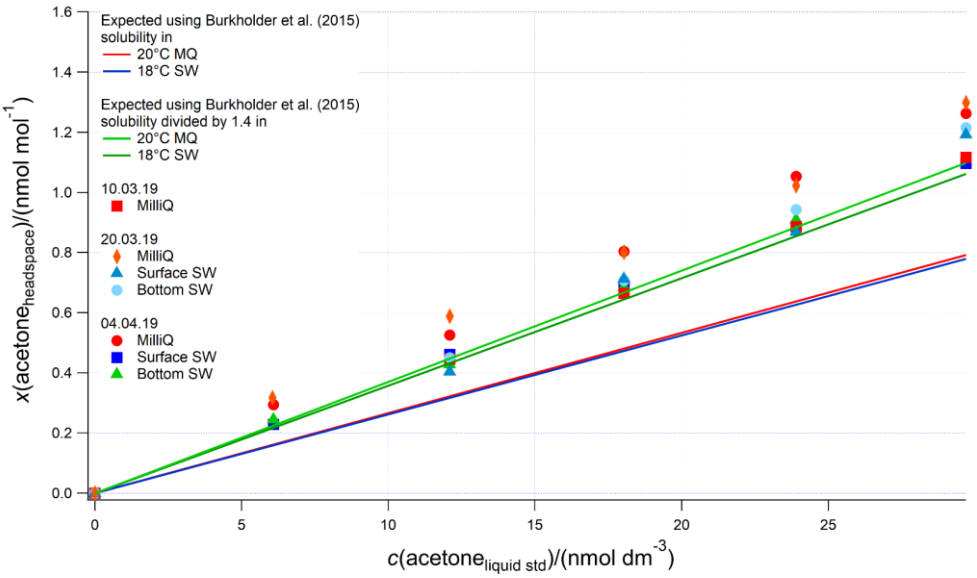

Figure 3.6 Evasion calibrations of acetone from the Antarctic deployment in different types of water. SW= seawater, MilliQ= MilliQ water. Bottom SW refers to seawater collected from well below the mixed layer, near the bottom of the water column; Surface SW refers to seawater collected from the underway seawater inlet. The average measured slope and standard deviation in the 4 seawater calibrations is (0.0388± 0.004) dm^3 mol^{-1} (10 % rel. std. dev.) and the average slope in the 4 MilliQ calibrations is (0.0398 ± 0.002) dm^3 mol^{-1} (5 % rel. std. dev.). Expected mole fractions are slightly different between MilliQ and SW mainly due to the lower seawater temperature.

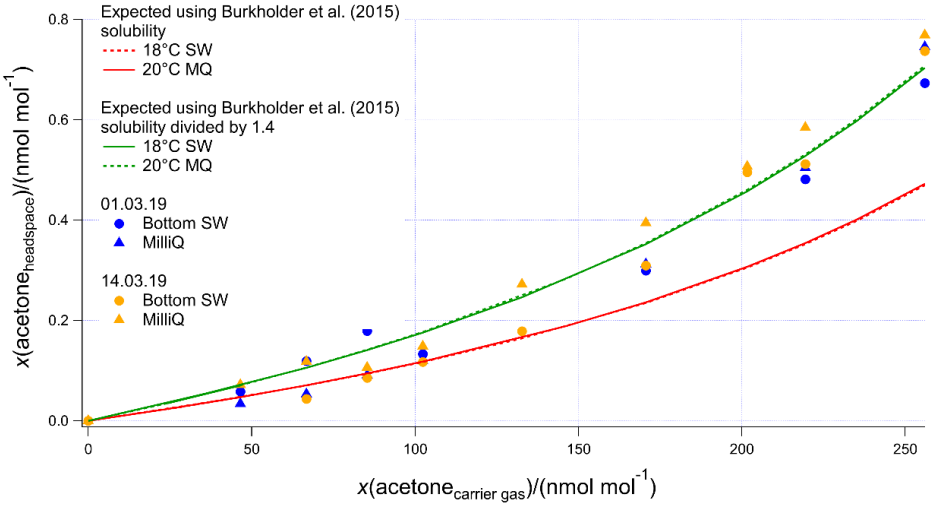

Figure 3.7 Invasion calibration for acetone from the Antarctic deployment using different types of water. SW= seawater, MQ= MilliQ water. Bottom SW refers to seawater collected from well below the mixed layer. The non-linear relationship is due to the addition of a large amount of standard gas to the zero air carrier gas, which alters the purging factor. This is accounted for in the computation of the expected equilibrator headspace mole fraction. Due to the fairly low head space mole fraction of acetone, invasion calibrations with high carrier gas mole fraction are more accurate.

Invasion and evasion calibrations for acetone are found to agree with each other only if the solubility of acetone is 30 % lower than that recommended by Burkholder et al. (2015) (Figure 3.6 and Figure 3.7). To calculate a solubility that agrees with my measurements, I divide the solubility recommended by Burkholder et al. (2015) by 1.4. The solubility recommended from my works is within the range of other previously published solubility values and previous laboratory calibrations of the SFCE. It is also within the uncertainty estimate by Burkholder et al. (2015).

The following figure illustrates the evasion calibration for methanol (Figure 3.8).

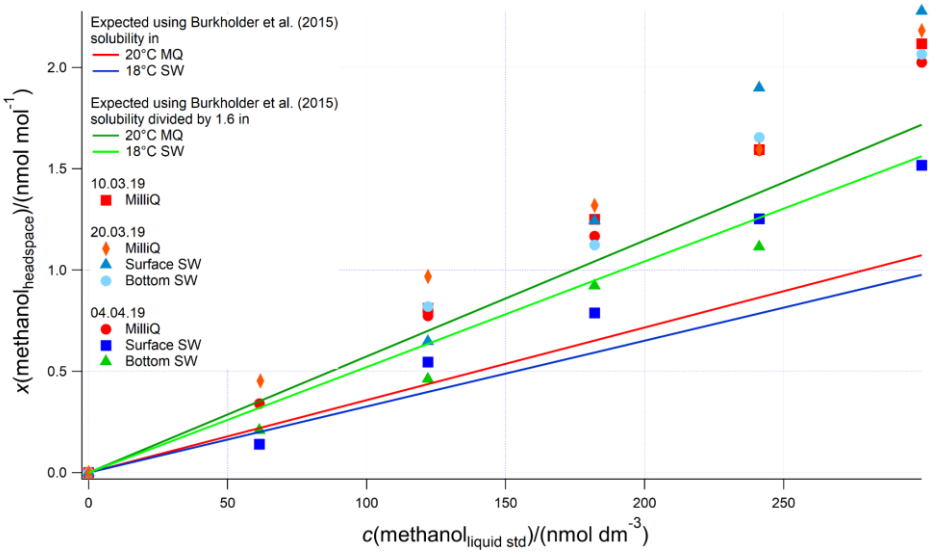

Figure 3.8 Evasion calibrations of methanol from the Antarctic deployment in different types of water. SW= seawater, MQ= MilliQ water. Bottom SW refers to seawater collected from well below the mixed layer, Surface SW refers to seawater collected from the underway seawater inlet. The average measured slope in the 4 seawater calibrations is (0.00624 ± 0.00121) dm^3 mol^{-1} (rel. std. dev. 19 %) and the average slope in the 4 MilliQ calibrations is (0.00678 ± 0.000254) dm^3 mol^{-1} (rel. std. dev. 3 %). Expected mole fractions are slightly different between MQ and SW mainly due to the lower seawater temperature.

For methanol, I infer an updated solubility from the evasion calibration alone (Figure 3.8). No invasion calibration for methanol could be obtained due to the extremely high solubility (and thus little methanol remaining in the gas phase at equilibrium). However, the agreement between acetone evasion and invasion calibrations provided some assurances in the serial dilution procedure during the Antarctic deployment. This is because methanol and acetone were dissolved together during the first step of the serial dilution. Therefore, I also suggest a 40 % lower solubility for methanol than what is recommended by Burkholder et al. (2015) (Figure 3.8). To calculate a solubility that agrees with my measurements, I divide the solubility recommended by Burkholder et al. (2015) by 1.6. This is within the uncertainty of the solubility value estimated by Burkholder et al. (2015). These updated solubilities of acetone and methanol are used throughout this thesis.

The evasion and invasion calibrations for acetaldehyde from the Antarctic deployment are shown in Figure 3.9 and Figure 3.10.

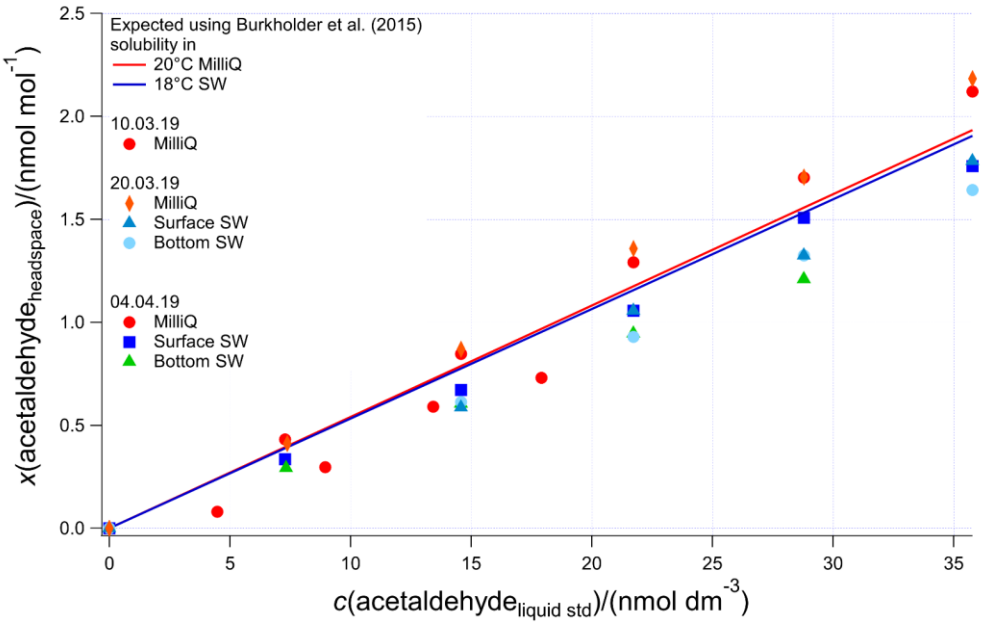

Figure 3.9 Evasion calibrations of acetaldehyde from the Antarctic deployment in different types of water. SW= seawater, MilliQ= MilliQ water. Bottom SW refers to seawater collected from well below the mixed layer, Surface SW refers to seawater collected from the ship's underway seawater inlet. The average measured slope in the 4 seawater calibrations is (0.0473 ±0.00313) dm3 mol-1 (rel. std. dev. 6 %) and the average slope in the 4 MilliQ calibrations is (0.0548 ±0.00767) dm3 mol-1 (rel. std. dev. 14 %). Expected mole fractions are slightly different between MilliQ and SW due to the lower seawater temperature.

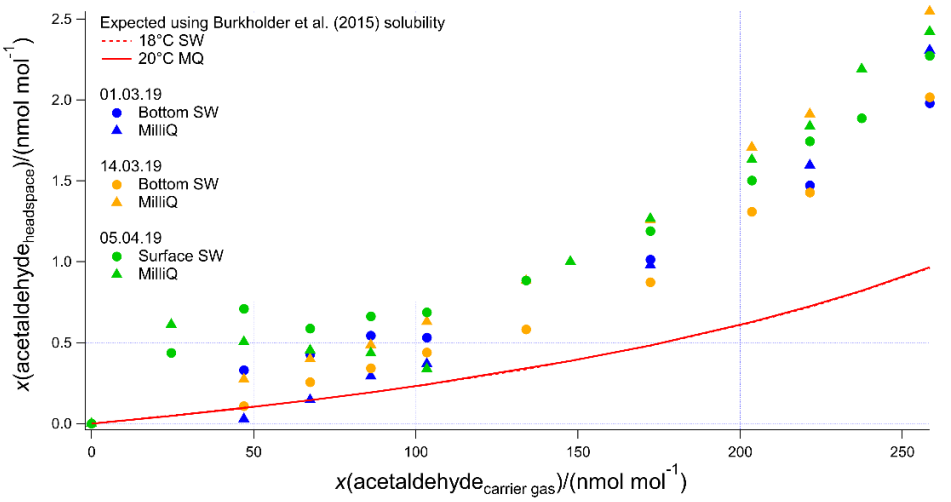

Figure 3.10 Invasion calibrations of acetaldehyde during the Antarctic deployment using different types of water. SW= seawater, MQ= MilliQ water. Bottom SW refers to seawater collected from well below the mixed layer, Surface SW refers to seawater collected from the ship's underway seawater inlet. The non-linear relationship is due to the changing gas flow as more standard gas is added to the zero air carrier gas, which alters the purging factor.

For acetaldehyde, results from invasion and evasion calibrations are found to be different from each other (Figure 3.9 and Figure 3.10). The evasion results agree with the recommended solubility (Burkholder et al., 2015) but the invasion results do not. This could be due to acetaldehyde hydration reactions occurring in the water, which affect the air – water exchange of acetaldehyde (Bell et al., 1956; Kurz and Coburn, 1967; Yang et al., 2014c). In fact, around 60 % of the acetaldehyde in solution is thought to be present as a hydrate (Bell et al., 1956), but only the un-hydrated form is likely available for air – sea exchange (Yang et al., 2014c). Bell et al. (1956) suggest a half-life of the hydration reaction of acetaldehyde between 6 and 60 seconds. Given that 37 s residence time in the segmented flow tube, it is possible that there is not enough time for complete hydration of acetaldehyde within the SFCE during invasion calibrations. The solubility of acetaldehyde recommended by Burkholder et al. (2015) is an apparent solubility that represents the sum of acetaldehyde and acetaldehyde hydrate. In our study, the evasion calibration is considered a more realistic analogue of the actual seawater measurement since water standards represent the sum of acetaldehyde and acetaldehyde hydrate. Therefore I use my evasion calibration results from the Antarctic deployment (in agreement with (Burkholder et al., 2015) for acetaldehyde calculations throughout this thesis.

3.6 Measurement sensitivity toward air: water flow ratio

Air and water at equal flow rates of 100 cm^3 min^{-1} are chosen to allow for sufficiently long equilibration time, large surface area for exchange, and so a high signal while satisfying the air flow requirements of the PTR-MS. They are also chosen such that the stripping of the

soluble compounds from the water phase during equilibration would be small (i.e. purging factor near 1). Additionally, the use of equal flows of air and water simplifies the calculation of the purging factor (Figure 3.12). The water flow is not routinely monitored during the Arctic deployment and decreased by up to 20% due to aging of the peristaltic pump tubing over the course of a few days. This could influence our measurement through at least changing (i) the equilibration time and hence the efficiency in the coil; (ii) the purging factor. To investigate the influence of these competing factors, an experiment is performed after the cruise measuring the same solution of liquid standard at different water flows into the equilibrator while keeping the air flow constant (Figure 3.11). Data are presented as the measured mole fractions divided by those at a water flow of 100 ml/min (i.e. standard setup).

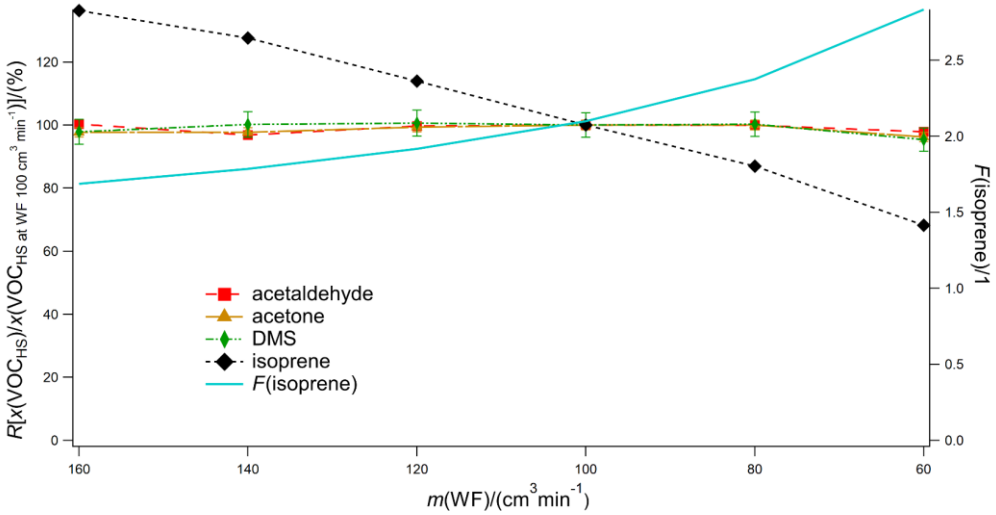

Figure 3.11 Relative signal as a function of water flow into the equilibrator. Error bars represent random error propagation where the initial error has been determined from the standard deviation of 10 consecutive 6 min blank measurements. *F*(isoprene) is the purging factor for isoprene. HS = Headspace, WF = water flow

The signals of acetone, acetaldehyde, and DMS are independent of the water flow into the equilibrator (Figure 3.11). These results provide additional experimental evidence that (i) VOCs with solubilities greater than or similar to DMS fully equilibrate in the coil, and (ii) the gas flow does not remove a large fraction of these gases from the water phase during the equilibration process (i.e. purging factor about 1). In contrast, the signal of isoprene declines with decreasing water flow. As the water flow decreases during this experiment, the purging factor increases at a comparable rate to the decrease in isoprene headspace mole fractions (Figure 3.11). This suggests that the change in purging factor is largely responsible for the change in the isoprene signal. Consequently, compared to the soluble

VOCs, for isoprene there is an additional uncertainty of about 20 % during the Arctic deployment due to variable water flow.

3.7 Measurement response time

A series of discrete liquid standards are swapped over rapidly to induce step changes in methanol, acetone and acetaldehyde (Figure 3.12). This is used to determine the response and delay times of the equilibrator and to test for any possible memory effect due to wall adsorption and desorption effects.

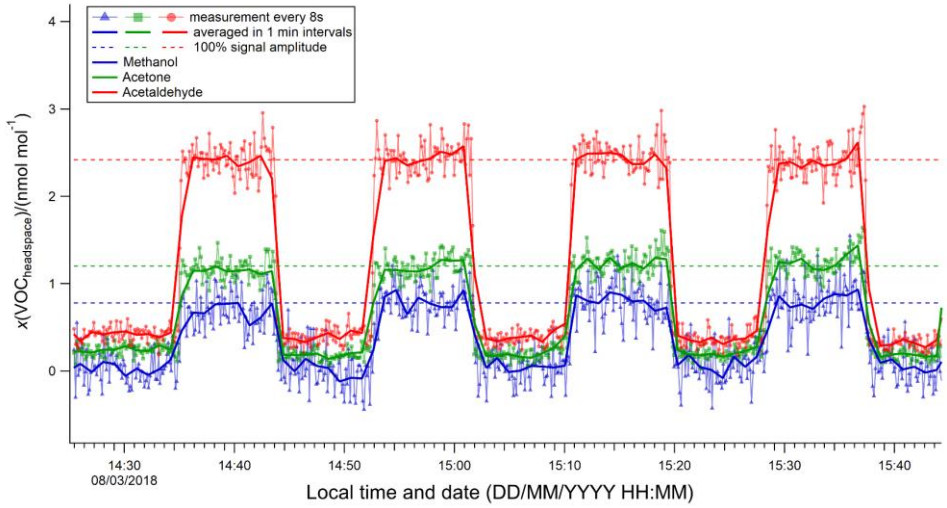

Figure 3.12 Instrument response to step changes in dissolved VOC concentration. The step size is 20 nmol dm^{-3} for acetone, 20 nmol dm^{-3} for acetaldehyde and 200 nmol dm^{-3} for methanol.

The residence time (37 s) in the equilibrator segmented flow tube is calculated from the flows of air and water into the equilibrator and the volume of the segmented flow tube. After that, there appears to be a delay time of approximately 30 s. So the total time between introducing a water change and observing a signal is about 67 s. The response time or e-folding time, defined as the time for the signal to reach $1 - \frac{1}{e}$ (i.e. about 68 % of the full signal), is less than 15 s (i.e. two measurement cycles in the PTR-MS here). The rapid rate of increase/decrease in VOC concentrations during this experiment suggests that there is little “carry over” or memory effect. Whilst the response time of the SFCE is extremely fast, measured dissolved gas concentrations need to be averaged over a longer time to reduce random noise and improve the precision of the measurement. The data from the Arctic and Antarctic deployments are averaged over 6 and 5 min at a minimum, respectively.

3.8 Measurement backgrounds for seawater analysis

The determination of appropriate backgrounds, a challenge for many analytical methods, is critical for the measurements of seawater VOC concentrations with the SFCE-PTR-MS system. This is due to the small signal compared to the background and the potentially large variability in the background over time. In the PTR-MS, the presence of a nonzero instrument background for most VOCs is due to a combination of (a) impurities in the PTR-MS (from e.g. source water reservoir and wall desorption), (b) interference of unwanted ions (e.g. from CO_2 (Herbig et al., 2009; Warneke et al., 2003b)) and (c) sample humidity (de Gouw et al., 2003; Yang et al., 2013c). In addition, any background artifacts related to the SFCE system also need to be considered.

For atmospheric measurements, ambient air measured through a Pt-catalyst is a well-established method for background determination (Dunne et al., 2018; de Gouw et al., 2003). In contrast, the community measuring dissolved VOCs using PTR-MS has not arrived at a consensus method of background determination. Kameyama et al. (2010) purged MilliQ water for 6 h in a bubble column equilibrator to obtain a background reading for isoprene. The highly soluble methanol, acetone and acetaldehyde remained in solution even after purging. Thus, they used pure nitrogen carrier gas to estimate the backgrounds for these compounds roughly once a week. Yang et al. (2014a) (using the method described by Beale et al. (2011)) also used pure nitrogen carrier gas as a background for methanol, acetone and acetaldehyde. However, the use of nitrogen carrier gas might not be optimal as it does not take into account for example humidity and CO_2 dependencies in the PTR-MS measurement.

To address this challenge, I collected several different types of backgrounds in an attempt to find the most appropriate ones for seawater measurements (Sect. 3.8.1). I also regularly measured deep seawater (Sect. 3.8.1), where I might expect low concentrations of these VOCs (due to their predominant photochemical and biological sources as well as microbial consumption). My choice of the background for each compound is discussed in detail (Sect. 3.8.2). Such an extensive approach of collecting multiple backgrounds and comparing them (Sect. 3.8.3 and Sect.3.8.4) has not been attempted before for VOC measurements to the best of my knowledge. The section is rounded up with a few concluding remarks (Sect. 3.8.5).

3.8.1 Different approaches for estimating backgrounds for seawater VOC measurements

The ideal background for seawater VOC measurements would be VOC-free seawater. However, I am unable to generate or obtain seawater that is free of methanol, acetone or acetaldehyde due to the high solubility and ubiquity of these gases. Additionally, it is debatable whether any natural seawater may be free of many of these VOCs due to a lack of knowledge about the cycling of these compounds. In the absence of a truly VOC-free seawater, a surrogate blank is necessary. Ideally, this surrogate should have the same property (e.g. humidity and CO_2 mole fractions) as the equilibrator headspace, but none of the VOCs.

The impact of humidity on the PTR-MS measurement is fairly well documented, particularly in the breath analysis literature (Schwarz et al., 2009; Trefz et al., 2018; Warneke et al., 2001) and is already discussed in a previous chapter. For VOCs with a humidity sensitivity, it is thus preferred that the background measurement has the same humidity level as when measuring the water sample.

In addition to humidity, the amount of CO_2 could also influence the PTR-MS signal (Trefz et al., 2018). While most components of bulk air do not react within the PTR-MS, a small fraction of CO_2 can be ionised after passing through the drift tube (Warneke et al., 2003b). Ionised CO_2 (HCO_2^+, *m/z* 45) and a CO_2 hydronium cluster ($CO_2(H_3O^+)$, *m/z* 63) have been shown to contribute to the background of acetaldehyde (Warneke et al., 2003b) and DMS, respectively (Herbig et al., 2009). The sensitivity of isoprene (*m/z* 69) (Schwarz et al., 2009; Trefz et al., 2018) has been found to be slightly higher at higher CO_2. The CO_2 effects on the background and sensitivity have been found to be very dependent on the settings of the PTR-MS (Herbig et al., 2009; Schwarz et al., 2009; Trefz et al., 2018). I only became aware of the potential effects of CO_2 on the measurements after the two field deployments and did not have a chance to quantify these effects on our PTR-MS in situ. However, experiments recently done on our PTR-MS instrument qualitatively confirmed the effect of CO_2 on the background of acetaldehyde. To address this, I try to use a measurement background with a similar amount of CO_2 as the water sample where possible.

Below, I detail the different approaches for estimating the measurement backgrounds during the Antarctic campaign.

Zero air

Daily measurement of zero air carrier gas (defined in Sect. 3.2), bypassing the SFCE, is used to track any drift in the internal PTR-MS background. The use of zero air is similar in principle to the use of nitrogen carrier gas by Beale et al. (2011), Yang et al. (2014a) and Kameyama et al. (2010). Zero air contains essentially no humidity nor CO_2, which could affect the measurements of some VOCs (de Gouw and Warneke, 2007; Herbig et al., 2009). Out of the compounds monitored here, I find that DMS and methanol display obvious humidity dependencies in the backgrounds, while the acetaldehyde background depends more strongly on CO_2. Thus zero air alone is probably not an accurate background for these VOCs.

Platinum(Pt)-catalyst

A Pt-catalyst blank was measured by directing ambient air through a Pt-catalyst (450 ºC) for 5 min every hour (automated by solenoid valves). Complete oxidation of VOCs in the Pt-Catalyst has been demonstrated previously for both dry air and air that is fully saturated with water at 20 ºC (Yang and Fleming, 2019). Furthermore, the Pt-catalyst does not significantly alter the humidity level (Yang and Fleming, 2019). The Pt-catalyst blank is the most suitable blank for the air measurements since it has the same humidity and CO_2 mole fraction (apart from the very small contribution from oxidised VOCs) as the ambient air (de Gouw et al., 2003; Yang et al., 2013c). Compared to other backgrounds, the Pt-catalyst blank also contains the closest CO_2 value to seawater samples, which is advantageous for compounds that show a dependency on CO_2. Additionally, the Pt-catalyst is measured hourly, allowing me to capture short term variability in the background. For example, a large change in background is typically observed after turning the PTR-MS off and on again. Thus, compared to the other daily blank measurements, the hourly catalyst measurement provides a more precise blank in the mean. The Pt-catalyst blank can thus be used as a seawater blank for compounds that do not display a humidity dependence of the background.

Wet equilibrator

Another background I determined daily is the “wet equilibrator” blank. Following a deep seawater measurement (Arctic deployment) or MilliQ water measurement (Antarctic deployment), I stopped the water flow into the equilibrator and purged the wet equilibrator with zero air for 20-30 min (last 5 min are used for the blank calculation). The

flow of zero air is expected to purge out much of the sparingly soluble gases from the droplets inside the equilibrator. As such, it should contain very low CO_2 mole fractions. The advantage of this blank is that humidity in the headspace remains largely constant and equal to the humidity during the seawater measurement, as small water droplets remain inside of the coil and are not substantially dried by the zero air during the 20-30 min. However, the wet equilibrator blank could overestimate the background if there is any outgassing of the VOCs from the SFCE itself. This is in part because the residence time of zero air during a wet equilibrator blank measurement is twice as long as during a normal measurement due to a lack of water flow, i.e. 1 min 14 s.

Wet equilibrator during Antarctic campaign

During the Antarctic campaign, the water bath was set to 25 ºC – higher than the equilibrated seawater temperature during normal measurement (18 ºC). Thus the humidity level during wet equilibrator blank is slightly higher than during normal measurement. In addition, heating to 25 ºC caused some VOCs (most obviously acetone and methanol) to outgas from the SFCE.

Wet equilibrator contamination from the PTFE jar during the Arctic deployment

During the Arctic deployment, the wet equilibrator blanks of methanol and acetone were higher than the bottom water samples, clearly suggesting that the wet equilibrator blanks were contaminated for these VOCs. The water bath was kept at 20 ºC throughout this deployment, ruling out a similar issue to the Antarctic deployment. I used a 200 cm^3 PTFE jar (theoretically inert) to separate the carrier gas from the seawater after equilibration during the Arctic deployment. Nevertheless, the most plausible explanation for this contamination seems to be outgassing of methanol and acetone from the walls of the PTFE jar itself. After the cruise, I replaced the PTFE jar with a PTFE tee fitting (Swagelok), and this effect vanished. It seems that switching to the PTFE tee improved the situation as it substantially reduced the time spent in the air water separator.

Contamination from the PTFE jar appears to be greatly suppressed during normal water measurement thanks to the very high solubility of methanol and acetone. This is consistent with the fact that the bottom water concentrations from the Arctic deployment are relatively low (mean bottom water concentration; methanol 17 nmol dm^{-3}, acetone 2.3 nmol dm^{-3}) and comparable to limited existing observations (Beale et al., 2013; Williams et

al., 2004). Still, acetone and methanol concentrations reported for the Arctic deployment could be biased slightly high due to this contamination.

Humid air

Daily, a "humid air" blank was measured following the wet equilibrator blank. This consisted of measuring the wet equilibrator air that was further passed through the Pt-catalyst. The humid air measurement has approximately the same humidity level as the seawater measurement, though very low CO_2 mole fractions. Scrubbing by the Pt-catalyst removes any VOCs outgassed during the wet equilibrator blank measurement.

MilliQ water

MilliQ water from the ship's system was measured daily. This is a useful reference but there is insufficient evidence to suggest that MilliQ water is free of VOCs. Any VOCs in the MilliQ water should manifest itself by increased and variable equilibrator headspace mole fractions compared to the other backgrounds. From experience, CO_2 mole fractions in MilliQ water are low.

Bottom water as a sampling "point check"

As per availability, bottom water was measured, which provided a useful reference point in the background selection process. Bottom water is defined here as the deepest seawater sample collected by the rosette at the station. This is between 290 m and 1750 m during the Arctic deployment and between 500 and 5000 m during the Antarctic deployment, i.e. well below the mixed layer. The chief advantage of using the bottom water measurement as a point check is that after equilibration the headspace has similar properties (humidity, temperature, exposure to the equilibrator, and collection protocol) as the headspace from surface seawater samples. Most of the other VOCs monitored here have photochemical or biological sources and are consumed microbially. Hence, I might expect their concentrations in bottom water to be lower than in surface waters. For example, it is well established that the concentration of DMS below the mixed layer is nearly zero (Rellinger et al., 2009). One consideration when comparing surface and deep water measurements is that bottom water in the Arctic and Antarctic contains much higher CO_2 levels compared to surface seawater (about 1.5 to 2 times as much) (Beaupré-Laperrière et al., 2020; Shadwick et al., 2015). This becomes important for VOCs that display a CO_2 sensitivity in the PTR-MS, especially acetaldehyde.

3.8.2 Background decision process

The different VOCs measured here span a large range in solubility, volatility and ease of contamination. Their detections by the PTR-MS also have different dependencies on sample humidity and CO_2 mole fractions. Thus, it is unlikely that the same type of background is appropriate for all the VOCs. In this section, I lay out my overall decision process about how to choose the best available background for each VOC.

First, if the background of a compound displays a strong dependence on humidity, I prefer to use a background that has the same humidity as during the seawater measurement. The humidity dependence may also be accounted for using my experimentally determined relationships. If the compound does not display a humidity dependence, I prefer to use the Pt-catalyst as a blank due to its higher frequency. The zero air measurement would also be suitable if the Pt-catalyst wasn't available.

Any background sensitivity towards CO_2 is more difficult to correct for because none of the backgrounds recorded contains the same CO_2 level as the equilibrator headspace.

In addition, I review if the concentrations calculated are realistic compared to a) previous literature values, and b) characterised instrument noise. If the computed concentrations appear unrealistic, I try to identify the most suitable background based on operational reasons and evidence at hand.

As mentioned in Sect. 3.8.1, a variety of seawater blanks were collected during the deployments. In this section, I would like to illustrate how these backgrounds relate to each other during the two deployments and how the decision making process for choosing the most optimal background is applied to each compound.

3.8.3 Backgrounds for the Antarctic deployment

Humidity levels during the background measurements

Given the potential importance of humidity on the VOC background, I first show the timeseries of sample humidity, monitored as $R_I(37/21)$ for the entire Antarctic campaign (Figure 3.13).

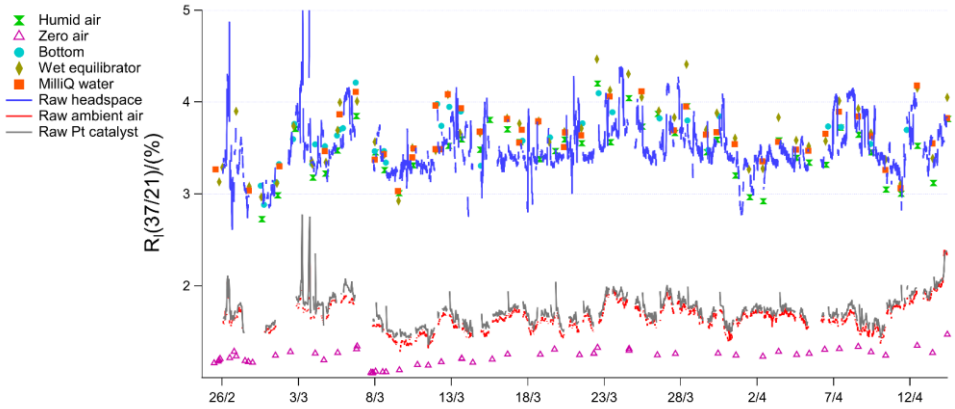

Figure 3.13 Timeseries of the sample humidity (R_I(37/21)) for different signals and blanks during the Antarctic deployment.

Figure 3.13 confirms that the lowest humidity is observed when measuring zero air. The Pt-catalyst has approximately the same humidity as the ambient air. Humid air, bottom seawater and MilliQ water display essentially the same humidity as the surface water samples (labelled as 'raw headspace').

The humidity of the wet equilibrator blank is higher than the equilibrator headspace by a mean absolute difference (± std. error) of (0.17±0.03) %. This is because during the deployment in the Antarctic, the water bath was kept at 25 ºC to account for the cold seawater. As a consequence, during the wet equilibrator blank measurement, the zero air probably warmed up more than during measurements of seawater. This led to higher humidity and likely outgassing of some VOCs, which would not be present during the measurement. This could explain why some of the compounds display a higher than expected wet equilibrator blank during this deployment.

Acetone

Raw mole fractions of equilibrator headspace, ambient air, and backgrounds for acetone are presented in Figure 3.14.

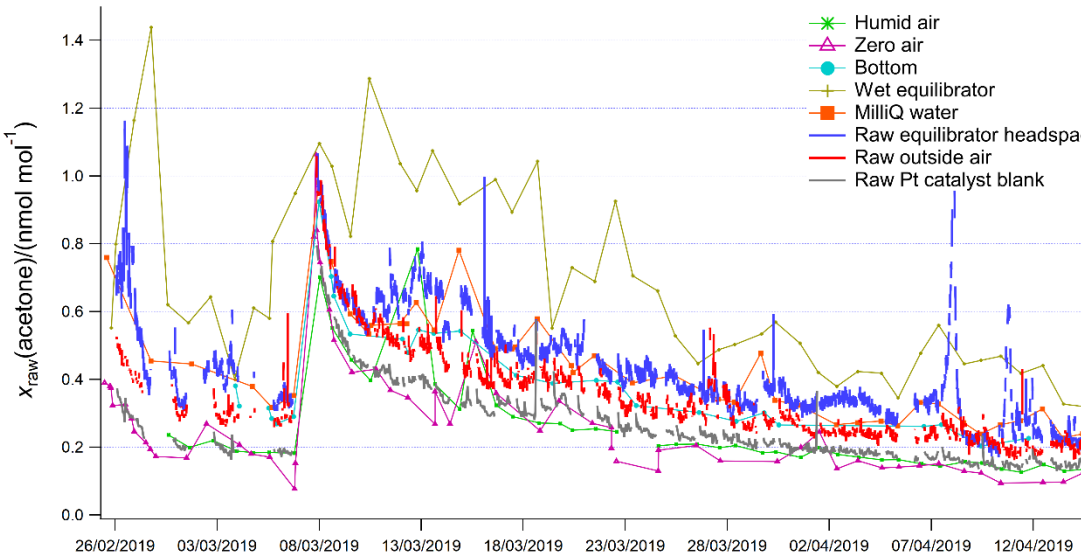

Figure 3.14 Timeseries of raw acetone equilibrator headspace surface and bottom seawater as well as raw ambient air measurements plotted with the raw measurements of the different blanks.

Acetone does not display a humidity dependence in the background (as illustrated by the agreement between zero air and humid air) and thus I prefer to use the Pt-catalyst as a blank. The Pt-catalyst, zero air and humid air blank give similar values, suggesting that the acetone signal is independent on CO_2. Using any of these three blanks would yield similar and realistic seawater concentrations. The wet equilibrator blank gives consistently higher readings than the surface water measurement. As mentioned previously, this may be because the water bath was kept at 25 ºC during this deployment. The increased temperature may have caused some of the acetone to outgas during the wet equilibrator measurement. MilliQ water is clearly not an appropriate blank for acetone as it gives a higher acetone value than the deep water sample.

Methanol

Equilibrator headspace, ambient air raw signal, and backgrounds for methanol are presented in Figure 3.15.

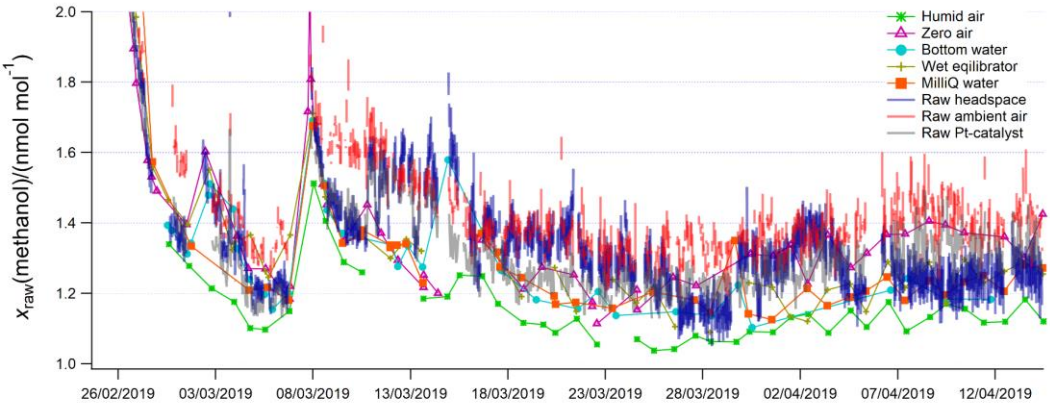

Figure 3.15 Timeseries of raw methanol equilibrator headspace surface and bottom seawater as well as raw ambient air measurements plotted with the raw measurements of the different blanks.

The background of methanol changes as a function of humidity (as illustrated by the offset between zero air and humid air). Pt-catalyst and zero air are thus not the most ideal backgrounds for seawater methanol measurement. The background of methanol seems largely independent of CO_2, as demonstrated by the good agreement between the zero air and Pt-catalyst. Similar to acetone, MilliQ water is not an appropriate blank as it gives higher raw values than surface seawater. Using the wet equilibrator as a blank, I calculate surface methanol concentrations down to -50 nmol dm^{-3}, which is far beyond the measurement noise (7 nmol dm^{-3}). The higher than expected wet equilibrator blank is likely due to outgassing due to the higher water bath temperature. The humid air blank is chosen as a blank here as it gives the most consistent and physically realistic surface seawater concentrations. It is also possible to apply a humidity-correction to zero air to estimate the methanol background, which I do for the Arctic deployment.

Acetaldehyde

Equilibrator headspace, ambient air raw signal, and backgrounds for acetaldehyde are presented in Figure 3.16.

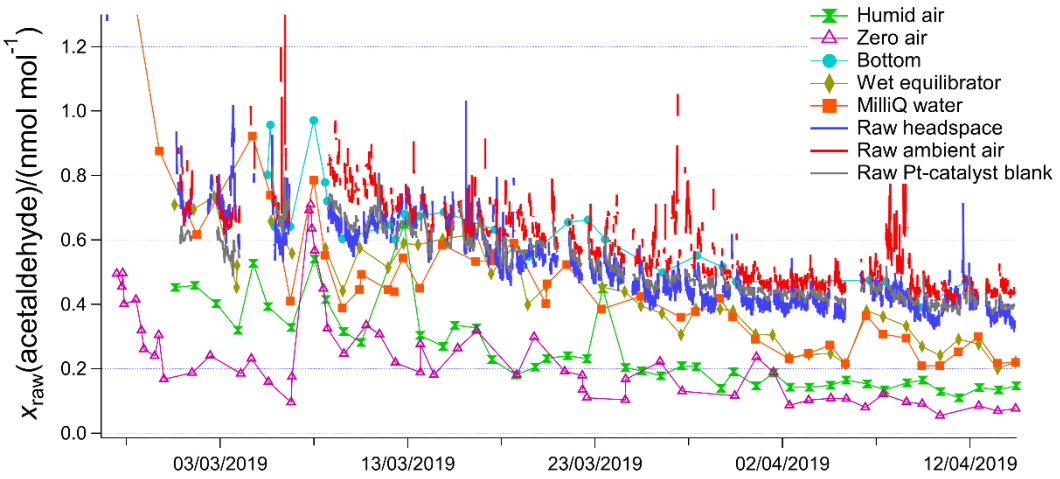

Figure 3.16 Timeseries of raw acetaldehyde equilibrator headspace surface and bottom seawater as well as raw ambient air measurements plotted with the raw measurements of the different blanks.

Acetaldehyde does not display a strong humidity dependence in the background (as demonstrated by the relatively small difference between humid air and zero air). However, acetaldehyde background depends strongly on CO_2 (Warneke et al., 2003c), consistent with the offset between zero air (~ no CO_2) and the Pt-catalyst (ambient atmospheric CO_2) backgrounds. Using the Pt-catalyst as a blank yields negative concentrations in surface water down to -4 nmol dm^{-3}, which seems unrealistic given the measurement noise (1 nmol dm^{-3}). This is possibly because CO_2 mole fractions in equilibrator headspace (calculated range of 170-235 µmol/mol from in situ fCO_2 assuming full equilibration) are lower than in the Pt-catalyst (around 400 µmol/mol). Thus using the Pt-catalyst leads to an overestimate of the acetaldehyde seawater background. Using the zero air or humid air as a blank (which does not account for the influence of CO_2 on the background) would give bottom water concentrations of on average 8.2 nmol dm^{-3}, which is much higher than I expect given the photochemical source of this compound combined with a rapid biological consumption. MilliQ water and the wet equilibrator agree relatively well (mean difference (± std. error) of (0.008±0.013) nmol mol^{-1}). For the measurements presented in this thesis, I choose the wet equilibrator as a blank as it gives more realistic bottom water concentrations of on average 3.1 nmol dm^{-3}. However, the MilliQ and wet equilibrator blanks also do not account for the influence of CO_2 on the signal. I recognise this represents a measurement bias that I am unable to quantify or account for. The uncertainty and possible bias associated with my choice is discussed in Sect.3.9.2.

Isoprene

Equilibrator headspace and ambient air raw signal and blanks for isoprene are presented in Figure 3.17.

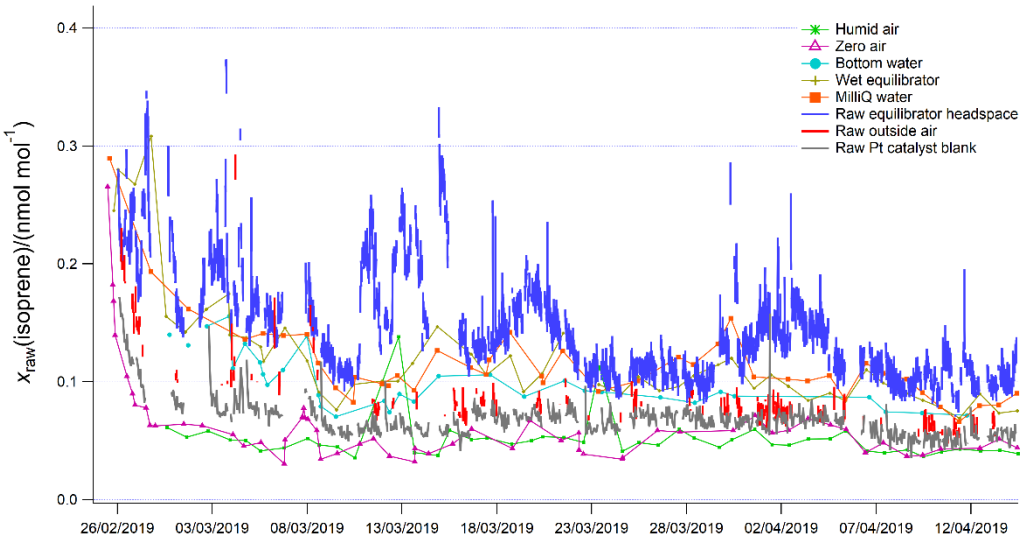

Figure 3.17 Timeseries of raw isoprene equilibrator headspace surface and bottom seawater as well as raw ambient air measurements plotted with the raw measurements of the different blanks.

The background of isoprene does not display a humidity dependence (as illustrated by the agreement between zero air and humid air). However, the background of isoprene does appear to display a dependence on CO_2 during this deployment (consistent with previous estimation by Schwarz et al. (2009)), as illustrated by the higher Pt-catalyst measurements compared to zero air/humid air. In contrast, using zero air/humid air would give a mean isoprene concentration in bottom water of 0.0095 nmol dm^{-3}, which is much higher than reported in previous measurements (Booge et al., 2018; Moore and Wang, 2006; Tran et al., 2013). The consequence of this background choice is considered in greater detail in my uncertainty analysis for isoprene in Sect.3.9.2.

DMS

Equilibrator headspace, ambient air raw signal, and backgrounds for DMS are presented in Figure 3.18.

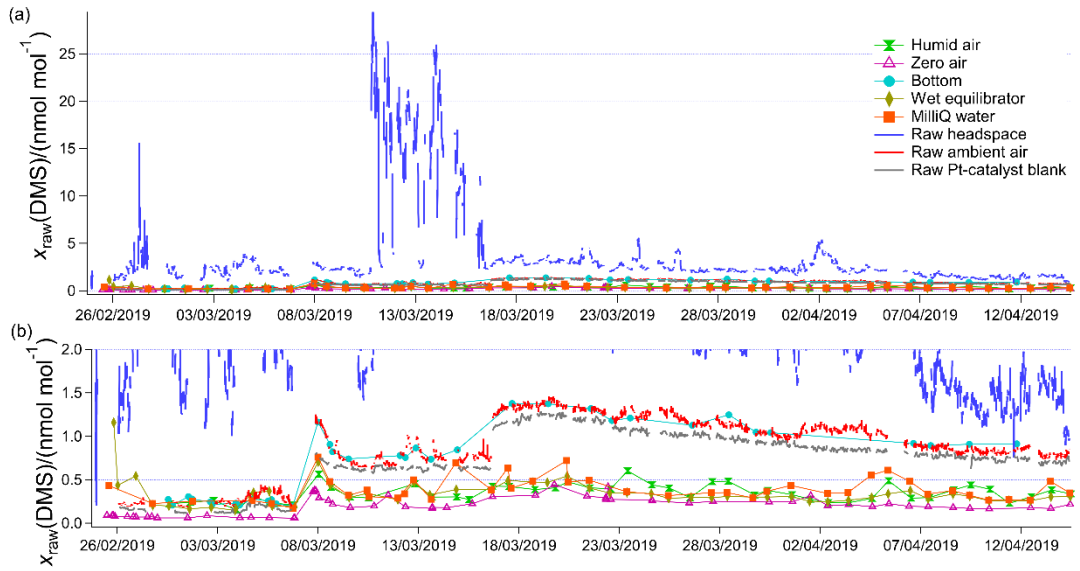

Figure 3.18 Timeseries of raw DMS equilibrator headspace surface and bottom seawater as well as raw ambient air measurements plotted with the raw measurements of the different blanks. Panel (a) shows the full range of readings, whereas panel (b) shows a focus from zero to two nmol mol^{-1}.

The backgrounds for DMS display a humidity dependence as illustrated by the consistent difference between zero air and humid air blanks. For the first 10 days of the campaign, the Pt-catalyst, bottom water, wet equilibrator, humid air, and MilliQ water all give comparable values. The reaction chamber of the PTR-MS was opened up for cleaning on 07/03/2019 and the source settings had to be changed to avoid formation of unwanted O_2^+ ions. Immediately following this, the Pt-catalyst blank and bottom water values grouped together at higher values, while wet equilibrator, humid air, and MilliQ water grouped together at lower values. The source settings had to be changed again on 17/03/2019 after cleaning the source, which led to a widening of this separation. The reason for this difference between the blanks is likely due to decreases in the source voltages after maintenance events (in this case the "Source out" voltage) and subsequent formation of CO_2 hydronium clusters (Herbig et al., 2009). The difference between zero air and Pt-catalyst does suggest a dependence of DMS signal on CO_2 after the maintenance events.

Using the wet equilibrator, zero air or humid air as a blank would lead to reporting DMS concentrations of up to 1.2 nmol dm^{-3} in bottom water during the latter part of the cruise. This seems unrealistic as DMS concentrations far below the mixed layer are generally considered to be near zero (Rellinger et al., 2009). Additionally, sudden increases in bottom water values immediately followed the PTR-MS maintenance events, suggesting that using the wet equilibrator, zero air or humid air as a blank would introduce a measurement artefact. The Pt-catalyst blank appears to account best for these short term changes in the

background related to maintenance events as it contains the most similar amount of CO_2 compared to the equilibrator headspace. I thus decide to use the Pt-catalyst as a blank for DMS and add the experimentally determined humidity dependence (determined as 0.11 nmol mol^{-1} during this deployment). This gives a mean bottom water concentration of 0.02 nmol dm^{-3} for this deployment, which seems realistic.

3.8.4 Backgrounds for the Arctic deployment

The Arctic deployment was carried out during an earlier stage in the method development and thus I only collected the zero air and wet equilibrator as a blank. Bottom water was collected as a "spot check". This gives me more limited choice of blanks compared to the Antarctic deployment. However, I believe that I am still able to estimate a reasonable set of backgrounds for the Arctic deployment with the insights gained from the Antarctic deployment.

Figure 3.19 illustrates how the blanks relate to each other and to the surface seawater and bottom seawater signals. Figure 3.19 also shows the smoothly interpolated background.

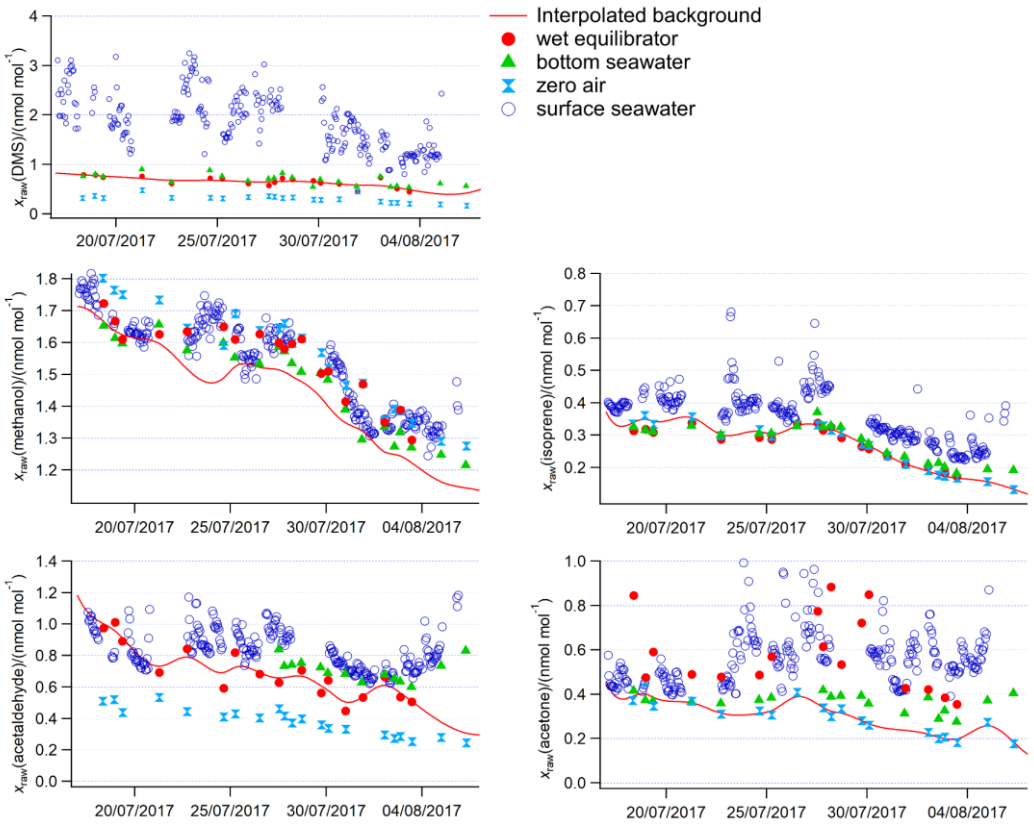

Figure 3.19 Timeseries of raw VOC equilibrator headspace surface and bottom seawater as well as raw zero air and wet equilibrator blanks for the Arctic deployment. Missing acetaldehyde bottom seawater measurements are due to a contamination from the CTD sampling Niskin bottle.

Background interpolation

Figure 3.19 shows the smoothly interpolated background. I decided to do a smooth interpolation instead of a linear interpolation (for both deployments) to account for the noise in the blank measurement.

DMS

I use the wet equilibrator as the blank for seawater DMS measurements in the Arctic. This gives near zero concentrations in bottom water, consistent with existing literature. Both the wet equilibrator and bottom water show markedly higher values than zero air, likely due to the humidity dependence in DMS measurement. During the Arctic deployment, the same source settings as at the beginning of the Antarctic campaign were applied throughout, which explains the absence of an obvious CO_2 dependence in the DMS background.

Methanol

Methanol background depends on humidity but not CO_2. Using the wet equilibrator as a blank gives meaningless concentrations down to - 50 nmol dm^{-3}, which is far beyond measurement noise (7 nmol dm^{-3}). Later it was discovered that the jar trap used during this deployment likely led to high methanol wet equilibrator backgrounds. Thus, the background for methanol is calculated using zero air and the experimentally determined humidity dependence in the background. The humidity dependence is a relatively large correction and thus a potential source of uncertainty. However, this humidity dependence was found to be nearly identical between the two deployments and relatively constant. The uncertainty associated with this correction is estimated in Sect.3.9.2.

Isoprene

Isoprene does not display a humidity dependence in the background. During this deployment, the wet equilibrator and the zero air agree reasonably well. Using either of the two blanks gives near zero bottom water concentrations, which seems realistic and suggests little influence of CO_2 on the isoprene signal during the Arctic deployment (similar to DMS). Therefore, zero air is used as a blank for isoprene during this deployment.

Acetaldehyde

Acetaldehyde background does not display a large humidity dependence but does depend strongly on CO_2. Similar to the Antarctic deployment, using zero air as a blank gives a mean bottom water concentration of 9.5 nmol dm^{-3}, which is far higher than I would expect due to

the short lifetime and photochemical source of this compound. Consistent with the Antarctic deployment, I choose to calculate acetaldehyde seawater concentrations using the wet equilibrator as a blank. The uncertainty and possible bias associated with this choice is discussed in Sect. 3.9.

Acetone

Acetone does not display a humidity dependence, nor a CO_2 dependence. I therefore decide to calculate seawater acetone concentrations using zero air as a blank. Similar to methanol, the wet equilibrator blank gives higher readings than the surface seawater, likely due to outgassing of acetone from the jar trap.

3.8.5 Concluding remarks

A table is shown here to summarise which blank is used for each deployment (Table 3.1).

Table 3.1: Summary of seawater blanks for each compound during the two deployments.

compound	Arctic measurements	Antarctic measurements
DMS	Wet equilibrator(≈ zero air + humidity)	Pt-catalyst + humidity
isoprene	Zero air	Pt-catalyst
methanol	Zero air+ humidity	Humid air(≈ zero air + humidity)
acetone	Zero air	Pt-catalyst (≈ zero air)
acetaldehyde	Wet equilibrator	Wet equilibrator

Table 3.1 summarises the different blanks chosen for the two deployments. The differences are due to the availability of the blanks and the varying influence of CO_2 (stronger for the latter half of the Antarctic deployment after a PTR-MS maintenance).

This section illustrates that estimating seawater blanks for these VOCs is very challenging. At the same time, this is a crucial step as the blank is a potential source of measurement bias and often displays large variability. Lacking VOC-free seawater, the choice of the most appropriate blank for seawater VOC measurements is sometimes ambiguous. In this thesis, I rely on an understanding of the PTR-MS instrument (largely the humidity and CO_2 dependencies) and comparison of bottom water measurements with previous literature reported values to make my best estimate. My discussions of these possible biases and measurement challenges will hopefully be a valuable contribution to the marine VOC community and spur further investigations.

It is possible that for different field deployments the most appropriate backgrounds are different. For example, during the Arctic deployment, the wet equilibrator and bottom water measurement of DMS agree very well, while they do not agree during the second part of the Antarctic deployment due to the slightly different source settings and probably the influence of CO_2.

Collecting a number of different types of blanks, not done previously by other investigators, allows me to more rigorously assess the impact of background choices on the seawater VOC concentrations. It is quite possible that further research will result in improved blanks for these compounds. For example, scrubbing the sample headspace air (rather than wet equilibrator air) with a catalyst might be a better way to ensure consistent humidity and CO_2 levels.

3.9 Uncertainties in the dissolved gas concentrations and ambient air mole fraction measurements

In this section, I estimate the uncertainties of the dissolved gas concentrations and air mole fractions presented in this thesis. This includes random noise (Sect. 3.9.1) and systematic bias (Sect. 3.9.2). A total measurement uncertainty is calculated using simple error propagation (Sect. 3.9.3).

3.9.1 Measurement precision

The analytical precision (1 σ) and the LOD (defined here as 3 σ) of this system are dictated by the noise of the PTR-MS measurement. In the air phase, this depends on the detector sensitivity and the averaging time. The seawater measurement precision additionally depends on the factors laid out in Sect. 3.3.2 (i.e. solubility, gas calibration slopes, equilibration efficiencies, and noise in the backgrounds). The VOC limit of detection and measurement precision are independently assessed for the Arctic and Antarctic deployments due to the slightly different PTR-MS settings/averaging times and calibration slopes.

Isoprene does not fully equilibrate in the equilibrator and the calibration slopes displayed a standard deviation of 16 %. To account for variable water flow and variable equilibration during the Arctic deployment, a blanket 20 % random measurement uncertainty is assumed in the calibration slope for isoprene only.

For both deployments, the background is smoothly interpolated, with the smoothing factor dependent on the noise of the PTR-MS measurement. The standard deviation of the

detrended blanks is calculated by subtracting the smooth interpolation. This represents measurement noise (1 σ) and is converted to ambient air mole fraction or dissolved gas concentration using the equations laid out in Sect. 3.3.2.

Hourly averages are used to calculate underway concentrations and fluxes. During the Antarctic deployment, each hourly average contains 10 min continuous ambient air measurements and 30 min equilibrator headspace measurement (values immediately following valve switching are excluded). During the Arctic deployment, each hourly average contains 18 min continuous equilibrator headspace measurement. Each blank measurement is 5 and 6 min long during the Antarctic and Arctic deployment respectively. Therefore the measurement noise is divided by the square root of the number of 5- or 6-min-segments in each hourly average to calculate the hourly measurement noise.

Table 3.2 illustrates that measurement noise is generally higher for the Arctic deployment, due to less frequent (daily) blanks, lack of gas phase calibrations and variable water flow. Out of the VOCs detected, the largest seawater measurement noise is generally observed for methanol, in part due to its very high solubility and the noise in the background.

Table 3.2 Ambient air and underway seawater measurement precision and LOD for both deployments. Hourly averages, to calculate the measurement noise of a single 5 min measurement (as e.g. applicable for CTD measurements), σ listed here should be multiplied by the square root of 6 or 3 for the Antarctic data or the Arctic data respectively. LOD = Limit of detection, σ = analytical precision

	Antarctic Underway Seawater		Antarctic Ambient Air		Arctic Underway Seawater	
compound	σ /(nmol dm^{-3})	LOD /(nmol dm^{-3})	σ /(nmol mol^{-1})	LOD /(nmol mol^{-1})	σ /(nmol dm^{-3})	LOD /(nmol dm^{-3})
DMS	0.006	0.018	0.012	0.036	0.04	0.12
isoprene	0.0003	0.0009	0.008	0.024	0.0012	0.0036
methanol	7	21	0.05	0.15	4	12
acetone	0.17	0.51	0.009	0.027	0.4	1.2
acetaldehyde	0.4	1.2	0.014	0.042	0.8	2.4

3.9.2 Measurement bias

I consider four sources of potential bias in the seawater VOC measurements: uncertainty in the solubility value, lack of regular gas calibrations, ambiguity in the choice of background and the effect of pressure within the equilibrator.

My mean acetaldehyde, DMS and isoprene calibrations agreed within 10 % compared to the solubility from Burkholder et al. (2015) or Karl et al. (2003), respectively. For methanol and acetone, I suggested a set of improved solubility values based on my own measurements, which come with a relative uncertainty estimated as 10 % (see Sect. 1.5). Thus, I assume a universal 10 % uncertainty in solubility for all VOCs as a potential bias in my data.

The regular gas phase calibrations during the Antarctic deployment captured a slow drift of 10 % in the slope, which has been accounted for by applying an interpolation of the calibration slopes. To account for the lack of regular gas calibrations during the Arctic deployment, this 10 % is further included as potential bias for this deployment.

For the air measurements, the widely used Pt-catalyst represents a very accurate background and is not expected to add substantial bias to my ambient air measurements. The choice of background, however, is very important for the seawater measurements but at time ambiguous. To estimate the potential measurement bias from the choice of background, I have calculated the dissolved gas concentration from the Antarctic deployment using different choices of backgrounds (Table 3.3).

Table 3.3 Mean underway surface water concentration from the Antarctic deployment computed using different backgrounds. Backgrounds indicated as subscript. The percentage difference is used to estimate the uncertainty bias in reported concentrations due to the choice of background (for each VOC, top: alternative background: bottom: chosen background for the Antarctic deployment). Methanol concentrations labelled as "zero air" are computed using the zero air blank and the experimentally determined humidity dependence. Acetaldehyde concentrations labelled as "CO2 effect" are computed by roughly accounting for the influence of CO_2 on the signal as explained in the text.

		R(difference)/(%)
$c(DMS_{wet\ equilibrator})$/(nmol dm^{-3})	2.93	11
$c(DMS_{Pt\text{-}catalyst})$/(nmol dm^{-3})	2.60	
$c(isoprene_{zero\ air})$/(nmol dm^{-3})	0.0170	23
$c(isoprene_{Pt\text{-}catalyst})$/(nmol dm^{-3})	0.0135	
$c(methanol_{zero\ air})$/(nmol dm^{-3})	86	24
$c(methanol_{humid\ air})$/(nmol dm^{-3})	67	
$c(acetone_{zero\ air})$/(nmol dm^{-3})	6.4	15
$c(acetone_{Pt\text{-}catalyst})$/(nmol dm^{-3})	5.5	
$c(acetaldehyde_{"CO2\ effect"})$/(nmol dm^{-3})	4.3	65
$c(acetaldehyde_{wet\ equilibrator})$/(nmol dm^{-3})	2.6	

Table 3.3 shows that for most VOCs detected, choosing a reasonable alternative background leads to a computed concentration that differs by <25 %. In the case of DMS,

these calculations possibly overestimate the true bias. A wealth of previous measurements show that DMS concentration in deep water should be about zero (which the catalyst blank yields for the Arctic deployment and the wet equilibrator yields for the Antarctic deployment).

The largest uncertainty by far is in the acetaldehyde measurements. This is due to the small signal to background ratio and relatively large differences between the backgrounds due to the influence of CO_2 on this compound. In this calculation, I try to account for the influence of CO_2 on the background to the best of my abilities. I assume that the difference between zero air and the Pt-catalyst is entirely due to the influence of CO_2 on the acetaldehyde background. This CO_2-sensitivity, scaled by the difference between CO_2 in equilibrator headspace air (see Chapter 5 for seawater CO_2 measurements) and atmospheric CO_2, is added to the zero air value to give a CO_2-corrected background. This calculation assumes full equilibration of CO_2 in the equilibrator and accounts for purging and headspace dilution. Previous measurements of acetaldehyde in seawater using equilibrators coupled to PTR-MS potentially possibly also suffer from the same artefact to a varying degree (Beale et al., 2013; Kameyama et al., 2009; Yang et al., 2014c). This uncertainty limits my ability to accurately estimate the saturation and air – sea flux of acetaldehyde. As a consequence, most of my discussion of these measurements will focus on relative distributions and ranges. Additionally, CO_2 abundance is much higher in deeper waters/below the mixed layer at the high latitudes (Beaupré-Laperrière et al., 2020; Shadwick et al., 2011). As a result, the shape of acetaldehyde depth profiles measured using this method could be impacted by this CO_2 interference. The implications of this are discussed in the relative chapters where the depth profile measurements for acetaldehyde are presented.

The equilibrator is operated at slight overpressure compared to ambient pressure (Sect. 3.2). From water displacement in the U-shaped drain, I calculate that the equilibrator is operated at 0.98 mbar above atmospheric pressure. Including this in the ideal gas law conversion factor in Eqn. 3.2, I calculate that by using ambient pressure, rather than the slightly higher true pressure in the equilibrator, I underestimate seawater concentrations by ≈ 0.1 %, which is negligible. The ambient pressure is also expected to vary. The standard deviation in ambient pressure during the deployment in the Antarctic was 15 mbar, which introduces an uncertainty of 1.5 % assuming the ambient pressure was about 1000 mbar. Given the much larger sources of uncertainty elsewhere (e.g. due to background correction), it's reasonable to neglect this pressure uncertainty. At the low, environmental

concentrations encountered here, there is no evidence in literature to suggest that these VOCs do not follow ideal gas law.

3.9.3 Overall measurement uncertainty

Using error propagation, the total uncertainty in the seawater measurements is computed and presented in Table 3.4. For this calculation, the measurement precision is converted to a percentage by dividing it by the cruise mean concentration or mole fraction. This total measurement uncertainty takes into account the measurement precision (Table 3.2) and potential biases (Table 3.3).

Table 3.4 Potential overall measurement uncertainty for both deployments.

	Arctic	Antarctic	
compound	$u[c(VOC_{seawater})]/(\%)$	$u[c(VOC_{seawater})]/(\%)$	$u[x(VOC_{ambient\ air})]/(\%)$
DMS	18	15	7
isoprene	27	25	15
methanol	30	27	29
acetone	23	20	11
acetaldehyde	69	67	28

Table 3.4 illustrates that the overall uncertainty of the seawater measurements is largely dictated by the background choice, as the estimated background bias is similar to the overall uncertainty. Table 3.4 confirms that the largest relative uncertainty is probably in the acetaldehyde seawater measurements. This large uncertainty is perhaps not surprising as the only direct air – sea flux measurements of acetaldehyde did not agree well with the computed flux using sea and air atmospheric acetaldehyde concentrations (Yang et al., 2014c). This implies that the acetaldehyde seawater measurements using PTR-MS could have been biased.

3.10 Conclusion

This chapter presents a ship-based equilibrator system coupled to a PTR-MS for measurements of a wide range of VOCs in seawater. Its main advantage lies in its unique design yielding a high degree of equilibration and a fast response time (less than 1 min). I find that with a 10 m segmented flow tube, the SFCE fully equilibrates for gases of similar or higher solubility than toluene and DMS.

Both invasion and evasion calibrations were carried out. Matching up the derived solubility from these two calibration methods provides an independent estimate of the gas solubility

at environmentally relevant concentrations in seawater. This approach enables me to determine the most appropriate solubility for isoprene, acetone and methanol out of literature values.

The largest uncertainty in the VOC measurements is due to the choice of background, which is often overlooked by previous investigators. I made several types of background measurements and discuss the rationale of my background choice for each deployment. This represents one of the novel, rigorous aspects of this work aiming at improving dissolved gas measurements using PTR-MS. The chapter is rounded up with an estimation of the uncertainty of the measurement. The potential overall air and seawater measurement uncertainty is generally less than 30 % and similar for both cruises. Uncertainty is lowest for DMS, while acetaldehyde measurements are highly uncertain (more than 60 %) due to an unquantified interference of CO_2 with the background. The discussion of this influence on the acetaldehyde seawater measurements represents one of the novel aspects of this work and should be addressed by future investigators.

4 Sea ice cover impacts dissolved organic gases in the Canadian Arctic

In the Arctic, sea ice cover varies seasonally. Waters influenced by sea ice tend to display higher biological and photochemical activity during summer. The Arctic is undergoing rapid climate change, leading to rapid reduction in sea ice cover. It is currently unknown how the biogeochemical processes in the sea ice zone influence dissolved concentrations of dimethyl sulfide, isoprene, methanol, acetone and acetaldehyde, largely due to a lack of measurements.

To address this, in this chapter I present VOC concentration measurements from near the surface to 60-m depth. These measurements were made in the Canadian Arctic Archipelago during the summer. Using a combination of underway measurements and a large number of depth profile measurements at different sea ice cover, I suggest that partial ice cover leads to higher surface seawater concentrations of these gases. The mean underway (3-4 m depth) seawater concentrations from this deployment are 38 nmol dm^{-3} methanol, 8.9 nmol dm^{-3} acetone, 4.6 nmol dm^{-3} acetaldehyde, 0.062 nmol dm^{-3} isoprene and 1.42 nmol dm^{-3} dimethyl sulfide. Depth profiles reveal enhanced concentrations for many of these compounds in the top 10 to 20 m of the water column, especially in partially ice-covered waters where concentrations tend to be the highest. This is the first comprehensive data set for the simultaneous measurement of methanol, acetone, acetaldehyde, DMS and isoprene which will help us better understand their distribution and the potential sources and sinks in the sea ice zone.

4.1 Introduction

The sea ice zone is characterised by unique seasonal biogeochemical processes. Their effects on the dissolved concentrations of VOCs are poorly known due to a lack of in situ measurements, which are required to pave the way for a more process-based understanding. The Arctic Ocean and the sea ice zone represent particularly under-sampled regions with no existing measurements of seawater concentrations of methanol, acetone and acetaldehyde particularly in partial sea ice cover. Based on atmospheric measurements, the Canadian Arctic sea ice zone in summer has been shown to be a sink for methanol and acetone (Sjostedt et al., 2012), and a source of dimethyl sulfide (DMS (Abbatt et al., 2019; Jarníková et al., 2018)) and other oxygenated VOCs (Mungall et al.,

2017, 2018)). Boudries et al. (2002) found that methanol, acetone and acetaldehyde represent about 90 % of all the detected oxygenated hydrocarbons in the atmosphere during a campaign in the high Arctic in spring at Alert. Snowpack photochemistry appears to be a source of acetone and acetaldehyde to the Arctic atmosphere in spring (Gao et al., 2012; Kos et al., 2014). Measurements of the seawater VOC concentrations will help to constrain the oceanic sources of these compounds. In the Arctic, the marginal ice zone can be 1.5-2 times more biologically productive than the open ocean due to frequent ice-edge blooms in summer (Perrette et al., 2011), which makes summer a key time of year and location to sample for biogenic VOCs. Missing this seasonal pulse in productivity could lead to underestimations of the annual biogenic VOC emissions of this region (Abbatt et al., 2019; Arrigo et al., 2011). Furthermore, seasonal sea ice melt leads to stratification in near surface waters, which in turn allows for very different biogeochemical conditions at different depths (Ahmed et al., 2020; Shadwick et al., 2013). Measuring VOCs at different depths could reveal the importance of different production and consumption processes.

In this chapter, I present depth profile (0-60 m) and shipborne underway seawater measurements of methanol, acetone, acetaldehyde, DMS and isoprene in the Canadian Arctic Archipelago during boreal summer (July-August 2017).

4.2 Cruise and sampling overview

In this section, I provide an overview for this Arctic deployment.

Underway seawater and depth profile concentrations of VOCs in the sea ice zone of the Canadian Arctic were measured on board the Ice Breaker CCGS *Amundsen*. The measurements were taken between 17/07/2017 and 08/08/2017 (Cruise 1702, leg 2b) (Figure 4.1).

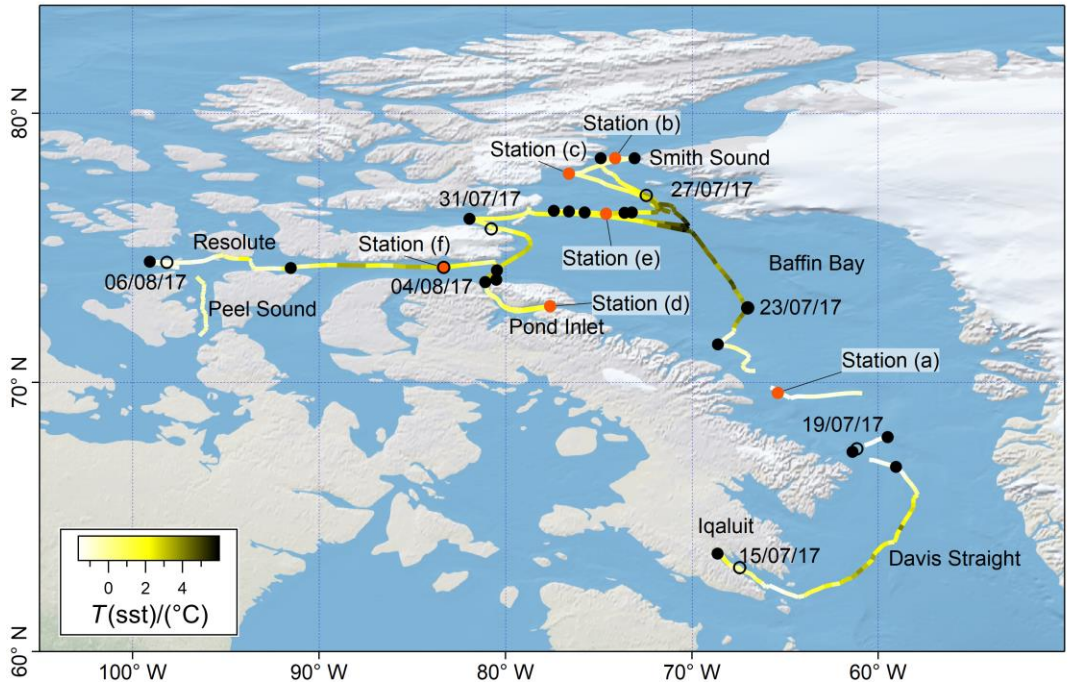

Figure 4.1 Cruise track of the sampling undertaken in the Arctic sea ice zone coloured by sea surface temperature (sst). Sampling dates are indicated as hollow circles marked with the date. The location of each CTD station where sampling was undertaken is indicated as a black closed dot. The CTD stations highlighted in this chapter are indicated as orange closed dots and labelled (Amundsen Science Data Collection, 2017). Interruptions in the cruise track and underway auxiliary data are due to failures in the ship underway logging system.

The research vessel travelled from Iqaluit northwards through Davis Straight and Baffin Bay to reach Smith Sound. In this area, more intense depth profile sampling was carried out. The vessel then travelled to Pond Inlet and Resolute. Sampling ended south of Resolute in Peel Sound.

I measured the VOC depth profiles from the near surface (2 m) to 60 m depth at a total of 21 stations. When logistically feasible on station, a handheld vertical 5 dm^3 Niskin bottle was deployed off the front starboard side of the ship to sample approximately the top 30 cm from the ocean surface. This was done by bringing the Niskin bottle up from approximately 3 m and firing it just before it reached the surface. The auxiliary data for the depth profiles were measured using sensors mounted on the CTD frame listed in Table 4.1.

Table 4.1 Sensors mounted on the CTD Rosette ***(Amundsen Science Data Collection, 2017)*****.**

Parameter	Sensor
Oxygen concentration	Seabird 43
Conductivity	Seabird 4
Chl *a*	Sea point Chlorophyll Fluorometer
PAR Irradiance	QCP-2300 Biosherical
Temperature	Seabird 3plus
Pressure	Paroscientific Digiquartz

The SFCE-PTR-MS system was set up in one of the labs located near the front of the ship with access to an underway water tap from the ship's main underway water supply. The SFCE nominally sampled from the bottom of a glass bottle, which was rapidly overflowed with the ship's underway water. During periods of high sea ice cover, as per decision by the ship's crew, the underway water inlet (located at 3-4 m depth) was turned off. The underway water flow rate was continuously monitored by the ship's crew and used for data quality control. A range of biogeochemical parameters were monitored continuously, including sst (monitored using Sea Bird SBE 38 Termosalinograph), sea surface salinity (sss) (monitored using Sea Bird SBE 45 MicroTSG Thermosalinograph) and Chl *a* fluorescence (monitored using Wetlabs WETStar Fluorometer).

4.3 Sea ice cover

This section describes how underway sea ice cover (SICs) is obtained from satellite data.

Before I dive into this, I would like to clarify that by sea ice cover, I am referring to the fractional sea ice cover (i.e., in %). I acknowledge that the satellite sea ice product I use here uses the term sea ice concentration, instead of sea ice cover. I decide to use the term sea ice cover throughout this thesis to avoid confusion with the actual concentrations of dissolved gases presented in this chapter. This leads to improved compliance with the true SI (International System of Units) definition of a concentration.

The AMSR2 passive microwave SIC satellite product (daily, 3.125 km resolution) (Ludwig et al., 2019; Spreen et al., 2008) is used to create a time series of SIC along the cruise track. This product is chosen due to its high spatial and temporal resolution as well as for complete coverage of the cruise track. For each daily satellite image, the SIC of the grid cell where the ship was located during that hour was used in the timeseries. Figure 4.2 shows

the underway SIC deduced from the AMSR2 satellite product and infrequent visual observations from the ship. The mean difference between these two SIC estimates is only 6 %, suggesting there is no major systematic bias. Visual SIC observations were made during CTD casts and thus I use those estimates to interpret my vertical profile measurements. I use the satellite SIC estimates for analysis of underway VOC measurements because of its wider spatial coverage.

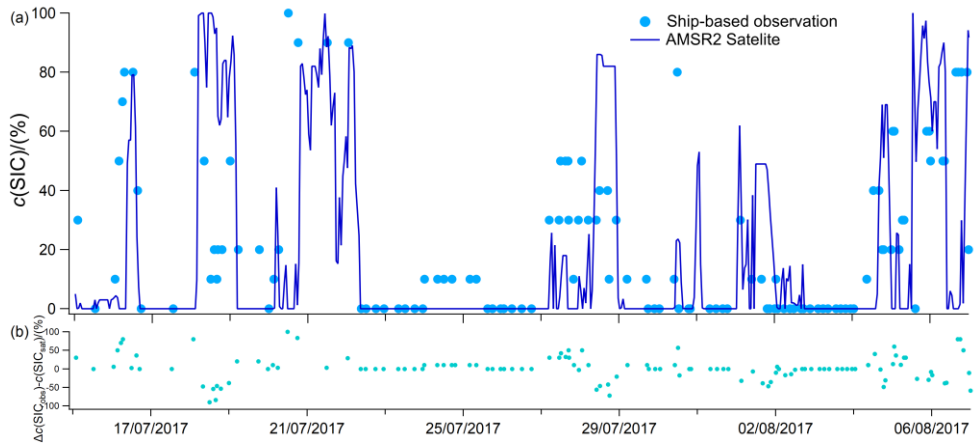

Figure 4.2 (a) SIC during the cruise estimated from satellite and ship-based observations and (b) the difference between two estimates. SIC were taken from the AMSR2 satellite (daily, 3.125 km resolution) and ship based observations.

In the analysis below, I mainly assess how the underway seawater VOC concentrations and depth profiles vary with SIC. These depth profiles represent measurements at different times and locations. Therefore, differences between these casts are possibly not only due to sea ice alone. I recognise that sea ice is a very heteogenous environment with respect to ice thickness (Hayashida et al., 2020), the presence of melt ponds (Gourdal et al., 2018), and types of sea ice (e.g. first year vs. multiyear ice (Lizotte et al., 2020). This heterogeniety likely leads to very dfferent biogeochemistry, affecting trace gas cycling. The analysis presented here does not explicitly take into consideration this variability, which I think is worthy of future research.

4.4 Analytical methods specific to this deployment

The SFCE-PTR-MS method was deployed in the field for the first time during this Arctic cruise. Here, I provide a brief recount of the analytical chemistry specific to this deployment.

To calibrate the PTR-MS, a gas phase calibration using a certified gas standard was carried out two months prior to the cruise when the PTR-MS was first installed on board. Results from this calibration, similar to those from post-cruise gas calibrations, were applied to the

cruise measurements (see Sect. 2.4.2.1). Post-cruise water phase calibrations of the SFCE (see Sect. 3.5) in the lab have shown that the equilibrator fully equilibrates for the soluble gases DMS, acetone, acetaldehyde and methanol, and has a mean equilibration efficiency of 68% for isoprene. The concentrations reported here were calculated using my experimentally determined solubility and equilibration efficiency where appropriate.

Water phase calibrations of the SFCE during the cruise would have been useful. However at the time I decided to focus more on making depth profile measurements, which was very labour intensive and time consuming. I also measured the VOC backgrounds daily with several approaches (see Sect. 3.8.1). Later analyses suggest that my decisions were justified, as post-cruise gas and waterside calibrations were very stable (varied by up to 10 % over 5 weeks), but VOC backgrounds varied by much more over the same time period (by up to 50 %). Similar to the deployment here, Kameyama et al. (2009) carry out gas phase calibrations of the PTR-MS in the field and use equilibration efficiencies determined in the laboratory to calculate dissolved concentrations. I would like to reiterate here that acetaldehyde concentrations from this deployment are highly uncertain due to an unquantified interference of CO_2 with the background (see Sect. 3.8.1). Discussion of the acetaldehyde concentrations in this chapter thus largely focusses on the shape of the depth profiles and the range in underway measurements. The concentration of CO_2 within the 60 m near the surface is not expected to vary drastically (Beaupré-Laperrière et al., 2020) and should thus not impact the shape of the acetaldehyde depth profiles during the Arctic campaign.

Because this deployment was carried out during the earlier stages of the method development, a more limited range of blanks was collected compared to the Antarctic deployment. However, knowledge gained from later deployments and comparison to bottom water samples allowed me to choose a reasonable blank. As noted in Sect. 3.9, the background value for seawater acetaldehyde measurement is quite uncertain. Thus the qualitative shapes of the acetaldehyde vertical profiles are of value, but the absolute concentrations are very likely biased.

Comparisons between near-surface CTD and underway measurements suggested an initial acetaldehyde contamination in the CTD rosette bottles due to the use of an air duster aerosol spray used near the rosette. The other VOCs were not affected. After use of the spray was stopped on 26/07/2017, the acetaldehyde contamination in the CTD measurements immediately disappeared. VOC measurements from the underway system

(2 h either side of the CTD cast) and from the near surface CTD (5 m depth) cast agree well overall. I calculate mean differences (± std. error) of (0±3) nmol dm^{-3} for methanol, (0.5±1.2) nmol dm^{-3} for acetone, (0.5±1.0) nmol dm^{-3} for acetaldehyde, (0.005±0.005) nmol dm^{-3} for isoprene and (0.13±0.10) nmol dm^{-3} for DMS.

4.5 Depth profiles reveal a unique influence of sea ice cover

The aim of this section is to investigate the effect of sea ice cover on the depth profile of these VOCs. To provide context, I share overview plots displaying the shapes of all the casts collected with some auxiliary data (Sect. 4.5.1). The trends in VOC profiles as a function of SIC are discussed in the second part (Sect. 4.5.2) and illustrated with selected casts along with more detailed auxiliary data.

4.5.1 Overview plots

Overview plots are shown to display the shapes of all the depth profiles collected. All profiles and corresponding auxiliary data have been grouped by SIC, plotted in sampling order and staggered along the x-axis for ease of viewing. The profiles have been offset against each other for the sake of visibility. A scale bar for VOC concentrations and auxiliary data is shown to compare casts. Profiles highlighted in the second part are highlighted in the overview plots using hollow circles.

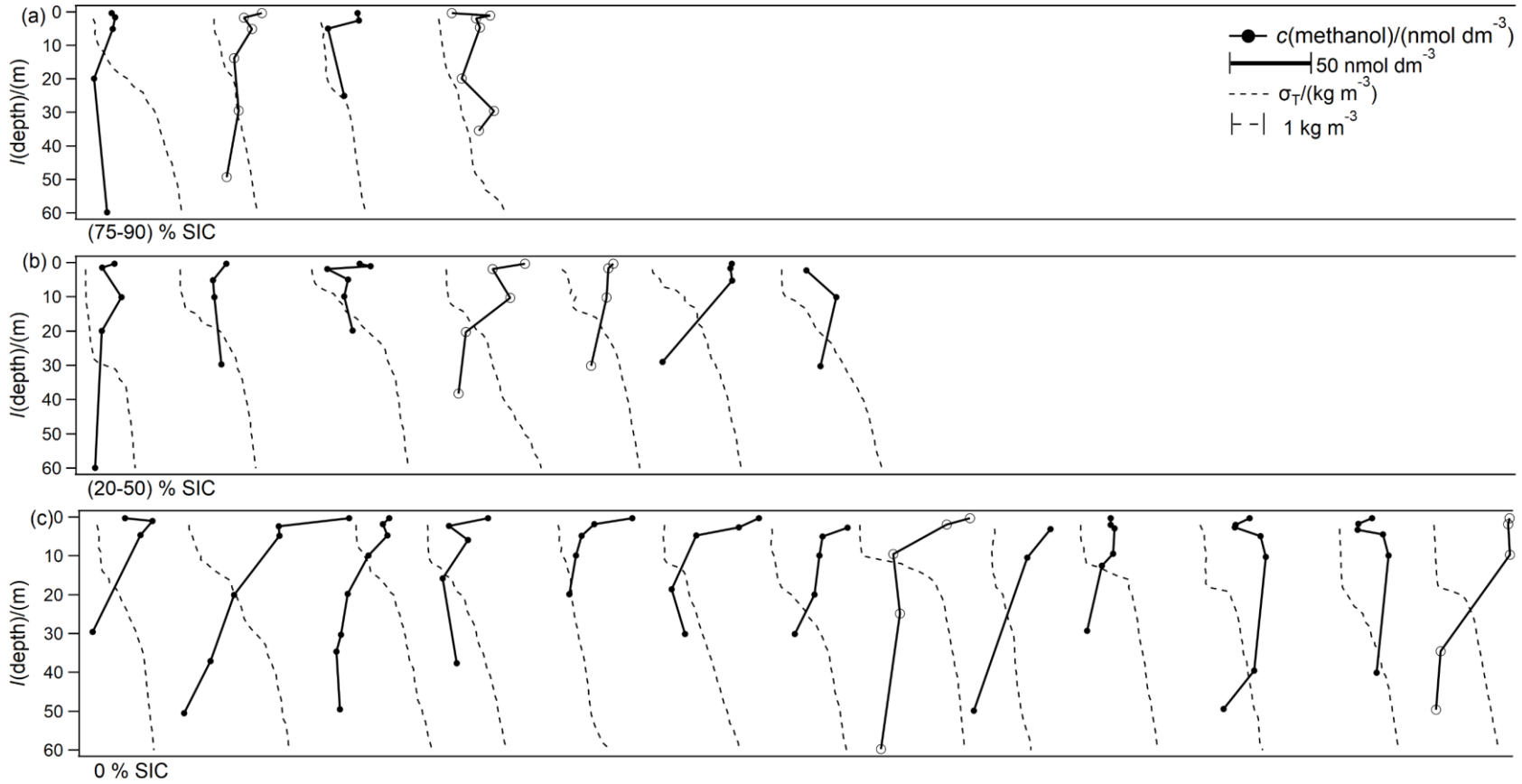

Figure 4.3 Overview plot displaying the shape of all methanol and density (σ_T) depth profiles grouped by SIC and staggered along the x-axis for ease of viewing. Labels indicate the SIC bin. The scale bars for methanol and density in panel (a) apply also to panels (b) and (c). Profiles with hollow markers are highlighted in Figure 4.8.

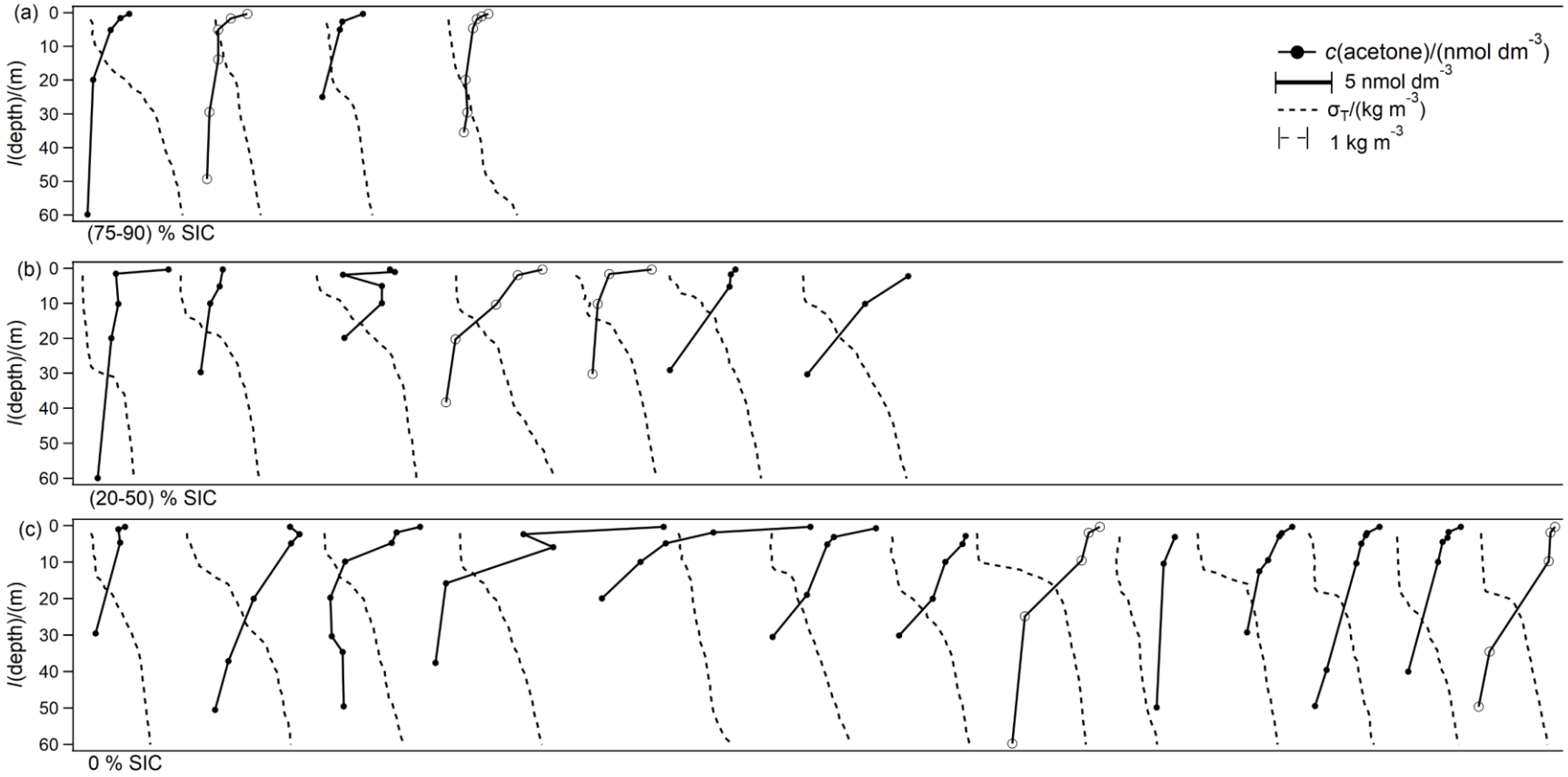

Figure 4.4 Overview plot displaying the shape of all acetone and density (σ_T) depth profiles grouped by SIC and staggered along the x-axis for ease of viewing. Labels indicate the SIC bin. The scale bars for acetone and density in panel (a) apply also to panels (b) and (c). Profiles with hollow markers are highlighted in Figure 4.8.

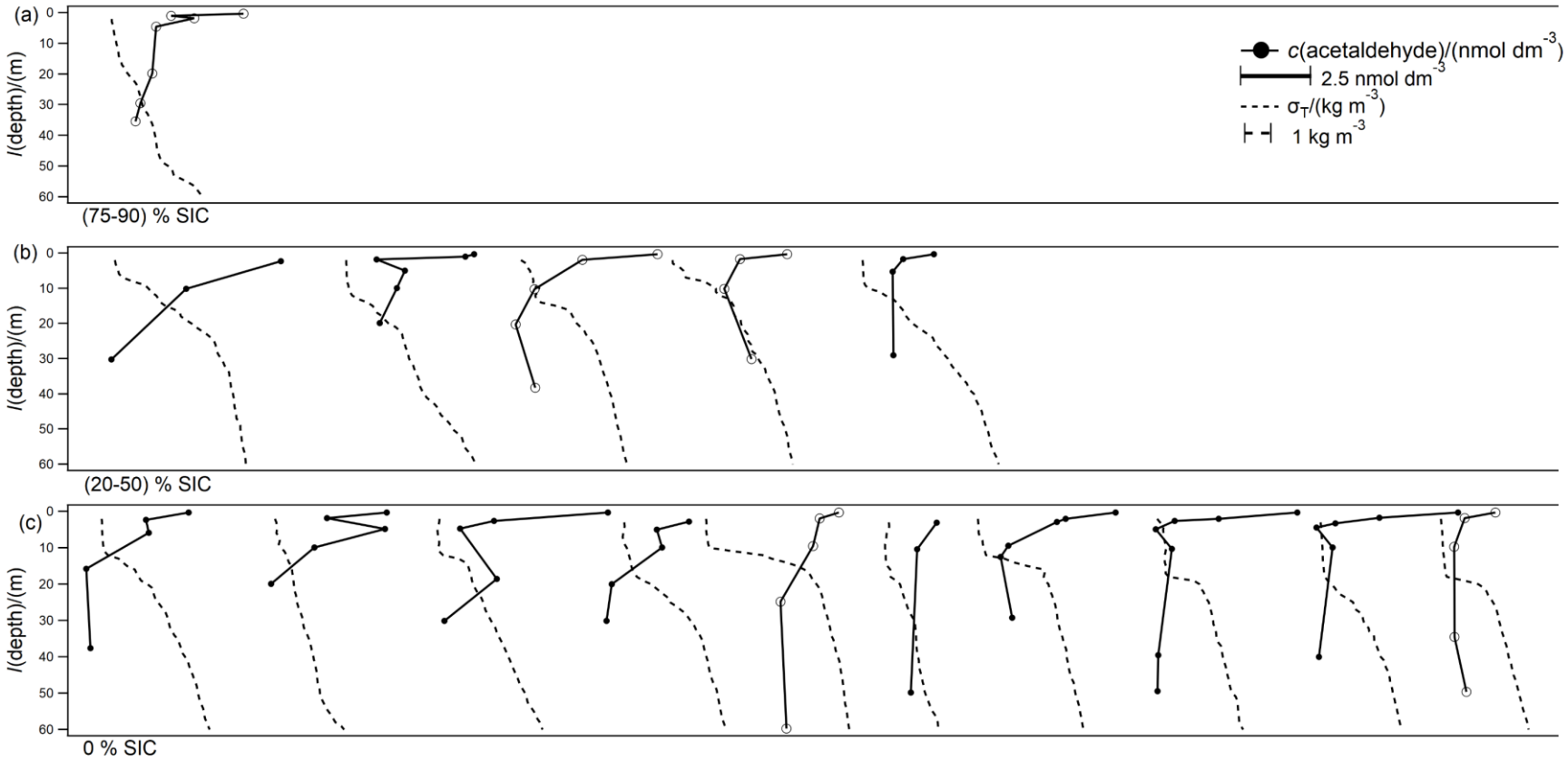

Figure 4.5 Overview plot displaying the shape of all acetaldehyde and density (σ_T) depth profiles grouped by SIC and staggered along the x-axis for ease of viewing. Labels indicate the SIC bin. The scale bars for acetaldehyde and density in panel (a) apply also to panels (b) and (c). Profiles with hollow markers are highlighted in Figure 4.8.

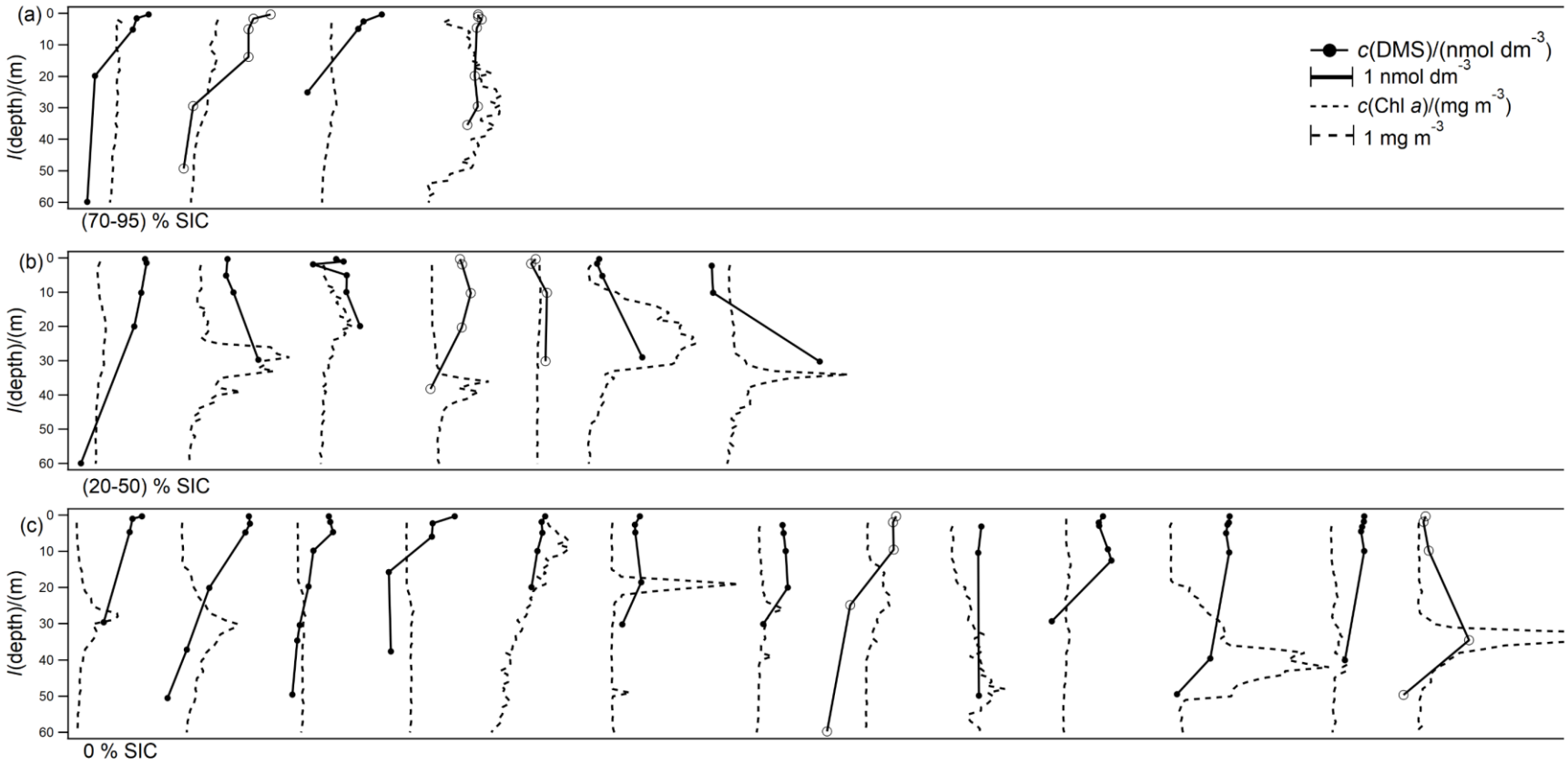

Figure 4.6 Overview plot displaying the shape of all DMS and Chl *a* depth profiles grouped by SIC and staggered along the x-axis for ease of viewing. Labels indicate the SIC bin. The scale bars for DMS and Chl *a* in panel (a) apply also to panels (b) and (c). Profiles with hollow markers are highlighted in Figure 4.8. One of the Chl *a* profiles is cut off in panel (c) for scale purposes.

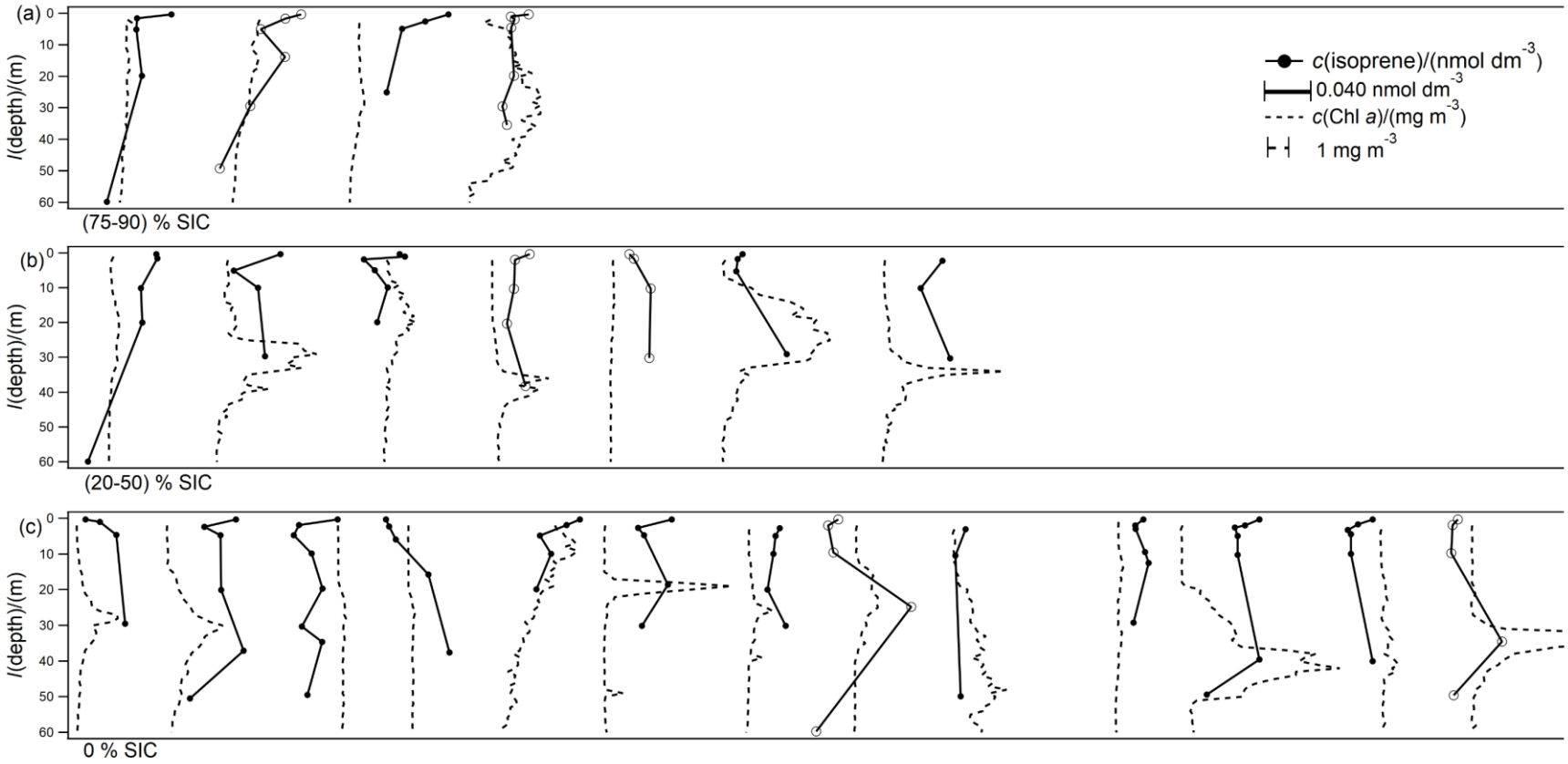

Figure 4.7 Overview plot displaying the shape of all isoprene depth profiles grouped by SIC and staggered along the x-axis for ease of viewing. Labels indicate the SIC bin. The scale bars for isoprene and Chl *a* in panel (a) apply also to panels (b) and (c). Profiles with hollow markers are highlighted in Figure 4.8. One of the Chl *a* profiles is cut off in panel (c) for scale purposes.

Figure 4.3-Figure 4.7 illustrate the variability in the data and also reveal some trends. It appears that SIC, stratification, mixed layer depth, and biology influence the vertical distributions of these VOCs. In the next section, individual casts and further auxiliary data are used to discern trends in the data.

4.5.2 The effect of SIC on VOC depth profiles

A selection of VOC depth profiles collected in the sea ice zone are presented in Figure 4.8, arranged by decreasing SIC. See Figure 4.1 for locations of individual CTD casts. These profiles are chosen from careful examinations of the overview plots as they; (i) represent the typical effect of sea ice on these compounds, (ii) present a higher number of samples collected near the surface and (iii) contain acetaldehyde concentrations which could not be determined for all profiles. I will discuss the effect of SIC on the biogeochemistry in the water column in general and the subsequent impact on the vertical VOC distributions.

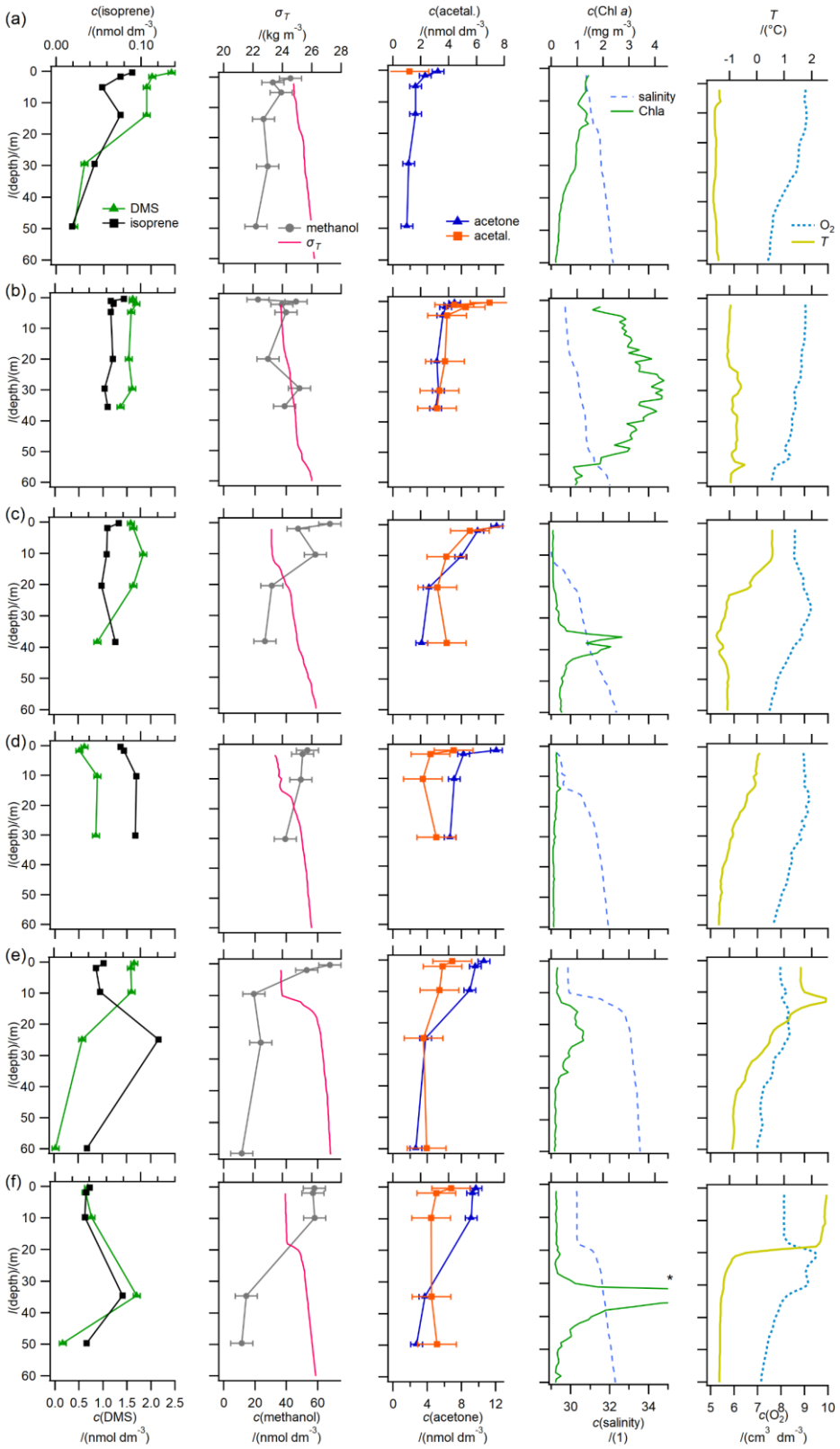

Figure 4.8 Depth profile concentrations arranged by decreasing SIC. Geographical locations of the stations a-f are indicated in Figure 4.1. SIC: (a) 90 %, (b) 75 %, (c) 50 %, (d) 20 %, (e) 0 %, (f) 0 %. (Aetal.=Acetaldehyde, Temp.=Temperature, * Chl a increases up to 13 mg dm^{-3} at the Chl a max). Error bars show measurement noise. (Amundsen Science Data Collection, 2017). Limited measurements of acetaldehyde during the early part of the cruise are due to contamination from the CTD and the single measurement came from the handheld Niskin bottle (30 cm depth).

Effect of SIC on water column biogeochemistry

As shown in Figure 4.8, a well-defined mixed layer was gradually formed as the SIC decreased. The stations with near full ice cover/during ice break up (following the definition of ice breakup by Ahmed et al. (2019)) (75 to 90 % SIC) shown here were weakly stratified but displayed very fine scale density gradients throughout the top 60 m, perhaps due to low wind-driven mixing. In these casts, high concentrations of Chl *a* were found near the surface. These may be in part due to under ice phytoplankton blooms or ice breakup-blooms ,which are frequent features of the Arctic sea ice zone (Levasseur, 2013; Perrette et al., 2011).

Stations with lower ice coverage (20 to 50 % SIC) tended to display a more defined, shallow mixed layer (ca. 10 m depth) and a deep Chl *a* maximum just below the mixed layer, similar to previous observations (Martin et al., 2010). The accumulation of dissolved oxygen near the deep Chl *a* maximum at some of the stations suggests that biology was very active at around this depth (Ardyna et al., 2013; Barber et al., 2015) and that gases produced at this depth were not efficiently vented to the atmosphere.

Ice-free casts (0 % SIC) display a deeper (ca. 20 m depth) and warmer mixed layer – useful indicators for how long these stations have been ice-free (Shadwick et al., 2013). Stratifications were stronger at these ice-free stations, and many of profiles displayed a very pronounced deep Chl *a* maximum located below the mixed layer. Next I discuss the VOCs profiles, grouped into oxygenated VOCs (methanol, acetone, acetaldehyde) and biogenic VOCs (DMS and isoprene).

Methanol

Casts with near full ice cover (75 to 90 % SIC) displayed somewhat similar concentrations of methanol throughout the top 60 m, while partially ice covered (20 to 50 % SIC) and ice-free casts displayed higher methanol concentrations in the mixed layer and near the surface. Some ice free casts display higher concentration in the top 2-5 m compared to the rest of the mixed layer (Figure 4.3, Figure 4.8). The few other methanol profiles collected in the temperate and tropical Atlantic indicate generally higher concentrations of methanol within the mixed layer than below (Beale et al., 2013; Williams et al., 2004; Yang et al., 2014c). In seawater, methanol is produced by a large range of phytoplankton (Davie-Martin et al., 2020; Mincer and Aicher, 2016) and consumed by bacteria (Dixon and Nightingale, 2012; Sargeant et al., 2016). Higher concentrations near the surface than below at stations

of low ice coverage are consistent with a biological source of methanol in seawater. However, there is no obvious relationship between methanol concentration and Chl *a*. This might be because the balance between biological production and consumption depends on the phytoplankton and bacteria species present (Mincer and Aicher, 2016; Sargeant et al., 2016). Methanol concentrations near the surface tend to be quite variable, which could be due to rapid changes in biological consumption rates with depth (Dixon and Nightingale, 2012). The shape of the methanol depth profiles presented here is remarkably similar to other compounds which display photochemical sources. The shape of these casts does suggest a likely role of light in the methanol depth profile distribution, though previous experiments suggest that direct photochemical production is negligible (Dixon et al., 2013). Higher light intensity has been shown to lead to higher biological methanol production rates (Halsey et al., 2017). Though those experiments used visible light, which is expected to penetrate deeper into the water column (≈ 40 – 50 m (Massicotte et al., 2018)) than ultra violet (UV) light (2-7 m (Tedetti and Semperv, 2006)). The very near surface enhancement in methanol concentrations (within the top ≈ 2 m) could have been in part due to cell lysis caused by damaging ultra violet (UV) light. Cell lysis has been suspected to possibly interfere with previous methanol production rate measurements (Davie-Martin et al., 2020). Lethal levels of UV light have been observed to depths of 2-3 m in the Arctic (Tedetti and Semperv, 2006). Since I only made measurements of concentrations, not rates, I am unable to comment definitively on the dominant production/consumption processes. This is the case for all VOCs discussed here.

Acetone

The stations with highest SIC (75 to 90 %) displayed a rapid decrease in acetone concentrations from the surface down to about 5 m. At stations with lower ice coverage, acetone concentrations decreased rapidly from the surface down to about 20-30 m. At some ice-free stations with a well-defined mixed layer, the concentrations of acetone in the mixed layer were very homogenous and higher than below the mixed layer (Figure 4.4, Figure 4.8). The acetone profiles could be explained by dominant photochemical production of acetone (De Bruyn et al., 2011; Dixon et al., 2013) in the recently ice uncovered water column. Because UV light is rapidly absorbed within the first 2-7 m of the Arctic water column (Tedetti and Semperv, 2006), the photochemical production is more concentrated near the surface. The fine scale vertical gradients of acetone in the ice-covered stations are probably preserved due low wind-driven mixing. As a more defined mixed layer forms, acetone produced at the surface is mixed deeper, forming a fairly

homogeneous profile within the mixed layer. The ice-free casts with homogeneously mixed layers are similar to previous measurements in the open ocean (Beale et al., 2013; Williams et al., 2004). I do not observe an obvious relationship between acetone and Chl *a* in these depth profiles. If light dependent biological production of acetone were an important process in the sea ice zone, I would have expected to detect substantial acetone concentrations at depths where Chl *a* peaked and around the penetration depth of visible light (≈ 40 – 50 m (Massicotte et al., 2018)) required for biological activity. Potentially up to 70 % of the primary productivity is occurring at the deep Chl *a* maximum (Burgers et al., 2020). Earlier incubation experiments suggest that biological production of acetone is negligible (Dixon et al., 2013), while more recent field campaigns (Schlundt et al., 2017) and culture experiments (Halsey et al., 2017) suggest that acetone may have a biological source. It is possible that some of the acetone observed below ≈ 10 m is produced from biological activity.

Acetaldehyde

Most acetaldehyde depth profiles display a rapid decrease in concentration from the surface to about 20 m (Figure 4.5, Figure 4.8). Acetaldehyde concentrations are highly uncertain due to an unquantified interference of CO_2 with the background. The amount of CO_2 within the 60 m near the surface is not expected to vary drastically (Beaupré-Laperrière et al., 2020) and should thus not impact the shape of the acetaldehyde depth profiles. Sharing some similarity to the acetone depth profiles, the rapid decrease of acetaldehyde concentrations from the surface likely suggests a dominant light-dependent source near the surface of the water column, which is supported by a range of scientific literature (Dixon et al., 2013; Mopper and Stahovec, 1986; Zhou and Mopper, 1997; Zhu and Kieber, 2019). In contrast to acetone, acetaldehyde almost never shows a homogenous profile within the mixed layer. This may be because acetaldehyde lifetime in seawater is too short (2 to 5 h (Dixon et al., 2013)) to be mixed homogenously, in contrast to acetone with its longer lifetime in seawater (5 to 55 days (Dixon et al., 2013)). These profiles from/near the sea ice zone are in contrast to previous measurements in the open ocean of the Atlantic where generally similar concentrations of acetaldehyde are observed at the surface and below the mixed layer (Beale et al., 2013; Yang et al., 2014c). These Arctic profiles compare best to depth profiles nearer to land (Beale et al., 2015; Kieber et al., 1990; Zhu and Kieber, 2019). This suggests there are light dependent production processes in these areas affecting acetaldehyde production, either related to terrestrial input or the influence of sea ice, which are not present in the open ocean. In the ocean, it is thought

that 7-53 % (Zhu and Kieber, 2019) or 16-68 % (Dixon et al., 2013) of acetaldehyde in seawater is produced from photochemical activity. The remainder is likely produced in a light-dependent manner from biological activity (Davie-Martin et al., 2020; Halsey et al., 2017). The wavelengths of visible light required to produce acetaldehyde from biological activity are expected to penetrate to ≈ 40 – 50 m (Massicotte et al., 2018), while the wavelengths responsible for photochemical production are expected to penetrate only to 2-7 m (Tedetti and Semperv, 2006). Additionally, the deep Chl *a* maximum only receives 3–10 % of the surface irradiance (Martin et al., 2010), but it is responsible for potentially up to 70 % of net community production (Burgers et al., 2020). Though I might expect a peak in acetaldehyde concentration if biological production was important at the deep Chl *a* maximum. The casts shown here generally show lower concentrations below 30 m, suggesting that the main source of acetaldehyde in this area is probably photochemistry, rather than biological production. Additionally, the acetaldehyde casts from this deployment show remarkable consistency, while Chl *a* (as an indicator for biological activity) was highly variable. This further supports that photochemical production in this area may be the dominant production process of acetaldehyde.

DMS

Stations with near full ice cover (75 to 90 % SIC) display highest concentrations of DMS within the surface 10 m. This could be due bottom-ice algae and ice edge blooms, which are known to be sources of DMS (Levasseur, 2013). Stations with partial sea ice cover (20 to 50 % SIC) and ice-free stations (0 % SIC) display higher concentrations of DMS at deeper depths (ca. 20 m), in part due to the establishment of more a stratified mixed layer (Figure 4.6, Figure 4.8). DMS maxima below the mixed layer are sometimes accompanied by deep Chl *a* maxima, qualitatively similar to previous observations of DMS profiles in oligotrophic waters (Simó et al., 1997) and the sea ice zone (Abbatt et al., 2019). Whether a DMS maximum occurs at the same depth as the deep Chl *a* maximum or not likely depends on the biological community composition (Galí and Simó, 2010; Levasseur, 2013).

Isoprene

Isoprene profiles some show qualitative similarities to the DMS profiles. The stations with highest ice cover (75 to 90 %) display the highest isoprene concentrations at the surface, and the concentrations decrease with depth over the upper 50 m. At lower SIC (20 to 50 %) and in ice-free casts (0 % SIC), the highest isoprene concentrations often occur below the surface, sometimes coinciding with the deep Chl *a* maximum (Figure 4.7, Figure 4.8).

Previous depth profiles from the open ocean showed that isoprene frequently displays subsurface maximum, which can be located either at, above or below the Chl *a* maximum and can be related to the oxygen maximum (Booge et al., 2018; Hackenberg et al., 2017; Tran et al., 2013). The subsurface maximum appears more consistently for isoprene than for DMS. This may be because the production of isoprene, predominantly from photosynthetic activity of phytoplankton, is less dependent on the biological community composition (Srikanta Dani et al., 2017). Additionally, the lifetime of isoprene in seawater is estimated as 7 (Palmer and Shaw, 2005) to 10 (Booge et al., 2018) days, much longer than DMS. This implies that isoprene profiles might be less responsive to rapid changes in biological community composition, thus favouring a more consistent distribution with depth compared to DMS. The deep isoprene maximum suggests that there is substantial isoprene production at depths of 10 m or deeper, also in the sea ice zone.

4.6 Underway seawater measurements

Compared to discrete CTD measurements, the underway measurements presented in this section have a much higher temporal and spatial coverage. Hence, they can be used to derive more robust statistics. I use the underway measurements when comparing to previous near surface concentrations measurements in other parts of the ocean. The underway measurements are in addition used to derive correlations with ancillary measurements and shed further light on the relevant biogeochemical processes.

Underway (3-4 m depth) seawater concentrations of methanol, acetone, acetaldehyde, DMS and isoprene are presented in Figure 4.9 along with the concentrations measured from the 5 m Niskin bottle. Underway sst, SIC, Chl *a* and sss are also presented.

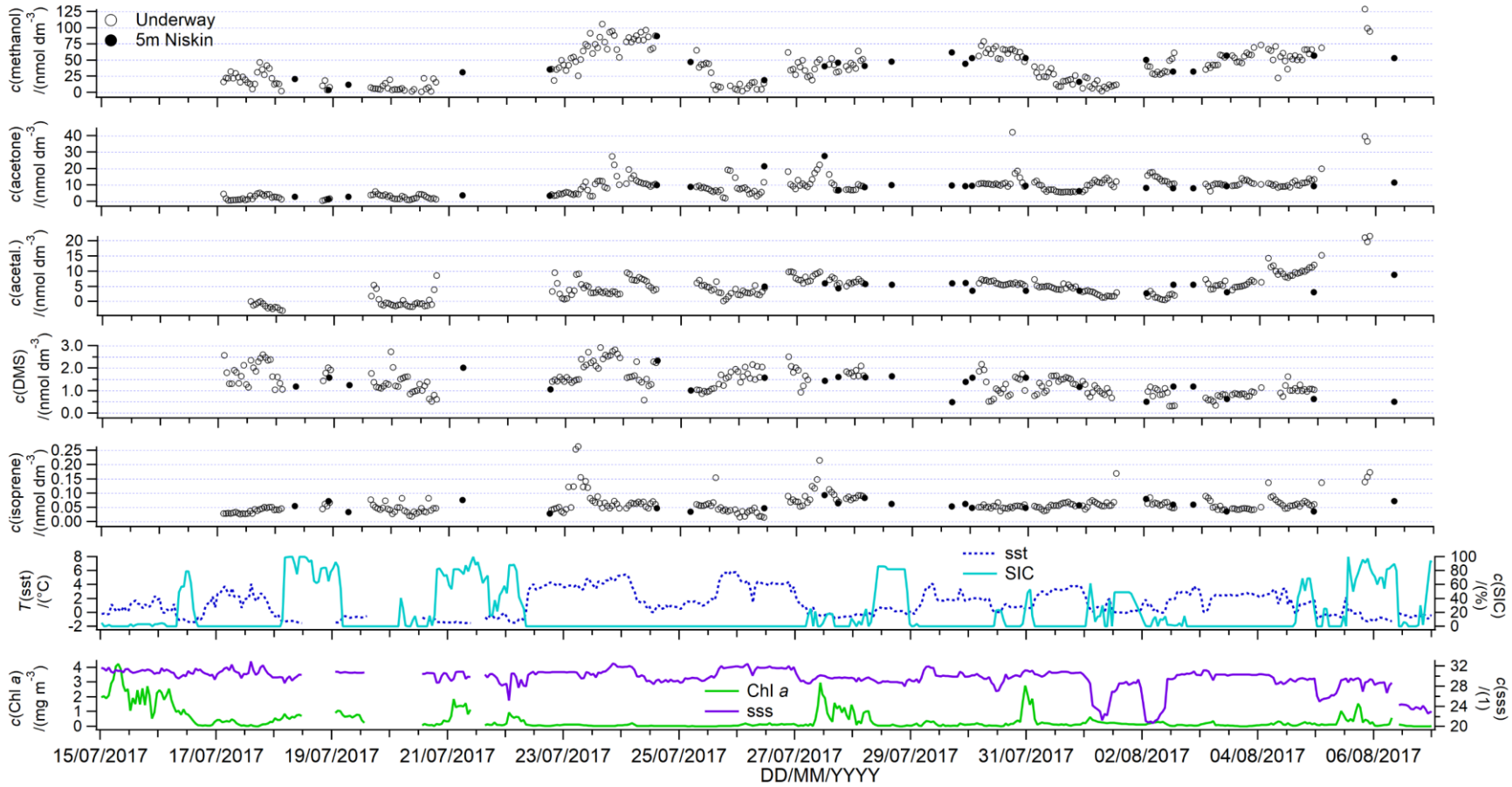

Figure 4.9 Underway surface seawater concentrations of dissolved VOCs measured in the sea ice zone of the Canadian Arctic. Auxiliary data plotted are sst, SIC, Chl *a* and sss.

Methanol

The mean concentration of methanol was 38 nmol dm^{-3} with a median of 36 nmol dm^{-3}, which is within the range of previous seawater measurements (Beale et al., 2013; Kameyama et al., 2010; Williams et al., 2004). Concentrations from this cruise compare well to measurements at UK shelf seas (Beale et al., 2015) and in the Atlantic (Yang et al., 2013a). They are higher than previous measurements in the Labrador Sea in October (Yang et al., 2014a), possibly due to higher seasonal biological activity during this cruise. Davie-Martin et al. (2020) also find higher methanol production rates in more productive waters. Methanol concentrations displayed a large range in concentrations (below limit of detection up to 129 nmol dm^{-3}). This suggests that methanol concentrations are probably not tightly coupled and governed by specific processes. Phytoplankton culture experiments suggest that methanol is produced by a large range of phytoplankton (Mincer and Aicher, 2016). Instead of being controlled by wide spread sources, such as production by a large range of phytoplankton (Mincer and Aicher, 2016), it is possible that methanol concentrations in the sea ice zone are heavily influenced by oxidation rates. Methanol oxidation rates tend to be (a) highly variable (Dixon et al., 2011; Dixon and Nightingale, 2012) and (b) influenced by the microbial species present (Sargeant et al., 2016, 2018). Methanol oxidation rates have also been shown to (c) influence seawater methanol concentrations in coastal waters (Beale et al., 2015).

Acetone

The mean (median) surface seawater acetone concentration measured during this deployment is 8.9 (9.1) nmol dm^{-3} while concentrations displayed a large from 0.3 to 46.7 nmol dm^{-3}. The mean concentration is similar to concentrations measured at UK coastal waters (Beale et al., 2015) and to previous high latitude measurements in the Labrador Sea in October (Yang et al., 2014a) and the Fram Straight in June/July (Hudson et al., 2007). Concentrations from this deployment are generally lower than other temperate and tropical open ocean measurements (Beale et al., 2013; Kameyama et al., 2010; Marandino et al., 2005a; Schlundt et al., 2017; Williams et al., 2004; Yang et al., 2014c). Acetone surface seawater concentrations have been shown to vary seasonally at a temperate site (highest concentrations in summer (Beale et al., 2015), possibly due to the slower oxidation rates and greater photochemical production during the warmer months (Dixon et al., 2014)). Using a machine learning technique, Wang et al. (2020a) also predicted the highest concentrations of acetone in the Arctic in June, July, August of around 8-12 nmol dm^{-3}, in

agreement with my measurements. Episodes of highest acetone concentrations tended to be observed in the sea ice zone of the Canadian Archipelago, possibly suggesting strong sources in sea ice near land.

Acetaldehyde

Mean (median) seawater acetaldehyde concentration was 3.7 (3.9) nmol dm^{-3}. I reiterate that the acetaldehyde concentration measurement is possibly biased due to uncertainty in the background value. Nevertheless, my mean concentration in the Arctic compares well with open ocean concentrations from the Atlantic (Beale et al., 2013; Yang et al., 2014c; Zhu and Kieber, 2019) and the Pacific (Kameyama et al., 2010) as well as measurements in shelf areas (Beale et al., 2015; Schlundt et al., 2017; Zhou and Mopper, 1997). There are episodes of high acetaldehyde concentrations (around 10 nmol dm^{-3}) during this cruise track, which is somewhat surprising given the extremely short lifetime of acetaldehyde in seawater (de Bruyn et al., 2017; Dixon et al., 2014). This suggests localised rapid production processes of acetaldehyde in this area. Production of acetaldehyde is thought to be due to mostly photochemistry (De Bruyn et al., 2011; Zhu and Kieber, 2019) and light-driven biological processes (Davie-Martin et al., 2020; Halsey et al., 2017). High biological (Burgers et al., 2020) and photochemical activity (Ratte et al., 1998; Zhu and Kieber, 2020) combined with 24 h daylight likely led to strong sources of acetaldehyde during episodes of this cruise track.

Correlations between the oxygenated VOCs

In this dataset, underway acetaldehyde and acetone significantly correlate (Figure 4.10a) (the slope and intercept of regressing acetaldehyde vs. acetone is 0.37 and 1.03 respectively, R^2 = 0.35, P=0.000, N=247). Acetaldehyde and methanol also significantly correlate in this dataset (Figure 4.10b) (the slope and intercept of regressing acetaldehyde vs. methanol is 0.08 and 0.34, R^2 = 0.34, P=0.000, N=248). Yang et al. (2014c) have observed similar correlations during a transatlantic transect with R^2 values of 0.29 (acetaldehyde vs. acetone) and 0.25 (acetaldehyde vs. methanol). Likewise, Schlundt et al. (2017) observed significant correlations between acetone and acetaldehyde surface seawater with R^2 values around 0.5 in the South China/Sulu Sea. The correlation between acetone and acetaldehyde is likely due to common photochemical sources in this area. Similarly, acetaldehyde and methanol likely correlate due to common biological sources. I could not find a correlation between methanol and acetone, possibly due predominant biological production of methanol and photochemical production of acetone.

All three oxygenated VOCs measured during this cruise generally display lower concentrations during the first week of sampling, which corresponds to sampling the sea ice zone of the more marine influenced Davis Straight and Baffin Bay area. This may suggest that these compounds display slightly higher concentrations nearer to land, i.e. in the channels of the Canadian Archipelago.

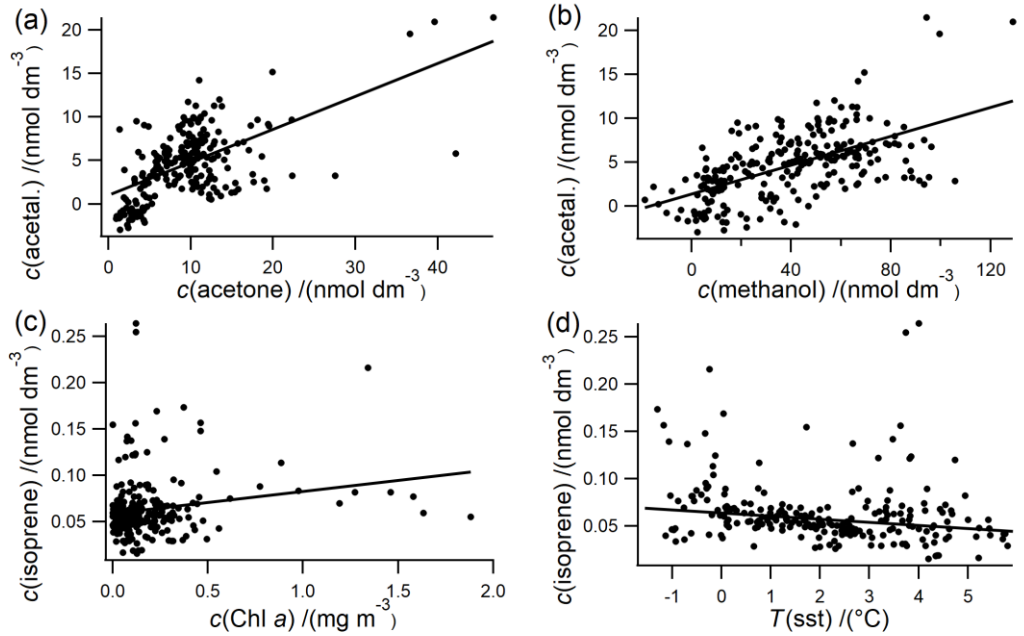

Figure 4.10 Scatter plot between (a) acetaldehyde and acetone as well as (b) acetaldehyde and methanol surface seawater concentrations. Scatter plot of isoprene surface seawater correlation with (c) Chl a and (d) sst.

DMS

The cruise mean DMS concentration was 1.42 nmol dm^{-3}, which is similar to the median concentration of 1.35 nmol dm^{-3}. This is within the range of concentrations measured by Jarnikova et al. (2018) but lower than measurements by Mungall et al. (2016) and Abbatt et al. (2019) in the same region at a similar time of year. Previous measurements generally show the lowest DMS concentrations before ice break up (Bouillon et al., 2002) and during the sea ice minimum (Luce et al., 2011; Motard-Côté et al., 2012).

There appears to be noticeable variability in surface DMS concentrations in the Arctic on both seasonal and inter-annual timescales (Collins et al., 2017). The seawater concentrations measured in Northern Baffin Bay during the cruise presented here show remarkably good agreement with concentrations of approximately 1 nmol dm^{-3} predicted by Galí et al (2019) based on a satellite algorithm. Their satellite algorithm suggests that the majority of the cruise sampling presented here has been carried out after peak DMS

concentrations in this area (Galí et al., 2019). This could be the reason why other investigators have recently measured higher concentrations in this area than me (Abbatt et al., 2019; Mungall et al., 2016).

Isoprene

The mean isoprene concentration was 0.063 nmol dm^{-3}, which is similar to the median concentration of 0.059 nmol dm^{-3}. This is suggesting a relatively normal distribution of isoprene concentrations during this deployment. Overall these isoprene concentrations appear relatively high compared to previous open ocean measurements (Hackenberg et al., 2017; Ooki et al., 2015). Measurements from this cruise compare better to measurements in very biologically productive areas (Baker et al., 2000; Matsunaga et al., 2002; Shaw et al., 2010) and in coastal regions (Baker et al., 2000; Hackenberg et al., 2017; Ooki et al., 2015, 2019; Shaw et al., 2010).

Previous authors have suggested Chl *a* as an indicator of surface isoprene concentrations (Hackenberg et al., 2017; Ooki et al., 2015; Rodríguez-Ros et al., 2020), as isoprene is produced by a range of phytoplankton (Shaw et al., 2010). However, I observe only a very weak positive correlation between underway isoprene and Chl *a* (Figure 4.10c). The slope and intercept of regressing underway isoprene vs. Chl *a* is 0.024 and 0.059 respectively (R^2 = 0.04, P=0.001, N=222). Hackenberg et al. (2017) and Ooki et al. (2015) have suggested a positive correlation between isoprene and sst from open ocean measurements. Contrary to those results, I observe a negative correlation between isoprene concentrations vs. sst during this cruise (Figure 4.10d). The slope and intercept of regressing underway isoprene vs. sst is -0.0030 and 0.0641 respectively (R^2 = 0.12, P=0.01, N=222). These correlations could be due the unique influence of sea ice cover on isoprene concentrations. By inference, parametrizations that predict surface isoprene concentrations as a function of Chl *a* and sst (Ooki et al., 2015; Rodríguez-Ros et al., 2020)), developed based on open ocean measurements, might not be very accurate in the sea ice zone.

4.7 Effect of seasonal sea ice coverage on surface seawater concentrations

The effect of sea ice coverage on the underway seawater VOC concentration is investigated in this section. Underway measurements are used to test whether the trends observed in the CTD depth profiles hold throughout the sampling track.

The hourly underway and 5 m CTD measurements of VOC concentrations have been plotted against the SIC at the time of sampling and bin averaged to 10 % SIC bins (Figure

4.11). A total of 61 hourly underway surface seawater measurements were taken in partial ice cover, which represents 23 % of the underway measurements shown here.

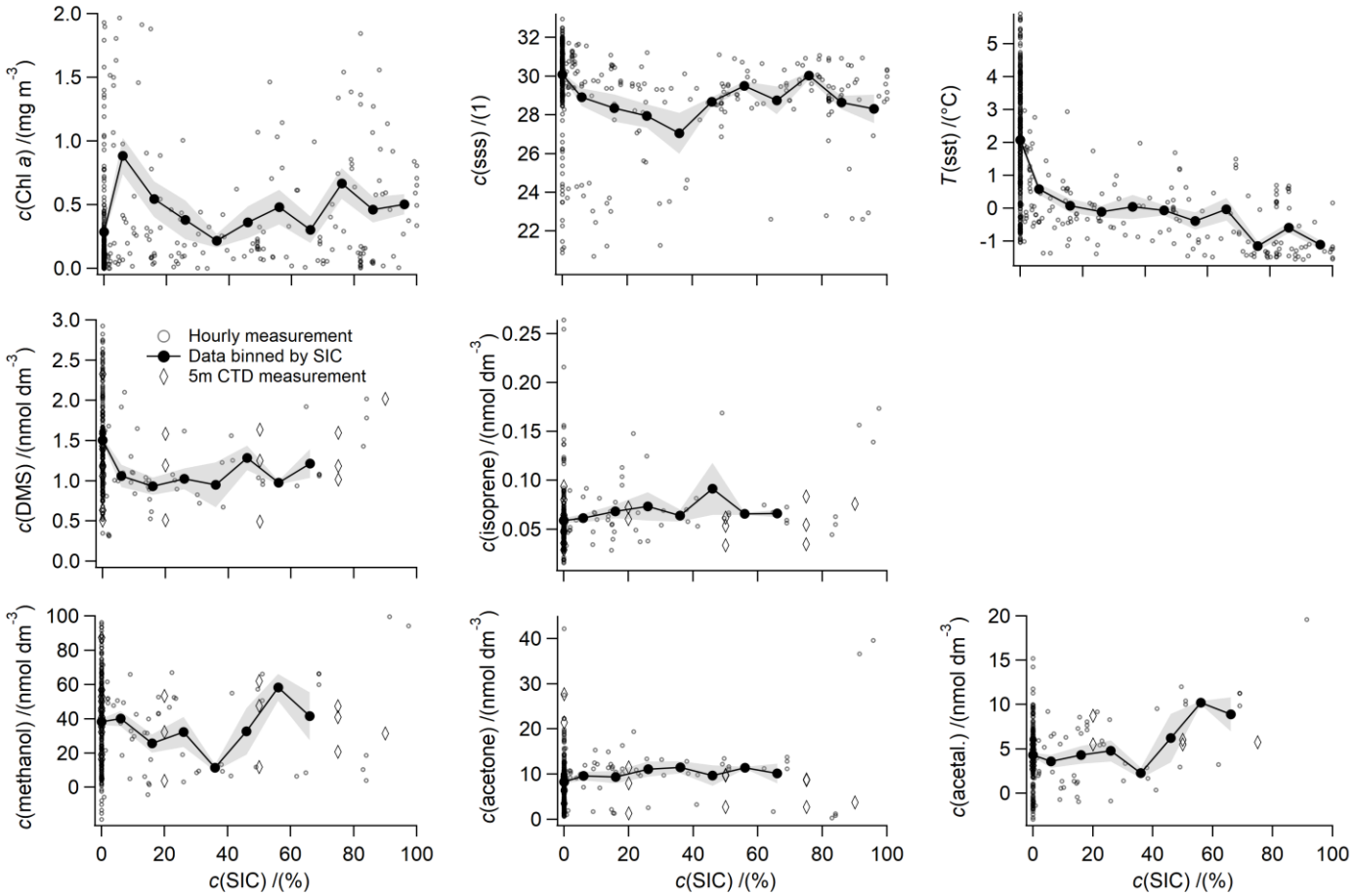

Figure 4.11 Underway auxiliary data and underway seawater VOC concentrations plotted against SIC. The standard error of the SIC bin is indicated as grey shaded area. VOC SIC bins have only been calculated for SIC up to 70 % due to scarcity of data at higher SIC.

Ancillary biogeochemical parameters

The sst gradually increases as the SIC decreases (Figure 4.11). This has been observed previously during an annual cycle in the sea ice zone and is due to ocean heat uptake (Shadwick et al., 2011). It is an indication of how long ago the ice breakup occurred. The data here show similarly low salinities in regions with and without sea ice cover. This is probably because most of the waters sampled here are affected by sea ice, regardless of the ice coverage at the time of sampling . Statistically higher surface Chl *a* concentrations are observed in partially sea ice covered ocean (mean 0.55 mg m^{-3}) compared to no sea ice cover (mean 0.27 mg m^{-3}) (*t*-test, *n1*=202, *n2*=57, *t* stat=-1.7, *t* critical=1.6, p=0.04). This is likely due to under-ice or ice edge blooms which form as the ice breaks up (Barber et al., 2015; Perrette et al., 2011).

Oxygenated VOCs

While near the surface methanol concentration does not appear to depend on SIC, there is a suggestion of acetaldehyde concentration increases with SIC. Excluding data at SIC=0, the slope and intercept of regressing underway acetaldehyde vs. SIC is 0.089 and 1.73 (R^2 = 0.29, P=0.001, N=38). Acetone displays significantly higher mean concentrations in sea ice covered waters (10.9 nmol dm^{-3}) compared to ice-free waters (8.3 nmol dm^{-3}) (*t*-test, *n1*=202, *n2*=61, *t* stat=2.5, *t* critical=1.6, p=0.01). However there doesn't appear to be an obvious relationship between acetone concentrations and SIC at intermediate SIC values.

Higher concentrations of acetone and acetaldehyde in partially sea ice covered ocean could be due to exposure of photolabile CDOM from under the sea ice. Acetone and acetaldehyde both have a photochemical source (Dixon et al., 2013; Kieber et al., 1990; Zhu and Kieber, 2018). The Arctic summertime is a hotspot for photochemical production of volatile organic compounds (Mungall et al., 2017; Ratte et al., 1998). The origin of CDOM has previously been shown to strongly influence the production rate of these compounds (De Bruyn et al., 2011), with unbleached CDOM appearing to be more effective (Zhu and Kieber, 2018). For acetaldehyde and acetone, biological production has also been suggested to be important (Halsey et al., 2017; Schlundt et al., 2017; Zhu and Kieber, 2019) and highest Chl *a* is also observed in partial ice cover. However, in light of an absence of a correlation between Chl *a* and acetone/acetaldehyde, it seems unlikely that these higher concentrations at partial ice cover may be caused by biological production.

Biogenic VOCs

Excluding data collected without sea ice cover, the slope and intercept of regressing underway DMS vs. SIC is 0.0057 and 0.94 respectively (R^2 0.12, P=0.01, N=42). The sea ice zone (Levasseur, 2013)

and the ice edge of the Canadian Arctic Archipelago (Abbatt et al., 2019) have previously been identified as strong sources of DMS. Jarnikova et al. (2018) observed higher surface DMS concentrations near strong gradients in SIC. Higher concentrations in partial sea ice cover could be due to production of DMSP induced by large shifts in salinity and temperature, which is further metabolised into DMS by bacteria (Levasseur, 2013; Wittek et al., 2020).

Excluding data collected without sea ice cover, the slope and intercept of regressing underway isoprene vs. SIC is 0.00024 and 0.057 respectively (R^2 = 0.19, P=0.001, N=42). It is possible that this correlation is driven by some of the points at SIC > 75 %. Higher isoprene concentrations at greater SIC could be due to ice edge blooms and higher biological production (indicated by Chl *a*) in partial sea ice cover. This further supports that isoprene concentrations in the marginal sea ice zone are controlled by different factors compared to the rest of the global ocean (Hackenberg et al., 2017; Ooki et al., 2015).

Potential role of mixed layer depth

It is possible that some of these lower concentrations of VOCs at lower SIC were caused by deepening of the mixed layer and consequent dilution, as opposed to a direct effect of sea ice on the production mechanism of these VOCs (this has been shown e.g. for DMS on a global scale (Vallina and Simó, 2007)). To investigate this, I test for correlations between mixed layer depth and VOC concentrations at 2 m at CTD stations. I determine mixed layer depth using data from all stations as the depth which displays a density of 0.3 kg m^{-3} higher compared to the density measured at a reference depth of 3 m (de Boyer Montégut et al., 2004). This gives a very shallow mean mixed layer of 8 m (range 4-18 m). I cannot find a significant correlation between mixed layer depth and any of the surface seawater concentrations. This suggests that the correlations in VOCs with SIC presented above were probably not primarily due to changing mixed layer depth as a function of sea ice cover. I note also that the mixed layer is poorly defined at many of these stations during this cruise and there is likely more exchange between the mixed layer and the underlying waters compared to ocean regions with stronger stratifications.

4.8 Summarising the impact of sea ice cover on seawater VOC concentrations

In this section, I draw on the patterns observed in the depth profiles and the underway data to comment on the overall impact of sea ice cover on the concentrations of these compounds.

To this end, Figure 4.12 is included here as an illustration.

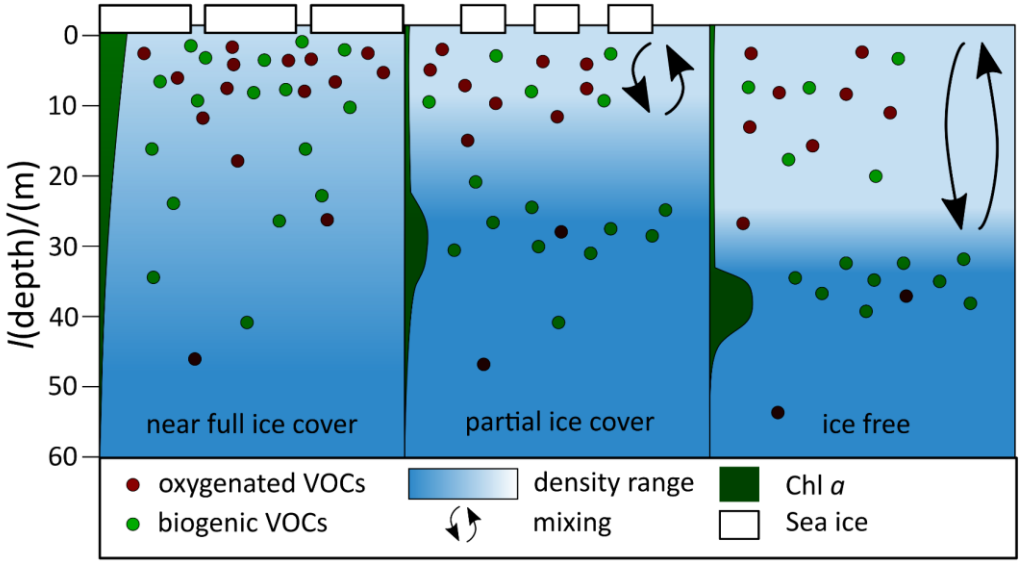

Figure 4.12 Schematic illustrating the effect of different sea ice covers in the Arctic on the concentrations of oxygenated and biogenic VOCs in seawater. Left: Near full ice cover (75 to 90 % SIC), Middle: Partial ice cover (20 to 50 % SIC), Right: Ice free (0 % SIC). Oxygenated VOCs: methanol, acetone, acetaldehyde. Biogenic VOCs: DMS, isoprene. Y-axis indicates depth (ca. 0-60 m).

In nearly full sea ice cover, I observe a weakly stratified water column with gradually decreasing concentrations of Chl *a* within the top 50 m. Oxygenated VOC concentrations display a rapid decrease from the surface within 5 m, although this is less pronounced for methanol. Highest concentrations of the biogenic VOCs are observed at the surface and concentrations decreased gradually within the top 50 m. Such fine scale concentration gradients of these VOCs are likely preserved due to slow mixing (little wind driven turbulence) and fine scale density gradients.

In partial ice cover, a shallow mixed layer of about 10 m is typically observed. Higher surface Chl *a* is observed in partial ice cover compared to ice-free waters. A deeper Chl *a* maximum is observed at some of these stations. The oxygenated VOCs typically display the highest underway concentrations in partial ice cover compared to ice-free. In partial ice cover, oxygenated VOCs also display steady decreases in concentrations from the surface to deeper waters. The biogenic VOCs display higher surface concentrations in partial sea ice cover compared to ice-free and show subsurface maxima, often coinciding with the deep Chl *a* maxima. Higher surface concentrations of biogenic VOCs in partial sea ice cover compared to ice-free waters are likely due to higher biological activity in partial sea ice cover.

In ice-free water, I typically observe a deeper mix layer of about 10 to 18 m. The lowest surface Chl *a* concentrations are often observed in ice-free waters, while a pronounced deep Chl *a* maximum is

observed at some of the stations. Concentrations of oxygenated VOCs, generally peaking near the surface, tend to be lower than in partial ice cover. Surface concentrations of biogenic VOCs are also lower in ice-free casts compared to partially ice-covered waters, with some stations displaying subsurface maxima.

This suggests that SIC exerts a strong influence on dissolved concentrations of VOCs via an interplay between physical drivers (e.g. wind driven mixing, stratification, light penetration) and biogeochemistry.

4.9 Conclusion

This chapter presents depth profiles and underway seawater measurements of methanol, acetone, acetaldehyde, DMS and isoprene in the marginal sea ice zone. The measurements were taken in the Canadian Arctic Archipelago during July/August 2017, i.e. during Arctic summer/sea ice melt. To the best of my knowledge, this represents the first measurements of seawater concentrations of these gases (except DMS) in the marginal sea ice zone and in the Canadian Archipelago.

The unique combination of depth profiles and surface underway measurements was used to assess the effect of sea ice on the concentrations on these compounds. I present overview plots to decipher patterns in the depth profiles and use correlation analyses to assess the surface underway distributions and possible sources of these gases. I generally observe gradually decreasing concentrations of oxygenated VOCs from the surface to about 20 .m in partial ice cover. I also observe higher surface seawater concentrations of oxygenated VOCs in partial sea ice cover compared to ice free, which could be due to photochemical production. Some of the profiles display highest concentrations of the biogenic VOCs at the deep Chl *a* maximum, due to high biological productivity at this depth. Surface underway concentrations of the biogenic VOCs were higher in partial ice cover compared to ice free, largely due to higher Chl *a* concentrations in partial sea ice cover.

The Arctic ocean undergoes strong seasonal variations related to the expansion and decline of sea ice. Measurements presented here suggest that sea ice abundance impacts the surface seawater concentrations of these VOCs. This dataset contains valuable measurements that will hopefully be helpful for elucidating the role of the polar oceans in the global cycling of these VOCs.

4.10 Acknowledgements

These measurements were made possible through a large range of collaborations. Many thanks to Brent Else for providing a berth on the CCGS *Amundsen* to make these measurements possible. I am thankful to Mohamed Ahmed, Dave Capelle and Brian Butterworth for maintaining the PTR-MS

before I joined the vessel. Many thanks to Tonya Burgers for helping me find my feet on the ship. I would particularly like to thank Jonathan Abbatt and Douglas Collins for shipping chemicals and providing a gas calibration standard. Many thanks to Martine Lizotte for providing pure acetaldehyde last minute during mobilisation. Final thanks go to the excellent crew of the CCGS *Amundsen* and the chief scientists Jean-Éric Tremblay and Martine Lizotte.

Some of the data presented herein were collected by the Canadian research icebreaker CCGS Amundsen and made available by the Amundsen Science program, which is supported by the Canada Foundation for Innovation Major Science Initiatives Fund. The views expressed in this publication do not necessarily represent the views of Amundsen Science or that of its partners.

I thank the Institute of Environmental Physics, University of Bremen for the provision of the merged MODIS-AMSR2 sea-ice concentration data at https://seaice.uni-bremen.de/data/modis_amsr2 (last access 11/01/2019).

5 Seawater and ambient air measurements of VOCs in the Atlantic sector of the Southern Ocean

In order to quantify their air – sea gas fluxes, I measured underway seawater concentrations and air mole fractions of methanol, acetone, acetaldehyde, dimethyl sulfide and isoprene in the Atlantic sector of the Southern Ocean, along an approximately 11000 km long transect at approximately 60° S in Feb-Apr 2019. Concentrations, mole fractions, oceanic saturations and calculated fluxes of these simultaneously sampled volatile organic compounds are presented here. To my knowledge these represent the first seawater measurements of methanol, acetone and acetaldehyde in the Southern Ocean. Campaign mean (± 1σ) surface water concentrations of dimethyl sulfide, isoprene, methanol, acetone and acetaldehyde were 2.60 (± 3.94), 0.0133 (± 0.0063), 67 (± 35), 5.5 (± 2.5) and 2.6 (± 2.7) nmol dm^{-3} respectively. In this dataset, seawater isoprene and methanol concentrations correlate positively. Furthermore, seawater acetone, methanol and isoprene concentrations correlated negatively with the fugacity of carbon dioxide, possibly due to a common biological origin. Campaign mean (± 1σ) air mole fractions of methanol, acetone and acetaldehyde were relatively low at 0.17 (± 0.08), 0.081 (± 0.031) and 0.049 (± 0.040) nmol mol^{-1}. I observe diel changes in averaged acetaldehyde concentrations in seawater and ambient air (and to a lesser degree also for acetone and isoprene), which suggest light-driven productions. Campaign mean (± 1σ) net fluxes of 4.3 (± 7.4) µmol m^{-2} d^{-1} DMS and 0.028 (± 0.021) µmol m^{-2} d^{-1} isoprene are determined where a positive flux indicates from the ocean to the atmosphere. Methanol was largely undersaturated in the surface ocean with a mean (± 1σ) net flux of -2.4 (± 4.7) µmol m^{-2} d^{-1}, but also had a few occasional episodes of outgassing. This section of the Southern Ocean varied from being a net source to a net sink for acetone and acetaldehyde this time of the year, depending on location, resulting in a mean net flux of -0.55 (± 1.15) µmol m^{-2} d^{-1} for acetone and -0.28 (± 1.22) µmol m^{-2} d^{-1} for acetaldehyde. To evaluate the importance of air sea exchange in controlling seawater concentrations, I also measured the depth profiles of VOCs. Depth profiles highlighted that surface concentrations are generally representative of mixed layer concentrations and that these VOCs typically display highest concentrations in the mixed layer. The data collected here will be important for constraining the oceanic source/sink of these gases and potentially help to elucidate the processes controlling surface concentrations of these compounds in seawater.

5.1 Introduction

To the best of my knowledge, acetone, acetaldehyde and methanol seawater concentrations in the Southern Ocean have not been measured previously. Thus, their air – sea fluxes and saturations in the Southern Ocean are largely unknown. The Southern Ocean is expected to play an important role in determining the air mole fractions of these compounds in the Southern Hemisphere due to the low land mass and so the paucity of dominant sources such as terrestrial vegetation.

The relatively few high resolution measurements of these VOCs in seawater (Asher et al., 2011; Kameyama et al., 2010; Royer et al., 2016; Tortell, 2005b; Tran et al., 2013) indicate that such short lived gases display spatial variability over scales of tens of kilometres (Asher et al., 2011; Royer et al., 2015) and at times diurnal variability (Takeda et al., 2014). During previous campaigns, ambient air and seawater have rarely been measured at a high enough frequency to explore such spatial/temporal variability (Williams et al., 2004; Yang et al., 2014a, 2014c). In addition to diurnal variability, high-resolution underway seawater concentrations enable investigators to capture hot spots that are important for estimating regional emissions (for example of DMS, Webb et al. (2019)).

In this chapter, I present hourly averaged ambient air and underway seawater and depth profile measurements of a suite of simultaneously measured gases (dimethyl sulfide, isoprene, acetone, acetaldehyde and methanol) from the Atlantic sector of the Southern Ocean during the transition from late austral summer into autumn. A fast alternation between underway ambient air and seawater measurement allows the fluxes and saturations of these gases to be determined at a fairly high resolution using the same instrument. Concurrent measurements of a broad range of gases also enables correlation analyses and identifications of common sources and sinks. By determining the fluxes and measuring these compounds in depth profiles, I will be able to discuss variability with depth and assess the importance of air – sea exchange in controlling surface seawater concentrations of these compounds – something rarely attempted before for OVOCs.

5.2 Cruise and sampling overview

The measurements were made during the ANDREXII cruise from 25/02 to 14/04 2019 on board of the RRS *James Clark Ross* (JCR), which is part of the ORCHESTRA project (https://orchestra.ac.uk/). The vessel transited from the Falkland Islands across Drake Passage to Elephant Island near the Antarctic Peninsula. The vessel then followed a transect along a latitude of approximately 60° S eastwards past the South Sandwich Islands. After that, the vessel transited further east until 30° E, and then followed a return track to repeat some stations and finished in the Falkland Islands. The sampling track of the ANDREXII cruise on board JCR is shown in Figure 5.1 and coloured by Chl *a*. The underway Chl *a* measurements (determined from underway WET Labs WSCHL fluorometer) drifted

substantially during the transect. Here they have been corrected using the fluorescence measured at 5–7 m by a sensor on the CTD rosette (Table 5.1), which itself has not been calibrated in the field against measurements of Chl *a*. Thus the Chl *a* measurements reported here are relatively uncertain. During this deployment, I sampled underway seawater while the vessel was in transit and measured seawater from different depths when the ship was on station. I typically sampled seawater from depths of 5, 25, 50, 75 and 100 m (35 depth profiles total). The auxiliary data for the depth profiles were measured using sensors mounted on the CTD frame listed in Table 5.1. A range of other physical and biogeochemical parameters were also measured underway, such as CO_2 fugacity ($f(CO_2)$) (Kitidis et al., 2012, 2017), sst measured using SBE38 Sea-Bird, and sss monitored using a SBE45 Sea-Bird Thermosalinograph. The $f(CO_2)$ of a seawater sample is one of the four parameters of the seawater carbonate system and refers to CO_2 fugacity as determined by equilibration of seawater with a carrier gas (Zeebe and Wolf-Gladrow, 2001). The time series of underway sss, sst as well as Chl *a* and $f(CO_2)$ data are shown in Figure 5.4.

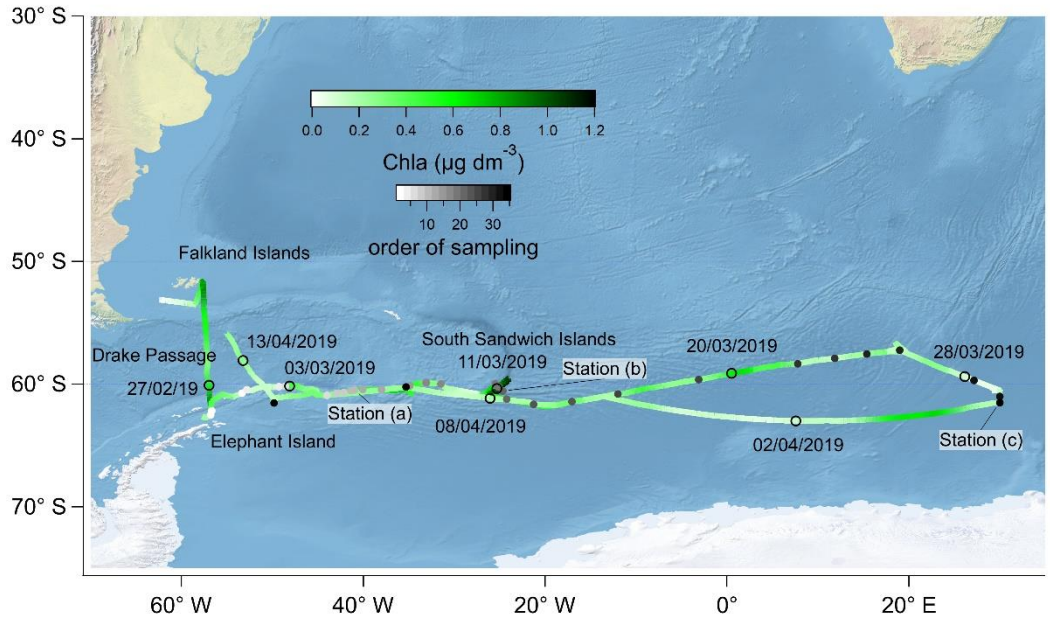

Figure 5.1 Map showing the cruise track of the Antarctic deployment coloured by underway Chl *a*. Hollow circles indicate the date at that location of the cruise track. Labelled stations ((a) to (c)) are highlighted in Sect. 5.8.2.

Table 5.1 A list of CTD depth profile variables and the sensors.

Parameter	Sensor
Oxygen	Seabird SBE43 dissolved oxygen sensor
Salinity	Seabird SBE4C conductivity sensors
Chl *a*	Chelsea Technologies Group AquaTracka Mk III fluorometer
Temperature	SBE35 Deep Ocean Standards Thermometer
Altimeter	Tritech PA200 altimeter

5.3 Installation of the SFCE for seawater measurements

As discussed in Chapter 3, VOCs in seawater and ambient air are measured with a Proton Transfer Reaction-Mass Spectrometer (PTR-MS, High Sensitivity Model by Ionicon) coupled to a segmented flow coil equilibrator (SFCE). The underway seawater inlet of the JCR is situated at approximately 5–7 m depth and set flush with the hull. The SFCE nominally samples from the bottom of a small (ca. 200 cm^3) glass vessel that is overflowing rapidly with underway seawater. In addition to the underway measurements, approximately once a day seawater sampled from the 5m Niskin bottle is measured to verify that the ship's underway seawater inlet does not affect the measured concentrations. There is no significant difference in any of the VOC concentrations sampled from the underway seawater inlet and the 5m Niskin bottle (*t*-test, n=35, $p<0.05$). To sample discrete CTD samples, the underway sampling is interrupted and the SFCE nominally samples from the bottom of a 1 dm^3 glass bottle, typically < 2h after the CTD comes on board.

A thermometer is installed at the seawater exhaust of the SFCE to continuously measure the seawater temperature. This reveals that when using the SFCE continuously with very cold seawater (cruise mean 1 ºC) and zero air cylinders mounted outside on deck, the seawater temperature in the coil only reaches 18 ºC (despite the water bath holding the SFCE set to 25 ºC). This is in contrast to earlier lab measurements and an Arctic deployment, during which the water exiting the SFCE was always 20 ºC with the zero air cylinder housed inside of the lab. The continuously recorded SFCE temperature is used to calculate the Henry's solubility and seawater VOC concentrations for this cruise. SFCE calibrations using MilliQ water (20 ºC) and cold seawater reveal that these gases fully equilibrate regardless of the initial temperature.

5.4 Atmospheric measurements and flux calculations

During this deployment, the SFCE-PTR-MS system was combined with a sampling setup to sample ambient air. In this section I show how the method is automated to measure both underway

seawater and the ambient atmosphere in alternation (Sect. 5.4.1). Details on the atmospheric sampling setup and filtering for ship stack contamination are provided in Sect. 5.4.2. and Sect. 5.4.3.

5.4.1 Combination of the SFCE with atmospheric sampling

The SFCE is combined with an ambient air sampling system to measure underway ambient air and seawater. A schematic of the tubing connections is shown in Figure 5.2. All tubing and connections are made of PTFE (Swagelok).

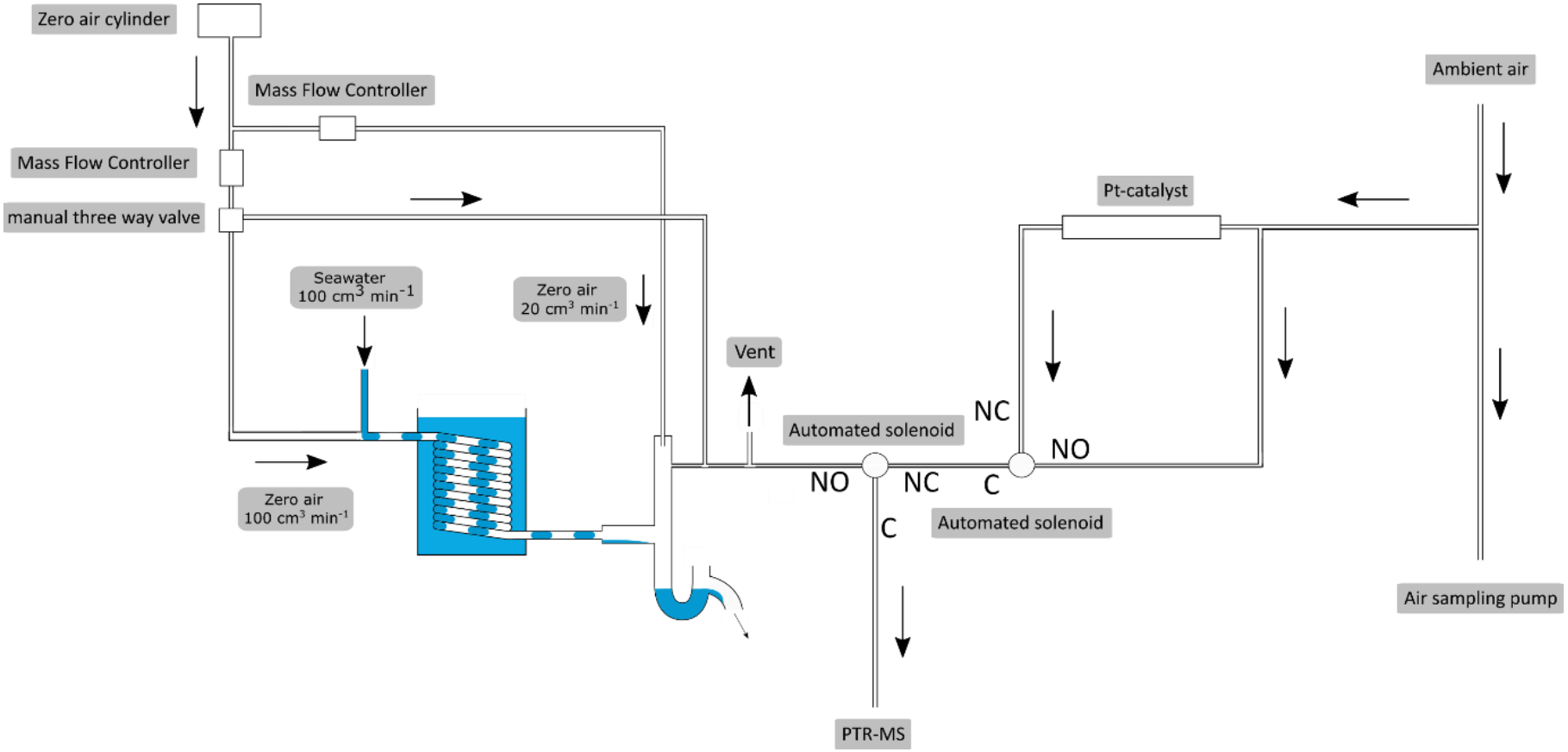

Figure 5.2 Valve connections showing how the SFCE-PTR-MS system is integrated into an existing system for ambient air sampling.

Arrows indicate flow direction. Solenoid Valves controlled by the PTR-MS are indicated as white circles with the letters indicating the valve configuration (C= common, NO= normally open, NC= normally closed).

5.4.2 Atmospheric measurements

For ambient air sampling, an air inlet was installed on a 40 cm pole extending forward from the railing of the walkway in front of the ship's bridge at approximately 16 m above the ocean surface. Ambient air was pumped towards the PTR-MS via a ~90 m PTFE (Polytetrafluoroethylene) air sampling tube (o.d. 9.5 mm, wall thickness 1.5 mm) using a Vacuubrand Diaphragm pump MD 4 NT at a flow rate of circa 30 dm^3 min^{-1}. The residence time of ambient air in the sampling tube was about 6 s, as calculated from the volume of the sampling tube and the gas flow rate. The PTR-MS subsampled from this main sampling tube, upstream of the Vacuubrand pump, at a flow of approximately 100 cm^3 min^{-1}. The sampling tube followed a complex path around the ship, had a number of tight turns, and was mostly sheltered from direct sunlight. I do not expect large particles to make it to the PTR-MS because of the tight turns in the main sampling tube as well as the low subsample flow.

The blank measurements for ambient air mole fractions were made by diverting ambient air through a custom-made Pt-catalyst at 450 ºC. A PTFE solenoid valve (1/8'', Takasago Fluid Systems, controlled by the PTR-MS) was installed downstream of the Pt-catalyst and was used to enable the PTR-MS to either sample outside air directly or outside air passed through the Pt-catalyst. The high efficiency of this Pt-catalyst at oxidizing all VOCs in air to CO_2 is demonstrated elsewhere (Yang and Fleming, 2019). A second PTFE solenoid valve was used to create an hourly measurement cycle of 40 min SFCE headspace (proportional to seawater concentration), 5 min ambient air scrubbed by the Pt-catalyst at 450 ºC (catalyst blank) and 15 min of ambient air measurements.

5.4.3 Filtering of Atmospheric VOC measurements

Ambient air measurements are filtered to remove the influence of ship stack contamination. Firstly, all measurements from during an 8 s sampling cycle are discarded if the mole fraction of benzene or toluene (two fossil fuel additives) is above a threshold of 0.2 nmol mol^{-1}. This is to eliminate small scale contamination from the ventilation pipes on the ship. Secondly, data are discarded if the relative wind speed is less than 4 m s^{-1}. Thirdly, only ambient air measurements with the wind coming from 10–70° either side of the bow are used for further analysis. These clean air sectors are derived from plotting all data against wind speed and direction. Note that air measurements with the wind blowing from the front are excluded to remove the influence of the foremast vents on my measurements. Filtering was carried out using 1 min averaged wind measurements from a Metek sonic anemometer installed on the foremast and resulted in the removal of 55 % of

the ambient air measurements overall. A large fraction of the air measurements is discarded due to the predominant westerly wind direction and the west-east orientation of the cruise track.

5.5 Light-driven contamination in the SFCE

The SFCE was installed near the starboard windows in the main lab. During the early part of the cruise, intense sunlight sometimes shined directly at the SFCE. This led to observations of extremely high headspace mole fractions that were presumably due light-driven production within the SFCE. This effect disappeared instantly after covering the air – water separating tee from direct sunlight. The exact cause of this light-driven contamination in the SFCE system is unclear. Temperature driven outgassing from infrared radiation appears unlikely as the effect disappeared instantly after covering up the air – water separating tee. Photochemical production of isoprene and carbonyl compounds at the sea surface microlayer from UV/visible light has been observed before (Brüggemann et al., 2018; Ciuraru et al., 2015). Although I do not expect substantial amounts of UV light to be present due to absorption by glass windows. Nevertheless, it could be that similar reactions were taking place on the water surfaces inside of the SFCE. The air – water separating tee of the SFCE was thereafter covered from direct sunlight and the blinds were kept closed from 04/03/19 onwards. The effect of this light reduction measure is illustrated in (Figure 5.3). Hence, daytime seawater concentrations of acetaldehyde, acetone and isoprene prior to 04/03/19 are not used in further analysis (deleted data between 7-19 h for acetaldehyde, 8-18 h for acetone, 8-13 h for isoprene, hours in solar time). Daytime data after 04/03/19 does not show any dependence on the ship's heading, indicating that this artefact has been satisfactorily dealt with.

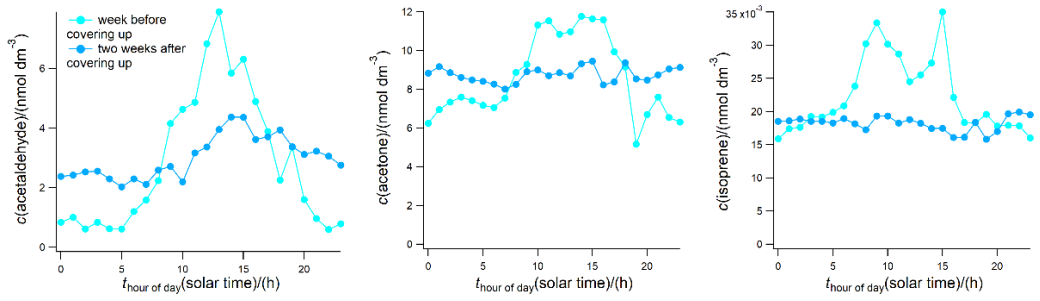

Figure 5.3 Underway seawater concentrations binned in 24 hourly bins for the week before and 2 weeks after protecting the SFCE equilibrator from sunlight on 04/03/19. This illustrates how light driven production of these compounds has been managed by protecting the equilibrator from direct sunlight.

5.6 Ambient air and seawater measurements, saturations, and air – sea fluxes

In the following sub-sections of Sect. 5.6, the ambient air mole fractions and seawater concentrations of DMS, isoprene, methanol, acetone and acetaldehyde as well as their saturations and fluxes are discussed. Saturations below 100 % indicate undersaturation in seawater (i.e. air–to–sea, or negative flux, net ocean sink). The cruise mean seawater concentrations in equilibrium with the atmosphere are indicated in the figure captions (calculated from the measured mean ambient air mole fractions). Measured seawater concentration lower than the equilibrium seawater concentration indicates undersaturation. Two versions of fluxes are presented; fluxes when both ambient air and seawater data are available, and continuous flux estimates despite missing ambient air data (e.g. wind direction out of sector). The latter used a smooth interpolation of the ambient air mole fractions.

Underway auxiliary data collected during this cruise is presented in Figure 5.4. This shows that the highest $f(CO_2)$ values of up to 450 µatm are observed from 01/03/19 through to 03/03/19, which corresponds to sampling of upwelling waters near the Antarctic Peninsula (Amos, 2001; Takahashi et al., 2009). The highest concentrations of Chl *a* (up to 1.2 µg dm^{-3}) are observed directly to the east of the South Sandwich Islands, where the ship undertook a detailed mapping of a phytoplankton bloom (Figure 5.4 shaded area).

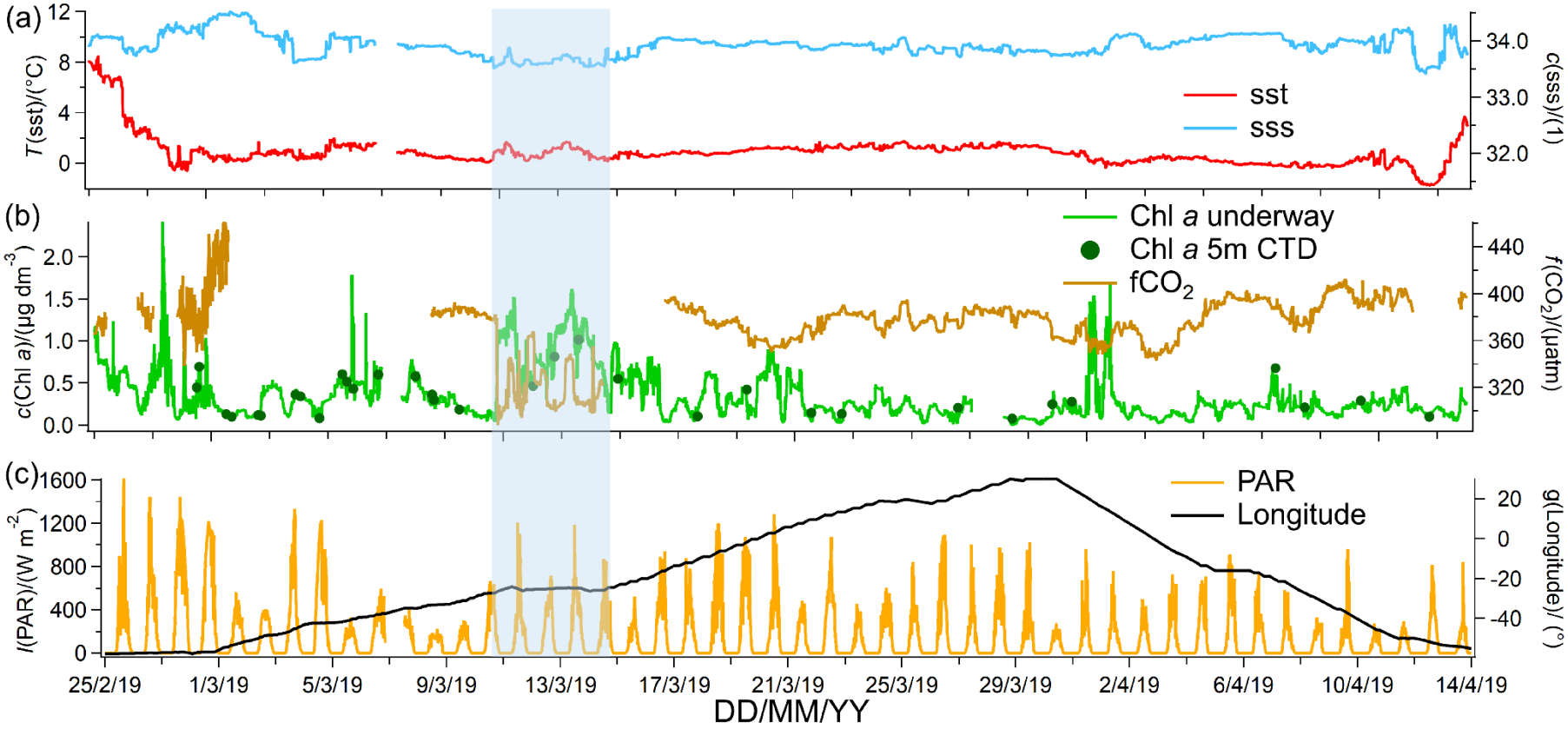

Figure 5.4: (a) Underway sst and sss, (b) Chl *a* concentration measured continuously underway and from the sensor installed on the CTD at 5-7 m depth as well as underway *f*(CO_2) and (c) PAR along with the longitude of the vessel's position. Sampling of the phytoplankton bloom east of the South Sandwich Islands is indicated with a shaded area.

5.6.1 Dimethyl sulfide

The time series of DMS measurements in ambient air and seawater as well as the corresponding fluxes and saturations are presented in Figure 5.5.

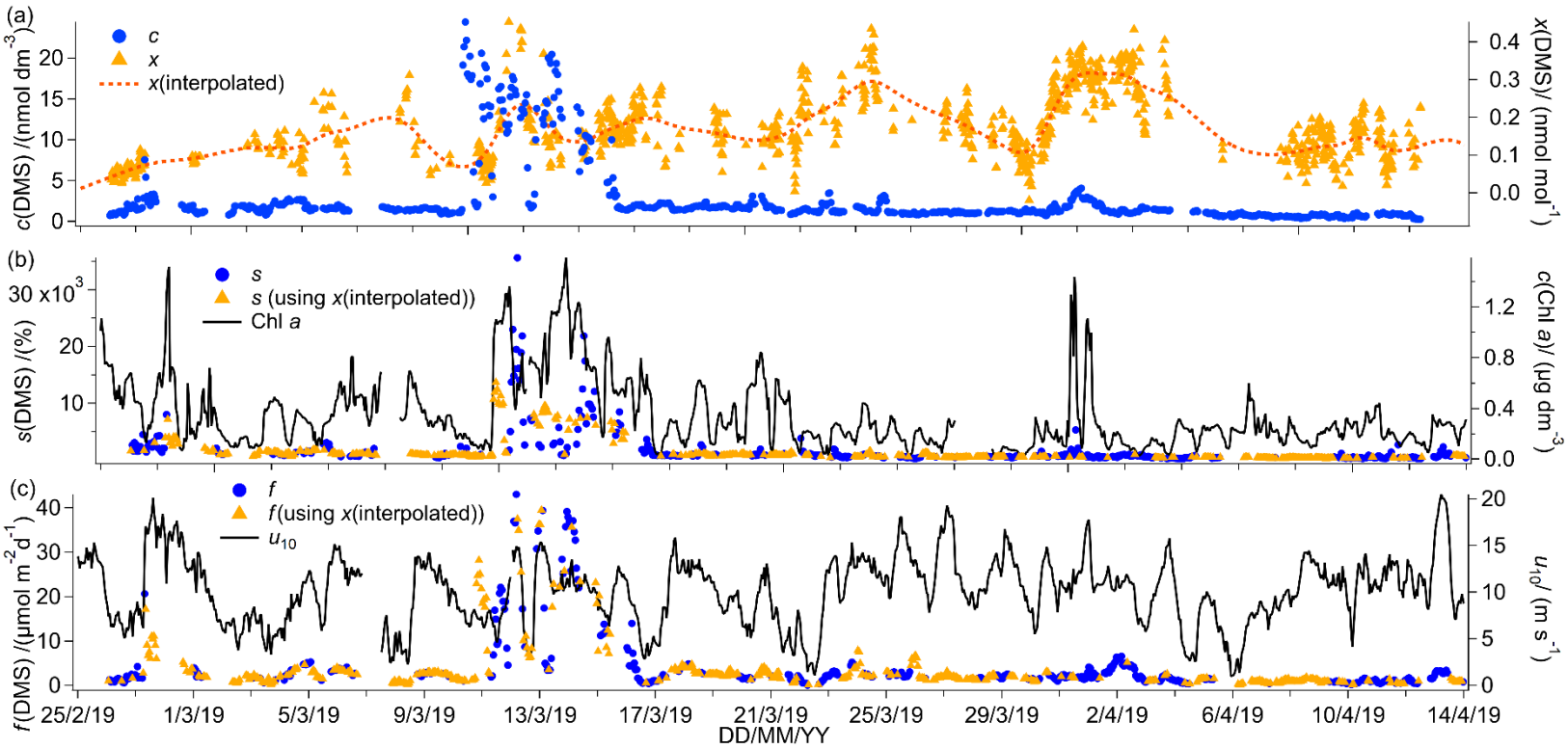

Figure 5.5 DMS ambient air, surface seawater measurements as well as fluxes and saturation. (a) Time series of DMS seawater concentrations as well as measured and interpolated marine boundary layer air mole fractions. (b) Time series of DMS saturations determined using the measured air mole fraction and interpolated air mole fraction with a time series of Chl a. (c) Time series of air – sea DMS fluxes calculated using the measured air mole fraction and interpolated air mole fraction and time series of wind speed. Cruise mean concentration at equilibrium with the atmosphere is 0.20 nmol dm^{-3}.

The campaign mean (temporally averaged) seawater concentration of DMS is 2.60 nmol dm^{-3}. The highest DMS seawater concentrations are observed near the Antarctic Peninsula upwelling region (around 28/02/19, up to 7.55 nmol dm^{-3}) and east of the South Sandwich Islands (around 13/03/19, up to 24.44 nmol dm^{-3}). Chl *a* is also elevated in those regions. These and other fine-scale hot spots of DMS are well resolved due to the use of continuous and fast-responding measurements. To remove the effect of ship sampling bias on the overall cruise mean (e.g. spending multiple days surveying a phytoplankton bloom), the DMS concentrations are first averaged in 1° longitudinal bins. The mean spatially averaged seawater DMS concentration for this campaign is 1.87 nmol dm^{-3} (confidence interval of the mean: 1.46-2.28 nmol dm^{-3}), similar to the Lana et al. (2011) climatology in this region and during these months (average of 1.5 nmol dm^{-3} and range: 0–3 nmol dm^{-3}).

Cruise mean and median ambient air mole fractions of DMS are 0.17 nmol mol^{-1} and 0.16 nmol mol^{-1} respectively. These values are comparable to previous measurements over the Southern Ocean at this time of year (Bell et al., 2015; Colomb et al., 2009; Curran et al., 1998; Guérette et al., 2019; Koga et al., 2014; Yang et al., 2011). Ambient air mole fractions are up to about 0.5 nmol mol^{-1} on occasions, and do not correlate with seawater concentrations. This is probably because air parcels travel much faster than seawater, leading to a decoupling between air and sea DMS distributions.

DMS is strongly supersaturated throughout this cruise track (mean saturation of 1884 %). The campaign mean DMS flux is 4.3 µmol m^{-2} d^{-1}. Fluxes are typically < 7 µmol m^{-2} d^{-1} but exceeded 30 µmol m^{-2} d^{-1} within the phytoplankton bloom encountered on around 13/03/2019. The mean DMS flux from this cruise compares well to direct measurements of DMS flux over the Southern Ocean (Bell et al., 2015; Yang et al., 2011).

5.6.2 Isoprene

The time series of isoprene ambient air and seawater measurements as well as the corresponding fluxes and saturations are presented in Figure 5.6.

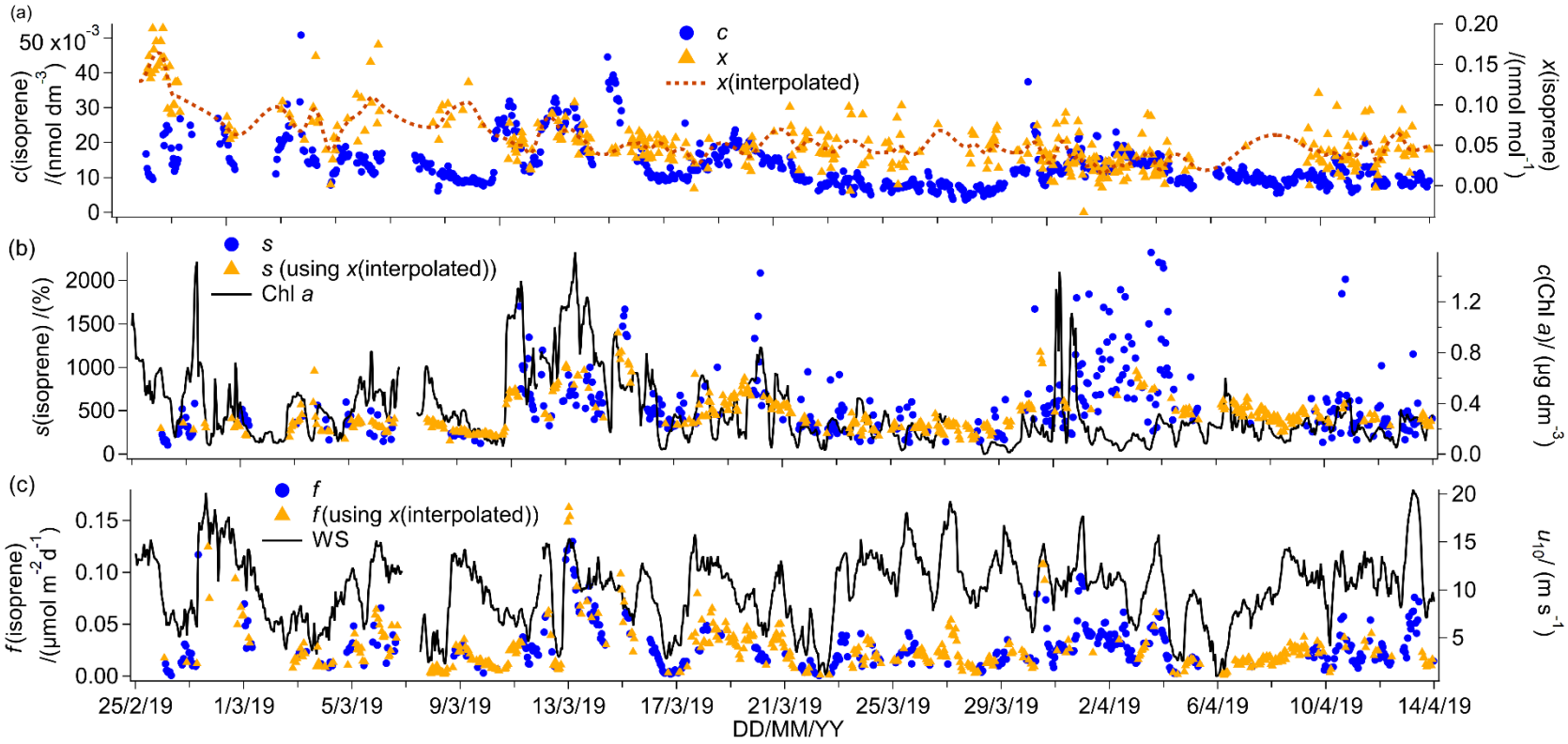

Figure 5.6 Isoprene ambient air, surface seawater measurements as well as fluxes and saturation. (a) Time series of isoprene seawater concentrations as well as measured and interpolated marine boundary layer air mole fractions. (b) Time series of isoprene saturations determined using the measured air mole fraction and interpolated air mole fraction as well as a time series of Chl a. (c) Time series of air – sea isoprene fluxes calculated using the measured air mole fraction and interpolated air mole fraction and time series of wind speed. Cruise mean concentration at equilibrium with the atmosphere is 0.0029 nmol dm^{-3}.

The campaign mean isoprene seawater concentration is 0.0133 nmol dm^{-3}. This is comparable to previous measurements in open ocean (Hackenberg et al., 2017; Ooki et al., 2015) and in the Southern Ocean (Kameyama et al., 2014). Isoprene concentrations as high as 0.040 nmol dm^{-3} are observed near the Antarctic Peninsula and in the phytoplankton bloom near the South Sandwich Islands. These areas are also associated with higher Chl *a* concentration and low $f(CO_2)$.

The slope and intercept of regressing underway isoprene vs. Chl *a* yields a slope of 0.0136 with an R^2 value of 0.35 and an intercept of 0.0087 (P= 0.000, N=799). There also appears to be a first order relationship between Chl *a* and seawater isoprene concentrations in other oceanic basins, but one that typically only explains 37 % (Kameyama et al., 2014), 12 % (Baker et al., 2000) or 52 % (Broadgate et al., 1997) of the variability in observed seawater isoprene concentrations. The regression slope from the cruise presented here, where SST is generally between 0 and 2 ºC, compares best to previous measurements in colder waters. For example, Ooki et al. (2015) find a slope of 0.0143 and intercept of 0.00223 isoprene in waters with temperatures between 3.3–17 ºC. Hackenberg et al. (2017) find slopes of 0.0379 and 0.0341 for SST below 20 ºC in the Atlantic and Arctic Oceans respectively. In General, there appears to be a positive temperature dependence in the isoprene: Chl *a* slope (Hackenberg et al., 2017; Ooki et al., 2015). It is worth reminding here that the underway Chl *a* measurements from this cruise are relatively uncertain.

The dataset presented here shows a significant negative correlation between isoprene vs. $f(CO_2)$ with a slope of -0.00013 and an intercept of 0.0589 (R^2 = 0.33, P=0.000, N=690). This is probably because isoprene is produced by phytoplankton (Dani and Loreto, 2017; Shaw et al., 2010), and high biological productivity tends to reduce seawater $f(CO_2)$ in phytoplankton blooms (Blain et al., 2007; Wingenter et al., 2004). A negative correlation between partial pressure of CO_2 and seawater isoprene concentrations has been reported previously for waters south of 53° S (Kameyama et al., 2014).

The mean ambient air mole fraction of isoprene on this cruise is 0.053 nmol mol^{-1} and the median is 0.045 nmol mol^{-1}, illustrating the positive skewness of the isoprene ambient air mole fractions. This positive skewedness is probably caused by biology- and wind speed-dependent emissions as well as the short lifetime of isoprene in the atmosphere that prevents it from being more fully mixed. Positively skewed atmospheric isoprene mole fractions have also been observed previously over the ocean (Kim et al., 2017). The mean of the measurements presented here compares best to previous measurements over the

Southern Ocean (Colomb et al., 2009; Nadzir et al., 2019; Yokouchi et al., 1999) as well as other biologically productive areas (Shaw et al., 2010).

Isoprene is consistently supersaturated throughout this cruise track, with a mean supersaturation of 760 % and flux of 0.028 µmol m^{-2} d^{-1}. The flux exceeds 0.07 µmol m^{-2} d^{-1} on occasions. These isoprene fluxes compare well to some published estimates from other oceans (Baker et al., 2000; Tran et al., 2013), but they are about 10-fold lower than an estimate from the Southern Ocean by Kameyama et al. (2014). This is probably due to the lower seawater concentrations measured during this campaign compared to the seawater concentrations reported by Kameyama et al. (2014). Fluxes from this cruise are also comparable to direct flux measurements in the Labrador Sea where mean isoprene fluxes were found to be dominated by episodic emissions (Kim et al., 2017).

5.6.3 Methanol

The time series of methanol ambient air and seawater measurements as well as the corresponding fluxes and saturations are presented in Figure 5.7.

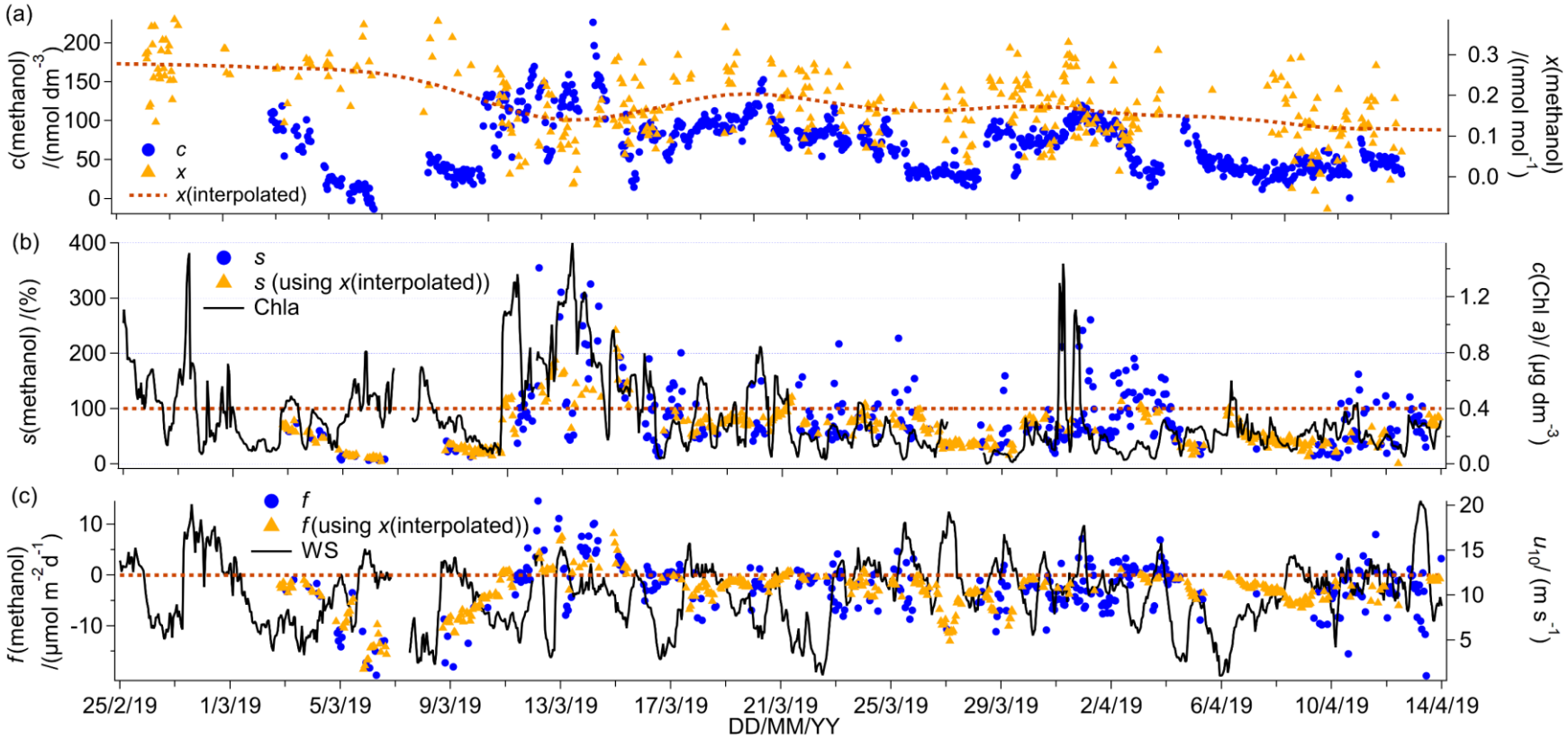

Figure 5.7 Methanol ambient air, surface seawater measurements as well as fluxes and saturation. (a) Time series of methanol seawater concentrations as well as measured and interpolated marine boundary layer air mole fractions. (b) Time series of methanol saturations determined using the measured air mole fraction and interpolated air mole fraction and time series of Chl a. (c) Time series of air – sea methanol fluxes calculated using the measured air mole fraction and interpolated air mole fraction and time series of wind speed. Cruise mean concentration at equilibrium with the atmosphere is 105 nmol dm^{-3}.

Median and mean seawater methanol concentrations are the same at 67 nmol dm^{-3}. The mean seawater concentration is within previously published measurements (Beale et al., 2013; Kameyama et al., 2009; Williams et al., 2004; Yang et al., 2013a, 2014a). Measurements using laboratory phytoplankton cultures suggest that methanol may be produced by a broad range of phytoplankton (Mincer and Aicher, 2016). The slope and intercept of regressing underway seawater concentrations of methanol vs. isoprene gives a significant positive relationship, where the slope is 3524 and the intercept is 22 (R^2 =0.38 P=0.000, N=771). However, seawater methanol concentrations do not correlate significantly with Chl *a*. The correlation between methanol and isoprene suggests that both compounds may be produced by similar phytoplankton species. Measurements of laboratory phytoplankton cultures show that cyanobacteria (*Synechococcus* and *Trichodesmium*) are strong producers of isoprene (Bonsang et al., 2010), but weak producers of methanol (Mincer and Aicher, 2016). *Phaeodactilum*, a temperate diatom, was found to produce large amounts of methanol (Mincer and Aicher, 2016) and moderate amounts of isoprene (Bonsang et al., 2010). *Emiliania Huxley*, a coccolithophore, was observed to produce moderate amounts of both isoprene and methanol (Bonsang et al., 2010; Mincer and Aicher, 2016). On this cruise, methanol significantly correlates with $f(CO_2)$, where a regression yields a slope of -0.97 and an intercept of 422 (R^2 = 0.55, P=0.000, N=651). This provides further evidence for the production of methanol by phytoplankton. No phytoplankton composition measurements were made during the cruise, so I am unable to comment further.

Ambient air mole fractions of methanol are quite low (mean= 0.17 nmol mol^{-1}, median= 0.17 nmol mol^{-1}), in agreement with previous measurements in the Southern Hemisphere (about 0.2 nmol mol^{-1} in the South Atlantic (Yang et al., 2013) and up to 0.54 nmol mol^{-1} above the Southern Indian Ocean (Colomb et al., 2009)). Lower ambient air mole fractions of methanol in the Southern Hemisphere compared to the Northern Hemisphere are probably due to the relatively sparse landmass and vegetation coverage.

The average methanol flux is calculated to be into the ocean with a mean saturation of 83 % and mean flux of -2.4 μmol m^{-2} d^{-1}. The cruise mean seawater concentration of methanol is 67 nmol dm^{-3}, while the concentration at equilibrium with the atmosphere is 105 nmol dm^{-3}. Highest seawater methanol concentrations of up to 226 nmol dm^{-3} are observed in the phytoplankton bloom encountered around 13/03/19. This is higher than previous high latitude measurements in the South Atlantic in the austral spring (Beale et al., 2013; Yang et al., 2014c) and in the Labrador sea in late boreal autumn (Yang et al., 2014a). Instead,

these measurements are similar in magnitude to measurements in the North Atlantic (Beale et al., 2013). The combination of high seawater methanol concentrations and relatively low ambient air mole fractions leads to episodes of outgassing (up to 10 µmol m^{-2} d^{-1}). Net sea–to–air transfer of methanol is somewhat unexpected given the extremely high solubility of methanol. Previous direct flux measurements of methanol along a meridional transect through the Atlantic (Yang et al., 2013a) and in the Labrador sea (Yang et al., 2014a) have shown that the flux of methanol was consistently into the ocean, with the largest air-to-sea flux in regions downwind of continents. Outgassing of methanol from the ocean has been suggested previously for some waters of the North Atlantic (Beale et al., 2013).

In this calculation, I note that the methanol flux is reasonably insensitive to the choice of solubility. If I instead calculate the methanol flux and seawater methanol concentrations using the recommended solubility by Burkholder et al. (2015), the mean seawater concentration of methanol, saturation and flux would be 125 nmol dm^{-3} (26 % higher) 82 % (unchanged), -2.4 µmol m^{-2} d^{-1} (essentially unchanged) respectively. Saturation and flux remain essentially unchanged here because the same solubility is used to calculate both the seawater concentration and concentration at equilibrium with the atmosphere, resulting in cancellation. The change in total gas transfer velocity due to the change in solubility is very small for methanol.

5.6.4 Acetone

The time series of acetone ambient air and seawater measurements as well as the corresponding fluxes and saturations are presented in Figure 5.8.

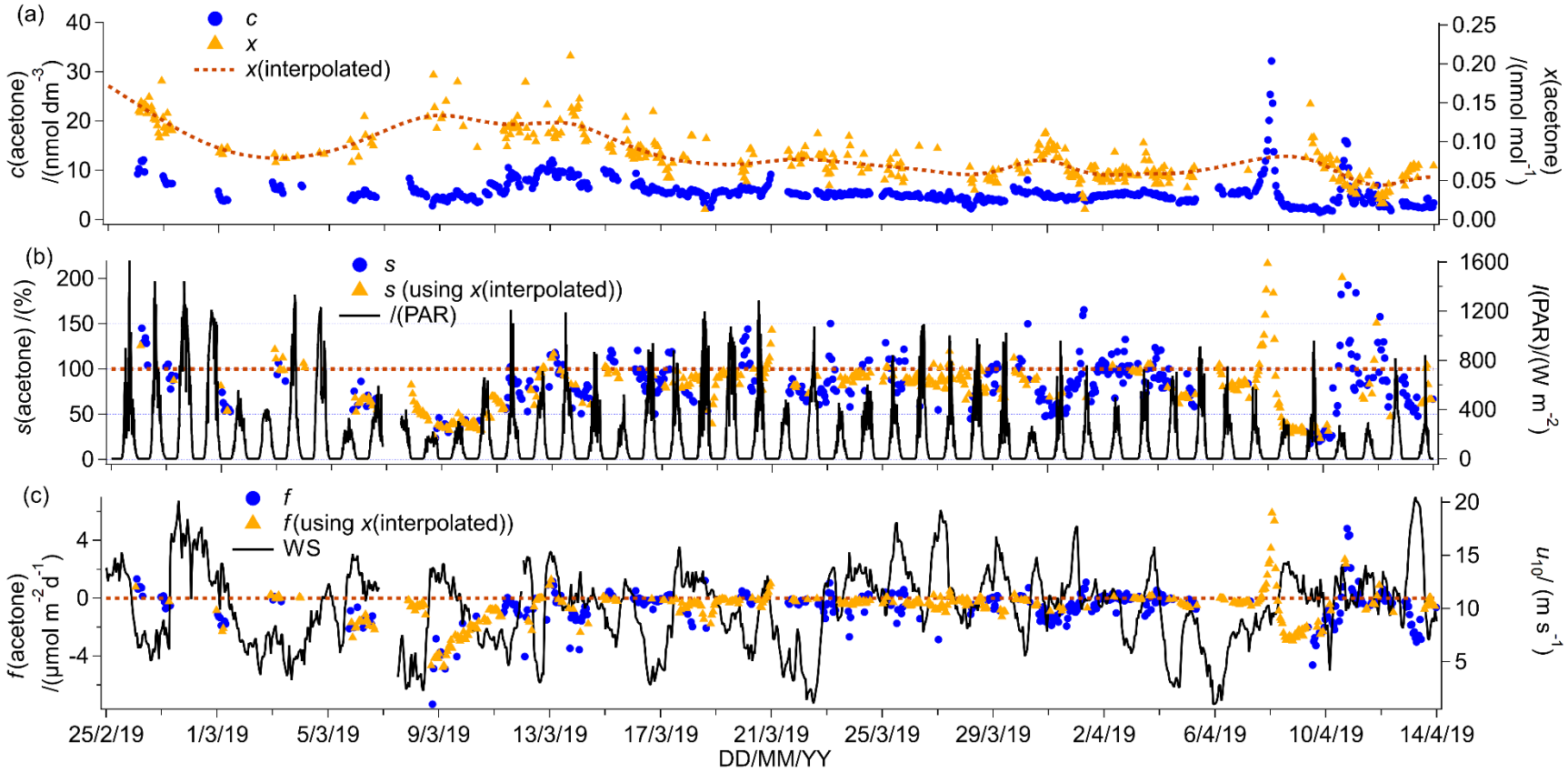

Figure 5.8 Acetone ambient air, surface seawater measurements as well as fluxes and saturation. (a) Time series of acetone seawater concentrations as well as measured and interpolated marine boundary layer air mole fractions. (b) Time series of acetone saturations determined using the measured air mole fraction and interpolated air mole fraction and time series of PAR. (c) Time series of air – sea acetone fluxes calculated using the measured air mole fraction and interpolated air mole fraction and time series of wind speed. Cruise mean concentration at equilibrium with the atmosphere is 6.8 nmol dm^{-3}.

The mean seawater acetone concentration of 5.5 nmol dm^{-3} compares well to previous high latitude measurements of less than 10 nmol dm^{-3} in the South Atlantic (Beale et al., 2013; Yang et al., 2014c) and in the Labrador sea (Yang et al., 2014a). Seawater acetone concentrations from this cruise are also similar to other open ocean measurements (Hudson et al., 2007; Kameyama et al., 2010; Marandino et al., 2005b; Schlundt et al., 2017). The median acetone concentration here is 5.1 nmol dm^{-3} and hence close to the campaign mean. Acetone is mostly thought to be a product of the photochemical degradation of organic matter but could also be directly produced by phytoplankton. The regression between acetone vs. $f(CO_2)$ yields a slope of -0.0469 and an intercept of 22 (R^2 = 0.55, P=0.000, N=671) after excluding high seawater acetone measurements from 08/04/19 and 10/04/19. These elevated data are considered strong outliers (and possibly represent questionable data) as values are higher than the upper quantile plus three times the interquartile range. This correlation of acetone with $f(CO_2)$ suggests a possible role for biology in the production of acetone. Previous investigators have found correlations between seawater acetone concentration and the abundance of haptophytes and pelagophytes (Schlundt et al., 2017), suggesting direct production by phytoplankton and/or bacterial communities associated with these phytoplankton. Taddei et al. (2009) have also observed higher emission of acetone in high Chl *a* areas in the remote South Atlantic. Acetone data presented here shows a weak, although significant positive correlation with Chl *a* concentration where regression analysis yields a slope of 4.84 and an intercept of 4.11 (R^2 = 0.07, P=0.000, N=750). From my data, it is not possible to comment whether photochemical of biological production is dominant for acetone. The underway acetone air and water concentrations on this transect were significantly higher during the day than at night, consistent with light-driven production (see Sect. 5.7).

The mean ambient air mole fraction of acetone measured during this cruise is very low (mean of 0.081 ±0.031 nmol mol^{-1} and median 0.076 nmol mol^{-1}). This is lower than mole fractions reported from clean marine air measurements of 0.188 nmol mol^{-1} at Cape Grim, Tasmania (Galbally et al., 2007), an average of 0.128 nmol mol^{-1} for air blowing off the Antarctic land mass (Legrand et al., 2012), and average marine air measurements of 0.127 nmol mol^{-1} over the South Atlantic at 55° S (Williams et al., 2010). The mean ambient air mole fraction reported here appears considerably lower than earlier modelled acetone air mole fraction over the Southern Ocean of 0.2 about nmol mol^{-1} (Fischer et al., 2012). An updated global budget of acetone predicts slightly lower air mole fractions over the Southern Ocean of 0.1-0.2 nmol mol^{-1} (Brewer et al., 2017). Both models possibly

overestimate air mole fractions above the Southern Ocean, since both have acetone seawater concentrations fixed at 15 nmol dm^{-3}, which is about three times the mean determined during this campaign.

The mean seawater saturation of acetone is 88 %, while the cruise mean seawater concentration at equilibrium with the atmosphere is 6.8 nmol dm^{-3} (cruise mean seawater concentration 5.5 nmol dm^{-3}). Saturations of between 50 and 200 % are typical for acetone (Schlundt et al., 2017; Yang et al., 2014a, 2014c). A mean flux into the ocean of -0.55 µmol m^{-2} d^{-1} during this cruise suggests that the Southern Ocean is generally a net acetone sink this time of the year. Using a *t*-test, the mean acetone flux is found to be significantly different from zero. The 95 % confidence interval of the campaign mean flux is -0.44 to -0.67 µmol m^{-2} d^{-1}. This is within the uncertainties of direct flux measurements of acetone over the Atlantic reported as a mean flux of -0.2 (propagated uncertainty 2.5) µmol m^{-2} d^{-1} (Yang et al., 2014c). The impact of terrestrial emissions on this Southern Ocean dataset appears to be minimal, as no correlation can be observed in the ambient air mole fractions 1) among all the VOCs, and 2) between atmospheric VOCs and atmospheric CO_2. This is contrary to observations by Yang et al. (2014c), who found that methanol, acetone and acetaldehyde ambient air concentrations correlated between each other and with CO_2. These earlier air measurements were taken along a transatlantic cruise, where different airmasses (some impacted by terrestrial emissions) were sampled (Yang et al., 2014c). Global models predict the Southern Ocean to be a weak sink for acetone (Brewer et al., 2017; Fischer et al., 2012), in agreement with my measurements. Confusingly, both global budgets of acetone (Brewer et al., 2017; Fischer et al., 2012) predict that the Southern Ocean is a sink for acetone, despite fixed seawater concentrations at 15 nmol dm^{-3} (for which I calculate outgassing, even at the higher air mole fractions that they predict). This is possibly because both models use the seawater solubility from Benkelberg et al. (1995) (similar to Burkholder et al. (2015)), which is about 30 % higher (more soluble) than the solubility derived from my measurements.

The mean acetone seawater concentration, saturation and flux changed to 8.0 nmol dm^{-3} (45 % increase), 88 % (unchanged) and -0.59 µmol m^{-2} d^{-1} (essentially unchanged) if I instead use the recommended solubility of Burkholder et al. (2015) in these calculations. The saturation and flux in my calculations remain effectively unchanged because the seawater concentration and concentration at equilibrium with the atmosphere change by the same factor, which cancel out. The change in total gas transfer velocity due to the change in solubility is very small for acetone.

5.6.5 Acetaldehyde

The time series of acetaldehyde ambient air and seawater measurements as well as the corresponding fluxes and saturations are presented in Figure 5.9.

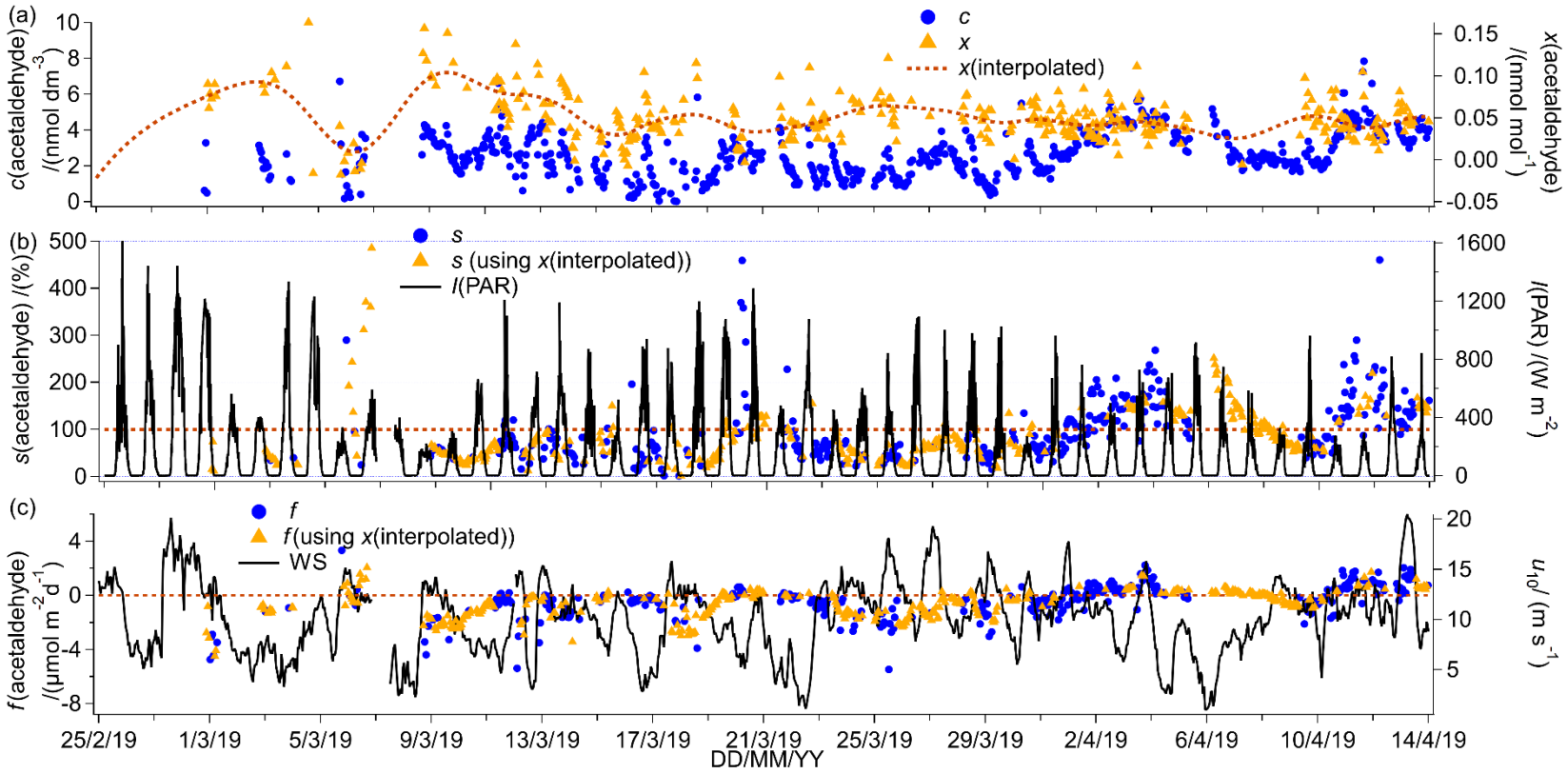

Figure 5.9 Acetaldehyde ambient air, surface seawater measurements as well as fluxes and saturation. (a) Time series of acetaldehyde seawater (SW) concentrations as well as measured and interpolated marine boundary layer air mole fractions. (b) Time series of acetaldehyde saturations determined using the measured air mole fraction and interpolated air mole fraction and time series of PAR. (c) Time series of air – sea acetaldehyde fluxes calculated using the measured air mole fraction and interpolated air mole fraction and time series of wind speed. Cruise mean concentration at equilibrium with the atmosphere is 3.1 nmol dm^{-3}.

The cruise mean seawater concentration of acetaldehyde is 2.6 nmol dm^{-3}, while the median concentration is 2.5 nmol dm^{-3}, suggesting a normal distribution. These acetaldehyde concentrations are relatively uncertain due to background uncertainties. The seawater concentrations measured here are generally lower than 6 nmol dm^{-3}, which compares well to other open ocean measurements (Beale et al., 2013; Kameyama et al., 2010; Schlundt et al., 2017; Williams et al., 2004; Yang et al., 2014c; Zhu and Kieber, 2018), but is lower than measurements near the coast in the English Channel (Beale et al., 2015) and off the West Coast of Florida (Mopper and Stahovec, 1986). No seawater concentrations of acetaldehyde are reported for the first four days of the deployment because of the longer time needed for acetaldehyde to be flushed from the tubing in the SFCE compared to the other VOCs. No significant correlations between seawater acetaldehyde concentrations with $f(CO_2)$ or with Chl *a* are observed, possibly due to rapid oxidation of acetaldehyde in seawater (Dixon et al., 2013) that prevents build-up of significant concentrations.

Mean ambient air mole fractions of acetaldehyde were 0.049 nmol mol^{-1} and appear fairly homogenous and low. Concentrations compare well with the previous atmospheric measurements of Legrand et al. (2012) who observe an average of 0.08 nmol mol^{-1} in ambient air off of the Antarctic continent. These values are consistent with the interhemispheric gradient in acetaldehyde concentrations, where lower ambient air mole fractions of acetaldehyde are generally observed in the Southern Hemisphere (Galbally et al., 2007; Guérette et al., 2019; Yang et al., 2014c). Acetaldehyde shows clear diurnal variability in both seawater and ambient air, which will be discussed in more detail in Section 5.7.

The cruise mean concentration at equilibrium with the atmosphere is calculated to be 3.1 nmol dm^{-3} (cruise mean seawater concentration 2.6 nmol dm^{-3}). Acetaldehyde saturation and fluxes reported from this deployment are highly uncertain due to uncertainties in the seawater concentrations. The mean saturation of acetaldehyde is 88 % with a standard deviation of 50 %, which is comparable to previously reported acetaldehyde saturations (Schlundt et al., 2017; Yang et al., 2014c). This suggests that saturation state possibly changes widely depending on location. The mean flux of acetaldehyde is -0.28 µmol m^{-2} d^{-1} and thus probably into the Southern Ocean this time of the year. Using a *t*-test, the mean acetaldehyde net flux is calculated as significantly different from zero. The 95% confidence interval of the mean acetaldehyde flux reported here is -0.51 to -0.25 µmol m^{-2} d^{-1}. The campaign mean acetaldehyde flux reported here is within the uncertainties of direct flux measurements across the Atlantic of 0.6 (propagated uncertainty 2.5) µmol m^{-2} d^{-1} (Yang et al., 2014c). The Southern Ocean appears to be a weaker acetaldehyde sink than the South China and Sulu Sea, where a flux of -10.11 µmol m^{-2} d^{-1} is estimated (Schlundt et al., 2017), probably due to the higher ambient air mole fractions during that measurement campaign. The fluxes from my works are

in approximate agreement with modelled acetaldehyde fluxes in the Southern Ocean by Wang et al. (2019), who predict that the Southern Ocean is near equilibrium with respect to acetaldehyde.

5.6.6 Summary of correlations in the underway data and critical analysis

In this section, a summary and critical analysis are provided of the surface seawater correlations from this deployment (Table 5.2).

Table 5.2 Summary of significant correlations between seawater variables highlighted during this Antarctic deployment. P-values and t values were determined using two-tailed tests.

correlation	Sign of the correlation	R^2	p-value	T value
c(isoprene), *c*(Chl *a*)	+	0.35	<0.0001	20.3
c(isoprene), *f*(CO_2)	-	0.33	<0.0001	-18.5
c(methanol), *c*(isoprene)	+	0.38	<0.0001	21.8
c(methanol), *f*(CO_2)	+	0.55	<0.0001	-28.5
c(acetone), *f*(CO_2)	-	0.55	<0.0001	-8.9
c(acetone), *c*(Chl *a*)	+	0.07	<0.0001	10.8

Table 5.2 illustrates that the correlations from this dataset are statistically significant (as demonstrated by t values and p-values). The number of data points for each correlation is sufficiently high (between 651 and 799) and thus the critical t-values are identical at 2.0. These correlations can generally only explain 55 % or less of the variability. This is likely because there are other factors that control the abundance of these compounds. Using these correlations to predict concentrations will thus only be of limited value. Nevertheless, these correlations can give some indication to the biogeochemical processes that control these gases in the surface of the Southern Ocean.

To look into the distribution of these data in more detail, scatter plots are shown in Figure 5.10, where the data collected in the bloom are highlighted.

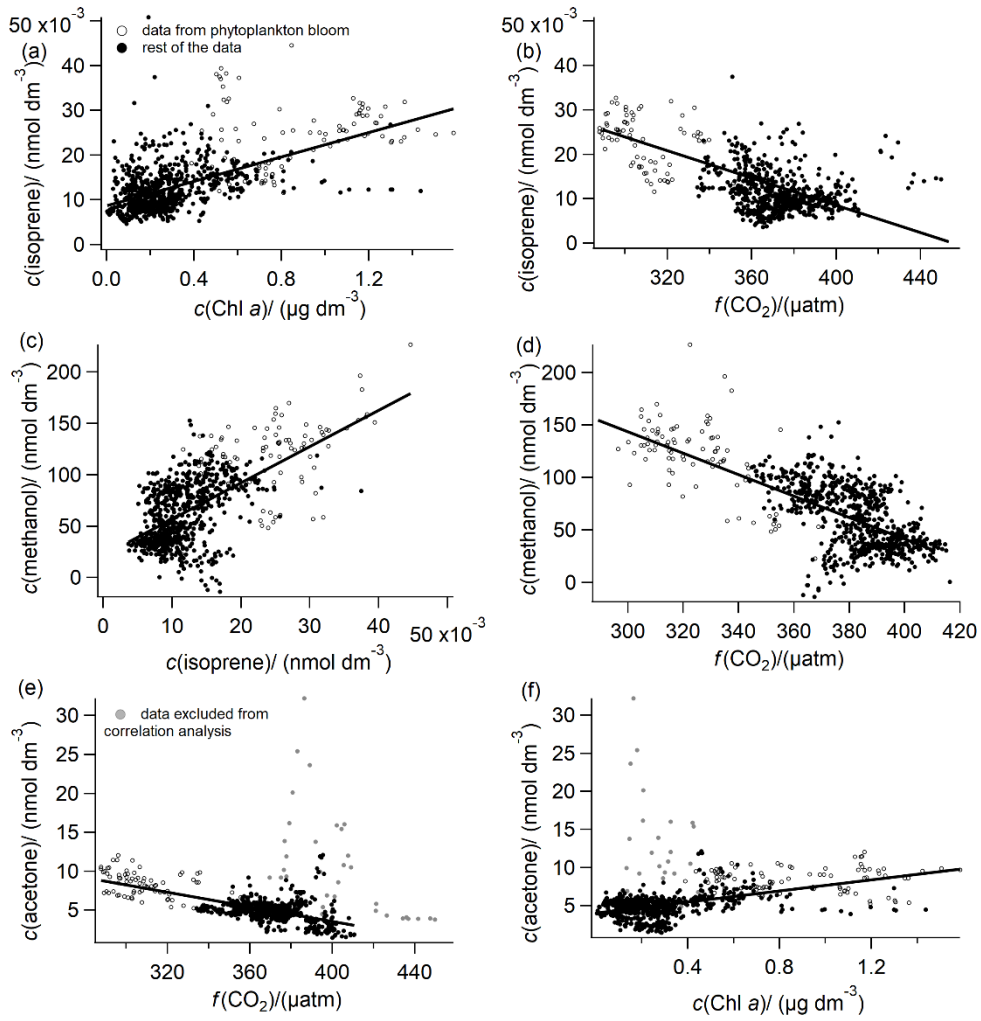

Figure 5.10 Scatter plots of the correlations highlighted in this analysis. Data collected during the phytoplankton bloom is highlighted as hollow circles.

Figure 5.10 illustrates that for many of the correlations, the data collected in the bloom tends to cluster on the extremity of the correlation. It seems that these points have a strong "leverage" on the overall correlation. Thus it is possible that some of these correlations were specific to this deployment and could be coincidental (e.g. waters inside and outside of the bloom have very different $f(CO_2)$, Chl *a*, and VOC concentrations).

5.7 Diurnal variations of acetaldehyde, acetone and isoprene in air and surface water concentrations

To investigate diurnal variability, the measurements of acetaldehyde, acetone and isoprene presented here are grouped in 24 hourly bins corresponding to the local solar time and then averaged. Diurnal variations are also presented as concentrations normalised by the respective daily mean concentrations and then binned. This second approach reduces the impact of spikes and short-term variability on the overall bin mean, as reflected by the generally lower relative standard

deviations. These results are shown in Figure 5.11. In the following discussion, time indicated as “h” refers to the hour of the day in local solar time.

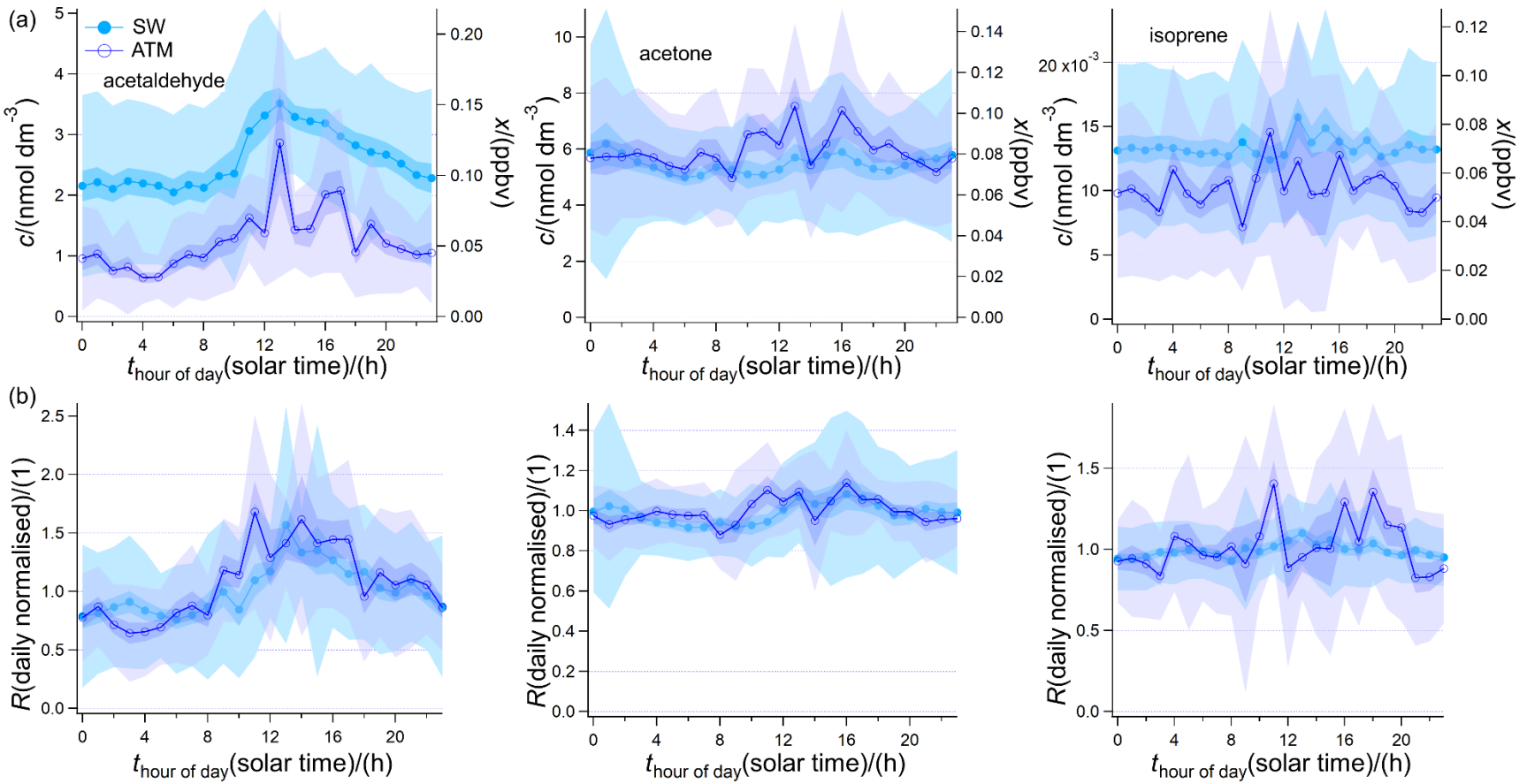

Figure 5.11 Diurnal variations in seawater and atmosphere of acetaldehyde, acetone and isoprene. This is expressed (a) as true 24 hourly averaged concentration/mole fractions and (b) daily normalised concentration where the hourly measured concentration is divided by the average of the 24 hours that this measurement is part of. Light shaded areas show the standard deviation of each hourly bin and the darker shaded areas show the standard error of each hourly bin.

Each hourly mean shown in Figure 5.11 is based on between a minimum of 8 (13–15 h) and a maximum of 25 (4 h) hourly measurements. Daytime is defined as 6–18 h for this analysis, which corresponds on average to the 12 hours of daylight. Hourly mean daytime acetaldehyde seawater concentration is 2.9 nmol dm^{-3}, which is 26 % higher than the mean night-time concentration of 2.3 nmol dm^{-3} (t=-3.7, P=0.002). Acetaldehyde air mole fractions are also found to be significantly different between daytime (avg: 0.061 nmol mol^{-1}) and night-time (avg: 0.040 nmol mol^{-1}, t=-3.7, P=0.001), a change of 53 %. Significantly different seawater acetone concentrations are also observed during daytime (avg: 6.3 nmol dm^{-3}) compared to night-time (avg: 5.8 nmol dm^{-3},t=-3.8, P=0.001), which amounts to 9 % difference. Acetone air mole fractions varied between on average 0.076 nmol mol^{-1} at night and 0.086 nmol mol^{-1} during the day, again a small (13 %) but significant difference (t=-3.5, P=0.003). Daytime seawater isoprene concentrations (avg: 0.0143 nmol dm^{-3}) are significantly higher than night-time concentrations (0.0133 nmol dm^{-3}, t=-3.3, P=0.004) by 8 %. Daytime isoprene air mole fractions (avg: 0.056 nmol mol^{-1}) are significantly higher than night-time isoprene air mole fractions (avg: 0.050 nmol mol^{-1}, t=-2.6, P=0.020) by 12 %. The large standard deviation compared to the standard error of each hourly bin illustrates the large variability in concentrations of these gases. The diurnal cycle becomes obvious in the overall bin-averages thanks to the large number of hourly underway samples, which reduces random noise and averages out much of the other variability. The amplitude of the daily cycle of any of these gases does not correlate to the light intensity, likely because of other sources of variability.

Over the southern Indian Ocean, previous investigators have found diel changes in ambient air acetaldehyde, acetone and isoprene mole fractions of up to a factor of 4, 10–15 % and up to a factor of 2 respectively with maxima when solar intensity was highest (Colomb et al., 2009). The amplitude and timing of these diurnal changes compares well to the observations presented here. The remoteness of the sampling location and the paucity of other sources possibly makes it easier to detect a diurnal cycle in the ambient air mole fractions in this dataset. It is possible that diurnal changes in atmospheric boundary layer hight (not measured on this transect) and subsequent dilution could also have some impact on the air mole fractions.

Acetone is mostly undersaturated during an average diurnal cycle and only between 14 and 15 h did the saturation increase up to 120 %. This suggests that acetone is most likely to outgas during the daytime when seawater concentrations typically peak. This is because the diel cycle in seawater acetone concentrations is greater than the diel cycle in atmospheric mole fractions. The 24 hourly averaged saturation of acetaldehyde shows a lot of variability. The mean daytime saturation of acetaldehyde is not found to be significantly different from the mean night-time saturation. I thus conclude that the diurnal cycles in acetone and acetaldehyde ambient air mole fractions and

seawater concentrations are most likely not driven by air – sea exchange, but instead by in situ processes. Binning the isoprene flux in 24 hourly bins also showed that the night-time flux is not significantly different from the daytime flux. This suggests that the higher daytime isoprene ambient air mole fractions are not due to increased outgassing of isoprene, but more likely due to in situ processes in seawater and the atmosphere.

5.8 VOC depth profiles

In this section, I discuss the depth profiles collected during this deployment. In the first sub-section, I show overview plots with all the depth profiles arranged in waterfall plots in the sampling order along with some of the auxiliary data. I move on by discussing the data using selected casts along with more extensive auxiliary data.

5.8.1 Overview plots

Waterfall plots displaying all of the casts in the order they were sampled (Figure 5.1) along with some auxiliary data are presented in this section. Casts are staggered along the x-axis for ease of viewing (Figure 5.12-Figure 5.16). The data are presented as unitless as it is offset by varying amounts on the waterfall graph to accommodate all of the casts. This allows me to focus on the shape of the depth profiles.

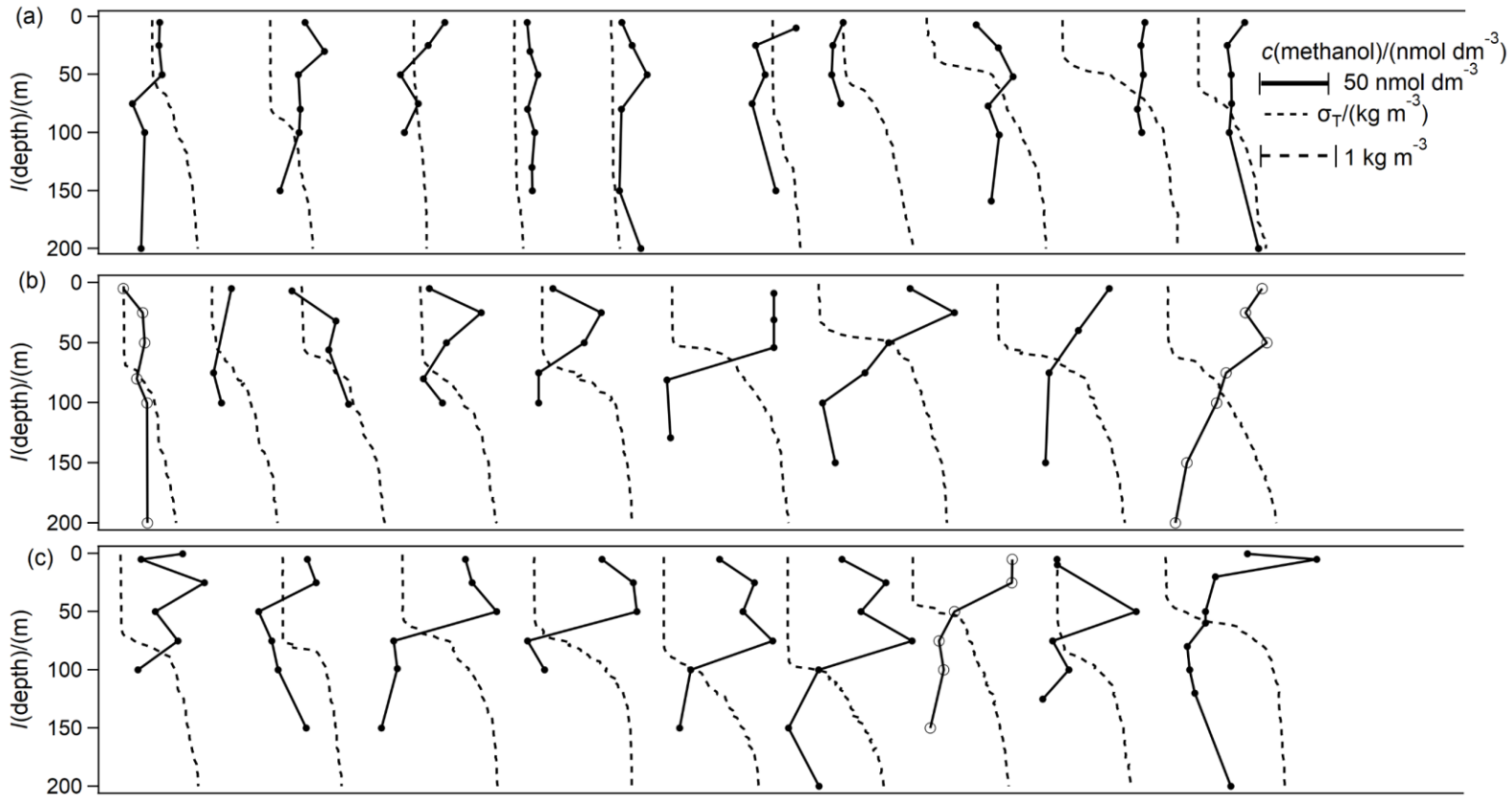

Figure 5.12 Overview plot displaying the shape of all methanol and density (σ_T) depth profiles staggered along the x-axis for ease of viewing. The scale bars for methanol and density in panel (a) also apply to panels (b) and (c). Profiles with hollow markers are highlighted in Figure 5.17.

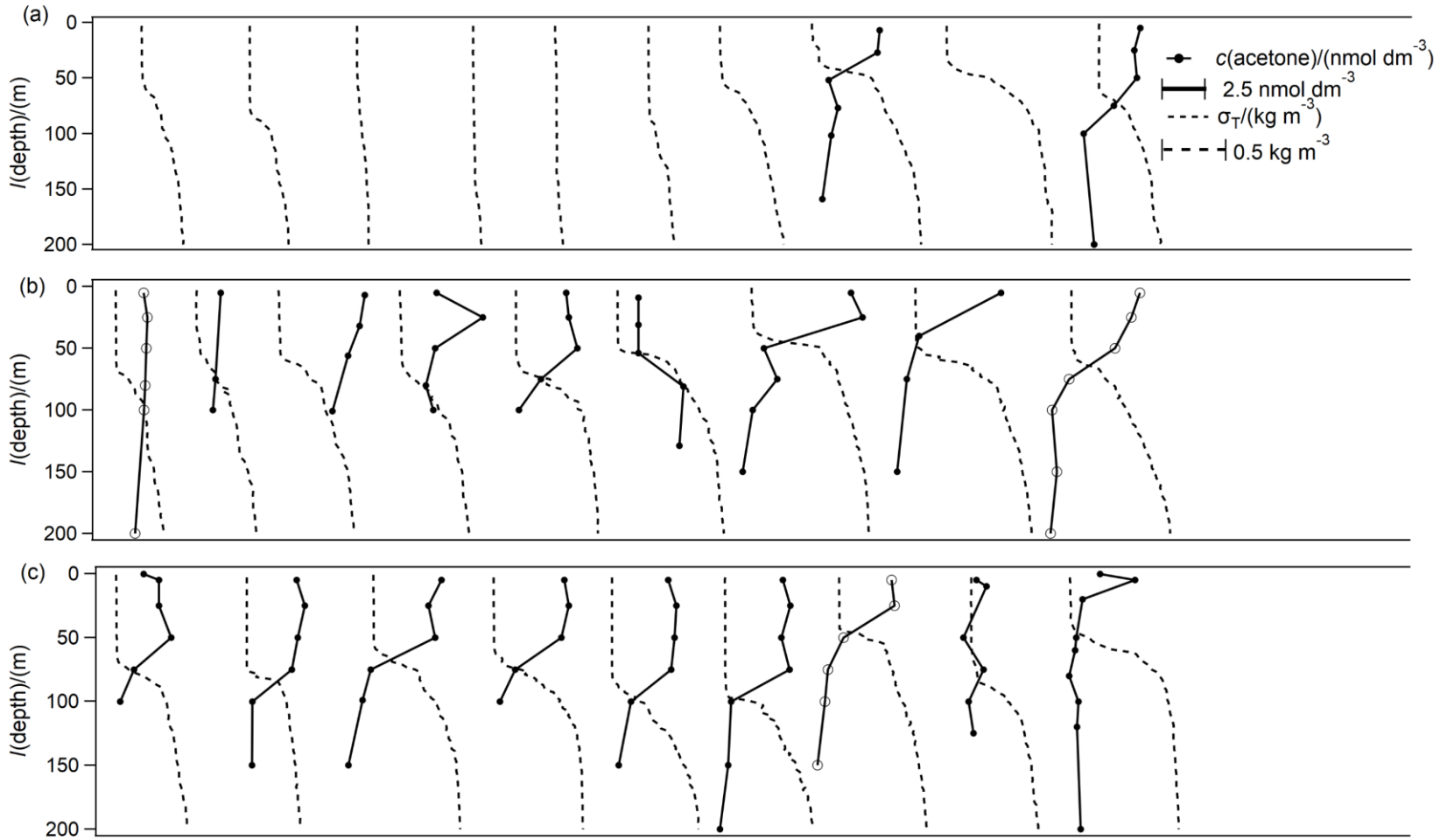

Figure 5.13 Overview plot displaying the shape of all acetone and density (σ_T) depth profiles staggered along the x-axis for ease of viewing. The scale bars for acetone and density in panel (a) also apply to panels (b) and (c). Profiles with hollow markers are highlighted in Figure 5.17.

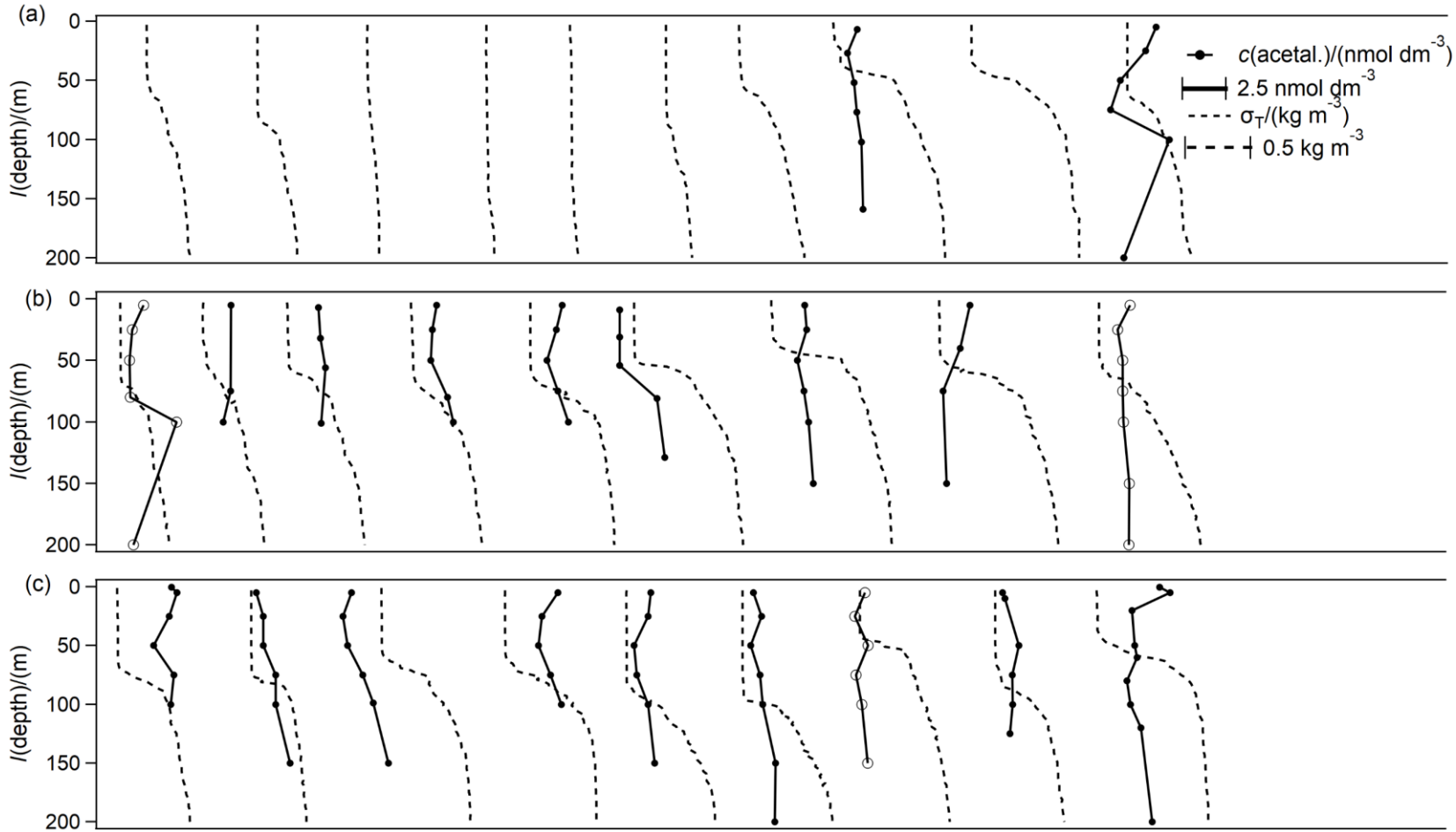

Figure 5.14 Overview plot displaying the shape of all acetaldehyde and density (σ_T) depth profiles staggered along the x-axis for ease of viewing. The scale bars for acetaldehyde and density in panel (a) also apply to panels (b) and (c). Profiles with hollow markers are highlighted in Figure 5.17. (acetal. = acetaldehyde)

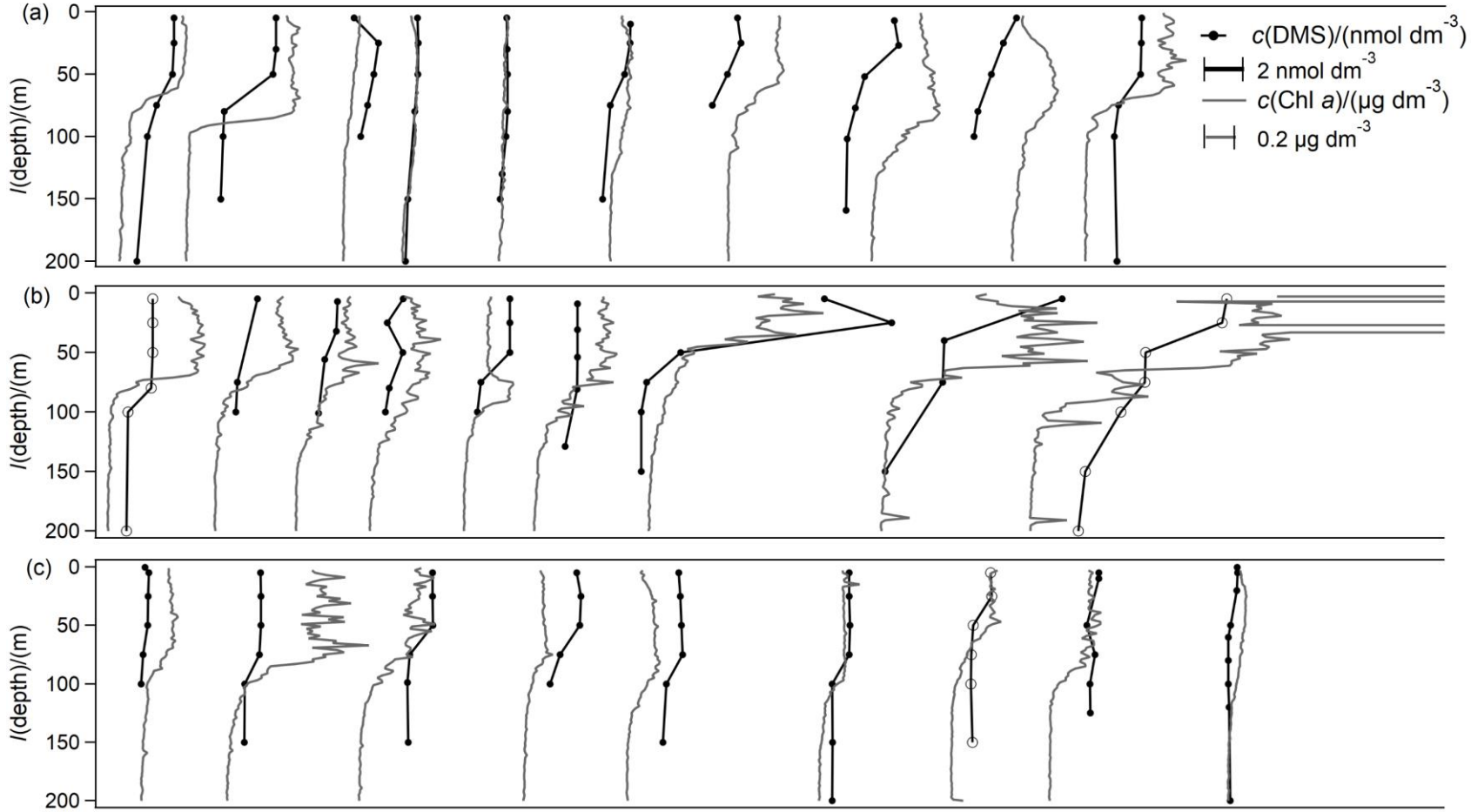

Figure 5.15 Overview plot displaying the shape of all DMS and Chl *a* depth profiles staggered along the x-axis for ease of viewing. The scale bars for DMS and Chl *a* in panel (a) also apply to panels (b) and (c). Profiles with hollow markers are highlighted in Figure 5.17. One of the Chl *a* profiles is cut off in panel (b) for scale purposes.

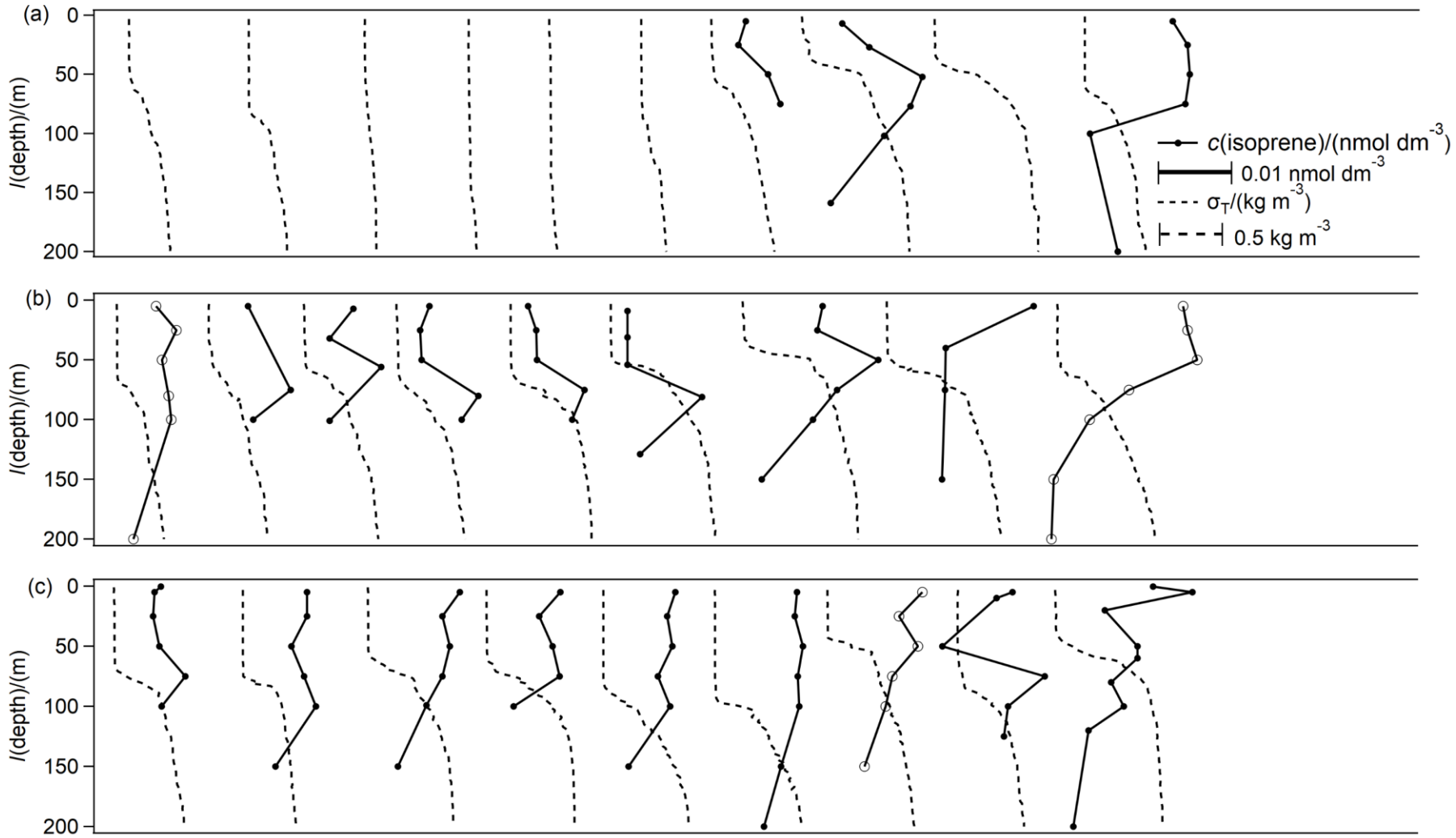

Figure 5.16 Overview plot displaying the shape of all isoprene and density (σ_T) depth profiles staggered along the x-axis for ease of viewing. The scale bars for isoprene and density in panel (a) also apply to panels (b) and (c). Profiles with hollow markers are highlighted in Figure 5.17.

Figure 5.12-Figure 5.16 show that these VOCs displayed a lot of variability, but there were also some clear patterns. In the next section 5.8.2, I discuss these patterns and what they suggest about the biogeochemical cycling of these VOCs.

5.8.2 Depth profile discussion

I chose these casts (Figure 5.17) as I perceive that they are representative of the overall pattern and cover the large sampling area. One of the casts highlighted (cast (b)) has been collected in the phytoplankton bloom.

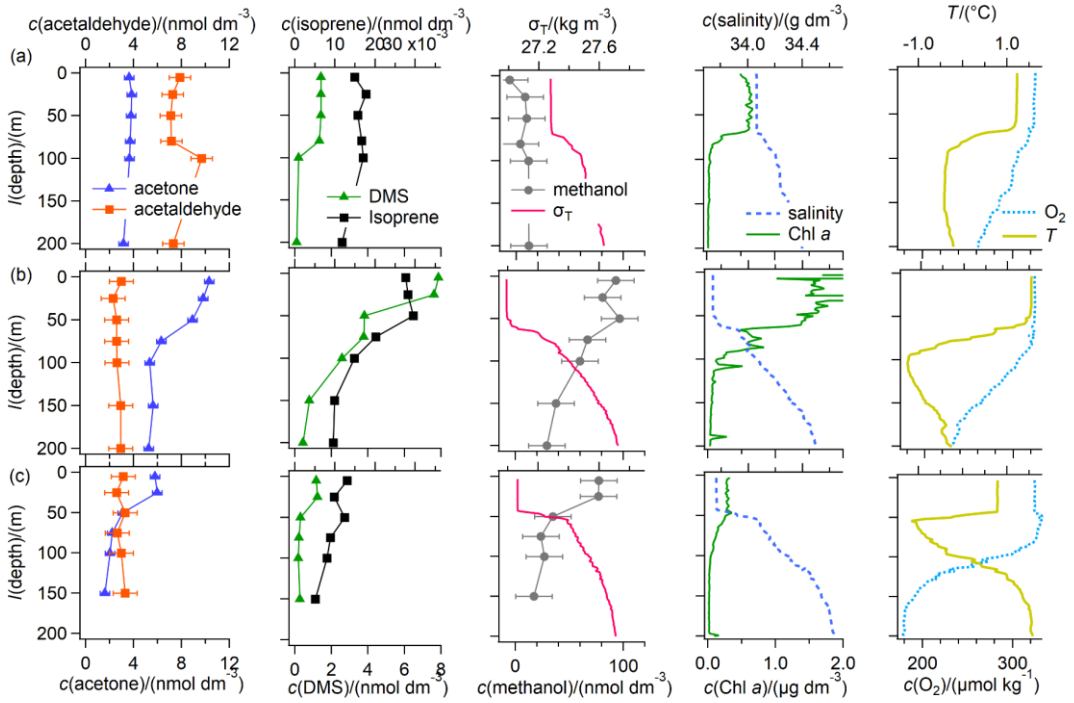

Figure 5.17 Selected depth profiles along with further auxiliary data. Location of the casts is indicated in Figure 5.1.

Water column biogeochemistry

The casts collected here are characterised by a well-defined mixed layer which is typically 40 to 100 m deep. The seawater temperature is typically near freezing and thus the density profile is shaped by the salinity profile (Rudels et al., 1991). The mixed layer is characterised by lower salinities indicating the influence of ice melt. The colder layer below the mixed layer is the winter cooled layer (Venables and Meredith, 2014). Most of the Chl *a* is homogenously distributed in the mixed layer, and a subsurface Chl *a* maximum is generally not observed. Chl *a* decreases slowly within 40 m below the mixed layer suggesting some biological activity just below the pycnocline. Similarly, oxygen is homogenously distributed within the mixed layer and decreases gradually within 100 m below the mixed layer.

Methanol

Methanol shows higher concentrations in the mixed layer than below the mixed layer at most stations. Methanol concentrations below the mixed layer are generally near the detection limit (Figure 5.12, Figure 5.17). Increased concentrations at the surface are qualitatively similar to most previous observations (Beale et al., 2013; Williams et al., 2004; Yang et al., 2014c) and consistent with a dominant biological source (Mincer and Aicher, 2016). Methanol concentrations within the mixed layer are sometimes quite variable. This variability is possibly due to methanol oxidation rates influencing dissolved concentrations as these oxidation rates are previously found to be highly variable with depth (Dixon and Nightingale, 2012). Nevertheless, the surface concentration is generally representative of the concentration in the rest of the mixed layer.

Acetone

Highest concentrations of acetone are measured in the mixed layer, while concentrations of acetone below the mixed layer are lower. Acetone concentrations within the mixed layer appear very homogenous (Figure 5.13, Figure 5.17). The acetone depth profiles reported here are similar to previous observations in the Atlantic (Beale et al., 2013; Williams et al., 2004; Yang et al., 2014c), supporting a predominantly light dependent source. From these data it is not obvious whether this light dependent source is biologically (Halsey et al., 2017; Schlundt et al., 2017) or photochemically (Dixon et al., 2013; Kieber et al., 1990) mediated.

Acetaldehyde

Generally, similar concentrations of acetaldehyde are observed in the surface waters and below the mixed layer (Figure 5.14, Figure 5.17). Some of the acetaldehyde profiles show slightly higher concentrations below the mixed layer. These patterns could be a measurement artifact - due to higher concentrations of CO_2 below the mixed layer and the consequence on the PTR-MS measurement (see Section 3.8). I would maybe expect slightly higher concentrations of acetaldehyde in the mixed layer compared to below, similar to measurements by Zhu and Kieber (2019). Higher concentration near the surface would be consistent with a dominant light dependent source. At the same time, the biological lifetime of acetaldehyde in surface seawater of several hours (Dixon et al., 2013) is likely too short to lead to a significant accumulation in the mixed layer. The rapid microbial consumption could be the reason why light dependent biological (Davie-Martin et al., 2020;

Halsey et al., 2017) or photochemical (De Bruyn et al., 2011; Zhu and Kieber, 2018) production of acetaldehyde are not obvious in the vertical concentration gradients.

DMS

Highest concentrations of DMS are observed in the mixed layer, while concentrations below the mixed layer are near zero (Figure 5.15, Figure 5.17). This is in line with previous observations (Rellinger et al., 2009; Royer et al., 2016; Turner et al., 1995). DMS is generally well mixed within the mixed layer; though in casts with the highest Chl *a* concentration, DMS concentration is the highest close to the surface and the concentration decreases gradually below the mixed layer. Some casts display occasional Chl *a* peaks below the mixed layer. Rellinger et al. (2009) have found that particulate matter exported from the mixed layer can contain DMS precursors and functional Chl *a* systems. These sinking, live cells release DMS, which leads to a gradual decrease in DMS concentrations below the mixed layer.

Isoprene

There is generally more isoprene in the surface mixed layer, while concentrations below the mixed layer are very low. Some of the depth profiles display highest concentrations at or just below the pycnocline (Figure 5.16, Figure 5.17). The isoprene depth profiles reported here are similar to previous observations (Booge et al., 2018; Moore and Wang, 2006; Tran et al., 2013). Thus, isoprene concentrations somewhat follow the shape of Chl *a* concentration with depth (Tran et al., 2013). Higher concentrations of isoprene at or below the pycnocline are probably due to local production and poor ventilation, leading to accumulation at those depths.

Importance of mixed layer depth

On a global scale, mixed layer depth has been shown to influence DMS concentrations (Vallina and Simó, 2007), while the effect of mixed layer depth is rather unknown for the other compounds monitored here. To investigate this, I correlate mixed layer depth with VOC concentration measured at 5 m.

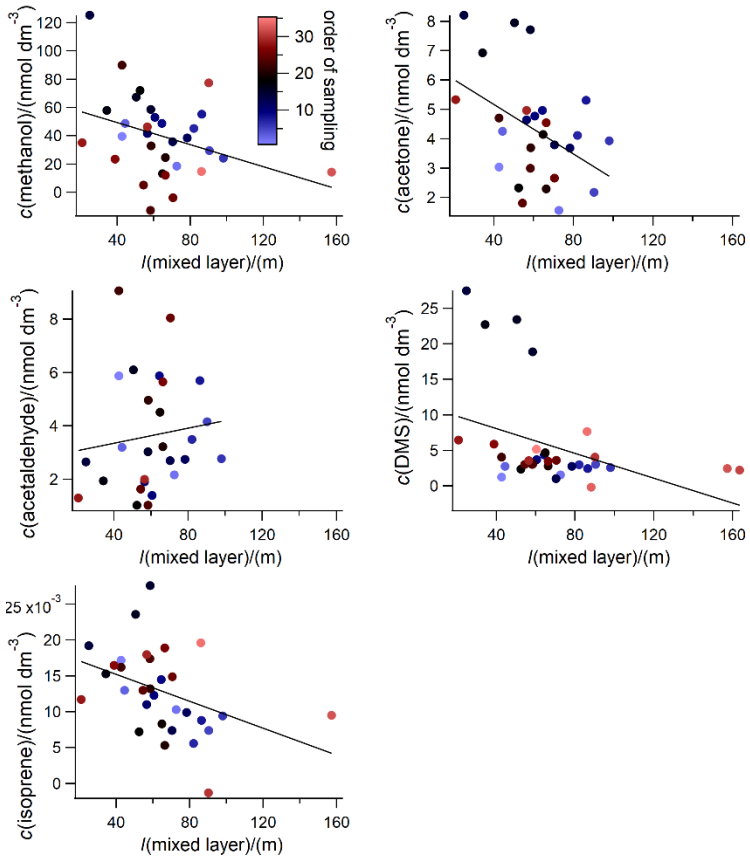

Figure 5.18 Surface seawater concentrations correlated with mixed layer depth at CTD stations. Markers have been coloured by the order the stations were sampled in.

Figure 5.18 highlights that a deeper mixed layer generally leads to lower surface VOC concentrations, possibly due to increased dilution. The mixed layer depth can explain 12 %, 19 %, 15 % and 17 % of the surface variability of methanol, acetone, DMS and isoprene respectively over this cruise track. Acetaldehyde is an exception to this trend, probably due to its short lifetime (Dixon et al., 2013) and thus consumption processes dominating its surface distributions. As such, color-coding of the markers suggests that stations sampled in proximity tend to cluster more tightly than all the data combined. This is probably because there are different production processes dominating in different areas and the mixed layer depth is one of the variables influencing VOC concentrations in that area.

Summary

To provide a brief summary on the distribution of these VOCs from the surface to 200 m depth, a schematic is presented (Figure 5.19).

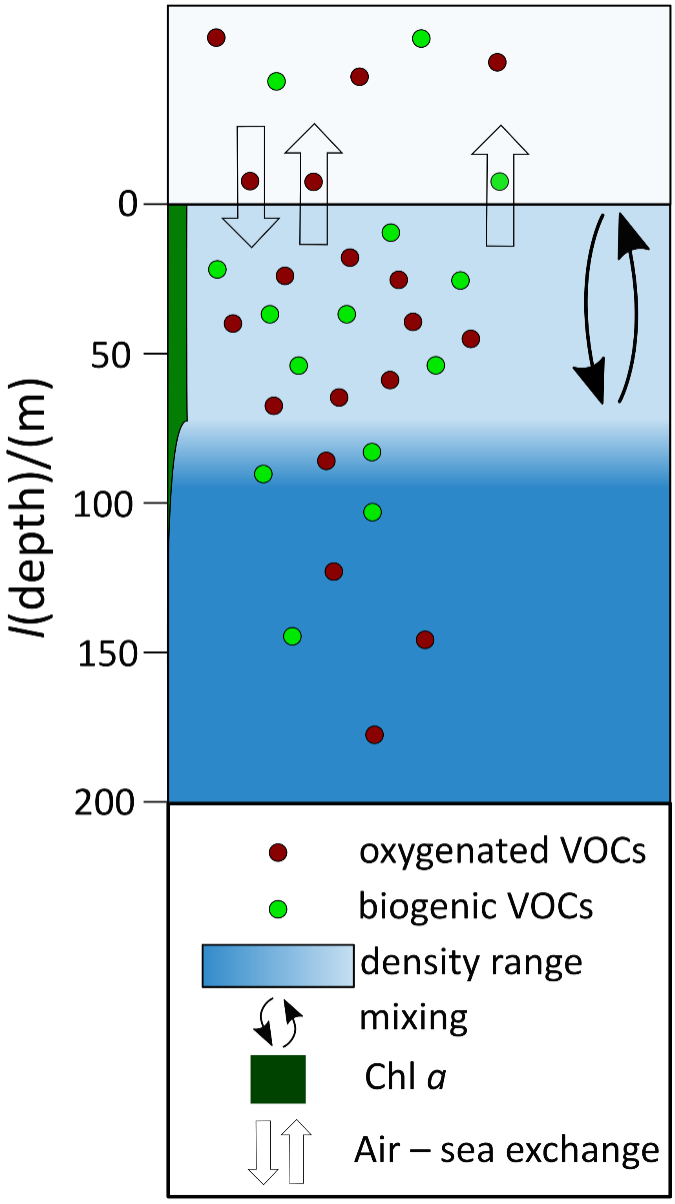

Figure 5.19 Schematic summarising depth profile distributions in the Antarctic of the VOCs monitored here.

Figure 5.19 summarises that the mixed layer during the Southern Ocean transect is fairly homogenous. This leads to similar concentrations of Chl *a* throughout the mixed layer and lower concentrations below the mixed layer. The oxygenated VOCs display higher concentrations in the mixed layer, than below. Biogenic VOCs are also generally well mixed in the mixed layer. Below the mixed layer, DMS concentrations decrease, often gradually within about 40 m, to near zero, while highest isoprene concentrations are sometimes observed at the bottom of the mixed layer. The air – sea flux of acetone and acetaldehyde can be in and out of the ocean, depending on location, while the methanol flux tends to be into the ocean. The biogenic VOCs, DMS and isoprene, are calculated to be emitted from

the ocean. My data also shows that a deeper mixed layer tends to coincide with lower surface VOC concentrations.

5.9 Conclusion

This chapter presents underway seawater and ambient air measurements of simultaneously measured DMS, isoprene, methanol, acetone and acetaldehyde. The measurements are taken in the Atlantic sector of the Southern Ocean along a 60° S transect during the transition from late austral summer into early autumn. The high resolution and frequent alternation between ambient air and seawater measurements allows me to derive the fluxes and saturations for all of these compounds at a high temporal resolution. To the best of my knowledge, this represents the first set of seawater concentrations and so fluxes for methanol, acetone and acetaldehyde in the Southern Ocean.

Seawater DMS concentrations display episodes of higher concentrations, while the mean is comparable to the climatology for this region at this time of year. Seawater isoprene concentrations are comparable to other open ocean measurements. Methanol seawater concentrations are higher than previous measurements in the North Atlantic (Yang et al., 2014a), while acetone and acetaldehyde seawater concentrations are generally quite low and comparable to other high latitude measurements. This dataset contains observational evidence for a statistically significant diurnal change in acetaldehyde, acetone and isoprene seawater and ambient air concentrations. Such a diurnal change in seawater concentrations has not been observed before in the open ocean.

The underway air measurements support that VOCs in the atmosphere above the Southern Ocean are predominantly influenced by marine conditions and not influenced by terrestrial emissions. Due to this remoteness of the sampling location, atmospheric mole fractions of methanol, acetone and acetaldehyde are very low. Methanol is transferred mostly from the atmosphere to the ocean during this cruise, giving a campaign mean flux of -2.3 µmol m^{-2} d^{-1}. However, episodes of higher methanol seawater concentrations are observed, which leads to somewhat unexpected and fine scale outgassing of methanol from the ocean. Acetone and acetaldehyde vary between being absorbed and emitted by the ocean, depending on location. This sector of the Southern Ocean is calculated to be on average a weak sink of acetone and acetaldehyde during this period, with a mean flux of -0.55 µmol m^{-2} d^{-1} and -0.24 µmol m^{-2} d^{-1} respectively. High resolution measurements provide more accurate confidence intervals of the flux since they account for fine scale variability in the

flux direction. The biogenic VOCs DMS and isoprene were both constantly emitted by the ocean throughout the cruise track.

Simultaneous measurement of multiple compounds allows possible common sources and sinks to be identified. For example, seawater methanol and isoprene concentrations are found to positively correlate, possibly due to some common biological sources for these two gases. Isoprene seawater concentrations are found to negatively correlate with $f(CO_2)$ and positively correlate with Chl *a*, supporting a biological origin for isoprene. Seawater acetone concentrations are found to correlate negatively with $f(CO_2)$, possibly pointing towards biological production of acetone in seawater. Acetaldehyde concentrations do not clearly correlate with the other gases, probably due to its very rapid oxidation by bacteria.

A large number of VOC depth profiles are presented in this chapter as overview plots which allows to detect trends in their distributions. These depth profiles generally show higher concentrations of oxygenated VOCs in the mixed layer and lower concentrations well below the mixed layer depth. DMS concentrations were highest in the mixed layer and gradually decreased below the mixed layer, while isoprene concentrations sometimes showed highest concentration at the base of the mixed layer. Correlations with mixed layer depth suggest that mixed layer depth exerts a relatively small influence over the whole cruise track, but is more important when controlling localised concentrations.

The VOC data presented here represent a unique dataset that can be used in models to elucidate more accurately the role of the ocean in the global cycling of methanol, acetone and acetaldehyde, as well as to further constrain the oceanic emissions of DMS and isoprene.

6 Conclusion

6.1 Introduction

Our understanding of the variability of methanol, acetone, acetaldehyde, DMS and isoprene in the marine environment has been limited in part by a lack of in situ concentration measurements. The polar regions are particularly undersampled with no prior observation of seawater methanol, acetone and acetaldehyde in the high latitudes. This is in part due to a lack of suitable methods for quantifying these compounds in seawater. This thesis provides detailed characterisation of an air – sea gas equilibrator coupled to PTR-MS for automated measurement of VOCs in seawater and ambient air. I present seawater measurements of these VOCs in the marginal sea ice zone of the Canadian Arctic Archipelago, focussing on the effect of sea ice on the distribution of these compounds in depth profile and surface underway measurements. The thesis also describes depth profile, underway seawater and ambient air measurements in the Southern Ocean. These measurements are used to compute the hourly air – sea fluxes and saturations. Correlations with underway auxiliary data provided new insights into what potentially controls the variability of these gases in the polar oceans.

The aims of this conclusion chapter are to:

1. comment on how the SFCE-PTR-MS setup improved our measurement capabilities and contributed to the field of VOC research.
2. compare key results from both field deployments.
3. critically discuss if these works closed knowledge gaps identified in the introduction satisfactorily.
4. speculate what the impact of these findings are in light of climate change.
5. identify the shortcomings in the works presented here and provide recommendations for future work.

This conclusion chapter is rounded up with a closing remark.

6.2 The SFCE-PTR-MS and its contributions to the field

The SFCE achieves a high degree of equilibration due to its design. Using a 10-m-long segmented flow tube, the SFCE achieves full equilibration for compounds more or equally soluble than toluene. The unique T-shaped air water separation system allows for rapid drainage of seawater without intrusion of lab air while allowing for an extremely fast response time.

The SFCE is versatile. Due to the relatively low water flow requirements of 100 cm^3 min^{-1}, the SFCE can be used for automated continuous measurements and discrete samples. The SFCE could be used to measure a broader range of compounds with a few adaptations.

The SFCE can be easily replicated and is inert. Previously only a few specialist research groups were able to make seawater VOC measurements. The SFCE presented in this thesis can be easily reproduced and coupled to another commercially available PTR-MS or other gas detectors. The SFCE is entirely made up of PTFE Teflon, which should minimize wall ad- and de-sorption effects. It also makes that the equilibrator is not very prone to biofouling and easy to clean.

Understanding of the PTR-MS underpins the SFCE-PTR-MS. The effects of humidity on the background and signal of the PTR-MS are characterised in detail. Settings of the PTR-MS have been optimised for measurement of soluble VOCs in equilibrator headspace. The effect of CO_2 (first identified in breath studies) is used to explain some of the differences between backgrounds.

Contributions to the field:

- **Detailed description of the data processing and derivation of the purging factor.** These equations can be used by other investigators using a similar setup. This should lead to greater consistency and improve reproducibility.
- **Two methods of calibration.** The SFCE can be calibrated using two different methods (invasion using a certified gas standard and evasion using serially diluted liquid standards). This should make calibrations and estimates of solubility more accurate.
- **Improved solubility for methanol and acetone**. Using both methods of calibration, I was able to determine the solubility of acetone, which should be more accurate than oft-used, published values. This also led me to infer an improved solubility for methanol. These solubilities were determined at environmentally relevant concentrations and should thus be more relevant to marine science. This should improve ocean source/sink estimates in global models.
- **Quantification of potential uncertainty through measurement of a variety of different backgrounds.** Estimating seawater VOC blanks is very challenging and crucial for determining dissolved gas concentrations when using PTR-MS coupled to an equilibrator. Few previous researchers carried out detailed characterisation of the seawater background. Through measuring a wide range of backgrounds, I close

some of the existing knowledge gaps, especially with regard to the humidity dependence in the VOC backgrounds. I highlight the potential uncertainty associated with the choice of background and hopefully spur further investigations.

6.3 Comparison of key findings from the Arctic and the Antarctic deployment: Implications for the wider field

Environmental settings

The two field deployments complement each other very well. Table 6.1 is used here to contrast the settings between the two cruises.

Table 6.1 Contrasting the settings between the two cruises.

comparison	Arctic	Antarctic
Environment	Sea ice zone	Open ocean
Sampling season	summer	Summer/autumn
Latitudes	About 60° N to 80° N	Around 60° S
Surface salinity	Very low (around 29)	Below global mean (34)
Surface temperature	Very variable (between +6 and -2 ºC)	Very low (around -1 ºC)
Episodes of high surface Chl *a*	above 2 mg m^{-3}	above 0.8 mg m^{-3}
Daily sunlight hours	24 h	Average 12 h

Table 6.1 contrasts the different environmental settings between the two cruises. The cruise in the Arctic took place in the sea ice zone during sea ice melt season/boreal summer at very high latitudes in the polar region and generally near land. As a consequence, surface salinity was generally very low due to freshwater input from melting sea ice. The surface temperature was very variable and generally higher in areas without sea ice cover. This warming of the mixed layer after sea ice melt is very characteristic for the Arctic (Shadwick et al., 2015). Episodes of very high surface Chl *a* were observed during this cruise, which is typical for the Arctic summer and related to sea ice melt leading to phytoplankton blooms (Barber et al., 2015; Perrette et al., 2011). Sampling at this time of year was characterised by 24 h sunlight leading to increased light-dependent biological and photochemical activity as well as a small difference between day and night.

Antarctic sampling occurred mainly in the open ocean during austral summer/autumn and thus later in the season compared to the Arctic cruise. Most of the measurements were taken at the edge of the polar circle. Surface salinity was lower than the global mean,

possibly due to ice berg meltwater input (Deppeler and Davidson, 2017). The sea surface temperature was very consistent and near freezing. Episodes of high Chl *a* were observed generally near islands and in upwelling areas. The Chl *a* concentrations observed during such events were generally less than half of what was observed in the Arctic. The daily average sunlight hours were around 12 h which leads to a more pronounced difference between day and night with effects on light-dependent processes.

As such the two cruises complement each other very well as they encompass a large range of polar environments. Together they provide new insights what influences VOC concentrations in the polar oceans.

Variability in the surface seawater concentrations of VOCs

In the introduction chapter, I highlight that the factors influencing surface variability of many of these compounds are largely unknown. In this section, I discuss compound by compound what my data from both polar regions revealed on this topic and what these new insights mean for the wider field. I also compare my findings to previous lower latitude measurements. To facilitate this discussion, the mean and range in the surface underway seawater concentrations from both deployments are shown in Table 6.2.

Table 6.2 Cruise mean and range in underway surface seawater concentrations measured during the Arctic and Antarctic cruise.

BLD= Below Limit of Detection

	c(Arctic cruise)/(nmol dm^{-3})		*c*(Antarctic cruise)/(nmol dm^{-3})	
compound	*mean*	*range*	*mean*	*range*
DMS	1.4	0.3 - 2.9	2.6	0.2 – 24.4
Isoprene	0.063	0.015 – 0.264	0.013	0.004 - 0.051
Methanol	37	BLD – 129.0	67	BLD - 227
Acetone	8.3	0.3 – 46.7	5.5	1.4 - 32.2
Acetaldehyde	3.7	BLD – 21.5	2.6	BLD – 7.9

Methanol. Methanol concentrations were on average about twice as high during the Antarctic deployment compared to the Arctic. In the Arctic, higher concentrations at the surface compared to below were generally measured in ice-free waters. In the Antarctic, highest concentrations were measured in specific areas of higher Chl *a*. During this deployment, methanol surface water concentrations were found to positively correlate

with underway isoprene and negatively with $f(CO_2)$ in the Antarctic, while no such correlations could be observed in the Arctic. Methanol concentrations in both polar regions displayed a very large range, suggesting a decoupling between sources and sinks of methanol. Earlier measurements at lower latitudes also find a very large range of methanol concentrations (Beale et al., 2013; Kameyama et al., 2010; Williams et al., 2004), while more recent measurements tend to show lower methanol concentrations (Beale et al., 2015; Yang et al., 2014a, 2014c). My higher resolution underway measurements largely span the range of these earlier observations. Previous laboratory experiments have shown that methanol is produced by a large range in phytoplankton species (Mincer and Aicher, 2016), while methanol consumption rates tend to display large variability (Dixon and Nightingale, 2012) and are dependent on specific microbial community composition (Sargeant et al., 2016). Overall, this is suggesting that methanol concentrations might be controlled by specific biological consumption processes.

Acetone. Acetone concentrations measured during the Arctic deployment were about 50 % higher compared to the Antarctic deployment. This could be due a) to 24 h daylight during the Arctic cruise, leading to increased light-dependent production of acetone , b) different abundance of precursor compounds, or c) terrestrial influences. Mean concentrations from both cruises are lower than measurements at lower latitudes which confirms the recent Wang et al. (2020a) global distribution based on machine learning. Lower concentrations at higher latitudes could be due to the influence of light or biological activity. Both cruise tracks showed a large range in acetone concentrations. This is largely due to very short (3 – 12 h) episodes of very high acetone concentrations, suggesting a decoupling between sources and sinks in specific areas. From these concentration measurements alone, it is hard to comment on the dominant production mechanism of acetone in seawater in the polar oceans – photochemical or light-dependent biological. Highest concentrations in partial sea ice cover support a dominant photochemical pathway. In the Antarctic, correlations with Chl *a* and $f(CO_2)$ suggest a biological source. However, given the very long distance of the transect and the different water masses sampled, these correlations may not be indicative of a direct causal link – correlation, not causation. I believe that my data is more in favour of a dominant photochemical pathway for acetone due to the higher concentrations in the Arctic and the diurnal change in seawater concentrations observed in the Antarctic.

Acetaldehyde. Absolute concentration measurements of acetaldehyde from both cruises were highly uncertain due to an unquantified interference of CO_2 in the background.

Bearing that in mind, acetaldehyde concentrations were slightly higher in the Arctic summer compared to what was measured in the Antarctic summer/autumn. Concentrations also displayed a much larger range in the Arctic compared to what was measured in the Antarctic. This could be due to a) enhanced photochemical or biological activity related to the abundance of terrestrial organic matter b) 24 h light and c) higher biological productivity in the Arctic summer. My mean concentrations from both cruises appear similar to previous measurements at lower latitudes in the open ocean (Yang et al., 2014c). Previous lower latitude measurements tend to find episodes of very high concentrations (more than 10 nmol dm^{-3}) near land (Beale et al., 2015; Schlundt et al., 2017). It seems that these phenomena also seem to be present in my Arctic cruise data. Comparison of data from my two cruises suggests that acetaldehyde concentrations are possibly controlled more by the proximity to land, rather than other factors changing with latitude. Acetaldehyde consumption rates were also found to be much higher in coastal waters (de Bruyn et al., 2017) compared to the open ocean (Dixon et al., 2013). Acetaldehyde did not show significant correlations with other environmental variables in the Arctic, nor in the Antarctic, which is similar to observations by Schlundt et al. (2017). This could be due to rapid biological consumption of acetaldehyde preventing significant accumulations in seawater. In the Arctic, acetaldehyde did correlate with acetone and methanol, possibly suggesting common sources in more terrestrially influenced environments. Due to the lack of other correlations it is difficult to comment on the dominant production pathway of acetaldehyde - biological or photochemical. Higher concentrations in partial ice cover could be due to either these processes. The comparison presented here suggests that acetaldehyde abundance is likely affected by proximity to land and rapid microbial consumption processes.

DMS. Higher mean concentrations and episodes of very high (more than 10 nmol dm^{-3}) concentrations of DMS were measured in the Antarctic summer/autumn compared to Arctic summer. This is probably due to sampling bias as the ship spent a few days mapping a high DMS area during the Antarctic cruise. The median DMS concentration from both field deployments are nearly identical (Antarctic: 1.39 nmol dm^{-3}, Arctic: 1.35 nmol dm^{-3}). Previous measurements show strong seasonal variability in DMS concentrations in the polar oceans .I observed highest DMS in higher sea ice cover, possibly due to a) rapid changes in salinity and temperature inducing production of DMSP (Wittek et al., 2020), a precursor to DMS and/or b) ice edge blooms which are known to be strong sources of DMS (Levasseur, 2013). In the Antarctic cruise, highest concentrations of DMS were observed in

the proximity of islands or in upwelling regions, probably due to higher biological activity in these areas. DMS is a very well researched compound and the findings here only make a relatively small contribution to the knowledge what controls DMS variability in surface ocean. My data suggests that in the Arctic, highest DMS concentrations are observed in partial sea ice, while in the Antarctic, highest DMS concentrations are observed in areas of high Chl *a*.

Isoprene. Isoprene concentrations measured in the Arctic summer were about three times higher and displayed a much larger range than measurements in the Antarctic summer/autumn. This is possibly due to different phytoplankton composition, higher biological productivity and terrestrial influences during the Arctic cruise. Isoprene significantly correlated with surface Chl *a* in both polar oceans and could explain more of the surface variability during the Antarctic cruise, compared to the Arctic cruise. Also at lower latitudes, isoprene correlates with Chl a (Hackenberg et al., 2017; Ooki et al., 2015). The slope of the correlation is about double in the Arctic compared to the Antarctic, which could be due to the net higher seawater concentrations during the Arctic cruise. During this Arctic cruise in the sea ice zone, isoprene correlates better with sst than with Chl *a*. The slope of the isoprene correlation with sst in the sea ice zone is negative, while in the open ocean, investigators typically report positive correlations between these two variables. This suggests that different parametrisations should be used when predicting isoprene concentrations in the sea ice zone. This is possibly reflecting that isoprene is controlled by different factors in the marginal sea ice zone compared to the open ocean.

Correlations between oxygenated VOCs. Methanol and acetone both correlated with acetaldehyde in the Arctic, but not in the Antarctic. This may suggest common sources for these oxygenated VOCs in more terrestrially influenced environments compared to the pristine marine environment that is the Southern Ocean. At the same time, the Antarctic cruise covered a very large area, sampling very different water masses and thus some of these correlations might not present themselves in the data.

Diurnal variations. In the introduction, I highlight that whether diurnal changes in the surface concentrations of these compounds exist is an ongoing scientific debate. I observed diurnal changes in seawater and ambient air concentrations of isoprene, acetone and acetaldehyde in the Antarctic. This implies light-driven productions of these compounds in the open ocean. Previous investigators have not been able to resolve such variability in the open ocean – but sometimes observed it in coastal areas. The absence of a diurnal change

in the seawater concentrations in the Arctic is probably due to the time of year as 24 h sunlight reduces any difference between daytime and night-time. Additionally, the Arctic cruise was in a very heterogenous environment, which makes it more challenging to tease out a subtle diurnal change from all the other sources of variability. Other factors, such as the sea ice cover, more strongly affected the surface concentrations of these VOCs in the Arctic.

Air – sea fluxes. In the introduction, I highlight that the global ocean source/sink strength is poorly quantified and there exist large discrepancies between modelled estimates and estimates based on observations, especially for the oxygenated VOCs and isoprene. To address this, I calculate air – sea fluxes for the Antarctic field deployment, listed in Table 6.3.

Table 6.3 Cruise mean underway air – sea flux calculated for the Antarctic cruise. Also shown are the standard deviation of the flux and the range in computed fluxes.

compound	*f*(Antarctic cruise)/(μmol m^{-2} d^{-1})	*σ(*flux*)*/(μmol m^{-2} d^{-1})	*f(range)*/(μmol m^{-2} d^{-1})
DMS	4.3	7.4	0.1-43.0
Isoprene	0.028	0.022	0.001-0.130
Methanol	-2.4	4.9	-19.8-14.5
Acetone	-0.55	1.15	-7.34-4.82
Acetaldehyde	-0.28	1.22	-5.48-3.33

These computed fluxes represent valuable estimates of the ocean source/sink strength in these areas and can be used as model inputs for this time of year. They highlight that the Southern Ocean is on average emitting the biogenic VOCs, DMS and isoprene. Over this cruise track, the ocean emitted two orders of magnitude more DMS compared to isoprene on a per area basis, possibly suggesting a higher particle forming potential of DMS compared to isoprene. For this cruise, the Southern Ocean is calculated to emit and absorb oxygenated VOCs, depending on location, resulting in a net weak sink. My high resolution flux estimates are consistent with previous observations in temperate waters of the Southern Hemisphere (Yang et al., 2014c). Results from this cruise suggest that the ocean is taking up much more methanol on a per area basis compared to the other oxygenated VOCs studied here. Only one episode of outgassing was observed which was surprising due to the high solubility of methanol. Measurements from this cruise showed that the

Southern Ocean is only a weak sink of these oxygenated VOCs, likely due to the very low ambient air mole fractions. I speculate that the Arctic Ocean is also constantly emitting the biogenic VOCs, DMS and isoprene. This is largely due to their short atmospheric lifetime and large supersaturation in seawater. Given the higher atmospheric mixing ratios of the oxygenated VOCs in the Arctic atmosphere compared to the Antarctic (Guimbaud et al., 2002; Sjostedt et al., 2012), I would expect the Arctic to be a net sink of methanol, acetone and acetaldehyde. Assuming that sea ice acts as a barrier to air – sea exchange (as suggested by Butterworth and Miller (2016)), I would expect more air – sea exchange in ice-free waters, compared to partially ice covered waters.

Overall, these represent valuable estimates that come with limitations when extrapolating over the whole year in particular. Both polar oceans undergo large seasonal variations and the sampling here only spanned summer/autumn, missing the extremely biologically productive spring which could control annual emissions.

Depth profiles. In the introduction I highlighted that the variability of these compounds with depth and the effect of water column biogeochemistry is poorly understood, partly due to the lack of measurements at different depths. One of the contributions of this thesis to the field is the large number of CTD depth profiles in both polar oceans. These depth profiles illustrated the variability of VOCs with depth and allowed me to tease out some trends, which I summarize here. Below, I contrast the vertical distributions of the VOCs sampled in this thesis in the Arctic and the Antarctic (Figure 6.1). This illustrates the effect of the biogeochemistry of the water column on these gases.

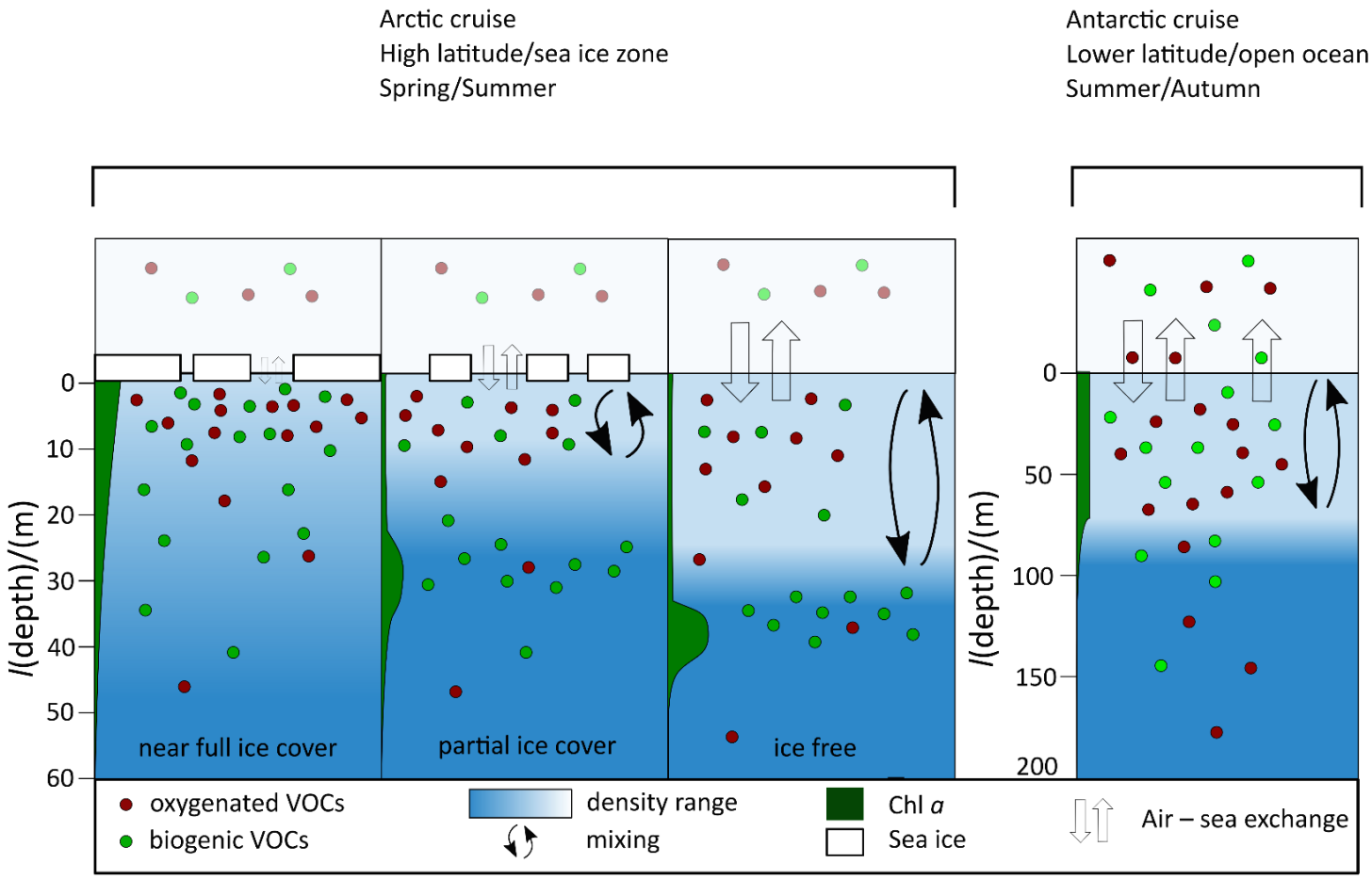

Figure 6.1 Comparison of the schematics describing depth profile distributions of VOCs during both deployments.

Water column biogeochemistry

Depth profiles collected in the Antarctic displayed a deep (mean 79 m) and well-defined mixed layer containing similar VOC concentrations throughout. The depth profiles in the Arctic however were characterised by a very complex surface water column with rapidly changing biogeochemistry in the surface 60 m, related to sea ice cover. This is also reflected in the VOC concentrations which displayed a lot of variability with depth. The mixed layer was typically very shallow (<10 m in areas covered with sea ice, and about 20 m away from sea ice). This is in part due to the lower wind speeds and proximity to land/influence of sea ice limiting wave fetch. The seasonal sea ice melt and deepening of the mixed layer often led to formation of a highly productive deep Chl *a* max, just below the mixed layer.

VOC variations with depth

In both polar oceans, the concentrations of these VOCs varied with depth. I generally found higher concentrations of these gases in the mixed layer and lower concentrations far below the mixed layer. In the Arctic, sea ice has a strong influence on these compounds. I generally observe higher surface concentrations of oxygenated and biogenic VOCs in partial ice cover. The deep Chl *a* max was often accompanied by a subsurface maximum concentration of the biogenic VOCs, which were supposedly produced at this depth and not efficiently vented. This is in line with a dominant biological source for these compounds. In partial ice cover, the oxygenated VOCs displayed a rapid decrease from the surface and tended to be mixed deeper as the sea ice melts and the mixed layer deepens, potentially suggesting a dominant light-dependent source. Air – sea fluxes were not determined in the Arctic, though I speculate that the largest fluxes tend to be observed in the ice free water column.

In the Antarctic, VOC concentrations in the mixed layer were generally very homogenous. I also generally observed lower surface concentrations in areas of deeper mixed layers, while no such correlation could be observed in the Arctic, possibly due to the poorly defined mixed layer depth or the complex biogeochemistry in the surface ocean influencing VOC concentrations.

These measurements illustrate the effects of water column biogeochemistry on dissolved concentrations of these gases and contrast depth profiles from the open ocean and the sea ice zone.

Extrapolations of these depth profiles to different latitudes and seasons in both polar oceans

These depth profiles complement each other very well, covering a large range of polar environments (near full ice cover to open ocean). I speculate that the distribution of VOCs in the sea ice zone is very similar in both polar environments. As such, vertical profiles in sea ice zones of the Antarctic would probably show greater near surface stratification. As a consequence, I would expect the concentrations of oxygenated VOCs to rapidly decrease with depth, as I observed in the Arctic. The Arctic casts in the sea ice zone were collected at an earlier time in the year. I speculate that going into autumn, the deepening of the mixed layer will continue and the casts in open water will probably look more similar to the ones I collected in the Antarctic. Deepening of the mixed layer likely contributes towards decreasing surface VOC concentrations in autumn and winter.

Thus, collecting a large range of depth profiles in both polar oceans and at complementing environmental settings allowed me to make guesses with regard to the distributions of these compounds at different latitudes and seasons in both polar regions.

6.4 Speculations on the effect of climate change

Climate change is predicted to have a huge impact globally and particularly on the polar regions. Using my measurements, I can make some speculations on the effect of climate change on dissolved VOC concentrations and air – sea fluxes.

In the Arctic, sea ice extent is already rapidly decreasing as a consequence of atmospheric warming and climate change (Maslanik et al., 2011). The first ice-free boreal summer is very hard to predict (Senftleben et al., 2020), but the sea ice extent is rapidly shrinking (Wang et al., 2020b). Sea ice is melting earlier and freezing up later in the season, leading to an overall longer ice-free period in the summer (about 20 days increase in the melt season over the last 30 years (Markus et al., 2009)). Multi-year ice is being lost rapidly (Maslanik et al., 2011), thus in the near future, most of the sea ice will probably be first year ice which is similar to what was sampled in this thesis . I speculate that in a changing climate, higher concentrations of these VOCs may occur in partial ice cover but VOC concentrations will decrease in ice-free waters, similar to observations presented in this thesis. However, the total area displaying this seasonal variation will decrease and migrate northwards with sea ice extent. Reduced sea ice extent may lead to lower seawater VOC concentrations. I expect the depth profiles in these newly formed open ocean regions to be more similar to the ones I collected in the Antarctic open ocean. The longer ice-free period

during summer will probably lead to net more annual air – sea exchange (Parmentier et al., 2013). This makes it more important to consider ocean fluxes in the high Arctic when modelling global ocean fluxes of these gases. At the moment, the high Arctic tends to be omitted from these global atmospheric budgets.

In the Antarctic, sea ice loss is not yet as dramatic as in the Arctic, though it will follow suit (Comiso et al., 2011) with likely a similar effect on VOC concentrations and fluxes as speculated for the Arctic. The Southern Ocean is predicted to experience shallowing of the mixed layer depths, a southward migration of ocean fronts and higher wind speeds (Deppeler and Davidson, 2017). My results suggest that shallower mixed layers are probably going to lead to higher VOC concentrations simply from less dilution. Shallower mixed layers will also lead to higher amounts of light experienced by organic matter and phytoplankton, increasing light-dependent production and diurnal variations. The southward migration of ocean fronts will change phytoplankton composition at the sampling location presented in this thesis. For a given latitude, it is possible that this breaks down some of the correlations observed here. Higher wind speeds will lead to more air – sea exchange, thus probably increasing the importance of the Southern Ocean in influencing VOC air mole fractions in the Southern Hemisphere and in global atmospheric budgets.

Overall, these predictions are highly speculative, and I recognize that the polar oceans are a hugely complex and interconnected environment which makes it hard to predict the effect of climate change on these VOCs. Nevertheless, the two sampling tracks complement each other very well which allows me to make some informed speculations.

6.5 Future recommendations

The SFCE-PTR-MS setup has been used to take measurements of VOCs in seawater and ambient air in the course of this thesis. My surface measurements show large spatial/temporal variability in VOC concentrations, while the large number of depth profiles highlights large variability with depth. These measurements represent useful model inputs and provide insights towards the factors influencing the variability of these compounds in seawater. It is evident that the scientific community still has yet to quantify the role of the oceans, and particularly the polar oceans, in the global atmospheric cycling of these VOCs. My measurements show that the Southern Ocean is a net weak sink of oxygenated VOCs, while it on average emits isoprene and DMS. Of course, my measurement technique is not without uncertainties and my measurements did not cover all regions of the ocean in all

seasons. The method development and fieldwork have raised potential future research questions which are discussed in this section.

6.5.1 Further instrument development

The choice of background is the largest source of uncertainty for methanol, acetone and acetaldehyde. OVOCs (particularly methanol and acetaldehyde) display very low signal to background ratios and the backgrounds of these compounds can be quite variable. A range of backgrounds has been collected, which allowed me to tease out different influences on the backgrounds and make an informed background choice. Nevertheless, for acetaldehyde, the remaining uncertainty due to background choice is very large. The best way to address this uncertainty would probably be to cross-calibrate the SFCE-PTR-MS measurement with a Gas Chromatograph-Mass Spectrometer or in situ derivatisation methods. A Time of Flight mass spectrometer would also allow to disentangle the influence of CO_2 on the background of acetaldehyde and DMS.

Investigating possible contaminations in the SFCE system. To further investigate the effect of light on the measurements with SFCE, the VOC backgrounds can be measured with laboratory/natural lights on and off. This can be done with natural and artificial (i.e. organics-free) seawater to tease out the possible effect of biology. Additionally, to exclude the unlikely possibility that the water bath housing the SFCE contributes to contamination via permeation of VOCs through the PTFE tube , the water bath could be spiked with VOCs while measuring VOC backgrounds.

Different seawater pump supplying water to the SFCE. An experiment with varying water flow rates revealed that the signal of sparingly soluble gases, such as isoprene, is dependent on the water flow rate into the equilibrator. The water flow for the SFCE is currently supplied by a peristaltic pump and the flow rate varied by 5 % (standard deviation) during field deployments but could decrease by up to 20 % after long periods of continuous operation. A different type of pump (e.g. a diaphragm pump) might be able to keep the water flow more constant. Care must be taken, such that the pump does not introduce contamination or rupture phytoplankton cells in seawater, which is known to release DMS and possibly other VOCs.

Measurement of different compounds. The SFCE can be used to detect a broad range of dissolved gases and is essentially only limited by the detector and its gas flow requirements. Next steps in the development could include measurement of terpenes which have a similar solubility to the oxygenated VOCs presented here. However, terpenes

present a complex fragmentation pattern in the PTR-MS. A time of flight detector could be used to distinguish different terpenes. Using a suitable detector, the SFCE has been used to detect carbon monoxide (Xie et al., 2001) and CO_2 (by our own research group). Less soluble compounds, such as methane and oxygen probably require a longer equilibration tube to achieve full equilibration. Less soluble compounds will also have a larger purging factor, which can lead to higher measurement errors. Isotopically labelled standards can easily be continuously added to the sample to continuously monitor the equilibration efficiency.

6.5.2 Further measurements of VOCs in the Southern Ocean

Higher spatial resolution. Higher resolution seawater measurements on the order of about one measurement every minute would allow information to be gained on the variability length scale of these compounds in the open ocean. It is useful to know over what area these compounds are typically homogenously mixed in the open ocean. This could inform global models of a suitable grid cell size for data integration and provide information on the dominant production mechanism.

Sea ice zone of the Southern Ocean and polynya. The measurements presented in this thesis were taken predominantly in open Southern Ocean. While a large area of the Antarctic is occupied by the Southern Ocean, significant biological productivity occurs in the sea ice zone and polynya. Antarctic Polynya are areas of open ocean surrounded by sea ice. Extremely high concentrations of DMS of up to 150 nmol dm^{-3} have been measured in such areas, indicating that Antarctic polynyas strongly impact atmospheric chemistry downwind and possibly the overall source/sink strength of the Southern Ocean. Measurements in the Antarctic sea ice zone during sea ice melt would answer the question of whether sea ice zones from the two poles are similar or not. A large number of depth profiles would be useful to compare how these compounds vary with depth in the sea ice zone.

Larger Temporal coverage. The Southern Ocean undergoes large seasonal changes for example in biological productivity and light intensity. These seasonal changes are particularly pronounced in the sea ice zone. These changes will affect dissolved gas fluxes and thus the annual ocean source/sink. Global models consistently highlight that the lack of surface seawater measurements during winter introduces potentially large uncertainties in their models and annual source/sink estimates. The cruise presented in this thesis was at the end of the summer when some biological productivity and photochemistry was still

present. To fully quantify the year-long oceanic sink/source of the Southern Ocean, measurements at earlier times of the year and during austral winter would be needed.

Further auxiliary data. One of the shortcomings of the cruise in the Antarctic is the lack of detailed auxiliary data. Further auxiliary data, such as information on dissolved carbon, light intensity/penetration, bacterial community composition and phytoplankton pigment measurements would have allowed me to comment in more detail on the variability of VOCs in seawater. Additionally, underway atmospheric measurements of e.g. particle size distribution/composition would have allowed comments on the effect of oceanic emissions on the atmospheric chemistry in the marine atmosphere.

6.5.3 Further measurements in the Arctic

Concurrent ambient air measurements. The air – sea flux of methanol, acetone and acetaldehyde is highly dependent on the ambient air concentration. However, ambient air mole fractions were not measured during the Arctic cruise. To provide estimates of the air – sea fluxes of these gases in the sea ice zone, concurrent measurements of ambient air mole fractions would be required.

Larger temporal coverage. The Arctic is characterized by strong seasonal variations in the atmosphere and in the water column. The data presented here suggests that sea ice melt influences the distribution of VOCs in seawater. To better understand the influence of sea ice melt, an annual study should be conducted measuring surface seawater and depth profile concentrations before and during sea ice melt, starting during the Arctic Haze period. Combined with ambient air measurements, this would give exciting insight into what controls the variability of these VOCs in the sea ice zone and enable to estimate the annual mean source/sink strength of this region.

Larger spatial coverage. One of the limitations of the Arctic dataset is that the measurements cover a relatively small, but biogeochemically exciting/variable area. To better constrain the net Arctic Ocean source/sink strength, measurements over a larger area would be required. Particularly seawater measurements of the far North Atlantic and in the Arctic Ocean would provide a lot of insight.

6.5.4 Elucidating the key biogeochemical processes at play

My measurements were of the standing stocks of VOCs (i.e. concentrations), which is most useful for evaluating spatial and temporal patterns and air – sea fluxes. However, in situ

rate measurements (e.g. biological production, photochemical production, microbial consumption) are needed to elucidate the key biogeochemical processes at play.

Culture Studies. Recent laboratory cultures suggest that phytoplankton may be a source of methanol, acetone and acetaldehyde. In my experience, it is very difficult to avoid some form of contamination of these compounds during measurements. This is made especially difficult in phytoplankton cultures which require long term incubation with many different utensils which could each add an unexpected contamination. Further, many of these incubation studies lack thorough characterization of the measurement technique used to take dissolved gas measurements. Finally, the literature may also be biased as only studies that find production of these gases by certain phytoplankton species tend to be reported. Thus, I would like to see laboratory culture studies addressing these issues. This would be useful to ascertain which phytoplankton species produce these compounds and potentially provide a better representation of the ocean flux in global models.

The SFCE for rate measurements. Due to its simple and versatile design, the SFCE could be used for a broad range of experiments and particularly rate measurements. For example, combined with a UV lamp the SFCE could be used to determine underway photochemical production rates. Similarly, I envisage to continuously add a radiolabelled standard from a gas canister with a mass flow controller to an extremely long SFCE leading to a long incubation time. This could be used to determine underway biological consumption rates at very high resolution.

Collaboration with modellers. It would be useful to work with global atmospheric modellers to scale up some of these observations. I would really like to provide a critical review for them of existing measurements and the potential uncertainties of using these measurements. This could lead to a more accurate representation of surface ocean concentrations in these models. Additionally, in my thesis I have highlighted the uncertainties surrounding solubility. Using a different solubility could potentially lead to different ocean fluxes and hopefully a more accurate representation. Working with global biogeochemical modellers would allow to predict more accurately the effect of climate change on the global emissions of these compounds, within the constrain of our understanding of the cycling of these gases in the marine environment.

6.6 Closing remarks

One of the most valuable lessons that I learned during my PhD can be summed up by a quote from my primary supervisor:

"After a cruise, everyone comes home with numbers. You just need to make sure they are the right numbers"

I think this was a mantra for me during the PhD and set me up for my future career. A large focus of my PhD has been on the analytical chemistry and coming up with good quality measurements. I have done a lot of thorough work by calibrating the instrument and determining the calibration slopes to apply to my measurement. I managed to compare home-made liquid standards to certified gas standards, leading to the suggestion of improved solubilities of these compounds and increasing confidence in my serial dilution procedure. In addition, I collected several different types of backgrounds in order to improve the accuracy of the measurements and minimize/estimate the measurement uncertainty.

It has been a privilege to take part in both field campaigns, even if at the time I was caught up in all the details of getting the measurements off the ground. The measurements from both field deployments are very valuable for global emission estimates. They also improved our understanding of what influences the variability in surface seawater concentrations of these VOCs and gave insights into the effect of sea ice. At the same time, many questions remain unanswered as single field deployments are usually unable to solve global problems. I believe that we should combine these measurements and those from other investigators with emerging computational techniques, namely artificial intelligence. This would allow us to calculate the global distributions of these compounds in surface seawater.

7 Appendix

7.1 Key to Figure 3.5

Table A1: Key to Figure 3.5: This table lists experimentally determined air over water dimensionless Henry solubilities of methanol, acetone and acetaldehyde at 20 ºC in MilliQ water as listed in Sander (2015) along with the in-text reference and the computed slope of the response in the SFCE in $dm^3\ mol^{-1}$. For full reference of the cited solubilities, please refer to Sander (2015). Experimentally determined calibration slope for methanol, acetone and acetaldehyde are (0.00786 ±0.00115) $dm^3\ mol^{-1}$, (0.0469 ±0.0145) $dm^3\ mol^{-1}$ and (0.0743 ±0.0190) $dm^3\ mol^{-1}$.

Reference	Henry solubility H / 1	$S_{predicted}$ / ($dm^3\ mol^{-1}$)
Methanol		
1. Li et al., (1993)	7378	0.00326
2. Snider and Dawson (1985)	7220	0.00333
3. Rytting et al., (1978)	7378	0.00326
4. Brunett et al., (1963)	7714	0.00312
5. Glew and Moelwyn-Hughes (1953)	7430	0.00324
6. Butler et al., (1935)	7714	0.00312
7. Vitenberg and Dobryakov (2008)	7044	0.00341
8. St.Pierre et al., (2014)	2212	0.01090
9. Helburn et al., (2008)	2616	0.00919
10. Teja et al., (2001)	6716	0.00358
11. Zhou et al., (2000)	8882	0.00271
12. Gupta et al., (2000)	6678	0.00360
13. Altschuh et al., (1999)	5367	0.00448
14. Burkholder et al. (2015)	6715	0.00358
Acetone		
15. Benkelberg et al., (1995)	891	0.0269
16. Hoff et al., (1993)	878	0.0274
17. Zhou and Mopper (1990)	1060	0.0227
18. Guitart et al., (1989)	746	0.0322
19. Hellmann et al., (1987)	341	0.0703
20. Snider and Dawson (1985)	802	0.0299
21. Schoene and Steinhanses (1985)	1062	0.0226
22. Sato and Nakajima (1979)	933	0.0258

Table A1: Key to Figure 3.5- continued

Reference	Henry solubility H / 1	$S_{predicted}$ / (dm^3 mol^{-1})
23. Vittenberg et al., (1975)	813	0.0295
24. Poulain et al., (2010)	946	0.0254
25. Ji and Evans (2007)	863	0.0278
26. Falabella et al., (2006)	744	0.0323
27. Strekowski and George (2005)	914	0.0263
28. Straver and de Loos (2005)	781	0.0308
29. Chai et al., (2005)	748	0.0321
30. Ayuttaya et al., (2001) (EPICS method)	325	0.0737
31. Ayuttaya et al., (2001) (static cell, linear form)	3.0587	5.93
32. Ayuttaya et al., (2001) (direct phase concentration method)	1725	0.0139
33. Burkholder et al. (2015)	901	0.0267
Acetaldehyde		
34. Ji and Evans (2007)	527	0.0455
35. Straver and de Loos (2005)	374	0.0641
36. Marin et al., (1999)	510	0.0470
37. Benkelberg et al., (1995)	439	0.0547
38. Zhou and Mopper (1990)	552	0.0435
39. Guitart et al., (1989)	242	0.0991
40. Betterton and Hoffmann (1988)	419	0.0572
41. Snider and Dawson (1985)	408	0.0589
42. Vitenberg et al., (1974)	298	0.0991
40. Betterton and Hoffmann (1988)	419	0.0572
41. Snider and Dawson (1985)	408	0.0589
42. Vitenberg et al., (1974)	298	0.0804
43. Buttery et al., (1969)	487	0.0493
44. Burkholder et al. (2015)	444	0.0541

7.2 Use of work, which has formed part of jointly-authored publications within this thesis

Chapter 2 and Chapter 3 are a greatly expanded version of a published paper:

Wohl, C., Capelle, D., Jones, A., Sturges, W. T., Nightingale, P. D., Else, B. G. T., and Yang, M.: Segmented flow coil equilibrator coupled to a proton-transfer-reaction mass spectrometer for measurements of a broad range of volatile organic compounds in seawater, Ocean Sci., 15, 925–940, https://doi.org/10.5194/os-15-925-2019, 2019.

Author contributions

CW and MY designed the equilibrator and worked on the raw data interpretation. CW carried out system performance tests. PDN, AJ, DC, and WTS provided input on the method development. CW carried out the deployment on board with help from MY during installation. Collaboration with BGTE made these measurements in the Canadian Arctic possible. CW prepared the paper with contributions from all co-authors.

Chapter 5 is a greatly expanded version of a published paper:

Wohl, C., Brown, I., Kitidis, V., Jones, A. E., Sturges, W. T., Nightingale, P. D., and Yang, M.: Underway seawater and atmospheric measurements of volatile organic compounds in the Southern Ocean, Biogeosciences, 17, 2593–2619, https://doi.org/10.5194/bg-17-2593-2020, 2020.

Author contributions

CW carried out the measurements and on-board calibrations under the supervision of MY. PDN, AEJ, MY, and WTS provided input to the set-up on-board. PDN and CW wrote the Collaborative Antarctic Support Scheme proposal to secure a berth on ANDREXII. IB measured underway seawater CO2 using the set-up installed with VK. CW analysed the data and prepared the manuscript with contributions from all co-authors.

8 List of references

Abbatt, J. P. D., Richard Leaitch, W., Aliabadi, A. A., Bertram, A. K., Blanchet, J. P., Boivin-Rioux, A., Bozem, H., Burkart, J., Chang, R. Y. W., Charette, J., Chaubey, J. P., Christensen, R. J., Cirisan, A., Collins, D. B., Croft, B., Dionne, J., Evans, G. J., Fletcher, C. G., Gali, M., Ghahremaninezhad, R., Girard, E., Gong, W., Gosselin, M., Gourdal, M., Hanna, S. J., Hayashida, H., Herber, A. B., Hesaraki, S., Hoor, P., Huang, L., Hussherr, R., Irish, V. E., Keita, S. A., Kodros, J. K., Köllner, F., Kolonjari, F., Kunkel, D., Ladino, L. A., Law, K., Levasseur, M., Libois, Q., Liggio, J., Lizotte, M., MacDonald, K. M., Mahmood, R., Martin, R. V., Mason, R. H., Miller, L. A., Moravek, A., Mortenson, E., Mungall, E. L., Murphy, J. G., Namazi, M., Norman, A. L., O'Neill, N. T., Pierce, J. R., Russell, L. M., Schneider, J., Schulz, H., Sharma, S., Si, M., Staebler, R. M., Steiner, N. S., Thomas, J. L., Von Salzen, K., Wentzell, J. J. B., Willis, M. D., Wentworth, G. R., Xu, J. W. and Yakobi-Hancock, J. D.: Overview paper: New insights into aerosol and climate in the Arctic, Atmos. Chem. Phys., 19(4), 2527–2560, doi:10.5194/acp-19-2527-2019, 2019.

Ahmed, M., Else, B. G. T., Burgers, T. M. and Papakyriakou, T.: Variability of Surface Water pCO2 in the Canadian Arctic Archipelago From 2010 to 2016, J. Geophys. Res. Ocean., 124(3), 1876–1896, doi:10.1029/2018JC014639, 2019.

Ahmed, M. M. M., Else, B. G. T., Capelle, D., Miller, L. A. and Papakyriakou, T.: Underestimation of surface pCO2 and air-sea CO2 fluxes due to freshwater stratification in an Arctic shelf sea, Hudson Bay, Elem. Sci. Anthr., 9(1), 0–21, 2020.

Alcolombri, U., Ben-Dor, S., Feldmesser, E., Levin, Y., Tawfik, D. S. and Vardi, A.: Identification of the algal dimethyl sulfide-releasing enzyme: A missing link in the marine sulfur cycle, Science (80-.)., doi:10.1126/science.aab1586, 2015.

Alvarez, L. A., Exton, D. A., Timmis, K. N., Suggett, D. J. and McGenity, T. J.: Characterization of marine isoprene-degrading communities, Environ. Microbiol., 11(12), 3280–3291, doi:10.1111/j.1462-2920.2009.02069.x, 2009.

Amos, A. F.: A decade of oceanographic variability in summertime near Elephant Island, Antarctica, J. Geophys. Res. Ocean., 106(C10), 22401–22423, doi:10.1029/2000jc000315, 2001.

Amundsen Science Data Collection: TSG and CTD data collected by the CCGS Amundsen in the Canadian Arctic. Processed data. TSG Version 2. CTD Version 1. Archived at www.polardata.ca, Canadian Cryospheric Information Network (CCIN), ArcticNet Inc.,

Québec, Canada., doi:TSG: https://doi.org/10.5884/12715. Accessed on 14/09/21.CTD: https://www.polardata.ca/pdcsearch/?doi_id=12713 Accessed on 14/09/21., 2017.

Andrews, S. J., Hackenberg, S. C. and Carpenter, L. J.: Technical Note : A fully automated purge and trap GC-MS system for quantification of volatile organic compound (VOC) fluxes between the ocean and atmosphere, Ocean Sci., 11, 313–321, doi:10.5194/os-11-313-2015, 2015.

Apel, E. C., Olson, J. R., Crawford, J. H., Hornbrook, R. S., Hills, A. J., Cantrell, C. A., Emmons, L. K., Knapp, D. J., Hall, S., Mauldin, R. L., Weinheimer, A. J., Fried, A., Blake, D. R., Crounse, J. D., St. Clair, J. M., Wennberg, P. O., Diskin, G. S., Fuelberg, H. E., Wisthaler, A., Mikoviny, T., Brune, W. and Riemer, D. D.: Impact of the deep convection of isoprene and other reactive trace species on radicals and ozone in the upper troposphere, Atmos. Chem. Phys., 12(2), 1135–1150, doi:10.5194/acp-12-1135-2012, 2012.

Archer, S. D., Gilbert, F. J., Nightingale, P. D., Zubkov, M. V., Taylor, A. H., Smith, G. C. and Burkill, P. H.: Transformation of dimethylsulphoniopropionate to dimethyl sulphide during summer in the North Sea with an examination of key processes via a modelling approach, Deep. Res. Part II Top. Stud. Oceanogr., 49(15), 3067–3101, doi:10.1016/S0967-0645(02)00072-3, 2002.

Ardelan, M. V., Holm-Hansen, O., Hewes, C. D., Reiss, C. S., Silva, N. S., Dulaiova, H., Steinnes, E. and Sakshaug, E.: Natural iron enrichment around the Antarctic Peninsula in the Southern Ocean, Biogeosciences, 7(1), 11–25, doi:10.5194/bg-7-11-2010, 2010.

Ardyna, M., Babin, M., Gosselin, M., Devred, E., Bélanger, S., Matsuoka, A. and Tremblay, J. E.: Parameterization of vertical chlorophyll a in the Arctic Ocean: Impact of the subsurface chlorophyll maximum on regional, seasonal, and annual primary production estimates, Biogeosciences, 10(6), 4383–4404, doi:10.5194/bg-10-4383-2013, 2013.

Ardyna, M., Lacour, L., Sergi, S., d'Ovidio, F., Sallée, J. B., Rembauville, M., Blain, S., Tagliabue, A., Schlitzer, R., Jeandel, C., Arrigo, K. R. and Claustre, H.: Hydrothermal vents trigger massive phytoplankton blooms in the Southern Ocean, Nat. Commun., 10(1), 1–8, doi:10.1038/s41467-019-09973-6, 2019.

Arévalo-Martínez, D. L., Beyer, M., Krumbholz, M., Piller, I., Kock, A., Steinhoff, T., Körtzinger, A. and Bange, H. W.: A new method for continuous measurements of oceanic and atmospheric N2O, CO and CO2: Performance of off-axis integrated cavity output spectroscopy (OA-ICOS) coupled to non-dispersive infrared detection (NDIR), Ocean Sci.,

doi:10.5194/os-9-1071-2013, 2013.

Arnold, S. R., Spracklen, D. V, Williams, J., Yassaa, N., Sciare, J., Bonsang, B., Gros, V., Peeken, I., Lewis, A. C., Alvain, S. and Moulin, C.: Evaluation of the global oceanic isoprene source and its impacts on marine organic carbon aerosol, Atmos. Chem. Phys., 9, 1253–1262, 2009.

Arrigo, K. R., Matrai, P. A. and Van Dijken, G. L.: Primary productivity in the Arctic Ocean: Impacts of complex optical properties and subsurface chlorophyll maxima on large-scale estimates, J. Geophys. Res. Ocean., 116(11), 1–15, doi:10.1029/2011JC007273, 2011.

Asher, E. C., Merzouk, A. and Tortell, P. D.: Fine-scale spatial and temporal variability of surface water dimethylsufide (DMS) concentrations and sea-air fluxes in the NE Subarctic Pacific, Mar. Chem., 126(1–4), 63–75, doi:10.1016/j.marchem.2011.03.009, 2011.

Aston, F. W.: Mass Spectrometry : Quadrupole Mass Filter, Mass Spectrom. Quadrupole Mass Filter, (1918), 2008.

Atkins, P. and Paula, J. De: Atkins' physical chemistry., 2009.

Atkinson, R.: Atmospheric chemistry of VOCs and NO(x), Atmos. Environ., 34(12–14), 2063–2101, doi:10.1016/S1352-2310(99)00460-4, 2000.

Baker, A. R., Turner, S. M., Broadgate, W. J., Thompson, A., McFiggans, G. B., Vesperini, O., Nightingal, P. D., Liss, P. S. and Jickells, T. D.: Distribution and sea-air fluxes of biogenic trace gases in the eastern Atlantic Ocean, Global Biogeochem. Cycles, 14(3), 871–886, doi:10.1029/1999GB001219, 2000.

Barak-Gavish, N., Frada, M. J., Ku, C., Lee, P. A., DiTullio, G. R., Malitsky, S., Aharoni, A., Green, S. J., Rotkopf, R., Kartvelishvily, E., Sheyn, U., Schatz, D. and Vardi, A.: Bacterial virulence against an oceanic bloom-forming phytoplankter is mediated by algal DMSP, Sci. Adv., doi:10.1126/sciadv.aau5716, 2018.

Barber, D. G., Hop, H., Mundy, C. J., Else, B., Dmitrenko, I. A., Tremblay, J. E., Ehn, J. K., Assmy, P., Daase, M., Candlish, L. M. and Rysgaard, S.: Selected physical, biological and biogeochemical implications of a rapidly changing Arctic Marginal Ice Zone, Prog. Oceanogr., 139, 122–150, doi:10.1016/j.pocean.2015.09.003, 2015.

Bates, K. H., Jacob, D. J., Wang, S., Hornbrook, R. S., Apel, E. C., Kim, M. J., Millet, D. B., Wells, K. C., Chen, X., Brewer, J. F., Ray, E. A., Commane, R., Diskin, G. S. and Wofsy, S. C.: The global budget of atmospheric methanol: new constraints on secondary, oceanic, and

terrestrial sources, J. Geophys. Res. Atmos., 1–23, doi:10.1029/2020jd033439, 2021.

Beale, R., Liss, P. S. and Nightingale, P. D.: First oceanic measurements of ethanol and propanol, Geophys. Res. Lett., 37(24), 1–5, doi:10.1029/2010GL045534, 2010.

Beale, R., Liss, P. S., Dixon, J. L. and Nightingale, P. D.: Quantification of oxygenated volatile organic compounds in seawater by membrane inlet-proton transfer reaction/mass spectrometry, Anal. Chim. Acta, 706(1), 128–134, doi:10.1016/j.aca.2011.08.023, 2011.

Beale, R., Dixon, J. L., Arnold, S. R., Liss, P. S. and Nightingale, P. D.: Methanol, acetaldehyde, and acetone in the surface waters of the Atlantic Ocean, J. Geophys. Res. Ocean., 118(10), 5412–5425, doi:10.1002/jgrc.20322, 2013.

Beale, R., Dixon, J. L., Smyth, T. J. and Nightingale, P. D.: Annual study of oxygenated volatile organic compounds in UK shelf waters, Mar. Chem., 171, 96–106, doi:10.1016/j.marchem.2015.02.013, 2015.

Beaupré-Laperrière, A., Mucci, A. and Thomas, H.: The recent state and variability of the carbonate system of the Canadian Arctic Archipelago and adjacent basins in the context of ocean acidification, Biogeosciences, 17(14), 3923–3942, doi:10.5194/bg-17-3923-2020, 2020.

Bell, R. P., Rand, M. H. and Wynne-Jones, K. M. A.: Kinetics of the hydration of acetaldehyde, Trans. Faraday Soc., 52(C), 1093–1102, doi:10.1039/tf9565201093, 1956.

Bell, T. G., Bruyn, W. De, Miller, S. D., Ward, B., Christensen, K. and Saltzman, E. S.: Air – sea dimethylsulfide (DMS) gas transfer in the North Atlantic : evidence for limited interfacial gas exchange at high wind speed, , 11073–11087, doi:10.5194/acp-13-11073-2013, 2013.

Bell, T. G., De Bruyn, W., Marandino, C. A., Miller, S. D., Law, C. S., Smith, M. J. and Saltzman, E. S.: Dimethylsulfide gas transfer coefficients from algal blooms in the Southern Ocean, Atmos. Chem. Phys., 15(4), 1783–1794, doi:10.5194/acp-15-1783-2015, 2015.

Benkelberg, H. J., Hamm, S. and Warneck, P.: Henry's law coefficients for aqueous solutions of acetone, acetaldehyde and acetonitrile, and equilibrium constants for the addition compounds of acetone and acetaldehyde with bisulfite, J. Atmos. Chem., 20(1), 17–34, doi:10.1007/BF01099916, 1995.

Blain, S., Tréguer, P., Belviso, S., Bucciarelli, E., Denis, M., Desabre, S., Fiala, M., Martin Jézéquel, V., Le Fèvre, J., Mayzaud, P., Marty, J. C. and Razouls, S.: A biogeochemical study of the island mass effect in the context of the iron hypothesis: Kerguelen Islands, Southern

Ocean, Deep. Res. Part I Oceanogr. Res. Pap., doi:10.1016/S0967-0637(00)00047-9, 2001.

Blain, S., Quéguiner, B., Armand, L., Belviso, S., Bombled, B., Bopp, L., Bowie, A., Brunet, C., Brussaard, C., Carlotti, F., Christaki, U., Corbière, A., Durand, I., Ebersbach, F., Fuda, J. L., Garcia, N., Gerringa, L., Griffiths, B., Guigue, C., Guillerm, C., Jacquet, S., Jeandel, C., Laan, P., Lefèvre, D., Lo Monaco, C., Malits, A., Mosseri, J., Obernosterer, I., Park, Y. H., Picheral, M., Pondaven, P., Remenyi, T., Sandroni, V., Sarthou, G., Savoye, N., Scouarnec, L., Souhaut, M., Thuiller, D., Timmermans, K., Trull, T., Uitz, J., Van Beek, P., Veldhuis, M., Vincent, D., Viollier, E., Vong, L. and Wagener, T.: Effect of natural iron fertilization on carbon sequestration in the Southern Ocean, Nature, 446(7139), 1070–1074, doi:10.1038/nature05700, 2007.

Blake, R. S., Monks, P. S. and Ellis, A. M.: Proton-transfer reaction mass spectrometry., Chem. Rev., 109(3), 861–896, doi:10.1021/cr800364q, 2009.

Blando, J. D. and Turpin, B. J.: Secondary organic aerosol formation in cloud and fog droplets: A literature evaluation of plausibility, Atmos. Environ., 34(10), 1623–1632, doi:10.1016/S1352-2310(99)00392-1, 2000.

Blomquist, B. W., Brumer, S. E., Fairall, C. W., Huebert, B. J., Zappa, C. J., Brooks, I. M., Yang, M., Bariteau, L., Prytherch, J., Hare, J. E., Czerski, H., Matei, A. and Pascal, R. W.: Wind Speed and Sea State Dependencies of Air-Sea Gas Transfer: Results From the High Wind Speed Gas Exchange Study (HiWinGS), J. Geophys. Res. Ocean., 122(10), 8034–8062, doi:10.1002/2017JC013181, 2017.

Bloss, W. J., Evans, M. J., Lee, J. D., Sommariva, R., Heard, D. E. and Pilling, M. J.: The oxidative capacity of the troposphere: Coupling of field measurements of OH and a global chemistry transport model, Faraday Discuss., 130, 425–436, doi:10.1039/b419090d, 2005.

Bonsang, B., Gros, V., Peeken, I., Yassaa, N., Bluhm, K., Zoellner, E., Sarda-Esteve, R. and Williams, J.: Isoprene emission from phytoplankton monocultures: The relationship with chlorophyll-a, cell volume and carbon content, Environ. Chem., doi:10.1071/EN09156, 2010.

Booge, D., Marandino, C. A., Schlundt, C., Palmer, P. I., Schlundt, M., Atlas, E. L., Bracher, A., Saltzman, E. S. and Wallace, D. W. R.: Can simple models predict large-scale surface ocean isoprene concentrations?, Atmos. Chem. Phys., 16(18), 11807–11821, doi:10.5194/acp-16-11807-2016, 2016.

Booge, D., Schlundt, C., Bracher, A., Endres, S., Zäncker, B. and Marandino, C. A.: Marine isoprene production and consumption in the mixed layer of the surface ocean- A field study over two oceanic regions, Biogeosciences, 15(2), 649–667, doi:10.5194/bg-15-649-2018, 2018.

Boucher, O. and Pham, M.: History of sulfate aerosol radiative forcings, Geophys. Res. Lett., doi:10.1029/2001GL014048, 2002.

Boudries, H., Bottenheim, J. W., Guimbaud, C., Grannas, A. M., Shepson, P. B., Houdier, S., Perrier, S. and Dominé, F.: Distribution and trends of oxygenated hydrocarbons in the high Arctic derived from measurements in the atmospheric boundary layer and interstitial snow air during the ALERT2000 field campaign, Atmos. Environ., 36(15–16), 2573–2583, doi:10.1016/S1352-2310(02)00122-X, 2002.

Bouillon, R. C., Lee, P. A., De Mora, S. J., Levasseur, M. and Lovejoy, C.: Vernal distribution of dimethylsulphide, dimethylsulphoniopropionate, and dimethylsulphoxide in the North Water in 1998, Deep. Res. Part II Top. Stud. Oceanogr., 49(22–23), 5171–5189, doi:10.1016/S0967-0645(02)00184-4, 2002.

de Boyer Montégut, C., Madec, G., Fischer, A. S., Lazar, A. and Iudicone, D.: Mixed layer depth over the global ocean: An examination of profile data and a profile-based climatology, J. Geophys. Res. C Ocean., 109(12), 1–20, doi:10.1029/2004JC002378, 2004.

Brewer, J. F., Bishop, M., Kelp, M., Keller, C. A., Ravishankara, A. R. and Fischer, E. V.: A sensitivity analysis of key natural factors in the modeled global acetone budget, J. Geophys. Res. Atmos., 122(3), 2043–2058, doi:10.1002/2016JD025935, 2017.

Broadgate, W. J., Liss, P. S., Penkett, S. A. and Penkett, A.: Seasonal emissions of isoprene and other reactive hydrocarbon gases from the ocean, Geophys. Res. Lett., 24(21), 2675–2678, doi:10.1029/97GL02736, 1997.

Brüggemann, M., Hayeck, N., George, C., Bonnineau, C., Pesce, S., Alpert, P. A., Perrier, S., Zuth, C., Hoffmann, T., Chen, J. and George, C.: Interfacial photochemistry at the ocean surface is a global source of organic vapors and aerosols, Nat. Commun., 9(1), 1–8, doi:10.1038/s41467-018-04528-7, 2018.

de Bruyn, W. J., Clark, C. D., Senstad, M., Barashy, O. and Hok, S.: The biological degradation of acetaldehyde in coastal seawater, Mar. Chem., 192, 13–21, doi:10.1016/j.marchem.2017.02.008, 2017.

De Bruyn, W. J., Clark, C. D., Pagel, L. and Takehara, C.: Photochemical production of formaldehyde, acetaldehyde and acetone from chromophoric dissolved organic matter in coastal waters, J. Photochem. Photobiol. A Chem., 226(1), 16–22, doi:10.1016/j.jphotochem.2011.10.002, 2011.

Burgers, T. M., Tremblay, J.-É., Else, B. G. T. and Papakyriakou, T. N.: Estimates of net community production from multiple approaches surrounding the spring ice-edge bloom in Baffin Bay, Elem. Sci. Anthr., 8(1), doi:10.1525/elementa.013, 2020.

Burkholder, J. B., Sander, S. P., Abbatt, J., Barker, J. R., Huie, R. E., Kolb, C. E., Kurylo, M. J., Orkin, V. L., Wilmouth, D. M. and Wine, P. H.: Chemical Kinetics and Photochemical Data for Use in Atmospheric Studies, Evaluation Number 18, JPL Publ., doi:10.1002/kin.550171010, 2015.

Butler, J. H., King, D. B., Lobert, J. M., Montzka, S. A., Yvon-Lewis, S. A., Hall, B. D., Warwick, N. J., Mondell, D. J., Aydin, M. and Elkins, J. W.: Oceanic distributions and emissions of short-lived halocarbons, Global Biogeochem. Cycles, 21(1), 1–11, doi:10.1029/2006GB002732, 2007.

Butterworth, B. J. and Miller, S. D.: Air-sea exchange of carbon dioxide in the Southern Ocean and Antarctic marginal ice zone, , doi:10.1002/2016GL069581.Received, 2016.

Cappellin, L., Karl, T., Probst, M., Ismailova, O., Winkler, P. M., Soukoulis, C., Aprea, E., Märk, T. D., Gasperi, F. and Biasioli, F.: On quantitative determination of volatile organic compound concentrations using proton transfer reaction time-of-flight mass spectrometry, Environ. Sci. Technol., 46(4), 2283–2290, doi:10.1021/es203985t, 2012.

Carpenter, L. J. and Nightingale, P. D.: Chemistry and Release of Gases from the Surface Ocean, Chem. Rev., 115(10), 4015–4034, doi:10.1021/cr5007123, 2015.

Carslaw, K. S., Lee, L. A., Reddington, C. L., Pringle, K. J., Rap, A., Forster, P. M., Mann, G. W., Spracklen, D. V., Woodhouse, M. T., Regayre, L. A. and Pierce, J. R.: Large contribution of natural aerosols to uncertainty in indirect forcing, Nature, doi:10.1038/nature12674, 2013.

Charlson, R. J., Lovelock, J. E., Andreae, M. O. and Warren, S. G.: Oceanic phytoplankton, atmospheric sulphur, cloud albedo and climate, Nature, 326(6114), 655–661, doi:10.1038/326655a0, 1987.

Ciuraru, R., Fine, L., Pinxteren, M. Van, D'Anna, B., Herrmann, H. and George, C.:

Unravelling New Processes at Interfaces: Photochemical Isoprene Production at the Sea Surface, Environ. Sci. Technol., 49(22), 13199–13205, doi:10.1021/acs.est.5b02388, 2015.

Claeys, M.: Formation of Secondary Organic Aerosols Through Photooxidation of Isoprene, Science (80-.)., 303(5661), 1173–1176, doi:10.1126/science.1092805, 2004.

Clayton McAuliffe: GC Determination of solutes by multiple phase equilibration, Chem. Tech., 1971.

Collins, D. B., Burkart, J., Chang, R. Y.-W. Y. W., Lizotte, M., Boivin-Rioux, A., Blais, M., Mungall, E. L., Boyer, M., Irish, V. E., Massé, G., Kunkel, D., Tremblay, J.-É. É., Papakyriakou, T., Bertram, A. K., Bozem, H., Gosselin, M., Levasseur, M. and Abbatt, J. P. D.: Frequent ultrafine particle formation and growth in Canadian Arctic marine and coastal environments, Atmos. Chem. Phys., 17(21), 13119–13138, doi:10.5194/acp-17-13119-2017, 2017.

Colomb, A., Gros, V., Alvain, S., Sarda-Esteve, R., Bonsang, B., Moulin, C., Klupfel, T. and Williams, J.: Variation of atmospheric volatile organic compounds over the Southern Indian Ocean (30-49 degrees S), Environ. Chem., 6(1), 70–82, doi:10.1071/en08072, 2009.

Comiso, J. C., Kwok, R., Martin, S. and Gordon, A. L.: Variability and trends in sea ice extent and ice production in the Ross Sea, J. Geophys. Res. Ocean., 116(4), doi:10.1029/2010JC006391, 2011.

Curran, M. A. J., Jones, G. B. and Burton, H.: Spatial distribution of dimethylsulfide and dimethylsulfoniopropionate in the Australasian sector of the Southern Ocean, J. Geophys. Res., 103, 16677–16689, doi:https://doi.org/10.1029/97JD03453, 1998.

Curson, A. R. J., Liu, J., Bermejo Martínez, A., Green, R. T., Chan, Y., Carrión, O., Williams, B. T., Zhang, S. H., Yang, G. P., Bulman Page, P. C., Zhang, X. H. and Todd, J. D.: Dimethylsulfoniopropionate biosynthesis in marine bacteria and identification of the key gene in this process, Nat. Microbiol., doi:10.1038/nmicrobiol.2017.9, 2017.

Dani, K. G. S. G. S. and Loreto, F.: Trade-Off Between Dimethyl Sulfide and Isoprene Emissions from Marine Phytoplankton, Trends Plant Sci., xx, 1–12, doi:10.1016/j.tplants.2017.01.006, 2017.

Davie-Martin, C. L., Giovannoni, S. J., Behrenfeld, M. J., Penta, W. B. and Halsey, K. H.: Seasonal and spatial variability in the biogenic production and consumption of volatile organic compounds (VOCs) by marine plankton in the North Atlantic Ocean, Frontiers

(Boulder)., 7(December), 1–15, doi:10.3389/fmars.2020.611870, 2020.

Deppeler, S. L. and Davidson, A. T.: Southern Ocean Phytoplankton in a Changing Climate, Front. Mar. Sci., 4(February), doi:10.3389/fmars.2017.00040, 2017.

Derwent, R. G., Parrish, D. D., Galbally, I. E., Stevenson, D. S., Doherty, R. M., Naik, V. and Young, P. J.: Uncertainties in models of tropospheric ozone based on Monte Carlo analysis: Tropospheric ozone burdens, atmospheric lifetimes and surface distributions, Atmos. Environ., doi:10.1016/j.atmosenv.2018.02.047, 2018.

DeVries, A. L. and Steffensen, J. F.: The Arctic and Antarctic Polar Marine Environments, Fish Physiol., 22(C), 1–24, doi:10.1016/S1546-5098(04)22001-5, 2005.

Dixon, J. L. and Nightingale, P. D.: Fine-scale variability in methanol uptake and oxidation: From the microlayer to 1000 m, Biogeosciences, 9(8), 2961–2972, doi:10.5194/bg-9-2961-2012, 2012.

Dixon, J. L., Beale, R. and Nightingale, P. D.: Microbial methanol uptake in northeast Atlantic waters., ISME J., 5(4), 704–16, doi:10.1038/ismej.2010.169, 2011a.

Dixon, J. L., Beale, R. and Nightingale, P. D.: Rapid biological oxidation of methanol in the tropical Atlantic: Significance as a microbial carbon source, Biogeosciences, 8(9), 2707–2716, doi:10.5194/bg-8-2707-2011, 2011b.

Dixon, J. L., Beale, R. and Nightingale, P. D.: Production of methanol, acetaldehyde, and acetone in the Atlantic Ocean, Geophys. Res. Lett., 40(17), 4700–4705, doi:10.1002/grl.50922, 2013.

Dixon, J. L., Beale, R., Sargeant, S. L., Tarran, G. A. and Nightingale, P. D.: Microbial acetone oxidation in coastal seawater, Front. Microbiol., 5(MAY), 1–9, doi:10.3389/fmicb.2014.00243, 2014.

Douglas, D. J.: Linear Quadrupoles in Mass Spectrometry, Mass Spectrom. Rev., 28, 937–960, 2009.

Dunne, E., Galbally, I. E., Cheng, M., Selleck, P., Molloy, S. B. and Lawson, S. J.: Comparison of VOC measurements made by PTR-MS, adsorbent tubes-GC-FID-MS and DNPH derivatization-HPLC during the Sydney Particle Study, 2012: A contribution to the assessment of uncertainty in routine atmospheric VOC measurements, Atmos. Meas. Tech., 11(1), 141–159, doi:10.5194/amt-11-141-2018, 2018.

Ellis, A. M. and Mayhew, C. A.: Proton Transfer Reaction Mass Spectrometry: Principles and Applications., 2014.

Exton, D. A., Suggett, D. J., Steinke, M. and McGenity, T. J.: Spatial and temporal variability of biogenic isoprene emissions from a temperate estuary, Global Biogeochem. Cycles, 26(2), 1–13, doi:10.1029/2011GB004210, 2012.

Fall, R.: Abundant Oxygenates in the Atmosphere: A Biochemical Perspective, Chem. Rev., 103(12), 4941–4951, doi:10.1021/cr0206521, 2003.

Fischer, E. V., Jacob, D. J., Millet, D. B., Yantosca, R. M. and Mao, J.: The role of the ocean in the global atmospheric budget of acetone, Geophys. Res. Lett., 39(1), 3–7, doi:10.1029/2011GL050086, 2012.

Galbally, I. E., Lawson, S. J., Weeks, I. A., Bentley, S. T., Gillett, R. W., Meyer, M. and Goldstein, A. H.: Volatile organic compounds in marine air at Cape Grim, Australia, Environ. Chem., 4(3), 178–182, doi:10.1071/EN07024, 2007.

Galí, M. and Simó, R.: Occurrence and cycling of dimethylated sulfur compounds in the Arctic during summer receding of the ice edge, Mar. Chem., 122(1–4), 105–117, doi:10.1016/j.marchem.2010.07.003, 2010.

Galí, M., Devred, E., Babin, M. and Levasseur, M.: Decadal increase in Arctic dimethylsulfide emission, Proc. Natl. Acad. Sci. U. S. A., 116(39), 19311–19317, doi:10.1073/pnas.1904378116, 2019.

Gantt, B., Meskhidze, N. and Kamykowski, D.: A new physically-based quantification of isoprene and primary organic aerosol emissions from the world ' s oceans, Atmos. Chem. Phys., 9, 4915–4927, 2009.

Gao, S. S., Sjostedt, S. J., Sharma, S., Hall, S. R., Ullmann, K. and Abbatt, J. P. D.: PTR-MS observations of photo-enhanced VOC release from Arctic and midlatitude snow, J. Geophys. Res. Atmos., 117(6), 1–10, doi:10.1029/2011JD017152, 2012.

Gourdal, M., Lizotte, M., Massé, G., Gosselin, M., Poulin, M., Scarratt, M., Charette, J. and Levasseur, M.: Dimethyl sulfide dynamics in first-year sea ice melt ponds in the Canadian Arctic Archipelago, Biogeosciences, doi:10.5194/bg-15-3169-2018, 2018.

de Gouw, J. a. and Warneke, C.: Measurements of Volatile Organic Compounds In the Earth's Atmosphere using Proton-Trasfer-Reaction Mass Spectrometry, Mass Spectrom. Rev., 26, 223–257, doi:10.1002/mas, 2007.

de Gouw, J. A., Goldan, P. D., Warneke, C., Kuster, W. C., Roberts, J. M., Marchewka, M., Bertman, S. B., Pszenny, A. A. P. and Keene, W. C.: Validation of proton transfer reaction-mass spectrometry (PTR-MS) measurements of gas-phase organic compounds in the atmosphere during the New England Air Quality Study (NEAQS) in 2002, J. Geophys. Res. Atmos., doi:10.1029/2003jd003863, 2003.

Guérette, É. A., Paton-Walsh, C., Galbally, I., Molloy, S., Lawson, S., Kubistin, D., Buchholz, R., Griffith, D. W. T., Langenfelds, R. L., Krummel, P. B., Loh, Z., Chambers, S., Griffiths, A., Keywood, M., Selleck, P., Dominick, D., Humphries, R. and Wilson, S. R.: Composition of clean marine air and biogenic influences on VOCs during the MUMBA campaign, Atmosphere (Basel)., 10(7), 1–30, doi:10.3390/atmos10070383, 2019.

Guimbaud, C., Grannas, A. M., Shepson, P. B., Fuentes, J. D., Boudries, H., Bottenheim, J. W., Dominé, F., Houdier, S., Perrier, S., Biesenthal, T. B. and Splawn, B. G.: Snowpack processing of acetaldehyde and acetone in the Arctic atmospheric boundary layer, Atmos. Environ., 36(15–16), 2743–2752, doi:10.1016/S1352-2310(02)00107-3, 2002.

Hackenberg, S. C., Andrews, S. J., Airs, R., Arnold, S. R., Bouman, H. A., Brewin, R. J. W., Chance, R. J., Cummings, D., Dall'Olmo, G., Lewis, A. C., Minaeian, J. K., Reifel, K. M., Small, A., Tarran, G. A., Tilstone, G. H. and Carpenter, L. J.: Potential controls of isoprene in the surface ocean, Global Biogeochem. Cycles, 644–662, doi:10.1002/2016GB005531, 2017.

Hales, B., Takahashi, T. and Bandstra, L.: Atmospheric CO2 uptake by a coastal upwelling system, Global Biogeochem. Cycles, 19, 1–11, doi:10.1029/2004GB002295, 2005.

Halsey, K. H., Giovannoni, S. J., Graus, M., Zhao, Y., Landry, Z., Thrash, J. C., Vergin, K. L. and de Gouw, J. a.: Biological cycling of volatile organic carbon by phytoplankton and bacterioplankton, Limnol. Oceanogr., 62(6), 2650–2661, doi:10.1002/lno.10596, 2017.

Hayashida, H., Carnat, G., Galí, M., Monahan, A. H., Mortenson, E., Sou, T. and Steiner, N. S.: Spatiotemporal Variability in Modeled Bottom Ice and Sea Surface Dimethylsulfide Concentrations and Fluxes in the Arctic During 1979–2015, Global Biogeochem. Cycles, doi:10.1029/2019GB006456, 2020.

Heald, C. . L. L., Goldstein, A. H., Allan, J. D., Aiken, A. C., Apel, E., Atlas, E. L., Baker, A. K., Bates, T. S., Beyersdorf, A. J., Blake, D. R., Campos, T., Coe, H., Crounse, J. D., DeCarlo, P. F., De Gouw, J. A., Dunlea, E. J., Flocke, F. M., Fried, A., Goldan, P., Griffin, R. J., Herndon, S. C., Holloway, J. S., Holzinger, R., Jimenez, J. L., Junkermann, W., Kuster, W. C., Lewis, A. C., Meinardi, S., Millet, D. B., Onasch, T., Polidori, A., Quinn, P. K., Riemer, D. D., Roberts, J. M.,

Salcedo, D., Sive, B., Swanson, A. L., Talbot, R., Warneke, C., Weber, R. J., Weibring, P., Wennberg, P. O., Worsnop, D. R., Wittig, A. E., Zhang, R., Zheng, J. and Zheng, W.: Total observed organic carbon (TOOC) in the atmosphere: A synthesis of North American observations, Atmos. Chem. Phys., 8(December), 17825–17871, doi:10.5194/acp-8-2007-2008, 2008.

Heikes, B. G.: Atmospheric methanol budget and ocean implication, Global Biogeochem. Cycles, 16(4), 1–13, doi:10.1029/2002GB001895, 2002.

Henze, D. K. and Seinfeld, J. H.: Global secondary organic aerosol from isoprene oxidation, Geophys. Res. Lett., 33(9), 6–9, doi:10.1029/2006GL025976, 2006.

Herbig, J., Müller, M., Schallhart, S., Titzmann, T., Graus, M. and Hansel, A.: On-line breath analysis with PTR-TOF, J. Breath Res., 3(2), doi:10.1088/1752-7155/3/2/027004, 2009.

Hudson, E. D., Okuda, K. and Ariya, P. A.: Determination of acetone in seawater using derivatization solid-phase microextraction, Anal. Bioanal. Chem., 388(5–6), 1275–1282, doi:10.1007/s00216-007-1324-x, 2007.

Huybrechts, T., Dewulf, J., Moerman, O. and Langenhove, H. Van: Evaluation of purge-and-trap – high-resolution gas chromatography – mass spectrometry for the determination of 27 volatile organic compounds in marine water at the ng 1-1 concentration level, J. Chromatogr., 893, 367–382, doi:10.1016/s0021-9673(00)00771-8, 2000.

Hyder, P., Edwards, J. M., Allan, R. P., Hewitt, H. T., Bracegirdle, T. J., Gregory, J. M., Wood, R. A., Meijers, A. J. S., Mulcahy, J., Field, P., Furtado, K., Bodas-Salcedo, A., Williams, K. D., Copsey, D., Josey, S. A., Liu, C., Roberts, C. D., Sanchez, C., Ridley, J., Thorpe, L., Hardiman, S. C., Mayer, M., Berry, D. I. and Belcher, S. E.: Critical Southern Ocean climate model biases traced to atmospheric model cloud errors, Nat. Commun., 9(1), doi:10.1038/s41467-018-05634-2, 2018.

Ito, A. and Kawamiya, M.: Potential impact of ocean ecosystem changes due to global warming on marine organic carbon aerosols, Global Biogeochem. Cycles, doi:10.1029/2009GB003559, 2010.

Jarníková, T. and Tortell, P. D.: Towards a revised climatology of summertime dimethylsulfide concentrations and sea-air fluxes in the Southern Ocean, Environ. Chem., 13(2), 364–378, doi:10.1071/EN14272, 2016.

Jarníková, T., Dacey, J., Lizotte, M., Levasseur, M. and Tortell, P.: The distribution of

methylated sulfur compounds, DMS and DMSP, in Canadian subarctic and Arctic marine waters during summer 2015, Biogeosciences, doi:10.5194/bg-15-2449-2018, 2018.

Johnson, J. E.: Evaluation of a seawater equilibrator for shipboard analysis of dissolved oceanic trace gases, Anal. Chim. Acta, 395(1–2), 119–132, doi:10.1016/S0003-2670(99)00361-X, 1999.

Johnson, M. T.: A numerical scheme to calculate temperature and salinity dependent air-water transfer velocities for any gas, Ocean Sci., 6(4), 913–932, doi:10.5194/os-6-913-2010, 2010.

Kameyama, S., Tanimoto, H., Inomata, S., Tsunogai, U., Ooki, A., Yokouchi, Y., Takeda, S., Obata, H. and Uematsu, M.: Equilibrator Inlet-Proton Transfer Reaction-Mass Spectrometry (EI-PTR-MS) for Sensitive , High-Resolution Measurement of Dimethyl Sulfide Dissolved in Seawater, Anal. Chem., 81(21), 9021–9026, 2009.

Kameyama, S., Tanimoto, H., Inomata, S., Tsunogai, U., Ooki, A., Takeda, S., Obata, H., Tsuda, A. and Uematsu, M.: High-resolution measurement of multiple volatile organic compounds dissolved in seawater using equilibrator inlet-proton transfer reaction-mass spectrometry (EI-PTR-MS), Mar. Chem., 122(1–4), 59–73, doi:10.1016/j.marchem.2010.08.003, 2010.

Kameyama, S., Tanimoto, H., Inomata, S., Suzuki, K., Komatsu, D. D., Hirota, A., Konno, U. and Tsunogai, U.: Application of PTR-MS to an incubation experiment of the marine diatom Thalassiosira pseudonana, Geochem. J., 45(5), 355–363, doi:10.2343/geochemj.1.0127, 2011.

Kameyama, S., Yoshida, S., Tanimoto, H., Inomata, S., Suzuki, K. and Yoshikawa-Inoue, H.: High-resolution observations of dissolved isoprene in surface seawater in the Southern Ocean during austral summer 2010-2011, J. Oceanogr., 70(3), 225–239, doi:10.1007/s10872-014-0226-8, 2014.

Karl, T., Yeretzian, C., Jordan, A. and Lindinger, W.: Dynamic measurements of partition coefficients using proton-transfer-reaction mass spectrometry (PTR-MS), Int. J. Mass Spectrom., 223–224, 383–395, doi:10.1016/S1387-3806(02)00927-2, 2003.

Kettle, A. J. and Andreae, M. O.: Flux of dimethylsulfide from the oceans: A comparison of updated data sets and flux models, J. Geophys. Res. Atmos., 105(D22), 26793–26808, doi:10.1029/2000JD900252, 2000.

Khan, M. A. H., Cooke, M. C., Utembe, S. R., Archibald, A. T., Maxwell, P., Morris, W. C., Xiao, P., Derwent, R. G., Jenkin, M. E., Percival, C. J., Walsh, R. C., Young, T. D. S., Simmonds, P. G., Nickless, G., O'Doherty, S. and Shallcross, D. E.: A study of global atmospheric budget and distribution of acetone using global atmospheric model STOCHEM-CRI, Atmos. Environ., 112, 269–277, doi:10.1016/j.atmosenv.2015.04.056, 2015.

Kieber, R., Zhou, X. and Mopper, K.: Formation of carbonyl-compounds from UV-induced photodegradation of humic substances in natural-waters - fate of riverine carbon in the sea, Limnol. Oceanogr., 35(7), 1503–1515 [online] Available from: http://apps.webofknowledge.com/full_record.do?product=UA&search_mode=GeneralSearch&qid=47&SID=4AGMqC1BIln9jo2qV5U&page=1&doc=2, 1990.

Kiene, R. P. and Bates, T. S.: Biological removal of dimethyl sulphide from sea water, Nature, 345, 702–705, doi:10.1038/258748a0, 1990.

Kiene, R. P. and Linn, L. J.: The fate of dissolved dimethylsulfoniopropionate (DMSP) in seawater: Tracer studies using 35S-DMSP, Geochim. Cosmochim. Acta, 64(16), 2797–2810, doi:10.1016/S0016-7037(00)00399-9, 2000.

Kiene, R. P., Linn, L. J. and Bruton, J. A.: New and important roles for DMSP in marine microbial communities, J. Sea Res., 43(3–4), 209–224, doi:10.1016/S1385-1101(00)00023-X, 2000.

Kim, J., Jun Yoon, Y., Gim, Y., Jin Kang, H., Hee Choi, J., Park, K. T. and Yong Lee, B.: Seasonal variations in physical characteristics of aerosol particles at the King Sejong Station, Antarctic Peninsula, Atmos. Chem. Phys., 17(21), 12985–12999, doi:10.5194/acp-17-12985-2017, 2017a.

Kim, M. J., Novak, G. A., Zoerb, M. C., Yang, M., Blomquist, B. W., Huebert, B. J., Cappa, C. D. and Bertram, T. H.: Air-Sea exchange of biogenic volatile organic compounds and the impact on aerosol particle size distributions, Geophys. Res. Lett., doi:10.1002/2017GL072975, 2017b.

Kim, M. J., Novak, G. A., Zoerb, M. C., Yang, M., Blomquist, B. W., Huebert, B. J., Cappa, C. D. and Bertram, T. H.: Air-Sea exchange of biogenic volatile organic compounds and the impact on aerosol particle size distributions, Geophys. Res. Lett., 44(8), 3887–3896, doi:10.1002/2017GL072975, 2017c.

Kitidis, V., Hardman-Mountford, N. J., Litt, E., Brown, I., Cummings, D., Hartman, S., Hydes,

D., Fishwick, J. R., Harris, C., Martinez-Vicente, V., Woodward, E. M. S. and Smyth, T. J.: Seasonal dynamics of the carbonate system in the Western English Channel, Cont. Shelf Res., 42, 30–40, doi:10.1016/j.csr.2012.04.012, 2012.

Kitidis, V., Brown, I., Hardman-Mountford, N. and Lefèvre, N.: Surface ocean carbon dioxide during the Atlantic Meridional Transect (1995–2013); evidence of ocean acidification, Prog. Oceanogr., 158, 65–75, doi:10.1016/j.pocean.2016.08.005, 2017.

Koga, S., Nomura, D. and Wada, M.: Variation of dimethylsulfide mixing ratio over the Southern Ocean from 36°S to 70°S, Polar Sci., 8(3), 306–313, doi:10.1016/j.polar.2014.04.002, 2014.

Korhonen, H., Carslaw, K. S., Spracklen, D. V., Mann, G. W. and Woodhouse, M. T.: Influence of oceanic dimethyl sulfide emissions on cloud condensation nuclei concentrations and seasonality over the remote Southern Hemisphere oceans: A global model study, J. Geophys. Res. Atmos., 113(15), 1–16, doi:10.1029/2007JD009718, 2008.

Kos, G., Kanthasami, V., Adechina, N. and Ariya, P. a.: Volatile organic compounds in Arctic snow: concentrations and implications for atmospheric processes, Environ. Sci. Process. Impacts, 16(11), 2592–2603, doi:10.1039/C4EM00410H, 2014.

Ksionzek, K. B., Lechtenfeld, O. J., McCallister, S. L., Schmitt-Kopplin, P., Geuer, J. K., Geibert, W. and Koch, B. P.: Dissolved organic sulfur in the ocean: Biogeochemistry of a petagram inventory, Science (80-.)., doi:10.1126/science.aaf7796, 2016.

Kurz, J. L. and Coburn, J. I.: The Hydration of Acetaldehyde. II. Transition-State Characterization, J. Am. Chem. Soc., 89(14), 3528–3537, doi:10.1021/ja00990a600, 1967.

Lana, A., Bell, T. G., Simó, R., Vallina, S. M., Ballabrera-Poy, J., Kettle, A. J., Dachs, J., Bopp, L., Saltzman, E. S., Stefels, J., Johnson, J. E. and Liss, P. S.: An updated climatology of surface dimethlysulfide concentrations and emission fluxes in the global ocean, Global Biogeochem. Cycles, 25(1), doi:10.1029/2010GB003850, 2011.

Land, P. E., Shutler, J. D., Bell, T. G. and Yang, M.: Exploiting satellite earth observation to quantify current global oceanic DMS flux and its future climate sensitivity, J. Geophys. Res. Ocean., 119, 7725–7740, doi:10.1002/jgrc.20224, 2014.

Lee, G., Choi, H. S., Lee, T., Choi, J., Park, J. S. and Ahn, J. Y.: Variations of regional background peroxyacetyl nitrate in marine boundary layer over Baengyeong Island, South Korea, Atmos. Environ., doi:10.1016/j.atmosenv.2012.07.075, 2012.

Legrand, M., Gros, V., Preunkert, S., Sarda-Estve, R., Thierry, A. M., Pépy, G. and Jourdain, B.: A reassessment of the budget of formic and acetic acids in the boundary layer at Dumont d'Urville (coastal Antarctica): The role of penguin emissions on the budget of several oxygenated volatile organic compounds, J. Geophys. Res. Atmos., 117(6), 1–15, doi:10.1029/2011JD017102, 2012.

Leighton, D. T. and Calo, J. M.: Distribution Coefficients of Chlorinated Hydrocarbons in Dilute Air-Water Systems for Groundwater Contamination Applications, J. Chem. Eng. Data, 26(4), 382–385, doi:10.1021/je00026a010, 1981.

Leng, C., Kish, J. D., Kelley, J., Mach, M., Hiltner, J., Zhang, Y. and Liu, Y.: Temperature-dependent Henry's law constants of atmospheric organics of biogenic origin, J. Phys. Chem. A, 117(40), 10359–10367, doi:10.1021/jp403603z, 2013.

Levasseur, M.: Impact of Arctic meltdown on the microbial cycling of sulphur, Nat. Geosci., 6(9), 691–700, doi:10.1038/ngeo1910, 2013.

Lewis, A. C., Hopkins, J. R., Carpenter, L. J., Stanton, J., Read, K. A. and Pilling, M. J.: Sources and sinks of acetone, methanol, and acetaldehyde in North Atlantic marine air, Atmos. Chem. Phys., 5(7), 1963–1974, doi:10.5194/acp-5-1963-2005, 2005.

Lindinger, W. and Jordan, A.: Proton-transfer-reaction mass spectrometry (PTR–MS): on-line monitoring of volatile organic compounds at pptv levels, Chem. Soc. Rev., 27(5), 347–354, doi:10.1039/a827347z, 1998.

Lindinger, W., Hansel, A. and Jordan, A.: On-line monitoring of volatile organic compounds at pptv levels by means of proton-transfer-reaction mass spectrometry (PTR-MS) medical applications, food control and environmental research, Int. J. Mass Spectrom. Ion Process., 173(3), 191–241, doi:10.1016/S0168-1176(97)00281-4, 1998.

Liss, P. S. and Lovelock, J. E.: Climate change: The effect of DMS emissions, Environ. Chem., 4(6), 377–378, doi:10.1071/EN07072, 2007.

Liss, P. S. and Slater, P. G.: Flux of Gases across the Air-Sea Interface, Nature, 247, 181–184, doi:10.1038/247181a0, 1974.

Lizotte, M., Levasseur, M., Law, C. S., Walker, C. F., Safi, K. A., Marriner, A. and Kiene, R. P.: Dimethylsulfoniopropionate (DMSP) and dimethyl sulfide (DMS) cycling across contrasting biological hotspots of the New Zealand subtropical front, Ocean Sci., 13(6), 961–982, doi:10.5194/os-13-961-2017, 2017.

Lizotte, M., Levasseur, M., Galindo, V., Gourdal, M., Gosselin, M., Tremblay, J. E., Blais, M., Charette, J. and Hussherr, R.: Phytoplankton and dimethylsulfide dynamics at two contrasting Arctic ice edges, Biogeosciences, 17(6), 1557–1581, doi:10.5194/bg-17-1557-2020, 2020.

Luce, M., Levasseur, M., Scarratt, M. G., Michaud, S., Royer, S. J., Kiene, R., Lovejoy, C., Gosselin, M., Poulin, M., Gratton, Y. and Lizotte, M.: Distribution and microbial metabolism of dimethylsulfoniopropionate and dimethylsulfide during the 2007 Arctic ice minimum, J. Geophys. Res. Ocean., 116(11), 4–11, doi:10.1029/2010JC006914, 2011.

Ludwig, V., Spreen, G., Haas, C., Istomina, L., Kauker, F. and Murashkin, D.: The 2018 North Greenland polynya observed by a newly introduced merged optical and passive microwave sea-ice concentration dataset, Cryosphere, 13(7), 2051–2073, doi:10.5194/tc-13-2051-2019, 2019.

Luo, G. and Yu, F.: A numerical evaluation of global oceanic emissions of α-pinene and isoprene, Atmos. Chem. Phys., 10(4), 2007–2015, doi:10.5194/acp-10-2007-2010, 2010.

Malin, G. and Steinke, M.: Coccolithophore-derived production of dimethyl sulphide, in Coccolithophores: From Molecular Processes to Global Impact, Springer Berlin Heidelberg, 2010. [online] Available from: http://repository.essex.ac.uk/5676/1/Malin and Steinke CoccoBook 2004.pdf, 2010.

Marandino, C. A., De Bruyn, W. J., Miller, S. D., Prather, M. J. and Saltzman, E. S.: Oceanic uptake and the global atmospheric acetone budget, Geophys. Res. Lett., 32(15), 1–4, doi:10.1029/2005GL023285, 2005a.

Marandino, C. A., De Bruyn, W. J., Miller, S. D., Prather, M. J., Saltzman, E. S., Bruyn, W. J. De, Miller, S. D., Prather, M. J., Saltzman, E. S., De Bruyn, W. J., Miller, S. D., Prather, M. J., Saltzman, E. S., Bruyn, W. J. De, Miller, S. D., Prather, M. J., Saltzman, E. S., De Bruyn, W. J., Miller, S. D., Prather, M. J., Saltzman, E. S., Bruyn, W. J. De, Miller, S. D., Prather, M. J. and Saltzman, E. S.: Oceanic uptake and the global atmospheric acetone budget, Geophys. Res. Lett., 32(15), 1–4, doi:10.1029/2005GL023285, 2005b.

Markus, T., Stroeve, J. C. and Miller, J.: Recent changes in Arctic sea ice melt onset, freezeup, and melt season length, J. Geophys. Res. Ocean., 114(12), 1–14, doi:10.1029/2009JC005436, 2009.

Martin, J., Tremblay, J. É., Gagnon, J., Tremblay, G., Lapoussière, A., Jose, C., Poulin, M.,

Gosselin, M., Gratton, Y. and Michel, C.: Prevalence, structure and properties of subsurface chlorophyll maxima in Canadian Arctic waters, Mar. Ecol. Prog. Ser., 412, 69–84, doi:10.3354/meps08666, 2010.

Maslanik, J., Stroeve, J., Fowler, C. and Emery, W.: Distribution and trends in Arctic sea ice age through spring 2011, Geophys. Res. Lett., 38(13), 2–7, doi:10.1029/2011GL047735, 2011.

Massicotte, P., Bécu, G., Lambert-Girard, S., Leymarie, E. and Babin, M.: Estimating underwater light regime under spatially heterogeneous sea ice in the Arctic, Appl. Sci., 8(12), 1–19, doi:10.3390/app8122693, 2018.

Matrai, P. A.: Dynamics of the vernal bloom in the marginal ice zone of the Barents Sea: Dimethyl sulfide and dimethylsulfoniopropionate budgets, J. Geophys. Res. C Ocean., 102(C10), 22965–22979, doi:10.1029/96JC03870, 1997.

Matsunaga, S., Mochida, M., Saito, T. and Kawamura, K.: In situ measurement of isoprene in the marine air and surface seawater from the western North Pacific, Atmos. Environ., 36(39–40), 6051–6057, doi:10.1016/S1352-2310(02)00657-X, 2002.

McCarty, P. L. and Reinhard, M.: Trace organics removal by advanced wastewater treatment, J. Water Pollut. Control Fed., 52(7), 1907–1922 [online] Available from: http://www.scopus.com/inward/record.url?eid=2-s2.0-0019044534&partnerID=40&md5=6b288cf153541571bec06854caabc93c, 1980.

McFiggans, G., Mentel, T. F., Wildt, J., Pullinen, I., Kang, S., Kleist, E., Schmitt, S., Springer, M., Tillmann, R., Wu, C., Zhao, D., Hallquist, M., Faxon, C., Le Breton, M., Hallquist, Å. M., Simpson, D., Bergström, R., Jenkin, M. E., Ehn, M., Thornton, J. A., Alfarra, M. R., Bannan, T. J., Percival, C. J., Priestley, M., Topping, D. and Kiendler-Scharr, A.: Secondary organic aerosol reduced by mixture of atmospheric vapours, Nature, doi:10.1038/s41586-018-0871-y, 2019.

Medeiros, D. J., Blitz, M. A., James, L., Speak, T. H. and Seakins, P. W.: Kinetics of the Reaction of OH with Isoprene over a Wide Range of Temperature and Pressure Including Direct Observation of Equilibrium with the OH Adducts, J. Phys. Chem. A, doi:10.1021/acs.jpca.8b04829, 2018.

Merzouk, A., Levasseur, M., Scarratt, M., Michaud, S., Lizotte, M., Rivkin, R. B. and Kiene, R. P.: Bacterial DMSP metabolism during the senescence of the spring diatom bloom in the

Northwest Atlantic, Mar. Ecol. Prog. Ser., doi:10.3354/meps07664, 2008.

Millet, D. B., Jacob, D. J., Custer, T. G., de Gouw, J. a., Goldstein, a. H., Karl, T., Singh, H. B., Sive, B. C., Talbot, R. W., Warneke, C. and Williams, J.: New constraints on terrestrial and oceanic sources of atmospheric methanol, Atmos. Chem. Phys., 8(2), 6887–6905, doi:10.5194/acpd-8-7609-2008, 2008.

Millet, D. B., Guenther, A., Siegel, D. a., Nelson, N. B., Singh, H. B., de Gouw, J. a., Warneke, C., Williams, J., Eerdekens, G., Sinha, V., Karl, T., Flocke, F., Apel, E., Riemer, D. D., Palmer, P. I. and Barkley, M.: Global atmospheric budget of acetaldehyde: 3-D model analysis and constraints from in-situ and satellite observations, Atmos. Chem. Phys., 10, 3405–3425, doi:10.5194/acp-10-3405-2010, 2010.

Mincer, T. J. and Aicher, A. C.: Methanol production by a broad phylogenetic array of marine phytoplankton, PLoS One, 11(3), 1–17, doi:10.1371/journal.pone.0150820, 2016.

Miyazaki, Y., Coburn, S., Ono, K., Ho, D. T., Pierce, R. B., Kawamura, K. and Volkamer, R.: Contribution of dissolved organic matter to submicron water-soluble organic aerosols in the marine boundary layer over the eastern equatorial Pacific, Atmos. Chem. Phys., 16(12), 7695–7707, doi:10.5194/acp-16-7695-2016, 2016.

Mochalski, P., King, J., Kupferthaler, A., Unterkofler, K., Hinterhuber, H. and Amann, A.: Measurement of isoprene solubility in water, human blood and plasma by multiple headspace extraction gas chromatography coupled with solid phase microextraction, J. Breath Res., 5(4), 1–8, doi:10.1088/1752-7155/5/4/046010, 2011.

Moore, R. M. Ã. and Wang, L.: The influence of iron fertilization on the fluxes of methyl halides and isoprene from ocean to atmosphere in the SERIES experiment, Deep. Res. Part II Top. Stud. Oceanogr., 53, 2398–2409, doi:10.1016/j.dsr2.2006.05.025, 2006.

Mopper, K. and Kieber, D. J.: Distribution and biological turnover of dissolved organic compounds in the water column of the Black Sea, Deep. Res. Part I-Oceanographic Res. Pap., 38(2), S1021–S1047, doi:10.1016/S0198-0149(10)80022-6, 1991.

Mopper, K. and Stahovec, W. L.: Sources and sinks of low molecular weight organic carbonyl compounds in seawater, Mar. Chem., 19(4), 305–321, doi:10.1016/0304-4203(86)90052-6, 1986.

Motard-Côté, J., Levasseur, M., Scarratt, M. G., Michaud, S., Gratton, Y., Rivkin, R. B., Keats, K., Gosselin, M., Tremblay, J. É., Kiene, R. P. and Lovejoy, C.: Distribution and metabolism of

dimethylsulfoniopropionate (DMSP) and phylogenetic affiliation of DMSP-assimilating bacteria in northern Baffin Bay/Lancaster Sound, J. Geophys. Res. Ocean., 117(2), doi:10.1029/2011JC007330, 2012.

Müller, J.-F. F., Liu, Z., Nguyen, V. S., Stavrakou, T., Harvey, J. N., Peeters, J., Chameides, W., Walker, J. C. G., Logan, J. A., Prather, M. J., Wofsy, S. C., Mcelroy, M. B., Zeng, G., Pyle, J. A., Young, P. J., Jacob, D. J., Millet, D. B., Singh, H. B., Burkert, J., Archibald, A. T., Petit, A. S., Percival, C. J., Harvey, J. N., Shallcross, D. E., Bossolasco, A., Faragó, E. P., Schoemaecker, C., Fittschen, C., Fittschen, C., Whalley, L. K., Heard, D. E., Berresheim, H., Neeb, P., Sauer, F., Horie, O., Moortgat, G. K., Millet, D. B., Stavrakou, T., Paulot, F., Bian, H., Zhang, S., Zhang, H., Nguyen, T. L. B. L. B. L., McCarthy, M. C., Stanton, J. F., Alvarez-Idaboy, J. R., Mora-Diez, N., Vivier-Bunge, A., Alvarez-Idaboy, J. R., Mora-Diez, N., Boyd, R. J., Vivier-Bunge, A., Peeters, J., Nguyen, V. S., Müller, J.-F. F., Miller, W. H., Handy, N. C., Adams, J. E., Baboul, A. G., Schlegel, H. B., Hratchian, H. P., Glowacki, D. R., Liang, C. H., Morley, C., Pilling, M. J., Robertson, S. H., Harvey, J. N., Troe, J., Guenther, A., Sommariva, R., Singh, H. B., Brune, W. H., Crawford, J. H., Flocke, F., Jacob, D. J., Vaghjiani, G. L., Ravishankara, A. R., Stavrakou, T., Khan, M. A. H., Read, K. A., Yang, M., Talbot, R. W., Millet, D. B., Jenkin, M. E., Saunders, S. M., Pilling, M. J., Goerigk, L., Grimme, S., Werner, H.-J., Knowles, P. J., Knizia, G., Manby, F. R., Schütz, M., Dunning, T. H., Neese, F., Peterson, K. A., Adler, T. B., Werner, H.-J., Alecu, I. M., et al.: The reaction of methyl peroxy and hydroxyl radicals as a major source of atmospheric methanol, Nat. Commun., 7(May), 13213, doi:10.1038/ncomms13213, 2016a.

Müller, J.-F. F., Liu, Z., Nguyen, V. S., Stavrakou, T., Harvey, J. N. and Peeters, J.: The reaction of methyl peroxy and hydroxyl radicals as a major source of atmospheric methanol, Nat. Commun., 7(May), 13213, doi:10.1038/ncomms13213, 2016b.

Müller, J. F., Stavrakou, T., Wallens, S., De Smedt, I., Van Roozendael, M., Potosnak, M. J., Rinne, J., Munger, B., Goldstein, A. and Guenther, A. B.: Global isoprene emissions estimated using MEGAN, ECMWF analyses and a detailed canopy environment model, Atmos. Chem. Phys., 8(5), 1329–1341, doi:10.5194/acp-8-1329-2008, 2008.

Mungall, E. L., Croft, B., Lizotte, M., Thomas, J. L., Murphy, J. G., Levasseur, M., Martin, R. V., Wentzell, J. J. B., Liggio, J. and Abbatt, J. P. D.: Dimethyl sulfide in the summertime Arctic atmosphere: Measurements and source sensitivity simulations, Atmos. Chem. Phys., 16(11), 6665–6680, doi:10.5194/acp-16-6665-2016, 2016.

Mungall, E. L., Abbatt, J. P. D., Wentzell, J. J. B., Lee, A. K. Y., Thomas, J. L., Blais, M.,

Gosselin, M., Miller, L. A., Papakyriakou, T., Willis, M. D. and Liggio, J.: A novel source of oxygenated volatile organic compounds in the summertime marine Arctic boundary layer, Proc. Natl. Acad. Sci., accepted, doi:10.1073/pnas.1620571114, 2017.

Mungall, E. L., Abbatt, J. P. D., Wentzell, J. J. B., Wentworth, G. R., Murphy, J. G., Kunkel, D., Gute, E., Tarasick, D. W., Sharma, S., Cox, C. J., Uttal, T. and Liggio, J.: High gas-phase mixing ratios of formic and acetic acid in the High Arctic, Atmos. Chem. Phys., 18(14), 10237–10254, doi:10.5194/acp-18-10237-2018, 2018.

Nadzir, M. S. M., Cain, M., Robinson, A. D., Bolas, C., Harris, N. R. P., Parnikoza, I., Salimun, E., Mustafa, E. M., Alhasa, K. M., Zainuddin, M. H. M., Ghee, O. C., Morris, K., Khan, M. F., Latif, M. T., Wallis, B. M., Cheah, W., Zainudin, S. K., Yusop, N., Ahmad, M. R., Hussin, W. M. R. W., Salleh, S. M., Hamid, H. H. A., Lai, G. T., Uning, R., Bakar, M. A. A., Ariff, N. M., Tuah, Z., Wahab, M. I. A., Foong, S. Y., Samah, A. A., Chenoli, S. N., Wan Johari, W. L., Zain, C. R. C. M., Rahman, N. A., Rosenstiel, T. N., Yusoff, A. H., Sabuti, A. A., Alias, S. A. and Noor, A. Y. M.: Isoprene hotspots at the Western Coast of Antarctic Peninsula during MASEC'16, Polar Sci., 20(December 2018), 63–74, doi:10.1016/j.polar.2018.12.006, 2019.

Nemecek-Marshall, M., Wojciechowski, C., Kuzma, J., Silver, G. M. and Fall, R.: Marine Vibrio species produce the volatile organic compound acetone, Appl. Environ. Microbiol., 61(1), 44–47, 1995.

Nemecek-Marshall, M., Wojciechowski, C., Wagner, W. P. and Fall, R.: Acetone formation in the vibrio family: A new pathway for bacterial leucine catabolism, J. Bacteriol., 181(24), 7493–7499, 1999.

Nightingale, P. D.: Air-Sea Gas Exchange, , 69–97, doi:10.1029/2008GM000774, 2009.

Nightingale, P. D., Malin, G., Law, C. S., Watson, J., Liss, P. S. and Liddicoat, I.: In situ evaluation of air-sea gas exchange parameterizations using novel conservative and volatile tracers, Global Biogeochem. Cycles, 14(1), 373–387, doi:10.1029/1999GB900091, 2000.

O'Dowd, C. D., Facchini, M. C., Cavalli, F., Ceburnis, D., Mircea, M., Decesari, S., Fuzzi, S., Young, J. Y. and Putaud, J. P.: Biogenically driven organic contribution to marine aerosol, Nature, 431(7009), 676–680, doi:10.1038/nature02959, 2004.

Ooki, A., Nomura, D., Nishino, S., Kikuchi, T. and Yokouchi, Y.: A global-scale map of isoprene and volatile organic iodine in surface seawater of the Arctic, Northwest Pacific, Indian, and Southern Oceans, J. Geophys. Res. Ocean., 120(6), 4108–4128,

doi:10.1002/2014JC010519, 2015.

Ooki, A., Shida, R., Otsu, M., Onishi, H., Kobayashi, N., Iida, T., Nomura, D., Suzuki, K., Yamaoka, H. and Takatsu, T.: Isoprene production in seawater of Funka Bay, Hokkaido, Japan, J. Oceanogr., 75(6), 485–501, doi:10.1007/s10872-019-00517-6, 2019.

Palmer, P. I. and Shaw, S. L.: Quantifying global marine isoprene fluxes using MODIS chlorophyll observations, Geophys. Res. Lett., 32(9), 1–5, doi:10.1029/2005GL022592, 2005.

Parmentier, F.-J. W., Christensen, T. R., Sørensen, L. L., Rysgaard, S., McGuire, a. D., Miller, P. a. and Walker, D. a.: The impact of lower sea-ice extent on Arctic greenhouse-gas exchange, Nat. Clim. Chang., 3(3), 195–202, doi:10.1038/nclimate1784, 2013.

Pellichero, V., Sallée, J. B., Schmidtko, S., Roquet, F. and Charrassin, J. B.: The ocean mixed layer under Southern Ocean sea-ice: Seasonal cycle and forcing, J. Geophys. Res. Ocean., 122(9), 1608–1633, doi:doi:10.1002/ 2016JC011970, 2017.

Perrette, M., Yool, A., Quartly, G. D. and Popova, E. E.: Near-ubiquity of ice-edge blooms in the Arctic, Biogeosciences, 8(2), 515–524, doi:10.5194/bg-8-515-2011, 2011.

Ratte, M., Bujok, O., Spitzy, A. and Rudolph, J.: Photochemical alkene formation in seawater from dissolved organic carbon: Results from laboratory experiments, J. Geophys. Res., 103, 5707–5717, 1998.

Read, K. A., Lee, J. D., Lewis, A. C., Moller, S. J., Mendes, L. and Carpenter, L. J.: Intra-annual cycles of NMVOC in the tropical marine boundary layer and their use for interpreting seasonal variability in CO, J. Geophys. Res. Atmos., 114(21), 1–14, doi:10.1029/2009JD011879, 2009.

Read, K. A., Carpenter, L. J., Arnold, S. R., Beale, R., Nightingale, P. D., Hopkins, J. R., Lewis, A. C., Lee, J. D., Mendes, L. and Pickering, S. J.: Multiannual observations of acetone, methanol, and acetaldehyde in remote tropical Atlantic air: Implications for atmospheric OVOC budgets and oxidative capacity, Environ. Sci. Technol., 46(20), 11028–11039, doi:10.1021/es302082p, 2012.

Rellinger, A. N., Kiene, R. P., del Valle, D. A., Kieber, D. J., Slezak, D., Harada, H., Bisgrove, J. and Brinkley, J.: Occurrence and turnover of DMSP and DMS in deep waters of the Ross Sea, Antarctica, Deep. Res. Part I Oceanogr. Res. Pap., 56(5), 686–702, doi:10.1016/j.dsr.2008.12.010, 2009.

Rodríguez-Ros, P., Galí, M., Cortés, P., Robinson, C. M., Antoine, D., Wohl, C., Yang, M. X. and Simó, R.: Remote Sensing Retrieval of Isoprene Concentrations in the Southern Ocean, Geophys. Res. Lett., 47(13), 1–10, doi:10.1029/2020GL087888, 2020.

Royer, S. J., Mahajan, A. S., Galí, M., Saltzman, E. and Simõ, R.: Small-scale variability patterns of DMS and phytoplankton in surface waters of the tropical and subtropical Atlantic, Indian, and Pacific Oceans, Geophys. Res. Lett., 42(2), 475–483, doi:10.1002/2014GL062543, 2015.

Royer, S. J., Galí, M., Mahajan, A. S., Ross, O. N., Pérez, G. L., Saltzman, E. S. and Simó, R.: A high-resolution time-depth view of dimethylsulphide cycling in the surface sea, Sci. Rep., 6(November 2015), 1–13, doi:10.1038/srep32325, 2016.

Rudels, B., Larsson, A. and Sehlstedt, P.: Stratification and water mass formation in the Arctic Ocean : some implications for the nutrient distribution Stratification and water mass formation in the Arctic Ocean : some implications for the nutrient distribution, Polar Res., 10(1), 19–32, doi:10.3402/polar.v10i1.6724, 1991.

Saltzman, E. S., de Bruyn, W. J., Lawler, M. J., Marandino, C. A. and McCormick, C. A.: A chemical ionization mass spectrometer for continuous underway shipboard analysis of dimethylsulfide in near-surface seawater, Ocean Sci., doi:10.5194/os-5-537-2009, 2009.

Sander, R.: Compilation of Henry's law constants (version 4.0) for water as solvent, Atmos. Chem. Phys., 15(8), 4399–4981, doi:10.5194/acp-15-4399-2015, 2015.

Sargeant, S. L., Colin Murrell, J., Nightingale, P. D. and Dixon, J. L.: Seasonal variability in microbial methanol utilisation in coastal waters of the western English Channel., Mar. Ecol. Prog. Ser., 550, 53–64, 2016.

Schade, G. W. and Goldstein, A. H.: Seasonal measurements of acetone and methanol: Abundances and implications for atmospheric budgets, Global Biogeochem. Cycles, 20(1), doi:10.1029/2005GB002566, 2006.

Schlundt, C., Marandino, C. A., Tegtmeier, S., Lennartz, S. T., Bracher, A., Cheah, W., Krüger, K., Quack, B., Marandino, C. A., Tegtmeier, S., Lennartz, S. T., Bracher, A., Cheah, W., Krüger, K., Quack, B. and Marandino, C. A.: Oxygenated volatile organic carbon in the western Pacific convective center: Ocean cycling, air-sea gas exchange and atmospheric transport, Atmos. Chem. Phys., 17(17), 10837–10854, doi:10.5194/acp-17-10837-2017, 2017.

Schwarz, K., Filipiak, W. and Amann, A.: Determining concentration patterns of volatile compounds in exhaled breath by PTR-MS, J. Breath Res., 3, 1–15, doi:10.1088/1752-7155/3/2/027002, 2009.

Senftleben, D., Lauer, A. and Karpechko, A.: Constraining uncertainties in CMIP5 projections of September Arctic sea ice extent with observations, J. Clim., 33(4), 1487–1503, doi:10.1175/JCLI-D-19-0075.1, 2020.

Shadwick, E. H., Thomas, H., Chierici, M., Else, B., Fransson, A., Michel, C., Miller, L. A., Mucci, A., Niemi, A., Papakyriakou, T. N. and Tremblay, J. É.: Seasonal variability of the inorganic carbon system in the Amundsen Gulf region of the Southeastern Beaufort Sea, Limnol. Oceanogr., 56(1), 303–322, doi:10.4319/lo.2011.56.1.0303, 2011.

Shadwick, E. H., Trull, T. W., Thomas, H. and Gibson, J. A. E.: Vulnerability of polar oceans to anthropogenic acidification: Comparison of arctic and antarctic seasonal cycles, Sci. Rep., 3, doi:10.1038/srep02339, 2013.

Shadwick, E. H., Trull, T. W., Tilbrook, B., Sutton, A. J., Schulz, E. and Sabine, C. L.: Seasonality of biological and physical controls on surface ocean CO2 from hourly observations at the Southern Ocean Time Series site south of Australia, Global Biogeochem. Cycles, 29(2), 223–238, doi:10.1002/2014GB004906, 2015.

Sharkey, T. D.: Emission of low molecular mass hydrocarbons from plants, Trends Plant Sci., 1(3), 78–82, doi:10.1016/S1360-1385(96)80038-0, 1996.

Shaw, S. L., Gantt, B. and Meskhidze, N.: Production and Emissions of Marine Isoprene and Monoterpenes: A Review, Adv. Meteorol., 2010(1), 1–24, doi:10.1155/2010/408696, 2010.

Sheehan, C. E. and Petrou, K.: Dimethylated sulfur production in batch cultures of Southern Ocean phytoplankton, Biogeochemistry, doi:10.1007/s10533-019-00628-8, 2020.

Simo, R., Pedros-Alio, C., Malin, G. and Grimalt, J. O.: Biological turnover of DMS, DMSP and DMSO in contrasting open-sea waters, Mar. Ecol. Prog. Ser., 203, 1–11, doi:10.3354/meps203001, 2000.

Simó, R., Grimalt, J. O. and Albaigés, J.: Dissolved dimethylsulphide, dimethylsulphoniopropionate and dimethylsulphoxide in western Mediterranean waters, Deep. Res. Part II Top. Stud. Oceanogr., doi:10.1016/S0967-0645(96)00099-9, 1997.

Simó, R., Saló, V., Almeda, R., Movilla, J., Trepat, I., Saiz, E. and Calbet, A.: The quantitative role of microzooplankton grazing in dimethylsulfide (DMS) production in the NW

Mediterranean, Biogeochemistry, 141(2), 125–142, doi:10.1007/s10533-018-0506-2, 2018.

Sims, R. P., Schuster, U., Watson, A. J., Yang, M., Hopkins, F. E., Stephens, J. and Bell, T. G.: A measurement system for vertical seawater profiles close to the air-sea interface, Ocean Sci., 13(5), 649–660, doi:10.5194/os-13-649-2017, 2017.

Singh, H. B., Kanakidou, M., Crutzen, P. J. and Jacob, D. J.: High concentrations and photochemical fate of oxygenated hydrocarbons in the global troposphere, Nature, 378(6552), 50–54, doi:10.1038/378050a0, 1995.

Singh, H. B., Salas, L. J., Chatfield, R. B., Czech, E., Fried, A., Walega, J., Evans, M. J., Field, B. D., Jacob, D. J., Blake, D., Heikes, B., Talbot, R., Sachse, G., Crawford, J. H., Avery, M. A., Sandholm, S. and Fuelberg, H.: Analysis of the atmospheric distribution, sources, and sinks of oxygenated volatile organic chemicals based on measurements over the Pacific during TRACE-P, J. Geophys. Res. D Atmos., 109(15), doi:10.1029/2003JD003883, 2004.

Sinha, V., Williams, J., Lelieveld, J., Ruuskanen, T. M., Kajos, M. K., Patokoski, J., Hellen, H., Hakola, H., Mogensen, D., Boy, M., Rinne, J. and Kulmala, M.: OH reactivity measurements within a boreal forest: Evidence for unknown reactive emissions, Environ. Sci. Technol., 44(17), 6614–6620, doi:10.1021/es101780b, 2010.

Sjostedt, S. J., Leaitch, W. R., Levasseur, M., Scarratt, M., Michaud, S., Motard-Cté, J., Burkhart, J. H. and Abbatt, J. P. D.: Evidence for the uptake of atmospheric acetone and methanol by the Arctic Ocean during late summer DMS-Emission plumes, J. Geophys. Res. Atmos., 117(12), 1–15, doi:10.1029/2011JD017086, 2012.

Snider, J. R. and Dawson, G. A.: Tropospheric Light Alcohols, Carbonyls, and Acetonitrile: Concentrations in the Southwestern United States and Henry'S Law Data, J. Geophys. Res., doi:10.1029/JD090iD02p03797, 1985.

Spracklen, D. V., Arnold, S. R., Sciare, J., Carslaw, K. S. and Pio, C.: Globally significant oceanic source of organic carbon aerosol, Geophys. Res. Lett., 35(12), 1–5, doi:10.1029/2008GL033359, 2008.

Spreen, G., Kaleschke, L. and Heygster, G.: Sea ice remote sensing using AMSR-E 89-GHz channels, J. Geophys. Res. Ocean., 113(2), 1–14, doi:10.1029/2005JC003384, 2008.

Srikanta Dani, K. G., Silva Benavides, A. M., Michelozzi, M., Peluso, G., Torzillo, G. and Loreto, F.: Relationship between isoprene emission and photosynthesis in diatoms, and its implications for global marine isoprene estimates, Mar. Chem., 189, 17–24,

doi:10.1016/j.marchem.2016.12.005, 2017.

Stacheter, A., Noll, M., Lee, C. K., Selzer, M., Glowik, B., Ebertsch, L., Mertel, R., Schulz, D., Lampert, N., Drake, H. L. and Kolb, S.: Methanol oxidation by temperate soils and environmental determinants of associated methylotrophs., ISME J., 7(5), 1051–64, doi:10.1038/ismej.2012.167, 2013.

Stavrakou, T., Guenther, A., Razavi, A., Clarisse, L., Clerbaux, C., Coheur, P. F., Hurtmans, D., Karagulian, F., De MaziÃre, M., Vigouroux, C., Amelynck, C., Schoon, N., Laffineur, Q., Heinesch, B., Aubinet, M., Rinsland, C. and Müller, J. F.: First space-based derivation of the global atmospheric methanol emission fluxes, Atmos. Chem. Phys., 11(10), 4873–4898, doi:10.5194/acp-11-4873-2011, 2011.

Taddei, S., Toscano, P., Gioli, B., Matese, A., Miglietta, F., Vaccari, F. P., Zaldei, A., Custer, T. and Williams, J.: Carbon dioxide and acetone air-sea fluxes over the southern Atlantic, Environ. Sci. Technol., 43(14), 5218–5222, doi:10.1021/es8032617, 2009.

Takahashi, T., Sutherland, S. C., Wanninkhof, R., Sweeney, C., Feely, R. A., Chipman, D. W., Hales, B., Friederich, G., Chavez, F., Sabine, C., Watson, A., Bakker, D. C. E., Schuster, U., Metzl, N., Yoshikawa-Inoue, H., Ishii, M., Midorikawa, T., Nojiri, Y., Körtzinger, A., Steinhoff, T., Hoppema, M., Olafsson, J., Arnarson, T. S., Tilbrook, B., Johannessen, T., Olsen, A., Bellerby, R., Wong, C. S., Delille, B., Bates, N. R. and de Baar, H. J. W.: Climatological mean and decadal change in surface ocean pCO2, and net sea-air CO2 flux over the global oceans, Deep. Res. Part II, 56, 554–577, doi:10.1016/j.dsr2.2008.12.009, 2009.

Takeda, K., Katoh, S., Mitsui, Y., Nakano, S., Nakatani, N. and Sakugawa, H.: Spatial distributions of and diurnal variations in low molecular weight carbonyl compounds in coastal seawater, and the controlling factors, Sci. Total Environ., 493, 454–462, doi:10.1016/j.scitotenv.2014.05.126, 2014.

Tedetti, M. and Semperv, R.: Penetration of Ultraviolet Radiation in the Marine Environment. A Review, Photochem. Photobiol., 82(24), 389–397, doi:10.1562/2005-11-09-lR-733, 2006.

Thomas, M. A., Suntharalingam, P., Pozzoli, L., Rast, S., Devasthale, A., Kloster, S., Feichter, J. and Lenton, T. M.: Quantification of DMS aerosol-cloud-climate interactions using the ECHAM5-HAMMOZ model in a current climate scenario, Atmos. Chem. Phys., 10(15), 7425–7438, doi:10.5194/acp-10-7425-2010, 2010.

Tortell, P. D.: Dissolved gas measurements in oceanic waters made by membrane inlet mass spectrometry, Limnol. Oceanogr. Methods, 3, 24–37, doi:10.4319/lom.2005.3.24, 2005a.

Tortell, P. D.: Small-scale heterogeneity of dissolved gas concentrations in marine continental shelf waters, Geochemistry, Geophys. Geosystems, 6(11), doi:10.1029/2005GC000953, 2005b.

Tran, S., Bonsang, B., Gros, V., Peeken, I., Sarda-Esteve, R., Bernhardt, A. and Belviso, S.: A survey of carbon monoxide and non-methane hydrocarbons in the Arctic Ocean during summer 2010, Biogeosciences, 10(3), 1909–1935, doi:10.5194/bg-10-1909-2013, 2013.

Trefz, P., Schubert, J. K. and Miekisch, W.: Effects of humidity, CO 2 and O 2 on real-time quantitation of breath biomarkers by means of PTR-ToF-MS, J. Breath Res., 12(2), doi:10.1088/1752-7163/aa9eea, 2018.

Turner, S. M., Nightingale, P. D., Broadgate, W. and Liss, P. S.: The distribution of dimethyl sulphide and dimethylsulphoniopropionate in Antarctic waters and sea ice, Deep Sea Res. II, 42, 1059–1080, 1995.

Udisti, R., Traversi, R., Silvia, B., Tomasi, C., Mazzola, M., Lupi, A. and Quinn, P. K.: Arctic Aerosols, in Physics and Chemistry of the Arctic Atmosphere, pp. 209–329, Springer Polar Sciences, Springer, Cham., 2020.

Vallina, S. M. and Simó, R.: Strong relationship between DMS and the solar radiation dose over the global surface ocean, Science (80-.)., 315(5811), 506–508, doi:10.1126/science.1133680, 2007.

Venables, H. J. and Meredith, M. P.: Feedbacks between ice cover, ocean stratification, and heat content in Ryder Bay, western Antarctic Peninsula, J. Geophys. Res. Ocean., doi:10.1002/2013jc009669, 2014.

Vitenberg, A. G., Ioffea, B. V., Dimitrova, Z. S. and Butaeva, I. L.: Determinatlon of gas-liquid partition by means of gas chromatographic analysis, J. Chromatogr., 112, 319–327 [online] Available from: http://www.sciencedirect.com/science/article/pii/S0021967300999643, 1975.

Wang, S., Hornbrook, R. S., Hills, A., Emmons, L. K., Tilmes, S., Lamarque, J., Jimenez, J. L., Campuzano-Jost, P., Nault, B. A., Crounse, J. D., Wennberg, P. O., Ryerson, T. B., Thompson, C. R., Peischl, J., Moore, F., Nance, D., Hall, B., Elkins, J., Tanner, D., Huey, L. G., Hall, S. R.,

Ullmann, K., Orlando, J. J., Tyndall, G. S., Flocke, F. M., Ray, E., Hanisco, T. F., Wolfe, G. M., St. Clair, J., Commane, R., Daube, B., Barletta, B., Blake, D. R., Weinzierl, B., Dollner, M., Conley, A., Vitt, F., Wofsy, S. C., Riemer, D. D. and Apel, E. C.: Atmospheric Acetaldehyde: Importance of Air-Sea Exchange and a Missing Source in the Remote Troposphere, Geophys. Res. Lett., 46, 2019GL082034, doi:10.1029/2019GL082034, 2019.

Wang, S., Apel, E. C., Schwantes, R. H., Bates, K. H., Jacob, D. J., Fischer, E. V., Hornbrook, R. S., Hills, A. J., Emmons, L. K., Pan, L. L., Honomichl, S., Tilmes, S., Lamarque, J. F., Yang, M., Marandino, C. A., Saltzman, E. S., de Bruyn, W., Kameyama, S., Tanimoto, H., Omori, Y., Hall, S. R., Ullmann, K., Ryerson, T. B., Thompson, C. R., Peischl, J., Daube, B. C., Commane, R., McKain, K., Sweeney, C., Thames, A. B., Miller, D. O., Brune, W. H., Diskin, G. S., DiGangi, J. P. and Wofsy, S. C.: Global Atmospheric Budget of Acetone: Air-Sea Exchange and the Contribution to Hydroxyl Radicals., 2020a.

Wang, Z., Li, Z., Zeng, J., Liang, S., Zhang, P., Tang, F., Chen, S. and Ma, X.: Spatial and Temporal Variations of Arctic Sea Ice From 2002 to 2017, Earth Sp. Sci., 7(9), 1–20, doi:10.1029/2020EA001278, 2020b.

Wanninkhof, R., Asher, W. E., Ho, D. T., Sweeney, C. and McGillis, W. R.: Advances in quantifying air-sea gas exchange and environmental forcing., Ann. Rev. Mar. Sci., 1, 213–244, doi:10.1146/annurev.marine.010908.163742, 2009.

Warneke, C., Van Der Veen, C., Luxembourg, S., De Gouw, J. A. and Kok, A.: Measurements of benzene and toluene in ambient air using proton-transfer-reaction mass spectrometry: Calibration, humidity dependence, and field intercomparison, Int. J. Mass Spectrom., 207(3), 167–182, doi:10.1016/S1387-3806(01)00366-9, 2001.

Warneke, C., De Gouw, J. A., Kuster, W. C., Goldan, P. D. and Fall, R.: Validation of atmospheric VOC measurements by proton-transfer-reaction mass spectrometry using a gas-chromatographic preseparation method, Environ. Sci. Technol., 37(11), 2494–2501, doi:10.1021/es026266i, 2003a.

Warneke, C., De Gouw, J. A., Kuster, W. C., Goldan, P. D. and Fall, R.: Validation of atmospheric VOC measurements by proton-transfer-reaction mass spectrometry using a gas-chromatographic preseparation method, Environ. Sci. Technol., 37(11), 2494–2501, doi:10.1021/es026266i, 2003b.

Warneke, C., De Gouw, J. A., Kuster, W. C., Goldan, P. D. and Fall, R.: Validation of atmospheric VOC measurements by proton-transfer-reaction mass spectrometry using a

gas-chromatographic preseparation method, Environ. Sci. Technol., 37(11), 2494–2501, doi:10.1021/es026266i, 2003c.

Webb, A. L., van Leeuwe, M. A., den Os, D., Meredith, M. P., J. Venables, H. and Stefels, J.: Extreme spikes in DMS flux double estimates of biogenic sulfur export from the Antarctic coastal zone to the atmosphere, Sci. Rep., 9(1), 1–11, doi:10.1038/s41598-019-38714-4, 2019.

Wells, K. C., Millet, D. B., Payne, V. H., Deventer, M. J., Bates, K. H., de Gouw, J. A., Graus, M., Warneke, C., Wisthaler, A. and Fuentes, J. D.: Satellite isoprene retrievals constrain emissions and atmospheric oxidation, Nature, 585(7824), 225–233, doi:10.1038/s41586-020-2664-3, 2020.

Williams, J., Pöschl, U., Crutzen, P. J., Hansel, A., Holzinger, R., Warneke, C., Lindinger, W. and Lelieveld, J.: An atmospheric chemistry interpretation of mass scans obtained from a proton transfer mass spectrometer flown over the tropical rainforest of Surinam, J. Atmos. Chem., 38(2), 133–166, doi:10.1023/A:1006322701523, 2001.

Williams, J., Holzinger, R., Gros, V., Xu, X., Atlas, E. and Wallace, D. W. R.: Measurements of organic species in air and seawater from the tropical Atlantic, Geophys. Res. Lett., 31(23), 1–5, doi:10.1029/2004GL020012, 2004.

Williams, J., Custer, T., Riede, H., Sander, R., Jöckel, P., Hoor, P., Pozzer, A., Wong-Zehnpfennig, S., Hosaynali Beygi, Z., Fischer, H., Gros, V., Colomb, A., Bonsang, B., Yassaa, N., Peeken, I., Atlas, E. L., Waluda, C. M., Van Aardenne, J. A. and Lelieveld, J.: Assessing the effect of marine isoprene and ship emissions on ozone, using modelling and measurements from the South Atlantic Ocean, Environ. Chem., 7(2), 171–182, doi:10.1071/EN09154, 2010.

Wingenter, O. W., Haase, K. B., Strutton, P., Friederich, G., Meinardi, S., Blake, D. R. and Rowland, F. S.: Changing concentrations of CO, CH4, C5H8, CH3Br, CH3I, and dimethyl sulfide during the Southern Ocean Iron Enrichment Experiments, Proc. Natl. Acad. Sci., 101(23), 8537–8541, doi:10.1073/pnas.0402744101, 2004.

Wittek, B., Carnat, G., Tison, J. L. and Gypens, N.: Response of dimethylsulfoniopropionate (DMSP) and dimethylsulfoxide (DMSO) cell quotas to salinity and temperature shifts in the sea-ice diatom Fragilariopsis cylindrus, Polar Biol., 43(5), 483–494, doi:10.1007/s00300-020-02651-0, 2020.

Woodhouse, M. T., Mann, G. W., Carslaw, K. S. and Boucher, O.: Sensitivity of cloud

condensation nuclei to regional changes in dimethyl-sulphide emissions, Atmos. Chem. Phys., 13(5), 2723–2733, doi:10.5194/acp-13-2723-2013, 2013.

Xie, H., C, Z. O., Wang, W. E. I. and Taylor, C. D.: A Simple Automated Continuous-Flow-Equilibration Method for Measuring Carbon Monoxide in Seawater, Environ. Sci. Technol., 35(7), 1475–1480, 2001.

Yang, M. and Fleming, Z. L.: Estimation of atmospheric total organic carbon (TOC) - paving the path towards carbon budget closure, Atmos. Chem. Phys., 19, 459–471, doi:10.5194/acp-19-459-2019, 2019.

Yang, M., Blomquist, B. W., Fairall, C. W., Archer, S. D. and Huebert, B. J.: Air - sea exchange of dimethylsulfide in the Southern Ocean : Measurements from SO GasEx compared to temperate and tropical regions, J. Geophys. Res., 116, 1–17, doi:10.1029/2010JC006526, 2011.

Yang, M., Nightingale, P. D., Beale, R., Liss, P. S., Blomquist, B. W. and Fairall, C. W.: Atmospheric deposition of methanol over the Atlantic Ocean., Proc. Natl. Acad. Sci. U. S. A., 110(50), 20034–9, doi:10.1073/pnas.1317840110, 2013a.

Yang, M., Archer, S. D., Blomquist, B. W., Ho, D. T., Lance, V. P. and Torres, R. J.: Lagrangian evolution of DMS during the Southern Ocean gas exchange experiment: The effects of vertical mixing and biological community shift, J. Geophys. Res. Ocean., 118(12), 6774–6790, doi:10.1002/2013JC009329, 2013b.

Yang, M., Beale, R., Smyth, T. and Blomquist, B. W.: Measurements of OVOC fluxes by eddy covariance using a proton-transfer- reaction mass spectrometer-method development at a coastal site, Atmos. Chem. Phys., 13(13), 6165–6184, doi:10.5194/acp-13-6165-2013, 2013c.

Yang, M., Blomquist, B. W. and Nightingale, P. D.: Air-sea exchange of methanol and acetone during HiWinGS: Estimation of air phase, water phase gas transfer velocities, J. Geophys. Res. Ocean., 119(10), 7308–7323, doi:10.1002/2014JC010227, 2014a.

Yang, M., Blomquist, B. W. and Nightingale, P. D.: Air-sea exchange of methanol and acetone during HiWinGS: Estimation of air phase, water phase gas transfer velocities, J. Geophys. Res. Ocean., 119, 7308–7323, doi:10.1002/2014JC010227, 2014b.

Yang, M., Beale, R., Liss, P. S., Johnson, M. T., Blomquist, B. W. and Nightingale, P.: Air-sea fluxes of oxygenated volatile organic compounds across the Atlantic Ocean, Atmos. Chem.

Phys., 14, 7499–7517, doi:10.5194/acp-14-7499-2014, 2014c.

Yaws, C. L. and Yang, H.-C.: Henry's law constant for compound in water, in: Thermodynamic and Physical Property Data, edited by C. L. Yaws, Gulf Publishing Company, Houston, TX., 1992.

Yokouchi, Y., Li, H. and Machida, T.: Isoprene in the marine boundary layer (Southeast Asian Sea,eastern Indian Ocean , and Southern Ocean): Comparison with dimethyl sulfide and bromoform, J. Geophys. Res., 104, 8067–8076, 1999.

Zeebe, R. E. and Wolf-Gladrow, D.: CO2 in Seawater: equilibrium, kinetics, isotopes. Chapter 1 Equilibrium, Elsevier Oceanogr. Ser., 2001.

Zhang, X. H., Liu, J., Liu, J., Yang, G., Xue, C. X., Curson, A. R. J. and Todd, J. D.: Biogenic production of DMSP and its degradation to DMS—their roles in the global sulfur cycle, Sci. China Life Sci., 62(10), 1296–1319, doi:10.1007/s11427-018-9524-y, 2019.

Zhao, J. and Zhang, R.: Proton transfer reaction rate constants between hydronium ion (H3O+) and volatile organic compounds, Atmos. Environ., 38(14), 2177–2185, doi:doi: 10.1016/j.atmosenv.2004.01.019, 2004.

Zhou, X. and Mopper, K.: Photochemical production of low-molecular-weight carbonyl compounds in seawater and surface microlayer and their air-sea exchange, Mar. Chem., 56(3–4), 201–213, doi:10.1016/S0304-4203(96)00076-X, 1997.

Zhou, X. . and Mopper, K.: Apparent Partition-Coefficients of 15 Carbonyl Compounds between Air and Seawater and between Air and Freshwater: Implications for Air Sea Exchange, Environ. Sci. Technol., 24(12), 1864–1869, doi:10.1021/es00082a013, 1990.

Zhu, L., Jacob, D. J., Kim, P. S., Fisher, J. A., Yu, K., Travis, K. R., Mickley, L. J., Yantosca, R. M., Sulprizio, M. P., De Smedt, I., Abad, G. G., Chance, K., Li, C., Ferrare, R., Fried, A., Hair, J. W., Hanisco, T. F., Richter, D., Scarino, A. J., Walega, J., Weibring, P. and Wolfe, G. M.: Observing atmospheric formaldehyde (HCHO) from space: Validation and intercomparison of six retrievals from four satellites (OMI, GOME2A, GOME2B, OMPS) with SEAC4RS aircraft observations over the southeast US, Atmos. Chem. Phys., 16(21), 13477–13490, doi:10.5194/acp-16-13477-2016, 2016.

Zhu, Y. and Kieber, D. J.: Wavelength- and Temperature-Dependent Apparent Quantum Yields for Photochemical Production of Carbonyl Compounds in the North Pacific Ocean, Environ. Sci. Technol., 52(4), 1929–1939, doi:10.1021/acs.est.7b05462, 2018.

Zhu, Y. and Kieber, D. J.: Concentrations and Photochemistry of Acetaldehyde, Glyoxal, and Methylglyoxal in the Northwest Atlantic Ocean, Environ. Sci. Technol., 53(16), 9512–9521, doi:10.1021/acs.est.9b01631, 2019.

Zhu, Y. and Kieber, D. J.: Global Model for Depth-Dependent Carbonyl Photochemical Production Rates in Seawater, Global Biogeochem. Cycles, 34(4), 1–20, doi:10.1029/2019GB006431, 2020.

Zou, Y., Wang, Y., Zhang, Y. and Koo, J. H.: Arctic sea ice, Eurasia snow, and extreme winter haze in China, Sci. Adv., doi:10.1126/sciadv.1602751, 2017.